

2.3 Preparation of gelatin/silk fibroin microspheres

Gelatin/silk fibroin microspheres prepared by water in oil (w/o) emulsion technique [8]. Briefly, an aqueous solution of 10 wt.% gelatin/silk fibroin was preheated up to 40 °C and added dropwise into 400 ml of soybean oil at 40 °C with constant stirring at 95 rpm for 15 min. Temperature was rapidly decreased to 4 °C to form the microspheres. The microspheres were washed with cold acetone and centrifuged at 9000 rpm 4 °C, for 5 min for complete cleaning of residual oils. Then they were fractionated through sieves (apertures of 710, OSAKA IIDA, Japan) and were airdried at 4 °C. Gelatin/silk fibroin microspheres were crosslinked using 0.05 %v/v of glutaraldehyde solution in acetone and were stirred at 4°C for 20 hours. The gelatin/silk fibroin microspheres were washed with glycine solution to block the unreacted glutaraldehyde before freeze-drying. Microspheres were kept in micro centrifuge tubes at -20 °C.

2.4 Size and morphology

Water swollen microspheres were observed under a microscope (Nikon, Japan). The average diameter of 100 microspheres for each sample was measured. Morphology of freeze-dried microspheres was observed using a scanning electron microscope (SEM, JSM-5410LV, Japan).

2.5 Crosslinking degree

Crosslinking degree was evaluated using the modified method by Bubins *et al.* [9]. Briefly, 5 mg of the gelatin/silk fibroin microspheres were weighed into test tubes. One milliliter of 0.5% 2,4,6-trinitrobenzene sulphonic acid (TNBS) and 4% NaHCO₃ were added. The mixture was incubated at 40 °C for 2 h. After that, 4 ml of 37% HCl (conc.) were added. The mixture was heated at 60 °C overnight. Absorbance of the solution was determined spectrophotometrically at 415 nm. The crosslinking degree was then calculated according to the equation(1):

$$\text{Crosslinking degree (\%)} = (1 - A_c/A_n) \times 100 \quad (1)$$

where A_c and A_n represent the absorbance of crosslinked and the non-crosslinked microspheres, respectively.

2.6 Water absorption

Ten milligrams of gelatin/silk fibroin microspheres were immersed into phosphate buffered saline pH 7.4 at 37 °C for 0.25, 0.5, 1, 2 and 3 h. Their wet weights (Ww) and dried weights (Wd) were measured. Water absorption of microspheres was calculated using the following expression:

$$\text{Water absorption(\%)} = [(Ww - Wd)/Ww] \times 100 \dots\dots\dots(2)$$

2.7 *In vitro* biodegradation

Ten milligrams of gelatin/silk fibroin microspheres were incubated at 37 °C, pH 7.4, in 1 U/ml of collagenase and 0.01% (w/v) sodium azide for 1, 3, 6, 8, 10 and 14 days [10]. The solution was changed

every 2 days to ensure continuous enzyme activity. After each time interval, the degraded scaffolds were taken out of the solution, rinsed with deionized water and centrifuged at 5,000 rpm for 5 min. The supernatant was freeze-dried and weighed. The remaining weight was calculated as follows:

$$\text{Remaining weight (\%)} = \frac{W_f}{W_i} \times 100 \dots\dots\dots(3)$$

where W_f and W_i represent the final and the initial weight of microspheres, respectively.

2.8 Statistical analysis

All experiments and measurements were performed in triplicate. Data are expressed as mean \pm standard deviations. Statistical analysis was performed using ANOVA. Statistics differences were considered as significant value at $p < 0.05$.

3. Results and Discussion

3.1 Morphology of gelatin/silk fibroin microspheres

Table 1 shows morphology of microspheres. G100SF0 had the largest average size while G50SF50 had the smallest average size. Average sizes of microspheres decreased with the increasing contents of silk fibroin. This result shows an effect of viscosity on size of microspheres since silk fibroin was more viscous than that of gelatin. Yield of gelatin microspheres was the highest. This suggested that gelatin microspheres have size distribution in narrow range. Morphology of the freeze-dried microspheres observed under a scanning electron microscope (SEM) are shown in Figure 1.

Table 1 Morphology of microsphere fabrication with different weightblending ratios.

| Samples | Yield (%wt) | Shape | Average size (µm) |
|---------|-------------|-------|---------------------------|
| G100SF0 | 97.16 | round | 858.42±41.93 ^a |
| G90SF10 | 84.71 | round | 832.97 ±9.44 ^b |
| G70SF30 | 83.64 | round | 785.24±17.66 ^c |
| G50SF50 | 74.60 | round | 735.83±13.19 ^d |

^{a-d} represented significant difference among the samples at $p < 0.05$

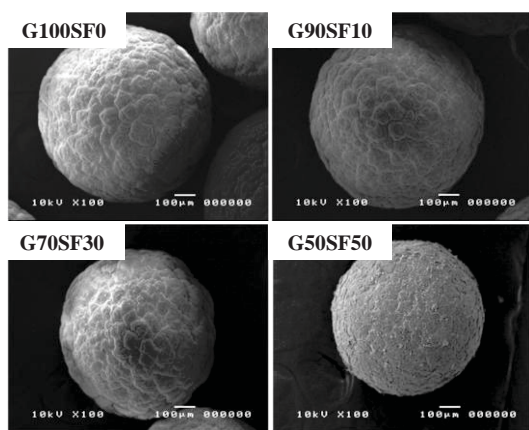


Figure 1. SEM photographs of gelatin/silk fibroin microspheres fabricated with different weight blending ratios

3.2 Crosslinking degree

Crosslinking degree of microspheres was determined by measuring the quantity of free amine groups using 2,4,6-trinitrobenzene sulphonic acid (TNBS) [9]. Figure 2 and 3 showed the amine contents of proteins before and after crosslinking. Crosslinking degree of microspheres increased with the increasing silk fibroin contents. The amine of gelatin was contributed by glutamine (11.3%), asparagine (8.3%), arginine (6.2%) and lysine (4.1%) [11]. The amine of silk fibroin was contributed by asparagine (1.9%), glutamine (1.7%), arginine (0.9%) and lysine (0.5%) [12]. The crosslinking of protein with glutaraldehyde has been affected by the amount of hydrophilic amino acids which usually located on the protein surface [12]. Silk fibroin contain low amine-containing amino acids than those of gelatin. Microspheres with high silk fibroin contents had higher crosslinking degrees compare to the gelatin microspheres due to the higher differences of amino groups before and after crosslink process while the total amount of $-NH_2$ groups (in the denominator in eq(1)) decreased at higher magnitude.

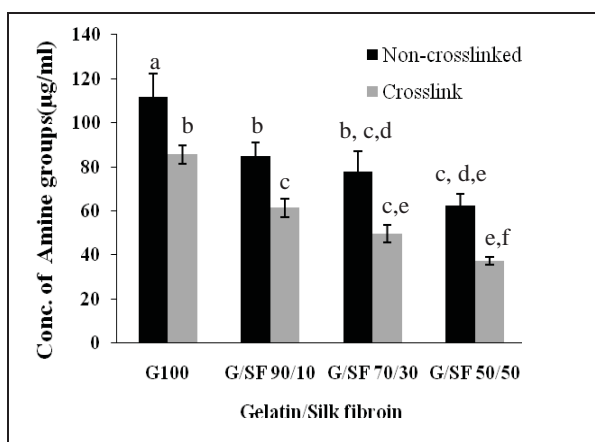


Figure 2. Concentration of amine groups in crosslinked and non-crosslinked microspheres. (a-f represented significant differences among the samples at $p < 0.05$)

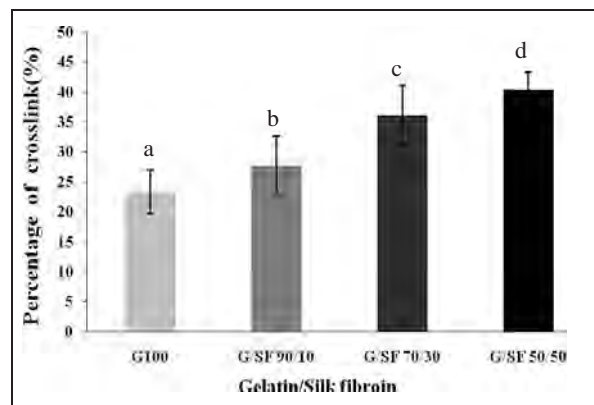


Figure 3. Crosslinking degree of gelatin/silk fibroin microspheres. (a-d represented significant differences among the samples at $p < 0.05$)

3.3 Water absorption of microspheres

Water absorption of G/SF microspheres prepared at 100/0, 90/10, 70/30, and 50/50 were 320.5%, 297.7%, 192.4% and 121.4%, respectively (Figure 4). The water absorption of microspheres decreased with the increasing silk fibroin contents. Silk fibroin is an insoluble fibrous protein with high crystallinity [10]. Blending of silk fibroin into gelatin microspheres decreased water absorption. Gelatin microspheres exhibited the highest water uptake capability. Water absorption of microspheres decreased with the increased crosslinking degree.

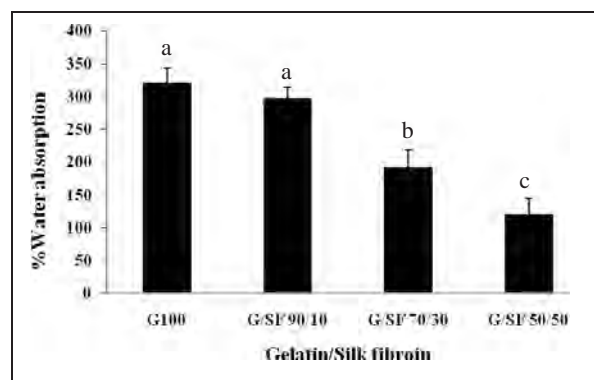


Figure 4. Water absorption of microspheres. (a-c represented significant difference among the samples at $p < 0.05$) at 37 °C, pH 7.4

3.4 In vitro biodegradation

In vitro biodegradation of gelatin/silk fibroin microspheres were estimated microspheres with collagenase a matrix metalloproteinase (MMP). This enzyme is secreted by macrophages as part of the body immune reaction to biomaterials [14]. The results are presented in Figure 5. It was found that the gelatin/silk fibroin microspheres had minimal degradation within 14 days at this condition. It was shown that the degradation was dependent on weight blending ratio of silk fibroin to gelatin. Gelatin

microspheres had the fastest degradation rate since collagenase can degrade collagen and gelatin rapidly. Blending of silk fibroin increases the crosslinking degree and extends degradation rate of the gelatin/silk fibroin microspheres, comparing to the gelatin microspheres.

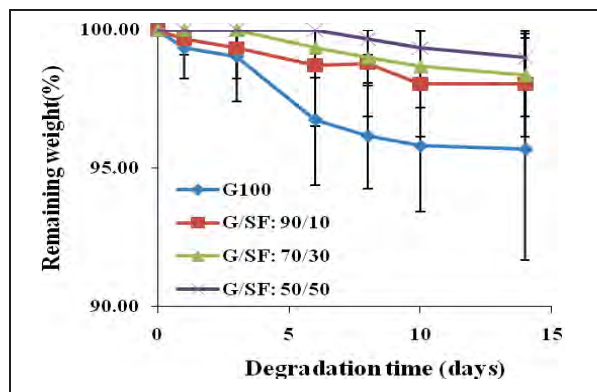


Figure 5. Remaining weight of gelatin/silk fibroin microspheres after degradation in 1 U/ml of collagenase at 37 °C, pH 7.4

4. Conclusions

We fabricated and characterized microspheres from gelatin and Thai silk fibroin using water-in-oil (w/o) emulsion and glutaraldehyde crosslinking with the different weight blending ratios. Morphology and sizes of microspheres depended on ratios of silk fibroin contents. Blending of SF reduced average size, water absorption but increased the crosslinking degree and delayed the degradation rate. We are currently evaluating the effect of the studied microspheres on cell growth.

Acknowledgement

This project is supported in parts by Chemical Engineering Research Unit for Value Adding of Bioresources (RU) and Chulalongkorn University Centenary Academic (The Biomedical Engineering Development project).

References

- [1] G. Antonios Mikos, S. Johnna Temenoff. *E.J. Biotechnol.* **Vol.3** No.2 (2000) 1-6
- [2] D. Zekorn. *Bibl Haematol.* **33:1** (1969) 31-40.
- [3] S. Freiberg, X.X. Zhu, *Int. J. Pharm.* **282** (2004) 1-18.
- [4] B. Lu, J.Q Zhang, H. Yang. *Int. J. Pharm.* **265** (2003) 1-11.
- [5] P. Wadbuaa, B. Promdonkoy, S. Maensiri, S. Siri. *Int. J. Biol. Macromol.* **46** (2010) 493-501
- [6] M. Okhawilai, R. Rangkupan, S. Kanokpanont, S. Damrongsakkul. *Int. J. Biol. Macromol.* **46** (2010) 544-550.
- [7] U.J. Kim, et al., *Biomaterials.* **26**(15). (2005) 2775- 2785.
- [8] Y. Tabata, Y. Ikada, K. Morimoto, H. Katsumata, T. Yabuta, K. Iwanaga, et al. *J Bioact Compat Polym.* **14** (1999) 371-384.
- [9] W.A. Bubnis and C.M. Ofner Iii. *Analytical Biochemistry.* **207**(1). (1992) 129-133.

- [10] P. Jetbumpenkul, et al. *Int. J. Biol. Macromol.* **50**(1) (2012) 7-13.
- [11] Y. Tabata, Y. Ikada. *Advanced Drug Delivery Reviews* **31**(1998) 287-301.
- [12] C. Vepari, D. L. Kaplan. *Progress in Polymer Science* **32** (2007) 991-1007.
- [13] F.A. Quiocho and F.M. Richards. *Proc. Natl. Acad. Sci.* **52** (1964) 833-839.
- [14] Li, M., M. Ogiso, and N. Minoura, *Biomaterials.* **24** (2003) 357-365.

DEVELOPMENT AND CHARACTERIZATION OF CHITOSAN BLENDED BACTERIAL CELLULOSE FILM

Kampole Intasorn¹, Muenduen Phisalaphong^{1*}

¹ Chemical Engineering Research Unit for Value Adding of Bioresources, Department of Chemical Engineering, Faculty of Engineering, Chulalongkorn University, Bangkok 10330, Thailand

* E-Mail: muenduen.p@chula.ac.th, Tel. +66 22186875, Fax. +66 22 186877

Abstract: Chitosan is a natural biopolymer derived by deacetylation of chitin, which composed of (1,4)-linked 2-amino-deoxy- β -D-glucan. It is non-toxic, biodegradable, biofunctional and biocompatible. It also has antibacterial property which is very useful for preparation of food antimicrobial packaging film. However, uses for chitosan films have been limited because of its weak mechanical properties. The purpose of this study is to improve mechanical property of chitosan based films by the incorporation of bacterial cellulose (BC). In the preparation, chitosan (minimum 85% deacetylated chitin; molecular weight 200,000) in acetic acid aqueous solution were thoroughly mixed with BC slurry at various weight ratios. The composite films were fabricated by casting and curing at 35°C. The mechanical properties of chitosan-BC films significantly depended on the weight ratio of BC. The water absorption capacity of the film was maximal at 548.15% obtained from the composite film with the ratio of chitosan : BC at 10:6. It was also showed that the CBC films had inhibitory effect on *S. aureus* growth.

1. Introduction

Currently, over 100 million tons of plastics are produced annually worldwide. Consumption and production of plastics have been continuously rising, so as to increase the amount of plastic waste. The management of plastic waste associated with serious environmental pollution from waste disposal and undegraded polymers [1]. To reduce the problem of plastic waste disposal, biodegradable polymers or biodegradable plastics have to be developed as substitutes for non-biodegradable plastics.

In food packaging, natural polysaccharides have been widely applied to producing degradable films. In particular, there has been a growing interest in starch, cellulose and their derivatives [2] with an abundant agricultural surplus raw material, since it can be produced at low cost with a large scale, non-allergic and thermal process ability [3]. A packaging material with extensively antimicrobial properties is also required and desirable for general use to improve the storage stability of various foods. For this purpose, the integration of antimicrobial substances in packaging material is useful. Because of its good film forming and antimicrobial properties, antimicrobial packaging films have been being developed using chitosan-based material [4].

Chitosan is derived by deacetylation of chitin, which is a major component of the shells of crustacean such as crab, shrimp and crawfish. It has received much attention for commercial applications in food

and biomedicine. Chitosan is non-toxic, biodegradable, biofunctional and biocompatible [5,6]. Moreover, it also has antibacterial properties [7, 8]. Nevertheless, uses for chitosan films have been limited because of its weak mechanical properties. Many works focused on improvement of properties of chitosan films. The properties of chitosan films could be improved by addition of other polymers [9]. The effect of chitosan concentration and type of solvent on the mechanical properties of chitosan has been studied [10].

Bacterial cellulose (BC) is cellulose, which is synthesized by *Acetobacter xylinum* using glucose as the carbon substrate. It has been recognized as a biologically appropriate property allowing for biomedical and tissue engineering applications [11, 12]. It has been reported for its high purity, strength and moldability [13]. BC has high mechanical strength, high water absorption capacity, high crystallinity, and highly pure fiber network structure [14].

Many works focused on improvement of properties of chitosan films by addition of other synthetic polymers. In this study, a novel antimicrobial biocomposite film has been developed. Chitosan-BC based films were prepared by casting method and were characterized for physical, mechanical and antimicrobial properties.

2. Materials and Methods

2.1 Materials

2.1.1 Chitosan powder which has minimum 85% deacetylated and molecular weight 200,000 from Seafresh Chitosan(Lab) Company Limited Bangkok 10500,Thailand was used for the study.

2.1.2 The *Acetobacter xylinum* strain was isolated from nata de coco, which was kindly supplied by Pramote Tammarate, the Institute of Food Research and Product Development, Kasetsart University, Bangkok, Thailand.

2.2 Preparation of composite films

Chitosan solution (1% w/v) was prepared by dissolving chitosan powder in 1% v/v acetic acid solution and stirring overnight. The pH of solution was adjusted to 5.0 with 1N NaOH. Then the chitosan solution was mixed with BC slurry at various weight ratios. Glycerol (2%v/v) was used as a plasticizer for

the mixture. The mixture was stirred until homogeneous. After that, it was poured into Petri plate and dried in an incubator at 35 °C for 5 days. Finally, Chitosan/BC (CBC) film was obtained.

2.3 Characterization of bio-films

2.3.1 The mechanical property testing

In this study, the tensile strength and elongation at break of CBC dried films were measured by Universal Testing Machine (Hounsfield H 10 KM, Redhill, England). The load cell capacity was 1 kN. The film samples were cut into strip-shaped specimens 10 mm width and 10 cm length. The test conditions followed ASTM D882 as a standard test method for tensile elastic properties. Two ends of the specimens were placed between the upper and lower jaws of the instrument, leaving a length of 6 mm of film in between the two jaws. Extension speed of the instrument was 2 mm/min. The tensile strength and break strain were the average value determined from at least five specimens.

2.3.2 The water absorption capacity (WAC)

The water absorption capacity (WAC) was determined by immersing the pre-weighted of dried samples in distilled water at room temperature until equilibration. Water content was determined by gravimetric method and calculated using the following formula:

$$WAC(\%) = \frac{W_h - W_d}{W_d} \times 100$$

Where W_h and W_d denoted the weight of hydrate and dry sample, respectively.

2.3.3 Antimicrobial ability testing

The antimicrobial properties of chitosan films were examined against 2 types of bacteria, *Escherichia coli* and *Staphylococcus aureus*. The films were cut into round-shaped sample of 0.5 grams according to the method described by ASTM E2149-10. The test or the control specimen was placed individually in a 250mL sterile Erlenmeyer flask and then the bacterial inoculum (50 mL) was added into the flask. The initial bacterial concentration was determined by performing serial dilutions and standard plate count techniques. The flask was then placed on the wrist-action shaker and was rotated at maximum stroke for 3 hours. After that, the bacterial concentration in each flask was determined. The bacteria concentration was the average value of three Petri dishes. The average value was converted into the colony-forming unit per milliliter (CFU/mL). The percent reduction of organisms was calculated from the values of the treated sample (A) compared to the untreated control (C).

$$\text{Reduction, \% (CFU/mL)} = \frac{C-A}{C} \times 100, \text{ where}$$

A = CFU/mL for the flask containing the treated substrate after the specified contact time.

C = CFU/mL for the flask containing the untreated substrate after the specified contact time.

3. Results and Discussion

3.1 Mechanical property

Figure 1. shows the effect of weight ratio of BC on tensile strength of the CBC films. The tensile strength property of the CBC dry films was significantly improved with the increase of weight ratio of BC. The CBC film with the ratio of chitosan:BC at 10:2 and 10:10 has tensile strength at 19.82 to 41.97 Mpa, respectively. Since BC has high mechanical strength [14], the incorporation of BC into the chitosan matrix considerably increased the overall mechanical performance of the composite films.

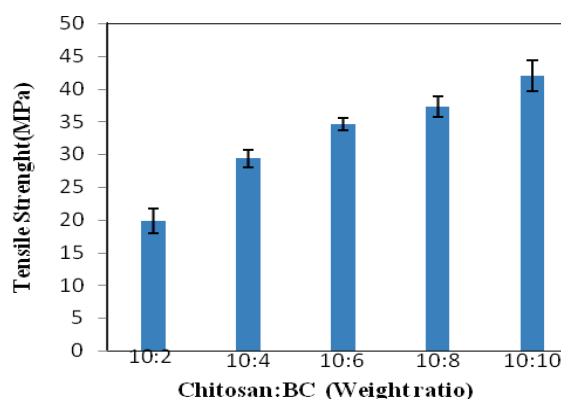


Figure 1. The tensile strength of CBC films in dry form.

Figure 2. shows the effect of weight ratio of BC on the percentage of elongation at break. It was found that the composite film exhibited the highest values of elongation at break (10.51%) at the weight ratios of chitosan: BC in the range of 10:4 to 10:6. However, the increased BC content higher than 10:6 could increase the stiffness of the films. As a result, it reduced flexibility of the composite films.

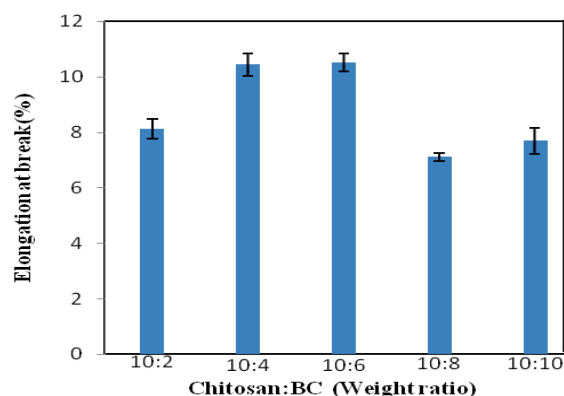


Figure 2. The Elongation at break (%) of CBC films in dry form.

3.2 Water adsorption capacity (WAC)

The effect of the BC slurry supplement on the water adsorption capacity (%WAC) of the composite films is shown in Figure 3. The maximum WAC at 548.2% was obtained at the weight ratio of chitosan:BC of 10:6, which was about 2 folds compared to that at the weight ratio of 10:2. Because BC has higher water holding capacity and hydrophilicity [15], the incorporation of BC into chitosan matrix for a certain amount resulted in the increase in WAC. However, at very high levels of BC supplement, it reduced the pore size of the composite films, resulting in lower WAC [16].

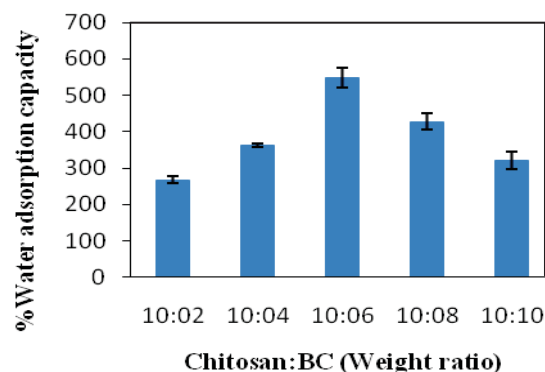


Figure 3. The water absorption capacity (%WAC) of CBC films.

3.3 Anti-microbial activity

E. coli and *S. aureus* were used for the antibacterial test of the chitosan films. The results are presented in Table 1.

Table 1: Antimicrobial activities of CBC films against *E. coli* and *S. aureus*.

| Micro-organism | Sample | The Number of bacterial | % reduction |
|------------------|----------------------|-------------------------|--------------------|
| <i>E. coli</i> | Control ^a | 3.8×10^5 | - |
| | Chitosan Mw.200,000 | 3.5×10^5 | 7.89 ^a |
| | Control ^b | 2.2×10^5 | - |
| | Chitosan:BC 10:6 | 6.5×10^5 | 0 ^b |
| <i>S. aureus</i> | Control ^c | 4.2×10^5 | - |
| | Chitosan Mw.200,000 | 2.9×10^5 | 30.95 ^c |
| | Control ^d | 3.2×10^5 | - |
| | Chitosan:BC 10:6 | 2.0×10^5 | 37.50 ^d |

^{a-d} refer to different control inoculums.

The antibacterial test of chitosan solutions resulted in 7.89 % reduction of *E. coli* and 30.95% reduction of *S. aureus*. The CBC films at chitosan: BC of 10:6 showed inhibitory effects against *S. aureus* (37.50% reduction). However, it had no inhibitory effect on *E. coli*. Nevertheless, the antibacterial

activity of chitosan is influenced by its degree of deacetylation, its concentration in solution, and the pH of the medium [17]

4. Conclusions

To modify the mechanical, physical and biological properties of chitosan based films, chitosan (85% DAC and MW 200,000) in acetic acid aqueous solution was blended with BC slurry at various weight ratios. Glycerol at 2% v/v was used as a plasticizer in order to increase the flexibility of the composite films. The results demonstrated that the mechanical properties of the CBC films depended on the weight ratio of BC. Based on the overall mechanical and physical properties, we suggested to use the formulation containing the weight ratio of chitosan:BC at 10:6 for the fabrication of thin films for food packaging. It was also showed that the CBC films had inhibitory effect on *S. aureus* growth.

Acknowledgements

The authors are grateful for the financial support from Integrated Innovation Academic Center: IIAC Chulalongkorn University Centenary Academic Development (Project Code: CU56-AM01) and partially supported by the Higher Education Research Promotion and National Research University Project of Thailand, Office of the Higher Education Commission (Project Code: AM667A).

References

- [1] Salleh, E., Muhamad, I., and Khairuddin, N. *Asian Chitin Journal*. **3**(2007) 55–68.
- [2] Weber, C.J., Haugaard, V., Festersen, R., and Bertelsen, G. *Food Addit Contam.* **19**(2002) 172–177.
- [3] L. Famá, A.M. Rojas, S. Goyanes and I. Gerschenson. *LWT* **38**(2004) 631–639.
- [4] Ban, W., Song, J., Argyropoulos, D. S., and Lucia, L. A. *American Chemical Society*. (2005).
- [5] Knorr, D. *Food Technol.* **38**(1984) 85–97.
- [6] Jayakumar, R., Prabakaran, M., Reis, R. L., and Mano, J. F. *Carbohydrate Polymers* **62**(2005) 142–158.
- [7] Kendra, D.F. and Hadwiger, L.A. *Exp. Mycol.* **8**(1984) 276–281.
- [8] Sudarshan, N.R., Hoover, D.G and Knorr, D. *Food Biotechnol.* **6**(1992) 257–272.
- [9] Hima Bindu, T.V.L., Vidyavathi, M., Kavitha, K., Sastry, T.P., *Trends in Biomaterials and Artificial Organs* **24** (2010) 122–130
- [10] Kienle-Sterzer CA, Rodriguez-Sanchez D, Rha C. *Makromol Chem.* **9** (1982) 183–1353.
- [11] Andrade, F. K., Pertile, R. N., Dourado, F., and Gama, F. M. *Cellulose:Structure and properties* (2010) 427–458.
- [12] Czaja, W. K., Young, D. J., Kawecki, M. and Brown, R. M. *Biomacromolecules* **8**(2007) 1–12.
- [13] Jonas, R and Farah, Luiz F. *Polymer Degradation and stability* **59**(1998) 101–106.
- [14] Vandamme, E.J.; Baets, S. De; Vanbaelen, A.; Joris, K. and Wulf, P.De. *Polymer Degradation and Stability* **59**(1998); 93–99.

- [15] Klemm, D., Schumann, D., Udhardt, U. & Marsch, S.
Progress in Polymer Science, **26**(2001)1561-1603.
- [16] Bu, X., Wang, L., and Ma, W. *Journal of Harbin Engineering University* **33** (2012); 989-995
- [17] Rabea, E.I., Badawy, M.E.-T., Stevens, C.V., Smagghe, G., and Steurbaut, W. *Biomacromolecules* **4** (2003) 1457-1

COMPUTATIONAL FLUID DYNAMICS MODELING OF FREE LUTEIN PURIFICATION IN A PREPARATIVE CHROMATOGRAPHY COLUMN

Weerapong Choopakdee¹, Phattanon Prasitchoke², Artiwan Shotipruk¹, Pimporn Ponpesh^{1*}

¹ Chemical Engineering Research Unit for Value Adding of Bioresources, Department of Chemical Engineering, Faculty of Engineering, Chulalongkorn University, Phayathai Rd., Patumwan, Bangkok, 10330 Thailand

² PTT Global Chemical Public Company Limited, Amphur Mueang Rayong, Rayong, 21150 Thailand

* E-mail: pimporn.p@chula.ac.th, Tel. +66 22186879, Fax. + 66 22 186877

Abstract: To develop a suitable mathematical model for adsorption behaviour of free lutein on silica gel in a preparative chromatography column, the transport phenomena inside the column was investigated using Computational Fluid Dynamics (CFD). The CFD software, Fluent, was used to simulate the chromatographic purification process in a column of 3.5 cm in diameter and 20 cm in height, and operated at an eluent flow rate of 10 ml/min. The eluent was composed of n-Hexane and Ethyl Acetate at the ratio of 70:30 v/v. Pulse injection of 10 sec pulse period was applied to introduce 10 ml and 40 µg/ml of free lutein sample. The simulated band profiles of free lutein as it moved through the column and the outlet free lutein concentration were found to be in good agreement with the experimental data.

1. Introduction

Marigold flowers are a major source of commercial free lutein production. Studies show that dietary intake of free lutein has been linked to the risk reduction of eyesight failure, coronary heart disease and cancer [1]. Column chromatography is an attractive method to purify free lutein from the marigold extract as it provides high purity and is easily scalable for industrial production [2,3]. In large-scale production of free lutein, trial and error has been applied for scaling procedure. It requires many resources and consumes much time. To reduce this problem, CFD simulation was applied in combination with experimental results to describe the phenomena of compound purification. Yu and Ching [4] has successfully applied CFD modeling to describe the band profiles (i.e., concentration profiles) behaviour in a nonlinear chromatographic column. They found that CFD modeling could correctly predict the peak behavior of the eluted components in the chromatographic column. Schmidt et al. [5] used CFD modeling to estimate the performance of chromatographic column and aid the selection of adsorption materials. They also found good agreement between the simulated and the experimental results.

In this study, a suitable mathematical model for adsorption behavior and chromatography of free lutein on silica gel will be developed. It will be applied to describe and predict the performances of lab scale preparative chromatographic purification of free lutein derived from marigold flowers through the use of CFD

simulation software (Fluent 12, ANSYS Inc., Lebanon, NH). The CFD model will then be used to guide the design of a large-scale chromatography column used for industrial production.

2. Materials and Methods

2.1 Problem description

The system consisted of a packed column with free lutein mixture and eluent solvent (i.e., hexane and ethyl acetate) entering at the bottom of the column (i.e., inlet) and leaving at the top (i.e., outlet). The bed was packed with silica beads to a height of 0.2 m. Isothermal condition was assumed in this study. Additional assumptions include constant mobile phase velocity throughout the column and negligible concentration gradient in radial direction. As a result, the distribution of mass transfer and flow parameters were also assumed to be axisymmetric. Furthermore, the compressibility of the mobile phase was assumed negligible. The system parameters are summarized in Table 1.

Table 1: Parameters of silica gel and packed bed column.

| Parameters | Value |
|------------------------------------|---------------------------|
| Bed height, L | 0.2 m |
| Column diameter, D | 0.035 m |
| Average diameter of silica, d_p | 30 µm |
| BET specific surface area | 480-540 m ² /g |
| Porosity of bed, ϵ_b | 0.30 |
| Porosity of particle, ϵ_p | 0.71 |
| Total porosity, ϵ_T | 0.73 |
| Superficial velocity, u_s | 1.7x10 ⁻⁴ m/s |
| Eluent | |
| (Hexane: Ethyl Acetate) | 70:30 v/v |
| Temperature | 30 °C |

A two-dimensional, half column was created for the computational domain. Since chromatographic processes normally involve high concentration gradient [6], the grids must be sufficiently fine throughout the column. The grid independent test was conducted to determine the optimal grid size and structure. As a

result, the grid number of 4,600 was applied in this study.

2.2 Adsorption kinetics

Batch method was used to determine adsorption isotherm of free lutein on silica gel. About 10 ml of free lutein with 10 µg/ml of initial concentration was agitated with 1 g of pre-treated silica gel in 125 ml conical flasks in an orbital shaker for 10 pieces of same. The temperature was maintained at 30 °C and agitation rate was 120 rpm. Silica gel was introduced to the flask at time zero and then the one by one flask was withdrawn at various time intervals to analyze concentration of free lutein.

From the experimental results, isothermal adsorption behaviour of free lutein on silica gel follows the linear adsorption model.

$$q = 6.0641y \quad (1)$$

, where q is the equilibrium concentration of free lutein in silica gel (µg/g) and y is the equilibrium concentration of free lutein in eluent (µg/ml).

2.3 Preparative chromatography model

The appropriate flow model was determined based on the flow regime. To estimate the flow regime, Reynolds number was applied and calculated from the following equation:

$$Re = \frac{\rho u_s d_p}{\mu(1-\varepsilon_T)} \quad (2)$$

, where ρ is fluid density, u_s is superficial fluid velocity through the column, d_p is the diameter of spherical particles, and μ is fluid dynamic viscosity. Based on the superficial velocity of the mobile phase of 1.40×10^{-4} m/s, the value of Reynolds number was approximately 0.0142. The Reynolds number was very low compared to the critical value for fully laminar flow through a packed bed (i.e., $Re < 10$) [7]. Therefore, the flow regime was laminar. In this study, the momentum balance has been solved by the equation of motion.

$$\frac{\partial}{\partial t}(\rho \bar{v}) + \nabla \cdot (\rho \bar{v} \bar{v}) = -\nabla p + \rho g + \mu \nabla^2 \bar{v} \quad (3)$$

, where \bar{v} is velocity. Thus, the momentum source term (i.e., pressure drop (∇p)) in porous media was calculated base on Darcy's law. It can be expressed as follows:

$$\nabla p = -\frac{\mu}{\alpha} \bar{v} \quad (4)$$

, where α is the permeability and can be approximated by the equation:

$$\alpha = \frac{d_p^2}{150} \frac{\varepsilon_b^3}{(1-\varepsilon_b)^2} \quad (5)$$

For mass balance equations, the most widely used chromatographic model is Equilibrium Dispersive Model [4,5,8]. The mass balance equation for the Equilibrium Dispersive Model follows:

$$\varepsilon_T \frac{\partial C_i}{\partial t} + (1-\varepsilon_T) \frac{\partial q_i}{\partial t} + u \frac{\partial C_i}{\partial z} = \varepsilon_e D_L \frac{\partial^2 C_i}{\partial z^2} \quad (6)$$

, where C_i is the concentration of component 'i' in the mobile phase, q_i is the concentration of component 'i' in the adsorbed phase, ε_T is the total porosity, u is the mobile phase velocity, ε_e is the external porosity, and D_L is the coefficient of axial dispersion.

The adsorption rate is additional source term of the species transport equation in Fluent. It must be incorporated into the software using User Defined Function (UDF) and can be expressed by the Linear Driving Force (LDF) Model.

$$\frac{dq}{dt} = k(q^* - q) \quad (7)$$

where k is the mass transfer coefficient of free lutein in eluent and obtained from dimensionless correlations, q^* is the absolute or equilibrium adsorption and calculated from equation (1). Dynamic adsorption (i.e., q) in equation (7) can be transformed by using finite difference technique to the following expression:

$$q_i = q_{i-1} + k(q_{i-1}^* - q_{i-1})(t_i - t_{i-1}) \quad (8)$$

The boundary conditions for species mass balance are the following:

$$\begin{aligned} \text{Inlet:} \quad & C_i(t,0) = C_0, \quad (0 < t \leq t_{\text{inject}}) \\ & C_i(t,0) = 0, \quad (0 \geq t_{\text{inject}}) \\ & \text{, where } C_0 = 40 \text{ µg/ml and } t_{\text{inject}} = 10 \text{ s,} \\ \text{Outlet:} \quad & \frac{\partial C_i}{\partial x} = 0, \quad \text{at any } t, \\ \text{Wall:} \quad & \frac{\partial C_i}{\partial y} = 0, \quad \text{at any } t. \end{aligned}$$

2.4 The correlations for model parameter estimation

In present work, the parameters in mass balance equation such as mass transfer coefficient (k_f) and axial dispersion coefficient (D_L) were obtained from the correlations available in literatures. For mass transfer coefficient, the correlation dependent on groups of dimensionless numbers such as Reynold number ($Re = \rho u_s d_p / \mu$) and Sherwood number ($Sh = k_f d_p / D_m$). They are summarized in Table 2.

Table 2: mass transfer coefficient correlations

| Correlations | Validity | Ref |
|--|---------------------------|------|
| $Sh = 1.13 Re^{0.21} Sc^{1/3} / \varepsilon$ | $Re < 10$ | [9] |
| $Sh = 1.11 Re^{0.28} Sc^{1/3} / \varepsilon$ | $Re < 10$ | [10] |
| $Sh = 1.85(1-\varepsilon/\varepsilon^2)^{1/3} Re^{1/3} Sc^{1/3}$ | $Re/(1-\varepsilon) < 10$ | [11] |

Mean mass transfer coefficient based on the three correlations shown in Table 2 for free lutein on silica gel is around 4.27×10^{-4} m/s.

Axial dispersion coefficient was estimated by Suzuki and Smith's correlation [12] as follows:

$$D_L = 0.44 D_m + 0.83 u_s d_p \quad (9)$$

, where D_m is molecular diffusivity of free lutein in eluent and can be approximated by Wilke and Chang [13].

$$\frac{D_M \mu_B}{T} = \frac{7.4 \times 10^{-8} (\phi_B M_B)^{0.5}}{V_A^{0.6}} \quad (10)$$

, where D_M is the mass diffusivity of free lutein diffusing through eluent, μ_B is the viscosity of eluent, T is the temperature of the system, ϕ_B is the associated parameter, M_B is the molecular weight of eluent and V_A is the critical volume of free lutein. For this study, D_M and D_L is equal to $1.02 \times 10^{-9} \text{ m}^2/\text{s}$ and $4.68 \times 10^{-9} \text{ m}^2/\text{s}$, respectively.

3. Results and Discussion

In Figure 1, the contours of velocity magnitude from the simulation are illustrated. The simulated result implies that the column is plug flow (i.e., negligible wall effect and, thus, uniform radial velocity). In addition, the axial velocity is constant, according to uniform porosity and homogeneous fixed bed assumptions.

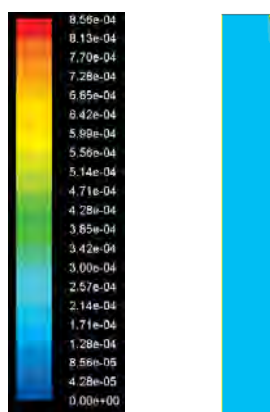


Figure 1. Contours of velocity magnitude of the mobile phase (liquid velocity of $1.7 \times 10^{-4} \text{ m/s}$ and initial bed height of 20 cm).

The simulated concentration profile of free lutein is shown in Figure 2. The colors represent the magnitude of free lutein concentration.

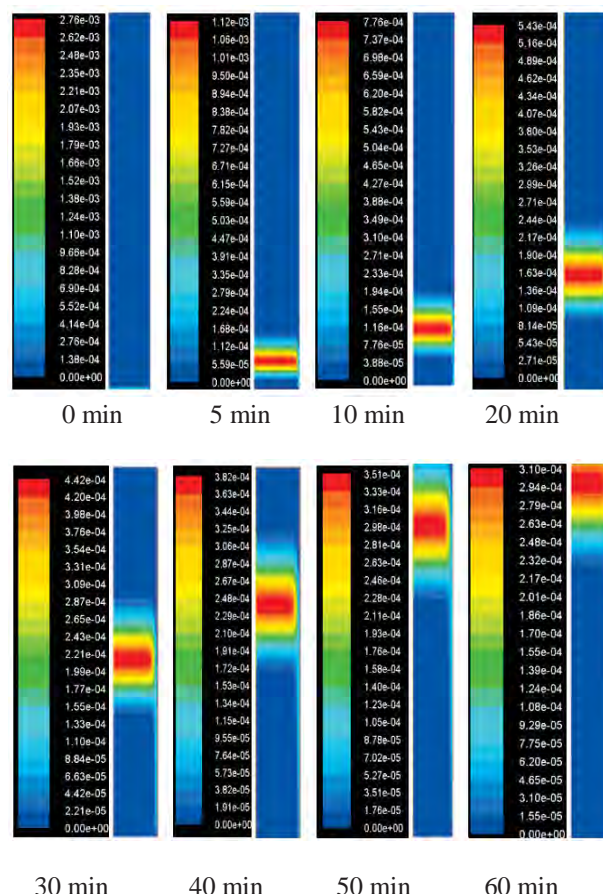


Figure 2. Simulated contours of mass fraction of free lutein at eluent velocity of $1.7 \times 10^{-4} \text{ m/s}$ with respect to time and for the initial bed height of 20 cm.

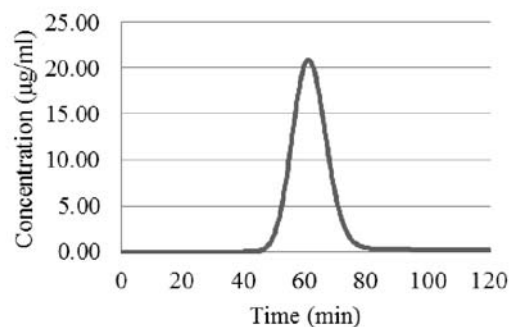


Figure 3. The pseudo elution chromatogram of outlet free lutein from the simulation.

Figure 2 shows that the concentration profile is flat and proceeds with uniform cross-sectional velocity (i.e., plug flow behavior). This characteristic is maintained throughout the profile migration. The broadening of the band width was caused by the axial diffusion of free lutein in the eluent. This is relevant to the broad peak of elution chromatogram illustrated in Figure 3. Figure 4 shows the concentration profile of free lutein from the experiment under the same conditions as those in the simulation. The region with dark colors represents free lutein, while the very light

yellow is other impurities being separated from the free lutein. The comparison between the simulated concentration profile (Figure 2) and the concentration profile from the experiment (Figure 4) shows that the simulated result is in good agreement with the experimental result. In other word, the CFD model can potentially predict the adsorption behavior of free lutein in lab-scale preparative chromatography column.

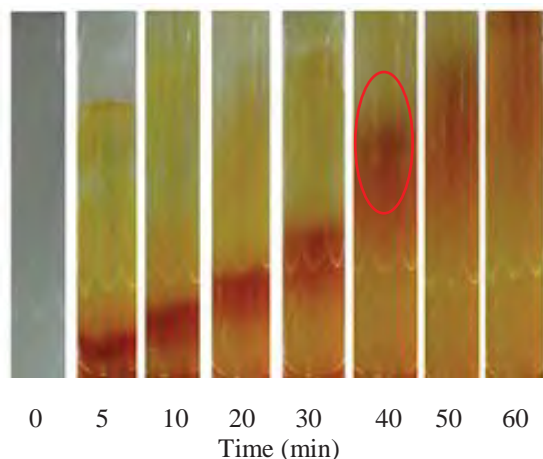


Figure 4. Concentration profile of free lutein from the experiment with eluent velocity of 1.7×10^{-4} m/s with respect to time and for the initial bed height of 20 cm. The areas with dark colors (circled) represent free lutein.

4. Conclusions

A suitable model of free lutein purification in a preparative chromatography was investigated using Computational Fluid Dynamics (CFD) simulation. The results show that CFD can be applied to predict transport phenomena inside the chromatographic column based on the information such as simulated band profile and elution chromatogram. Further study is underway to determine the critical parameters that influence column performances for free lutein purification. The results will be useful in developing operational and design guidelines which should be adaptable for large-scale production.

Acknowledgements

This research has been supported by PTT global chemical public company limited.

References

- [1] H.B. Sowbhagya, S.R. Sampathu and N. Krishnamurthy, *Food Rev. Int.* **20** (2004) 33-50.
- [2] S. Shibata, C. Ishihara and K. Matsumoto, *J. Agric. Food Chem.* **52** (2004) 6283-6286.
- [3] M. Hamburger, S. Adler, D. Baumann and A. Forg, *Fitoterapia*. **74** (2003) 328-338.
- [4] H.W. Yu and C.B. Ching, *J. Chromatogr.* **58** (2003) 793-796.
- [5] I. Schmidt, F. Lottes, M. Minceva, W. Arlt and E.H. Stenby, *Chemie Ingenieur Technik*. **83** (2011) 130-142.

- [6] H. Boysen, G. Wozeny, T. Laiblin and W. Arlt, *Chem Eng & Tech.* **26** (2003) 651-655.
- [7] M. Rhodes, in *Introduction to Particle Technology*, John Wiley & Sons, Chichester, UK (2008)
- [8] G. Guiochon, *J. Chromatogr A.* **965** (2002) 129-161.
- [9] S. Kumar, S.N. Upadhyay and V.K. Mathur, *Ind Eng Chem Proc Des Dev.* **16** (1977) 1-8.
- [10] P.N. Dwivedi and S.N. Upadhyay, *Ind Eng Chem Proc Des Dev.* **16** (1977) 157-165.
- [11] T. Kataoka, H. Yoshida and K. Ueyama, *J. Chem Eng Jpn.* **5** (1972) 132-136.
- [12] M. Suzuki M and J.M. Smith, *Chem Eng J.* **3** (1972) 256-264.
- [13] J.R. Welty, C.E. Wicks, R.E. Wilson and G.L. Rorrer, *Fundamental of momentum heat and mass transfer*, John Wiley & Sons, Inc., New York (2001)

SYNTHESIS OF GOLD NANOPARTICLES/MESOCELLULAR FOAM SILICA NANOCOMPOSITES USING ULTRASONIC IRRADIATION FOR BIOSENSOR APPLICATIONS

Nattawat Surathin¹, Joongjai Panpranot², Chanchana Thanachayanont³, Seeroong Prichanont^{1*}

¹ Chemical Engineering Research Unit for Value Adding of Bioresources, Department of Chemical Engineering, Faculty of Engineering, Chulalongkorn University, Phayathai Road, Bangkok, 10330 Thailand

² Department of Chemical Engineering, Faculty of Engineering, Chulalongkorn University, Phayathai Road, Bangkok, 10330 Thailand

³ National metal and Materials Technology Center, 114 Thailand Science Park, Paholyothin Road, Pathumthani, 12120 Thailand

* Author for correspondence; E-Mail: Seeroong.p@chula.ac.th, Tel. +66 22186860, Fax. +66 22 186877

Abstract: Mesocellular foam silica (MCF) is a porous material with unique properties such as large surface area, large pore volume, biocompatible, and modifiable surface. Gold nanoparticles (AuNPs) is conductive material commonly used in biosensors because of its good electron transfer and biocompatibility. Therefore, combination of two remarkable materials with immobilized enzyme for biosensor applications has high potential to improve sensor performances. The aim of this work was to study the synthesis of AuNPs/MCF nanocomposite for biosensor application. The experiments were divided into three parts. Firstly, MCF was synthesized using Pluronic 123 triblock copolymer (P123) as a template and tetraethyl orthosilicate (TEOS) as a silica source to give the MCF product with average pore diameters of 7.6 nm, surface area of 537.64 m²/g and pore volume 1.02 cm³/g. Secondly, The porous surface of modified MCF was refluxed in toluene solution at temperature of 100 °C using 3-aminopropyltriethoxysilane (APTS) to attach thiol functional group on porous surface of MCF for gold ion adsorption on MCF surface. Finally, gold nanoparticles were synthesized on MCF using ultrasonic hydrogen free radicals ($\cdot\text{H}$) and hydroxyl free radicals ($\cdot\text{OH}$) initiated by ultrasonic irradiation. These radicals acted as reducing equivalent converting Au^{3+} ion that prepared from chloroauric acid (HAuCl_4) to Au^0 atom and AuNPs adhere on porous surfaces of MCF. AuNPs - MCF nanocomposite was used for enzyme immobilization. The existence of gold nanoparticles helps enhancing potentially the electron transfer for biosensor application.

Keywords Mesocellular foam silica; Gold nanoparticles; Ultrasonic irradiation; Biosensor

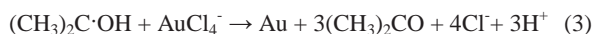
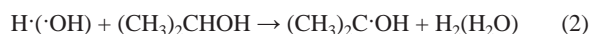
1. Introduction

Immobilization of enzymes has received significant attention due to its many advantages especially in enhancement of operational and storage stability of the enzymes. Various types of solid supports are used for enzyme immobilization such as zeolite, calcium carbonate, and mesoporous materials [1]. Among them, mesoporous silica materials have been proved to be effective for enzyme immobilization because of their high surface area, non-toxicity, and good biocompatibility [2].

Mesocellular foam silica (MCF) is a mesoporous silica materials with large surface area in the range of 500-1000 m²/g [3], and large pore volume 0.5-1.0 cm³/g [4] with surface functional group of silanol groups (Si-OH) [5]. Recently, MCF has been applied for immobilization of cholesteryl ester hydrolase (EC 3.1.1.13). The immobilized enzyme exhibited the ability to maintain its activity better than the free one [6]. Pandya et al. [7] also revealed that MCF is a promising material for immobilization of alpha-amylase due to its increased thermal stability, and tolerance towards pH and high substrate concentration. In addition, glucose oxidase was also found advantageously to be immobilized on the aminofunctionally modified surface of MCF since thermal stability and high catalytic activity for glucose oxidation could be achieved [8].

Although MCF has been reported as an excellent support for enzyme immobilization in terms of the ability to retain enzyme storage, and catalytic activity, the major drawback that bars MCF from its application in biosensors is its handicap in electron conduction. In order to overcome this problem, metal nanoparticles have been attached on the support surface for the enhancement of electron transfer [9]. Gold nanoparticles (AuNPs) are the most stable metal nanoparticles, of good electron conductivity, and high biocompatibility [10]. Fukuoka et al. [11] synthesized AuNPs that embedded into mesoporous silica type MCM-41 with the pore diameter of 2.7 nm. Chen et al. [12] also successfully synthesized gold nanoparticles embedded into porous silica materials using ultrasonic irradiation technique, and found that the average diameter of AuNPs within the pores was 5.2 nm.

The principle of ultrasonic irradiation technique is applied in this paper to synthesize AuNPs on MCF. The ultrasonic wave causes the formation, growth and splitting of water bubbles into hydrogen radicals ($\text{H}\cdot$), hydroxyl radicals ($\text{OH}\cdot$), and the secondary reducing radical ($(\text{CH}_3)_2\text{C}\cdot\text{OH}$) as described in equations (1) and (2). These radicals will act as reducing equivalents for the reduction of Au^{3+} ion from AuCl_4^- to Au^0 atom. Subsequently, AuNPs will be adhered on porous surfaces of MCF as shown in equations (3) and (4).



In this paper, we present the synthesis and characterization of AuNPs/MCF nanocomposites using ultrasonic irradiation technique. AuNPs/MCF nanocomposites synthesized in this work will be further applied as a novel enzyme immobilization matrix for biosensor applications.

2. Materials and Methods

2.1 Chemicals

Hydrogen tetrachloroaurate (III) ($\text{HAuCl}_4 \cdot 3\text{H}_2\text{O}$), and Tetraethoxysilane (TEOS, 98%) were purchased from Sigma-Aldrich. Pluronic P123 was procured from BASF. 1,3,5-Trimethylbenzene (TMB) was purchased from Suspelco. (3-aminopropyl) triethoxysilane (APTS) from Fluka. Hydrochloric acid from BHD laboratory supplies. Isopropanol 97%, and Toluene 97% were from Scitrader (Thailand). Deionized water was used in all experiments.

2.2 Syntheses of MCF

MCF was prepared by dissolving 2g of Pluronic P123 in 75 ml of 1.6 M HCl at 35-40 °C. Then 1 g of TMB was added, and mixed thoroughly by continuously constant stirring to homogeneity. Subsequently, 4.25 g of TEOS was added and the mixture was continuously stirred for 24 h at 40 °C. The mixing solution was then stirred at 120 °C for further 24 h. The occurred particles were then separated, washed with deionized water, and dried at ambient temperature of 30 °C. Residual water was removed from MCF by calcination at 500 °C for 6 h [13]. Pore sizes, surface area, and pore volumes of MCF were measured by N_2 -adsorption as described by the Brunauer, Emmett and Teller (BET) method using Micromeritics (ASAP 2020, USA). The synthesized MCF was also characterized by Transmission Electron Microscopy (TEM).

2.3 Modification of MCF with aminopropyl groups

Modification of MCF was performed by dissolving 1g of MCF in 10 ml of toluene solution containing 1% APTS by stirring at ambient temperature for 10 minutes. The mixture was transferred into a Teflon bottle, then heated up to 100 °C and left under this condition for 24 h. Adsorption of APTS on the porous surface of MCF was expected to be occurred in this step. The modified MCF was thereafter filtered, washed once with dry toluene, and twice with dichloromethane before being dried at 120 °C for 2 h [13].

2.4 Synthesis of gold nanoparticles on modified MCF

1 g of the achieved modified MCF was immersed into 50 ml of an aqueous solution mixture of 0.8 mmol/l of chloroauric acid and 0.2 mol/l of isopropanol for 24 hr. The solution was subsequently purged with argon gas to eliminate the oxygen trace and then transferred to a tightly closed erlenmeyer flask. The flask was then placed onto a sonication bath (Crest ultrasonic, CP360, USA). An ultrasonic irradiation of 40 kHz (input power of 100 W) was applied for 120 min. The achieved nanocomposites were then filtered, and dried at 120 °C for 12 h [12].

3. Results and Discussion

Figure 1 shows the nitrogen adsorption-desorption isotherm which was used to investigate pore diameter, pore volume, and surface area of MCF by using Brunauer – Emmett - Teller (BET) method [14]. The results of structural properties of MCF are presented in Table 1.

Table 1: Physical characteristics of MCF.

| Characteristics | MCF |
|--|-------|
| Pore diameter (nm) | 7.6 |
| Pore volume (cm^3/g) | 1.02 |
| Surface area (m^2/g) | 537.6 |

The MCF sample shows the characteristics of type IV isotherm with type H2 hysteresis loop according to the IUPAC classification at the relative pressure ranging from 0.4 to 1.0. The obtained material was therefore postulated to contain interconnecting channels with narrower windows and wide sections like as a bottleneck [15]. The results were similar to those recently reported by Na et al. [16] for the MCF materials with various pore sizes (4-18 nm).

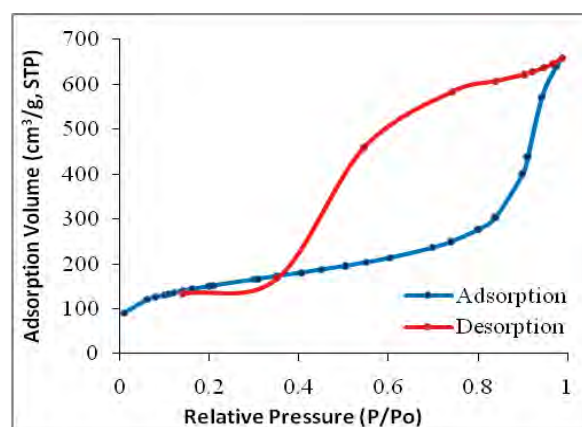


Fig. 1. Nitrogen adsorption – desorption isotherm of MCF.

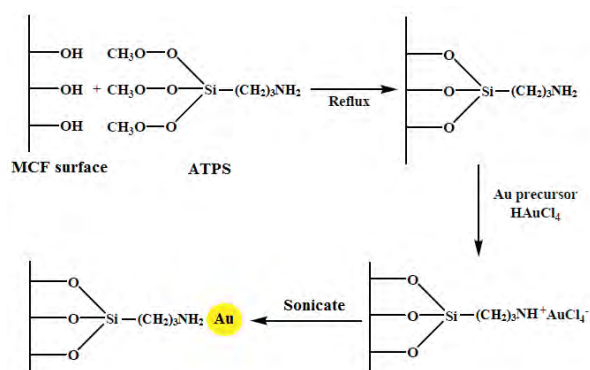


Fig. 2. Schematic diagram of the synthesized process of AuNPs/MCF nanocomposites by ultrasonication method.

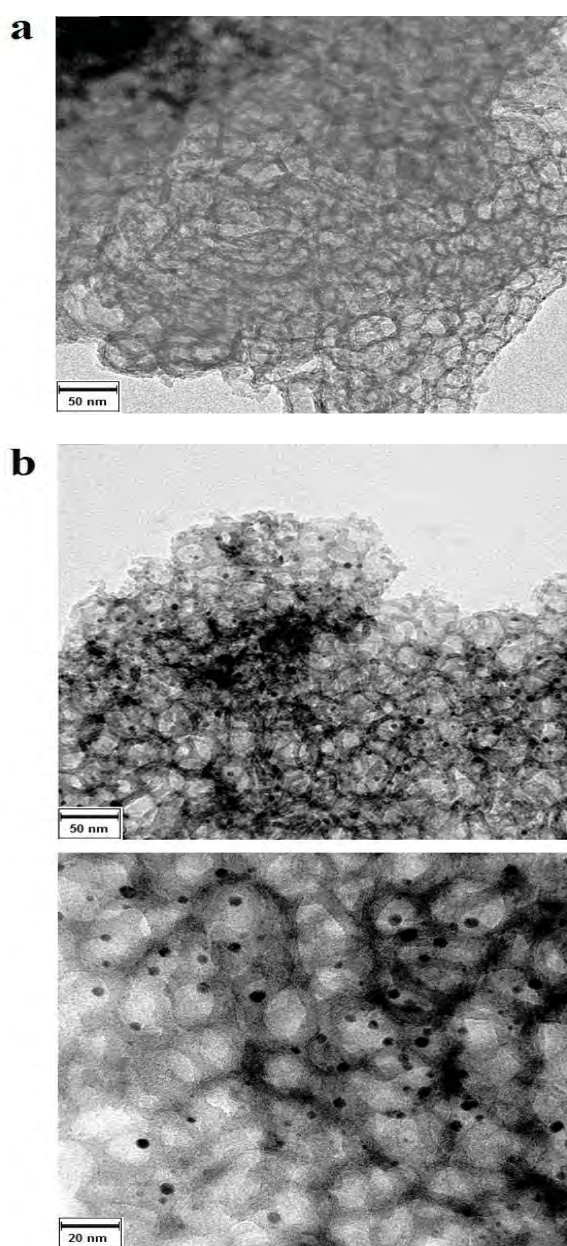


Fig. 3. TEM images of a) MCF b) AuNPs/MCF nanocomposites.

Figure 2 shows synthesizing step of AuNPs/MCF using ultrasonic irradiation technique. First, MCF was modified with APTS to attach a thiol functional group on its porous surface. Second, the modified MCF was immersed in hydrogen tetrachloroaurate ($\text{HAuCl}_4 \cdot 3\text{H}_2\text{O}$) which is a source of gold precursor generating AuCl_4^- ion that will be adsorbed on MCF surface. Finally, AuNPs were synthesized using ultrasonic irradiation with 40 kHz in isopropanol solution [12]. Free radicals that generated by the ultrasonic irradiation as described in equations (1) and (2) will reduce Au^{3+} ion to Au^0 atom, resulting in the adherence of AuNPs on porous surfaces of MCF.

Figure 3 shows TEM images of the synthesized MCF before and after adding gold nanoparticles. In Figure 3a shows cells of the framed structure which is the structural characteristics of MCF [16]. Mesostructure of MCF is favorable to be used for immobilization of enzyme since large spherical cells of 7.6 nm are big enough to accommodate the immobilized enzyme such as horseradish peroxidase and acetylcholinesterase with approximate size of 6.4×3.7 nm [13] and $4.5 \times 6.0 \times 6.5$ nm [17], respectively. These two enzymes are targeted biosensors for detecting phenol and pesticide compounds. In addition, the structural narrow windows prevent the leaching of enzyme [16]. Figure 3b shows TEM images of MCF after AuNPs synthesis using ultrasonication with 40 kHz for 120 mins. AuNPs were found homogeneously distributed throughout the surface of MCF. The average size of gold nanoparticles was 5 nm which is consistent with the results of Chen et al. [12] that synthesized AuNPs on mesoporous silica type SiO_2 by using ultrasonication technique with AuNPs products of 5.2 nm in size. The results indicate that AuNPs attach at the edges of MCF pores structure.

4. Conclusions

AuNPs/MCF nanocomposites were successfully synthesized using ultrasonic irradiation. The based MCF were of the average pore diameter of 7.6 nm, pore volume $1.02 \text{ cm}^3/\text{g}$, and surface area $537.6 \text{ m}^2/\text{g}$. AuNPs of approximate particle diameter of 5 nm were found homogeneously attached at ultrasonic at the edges of MCF pore structure after 120 mins of ultrasonic irradiation. AuNPs/MCF nanocomposites will be further applied for enzyme immobilization for biosensor applications.

Acknowledgements

This work was supported by Integrated Innovation Academic Center : IIAC Chulalongkorn University Centenary Academic Development Project.

Partially supported by the Higher Education Research Promotion and National Research University Project of Thailand, Office of the Higher Education Commission (FW0660I).

References

- [1] M. Indraneil, *Mesoporous Materials for Dental and Biotechnological applications, Curcumin Polymers and Enzymatic Saccharification of Biomass*, Licentiate Thesis, Drexel University, (2009).
- [2] H. Takahashi, R&D Review of Toyota CRDL **35** (2000) 12.
- [3] E.M. Johansson Samoson, *Controlling the pore size and morphology of mesoporous silica*, Licentiate Thesis, Linköping University, (2010).
- [4] K. Michal and J. Mieten, *Surface and structural properties of modified porous silicas*. Department of chemistry, Kent state University, Kent, Ohio (1998).
- [5] L.T. Zhuravlev, *Colloids and Surface A: Physicochemical and Engineering Aspect*. **173** (2000) 1-38.
- [6] T. Orita, M. Tomita, T. Nishida, and K. kato, *Materials Science and Engineering*. **238** (2012) 718–724.
- [7] H.P. Pandya, V.R. Jasra, B.L. Newalkar, N.P. Bhatt, *Microporous and Mesoporous Materials*. **77** (2005) 67–77.
- [8] X. Zhang, R.F. Guan, D.Q. Wu, K.Y. Chan, *J. Mol. Cata, B:Enzym*. **33** (2005) 43.
- [9] J. Chen, Y. Miao, N. He, X. Wu, S. Li, *Biotechnology Advances*. **22** (2004) 505-518.
- [10] D.C. Marie and A. Didier, *Chem. Rev.* **104** (2004) 293-346.
- [11] A. Fukuoka, H. Araki, Y. Sakamoto, N. Sugimoto, H. Tsukada, Y. Kumai, Y. Akimoto, M. Ichikawa, *Nano Lett.* **2002**, 2, 793–795.
- [12] A. chen, W.P. Cai, C.H. Liang, and L.D. Zhang, *Materials Research Bulletin*. **36** (2001) 335–342.
- [13] C. Wilaiwan, *The immobilization of horseradish peroxidase on Ag/mesoporous silica nanocomposite*, Licentiate Thesis, Chulalongkorn University, (2008).
- [14] T. Hyeon, M. Fang, and K.S. Suslick, *J. Am. Chem. Soc.* **118** (1996) 5492.
- [15] C.B. James, *Surface Area and Porosity Determinations by Physisorption Measurements and Theory*, Elsevier. (2006) 5492. 28-49.
- [16] N. Wei, W. Qi, S. He, and N.R. Zuo, *J. Porous Mater.* (2012).
- [17] J.L. Sussman, M. Harel, F. Frolow, C. Oefner, A. Goldman, L. Toker, I. Silman, *Science* **253** (1991) 872–879.

PREPARATION OF INTERPENETRATING NETWORK HYDROGEL FILMS BY ONE-POT POLYMERIZATION UNDER MICROWAVE IRRADIATION

Warunee Tanan, Kridsada Pananchai and Sayant Saengsuwan*

Laboratory of Advanced Polymers for Energy and Biomedical Applications (LAPEBA),
Department of Chemistry and Centre of Excellence for Innovation in Chemistry (PERCH-CIC),
Faculty of Science, Ubon Ratchathani University, Warinchamrab, Ubon Ratchathani, 34190 Thailand.

* Author for correspondence; E-Mail: sayants181@gmail.com, Tel. +66 85 415 9497, Fax. +66 45 288 379

Abstract: Poly (acrylamide-co-2-hydroxyethyl methacrylate) / poly(vinyl alcohol) (P(AM-co-HEMA)/PVA) interpenetrating network (IPN) hydrogel was successfully synthesized via one-pot solution polymerization with a microwave-assisted route to achieve fast reaction. IPN hydrogels were crosslinked by glutaraldehyde (GA) using ammonium persulfate (APS) as an initiator. The components of hydrogel were analyzed by Fourier transform infrared spectroscopy (FT-IR). FT-IR results showed the overlapping bands of N-H and O-H stretching at 3385 cm^{-1} , and exhibited vibration peaks of the C=O and C-O stretchings at 1670 and 1073 cm^{-1} , respectively. The morphological study showed pores and well organized nooks on the surface of hydrogels. Swelling behavior of hydrogels exhibited a rapid response. The water swelling of IPN hydrogels was about 600%, which was lower than that of hydrogel prepared by conventional method (800%). This was due to the higher network density of the IPN hydrogel prepared under microwave irradiation.

1. Introduction

Interpenetrating polymer network (IPN) hydrogels are a combination of more polymers in network that are crosslinked three-dimensional network structure of hydrophilic homopolymers or copolymers [1]. Due to the hydrophilicity characteristics, they can swell quickly in water or other biological fluid. The hydrogels have been widely used in the purification of waste water [2], controlled drug delivery [3] and tissue engineering [4]. They can be prepared by various methods including chemical and radiation induced crosslinking such as e-beam radiation, microwave irradiation, photo-initiated polymerization and plasma-induced grafting. As we all know that microwave irradiation is a special heating energy, which is used in the preparation of hydrogel. The method of microwave irradiation have been significant advantages such as rapid transfer of energy in the bulk of the mixture solution [5], accelerating reaction rate, improving yield and reducing the side effects [6]. Recently, many research used microwave-assisted for synthesis the hydrogel and polymeric biomaterials. Vijan et al. [7] reported the microwave irradiation in synthesis of acrylamide-grafted-gellan gum. The microwave irradiation results accelerate the reaction rate, which reduces reaction time. Thus, microwave assisted ceric (IV) induced graft copolymerization is an easy efficient. Sekhon [8] reviewed the overview of microwave-assisted in pharmaceutical

synthesis, and found that the obvious features of microwave technology like reduction of time for a chemical/pharmaceutical reaction. Sosnik et al. [9] used microwave irradiation as a versatile tool to synthesize organic and inorganic polymeric biomaterials. They found that the microwave irradiation for the fast, reproducible and scalable synthesis of polymeric materials has been thoroughly. Zhao et al. [10] synthesized the PNIPAAm hydrogels by microwave irradiation method and conventional hydrothermal method. The microwave irradiation had excellent advantages over the conventional hydrothermal method in improving properties of the hydrogels.

In this work, the IPN hydrogel of Poly(acrylamide-co-2-hydroxyethyl methacrylate)/poly(vinyl alcohol) (P(AM-co-HEMA)/PVA) was prepared via one-pot solution polymerization by using microwave-assisted. Then, it is compared with hydrogels synthesized by conventional method. Fourier transform infrared (FT-IR) spectroscopy was used to analyze the hydrogel compositions, and scanning electron microscope (SEM) was to observe their morphology of the hydrogels. The swelling behaviors of the resultant hydrogels were also studied. We will compare the characteristics properties and behavior swelling rate of hydrogels synthesized by two different methods.

2. Materials and Methods

2.1 Materials

2-Hydroxyethyl methacrylate (HEMA, 97%), acrylamide monomer (AM, 98.5%), ammonium persulfate (APS, 99%), ethylene glycol dimethacrylate (EGDMA, 98%), glutaraldehyde (GA, 50%), poly(vinyl alcohol) (PVA, 88%), N,N,N',N'-tetramethylethylen-diamine (TMEDA) and hydrochloric acid.

2.2 Preparation of IPN hydrogel films

Conventional method; the (PAM-co-HEMA)/PVA IPN hydrogel was prepared by free radical polymerization reaction. The detailed chemical compositions of the hydrogel are shown in Table 1. The mixed solution was bubbled with nitrogen for 30 min prior to the addition of the

initiator of APS. Then the polymerization was carried out at 50 °C for 24 h. After polymerization, glutaraldehyde and hydrochloric acid were added into the resultant solution under stirring to form crosslink reaction for 1 h. The resulting IPN hydrogel was transferred into petri dishes and dried for 9 h at 50 °C. Then, the hydrogel film was immersed in pure water for one day to remove all non-reactive materials and then was dried under vacuum at 30 °C for 24 h. The sample codes of hydrogel synthesized by conventional method as a 10% HEMA.

Microwave irradiation method; the reaction mixtures contained the same weight ratios as conventional method. In preparation of the IPN hydrogel, the monomer (acrylamide and 2-hydroxyethyl methacrylate), the polymer (poly (vinyl alcohol), cross-linker (glutaraldehyde and ethylene glycol dimethacrylate), and initiator (ammonium persulfate) were dissolved in distilled water. The mixed solution was bubbled with nitrogen for 1 h to eliminate dissolved oxygen that would be inhibitor for the reaction. The polymerization reaction was carried out in ME8IY microwave accelerator purchased from the Thai Samsung Electronics Company with adjustable and controllable temperature. The maximum power output was set at 300 W and the reaction time of 10 min. The resulting IPN hydrogel was transferred into petri dishes and dried for 9 h at 50 °C. And the sample was denoted as 10% HEMA-PM.

Table 1 the chemical compositions of the hydrogel.

| Symbol | HEMA (ml) | AM (g) | PVA (g) | H ₂ O (g) |
|----------|--------------|-----------|------------|-------------------------|
| 10% HEMA | 0.23 | 2.20 | 2.50 | 95.00 |

2.3 FT-IR analysis

The FT-IR spectra were used to analyze compositions of the hydrogel samples. The infrared samples were hydrogel film, approximately 3 mm x 3 mm placed in the sample holder. Spectra were recorded in the region of 4000-400 cm⁻¹ on a Fourier Transform Infrared (FT-IR) spectrophotometer (Perkin-Elmer 2000).

2.4 Morphology of the hydrogel

The morphologies of the hydrogels were characterized by Scanning Electron Microscope (SEM) (JEOL-JSM 5410 LV). The samples characterized were prepared by mounted onto stub, and then sputter-coating with a thin layer of gold under vacuum before measured.

2.3 Swelling behavior

The pre-weight dried hydrogel film samples were immersed in distilled water at room temperature to reach the equilibrium state. The hydrogels were drawn from water and then removing the water on the samples surface with filter paper. The equilibrium swelling of hydrogel sample was measured by gravimetrical method and then calculated the following equation

$$\%WC = [(W_s - W_d)/W_s] \times 100 \quad (1)$$

where W_d was the weight of dried sample, and W_s was the weight of swollen samples at different time. The mass swelling of hydrogel samples were obtained according to the equation [11-12].

$$\text{Mass swelling (\%)} = [(m_t - m_0)/m_0] \times 100 \quad (2)$$

where m_0 was initiated the weight of dried film, and m_t was the weight of swollen hydrogel.

3. Results and Discussion

3.1 Preparation of (PAM-co-HEMA)/PVA IPN hydrogel film

The hydrogel was successfully synthesized via one-pot copolymerization of AM, HEMA in PVA aqueous solution using microwave-assisted. In this work, APS was used as an initiator to initiate the radical polymerization, and GA and EGDMA are cross-linkers. This method shortened the reaction time of the polymerization and reduced the steps in the synthesis of hydrogel over the conventional method. The structures of (PAM-co-HEMA)/PVA IPN hydrogel and the synthesis route are shown in Scheme 1.

3.2 FT-IR of (PAM-co-HEMA)/PVA IPN hydrogel films

The FT-IR spectroscopy is used to confirm the compositions in the hydrogel samples. The absorption spectrum of 10% HEMA-PM and 10% HEMA hydrogel samples are showed in Fig. 1. The FT-IR spectra of both samples present the same characteristic peaks. FT-IR results showed the characteristic absorption band at 3000-2840 cm⁻¹, which related to the stretching vibration of C-H on the backbone. The absorption band at 3382 cm⁻¹ can be attributed to the characteristic peak of O-H and N-H. The peak of C=O and C-O groups appeared at 1670 cm⁻¹ and 1078 cm⁻¹, respectively. As a result, it can be concluded that the (PAM-co-HEMA)/PVA IPN synthesized by microwave irradiation method was successfully prepared.

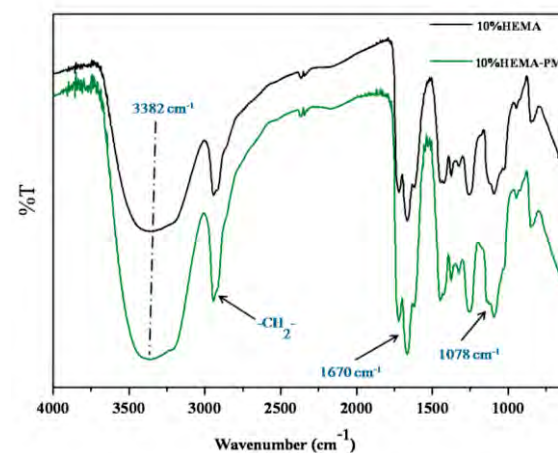
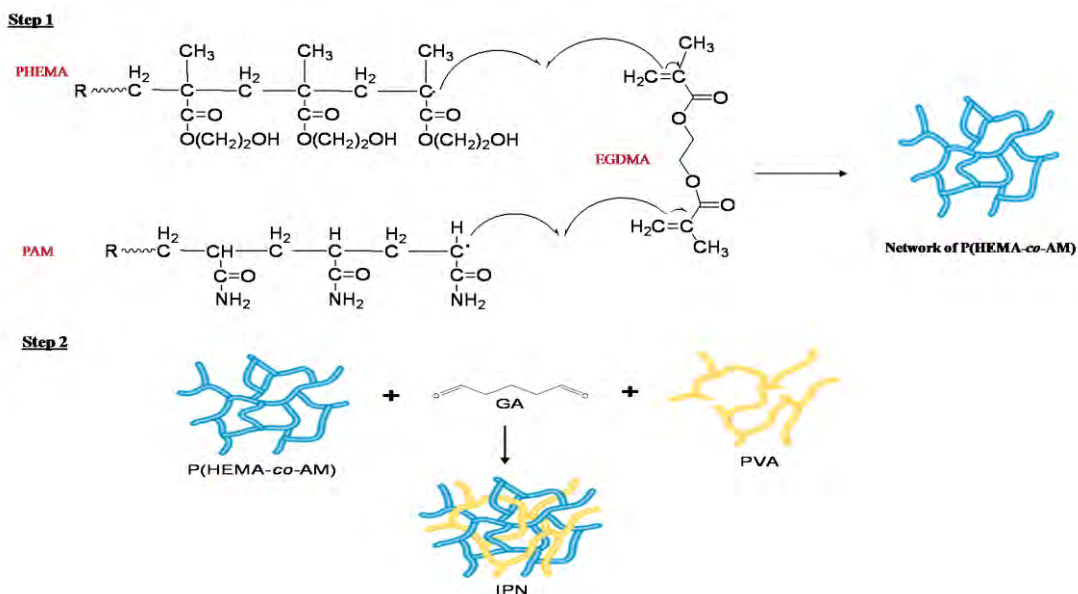


Figure 1. FTIR spectra of (PAM-co-HEMA)/PVA IPN hydrogels.



Scheme 1. The synthesis route of the (PAM-co-HEMA)/PVA IPN hydrogel [15].

3.3 SEM analysis

The morphology of the (PAM-co-HEMA)/PVA IPN hydrogels are shown in Fig. 2. It could be seen that the microstructure of hydrogels are three-dimensional networks having pores and well organized nooks in the surface of hydrogels. Thus, the natures of the pore/slit of the hydrogels render the hydrogels can be absorb and retain water within the structure. The porous hydrogels have potential application in the controlled release drug [13]. And the porosity of the hydrogels also affects their ability to absorb heavy metal ions [14].

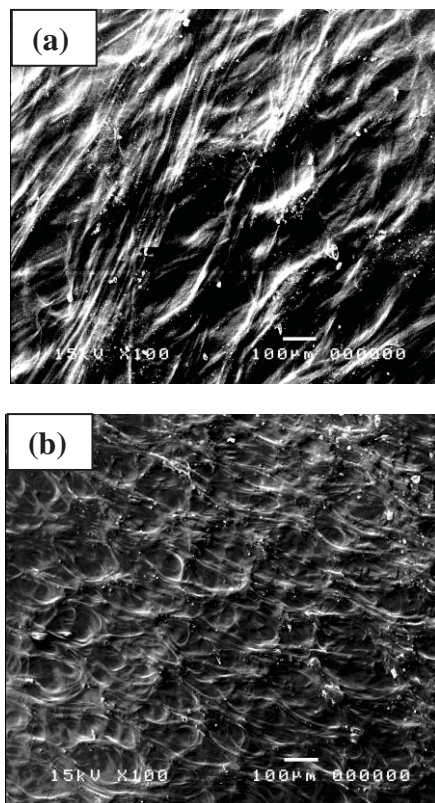


Figure 2. SEM photograph of (a) 10% HEMA-PM and (b) 10% HEMA hydrogels.

3.5 Swelling behavior

Swelling behavior of the hydrogels prepared was measured gravimetrically in distilled water at 27 °C. Fig. 3 shows the equilibrium swelling ratio of the hydrogel samples synthesized by conventional method (10% HEMA) and microwave irradiation method (10% HEMA-PM). From data, the samples show similar swelling behavior and fast reach the equilibrium only at 6 min. It can be seen that, 10% HEMA-PM can absorb water quickly and reaches to equilibrium faster than 10% HEMA. The mass swelling curves of the hydrogel samples are shown in Fig. 4. The percentage swellings of the samples were higher than 600%. As can be seen, the mass swelling of 10% HEMA is slightly higher than that 10% HEMA-PM. This is because the hydrogel prepared by microwave irradiation exhibited more crosslinked networks than hydrogel prepared by conventional methods. Therefore, the ability to absorb water of the 10% HEMA-PM hydrogel was decreased. However, the hydrogel prepared by microwave irradiation has good mechanical properties.

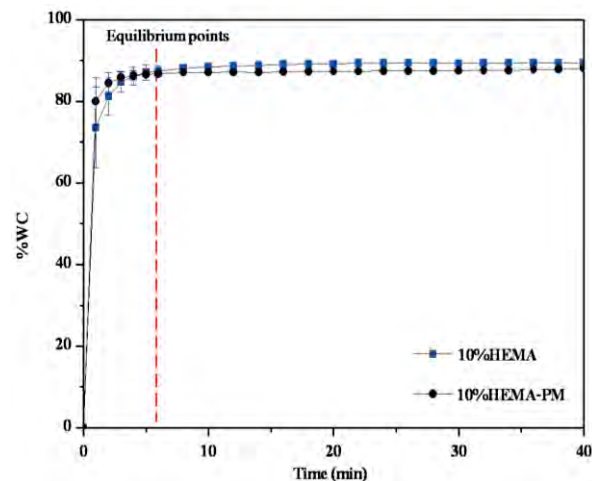


Figure 3. The equilibrium swelling ratio of the hydrogel samples.

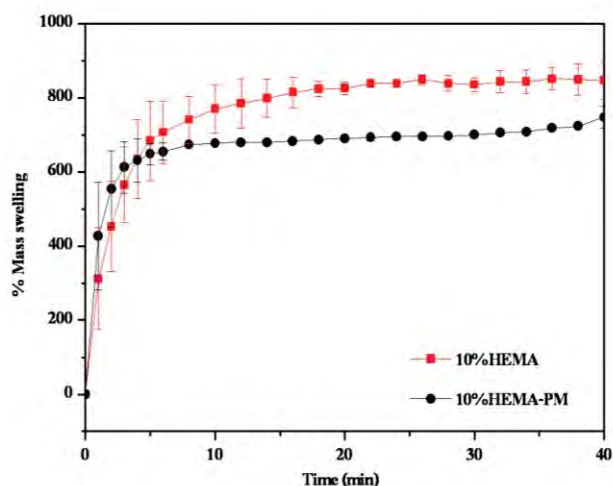


Figure 4. The mass swelling of the hydrogel samples.

4. Conclusions

The hydrogel prepared by one-pot microwave irradiation method can greatly shorten the reaction time, comparing with the hydrogel synthesized by conventional method. The FT-IR analysis confirms the compositions of hydrogel in the IPN networks. SEM photographs exhibited the microstructure of the IPN hydrogel films. The hydrogel prepared by microwave irradiation had swelling ratio higher than 600%. Nevertheless, the percentage swelling of hydrogel synthesis by microwave irradiation has slightly lower than that of hydrogel prepared by conventional method.

Acknowledgements

This work was fully supported by National Research Council of Thailand (NRCT). Center of Excellence for Innovation in Chemistry (PERCH-CIC), Commission of Higher Education, Ministry of Education and Ubon Ratchathani University are also acknowledged for some partial supports.

References

- [1] W.F. Lee and C.T. Huang, *Desalination*. **234** (2008) 195–203.
- [2] H.A. Essawy and H.S. Ibrahim, *React. Funct. Polym.* **61** (2004) 421–432.
- [3] D. Schmaljohann, *Adv. Drug. Del. Rev.* **58** (2006) 1655–1670.
- [4] J.L. Drury and D.J. Mooney, *Biomaterial.* **24** (2003) 4337–4351.
- [5] V. Singh, R. Sethi, A. Tewari, V. Srivastava and R. Sanghi, *Carbohydr Polym.* **54** (2003) 523–525.
- [6] H. P. Li, Z.d. Wang and T Yu, *Med. Chem. Res.* **20** (2011) 67–73.
- [7] V Vijan, S Kaity, S Biswas, J Isaac and A Ghosh, *Carbohydr. Polym.* **90** (2012) 496–506.
- [8] BS. Sekhon, *Int. J. Pharm. Techol. Res.* **2** (2010) 827–33.
- [9] A. Sosnik, G. Gotelli and G. A. Abrahamb, *Prog. Polym. Sci.* **36** (2011) 1050–1078.
- [10] Z. Zhao, Z. Li, Q. Xia, H. Xi and Y. Lin, *Eur. Polym. J.* **44** (2008) 1217–1224.

- [11] X.Z. Zhang, Y.Y. Yang and T.S. Chung, *Langmuir*. **18** (2002) 2538–2542.
- [12] Y. Xiang and D. Chen, *Eur. Polym. J.* **43** (2007) 4178–4187.
- [13] S. Amin, S. Rajabnezhad and K. Kohli, *Sci. Res. Essay*. **3(11)** (2009) 1175–1183.
- [14] Q. Tang, X. Sun, Q. Li, J. Lin and J. Wu, *J. Mater. Sci.* **44 (3)** (2009) 726–733.
- [15] Y. Yue, X. Sheng and P. Wang, *J. Eur Polym.* **45** (2009) 309–315.

BRADYKININ-A431 CELLS BINDING ASSAY BY QUARTZ CRYSTAL MICROBALANCE

Wannisa Sukjee¹, Peter A. Lieberzeit², Chak Sangma^{1*}

¹ Department of Chemistry, Faculty of Science, Kasetsart University, Chatuchak, Bangkok, 10400 Thailand

² Department of Analytical Chemistry, University of Vienna, Vienna, 1090 Austria

*E-mail: fscicsm@ku.ac.th,

Abstract: Bradykinin (BK) is an active peptide of the kinin group of G protein-coupled receptors which binds to two receptor types, named B1 and B2. Cell membrane of the human epidermoid A431 cell line expresses BK B2 receptors. In this work, the adhesion of bradykinin on A431 cultured on the poly(styrene-co-methyl methacrylate) coated on gold electrode was investigated with quartz crystal microbalance (QCM) technique. After bradykinin loading onto A431 there was a change in QCM signal. The results demonstrated that frequency was decreased with the increasing of BK concentration due to mass addition. The results showed a potential to use this method in applied in experiments related with BK receptor binding.

1. Introduction

Under a certain circumstance, scientists have to study systems in the most natural conditions *e.g.* experiments done with whole cells. A wide range of cells can be grown in culture and studied for their role in development and other biological processes. Cells could be miniature laboratories that can be leveraged for a range of assays from cytotoxic assays, apoptosis, metabolic assays which analyse cellular mechanisms such as cell growth, cell death, and cell function [1, 2]. In addition, cell-based assays can be used to study mechanisms of action such as receptor binding, receptor activation, cell signaling, ligand internalization, and subcellular localization [3].

Bradykinin (BK) belongs to a family of short, structurally similar peptides that are important metabolites of the kallikrein-kinin system [4]. Physiological and pathophysiological processes, including pain, inflammation, and regulation of blood pressure are mediated by bradykinins and their specific G-protein-coupled cell surface receptors that are coupled to multiple signal transduction pathways [5]. BK receptors are classified pharmacologically into two major subtypes, B1 and B2 [6].

Cell membranes of the human epidermoid cell line A431 express classical bradykinin (BK) B2 receptors [7], as assessed by BK binding studies. In addition to high affinity of BK to B2 receptors have been reported. In the present study we investigated the binding abilities of B2 receptors on A431 cells which are assessed by applying them onto quartz crystal microbalance (QCM) transducers and by tracing the subsequent frequency shifts following bradykinin exposure.

2. Materials and Methods

2.1 Materials and Chemicals

Bradykinin acetate salt powder ($\geq 98\%$), Azobisisobutyronitrile (AIBN) were purchased from Sigma-Aldrich. Styrene, Divinylbenzene, Methyl methacrylate were purchased from Merck. AT-cut quartz crystal sheets (10 MHz fundamental frequency) and the gold paste (for the screen printing of electrode over QCM sheets) were purchased from Great Microtama Electronics (Surabaya, Indonesia) and HERAEUS (Hanau, Germany).

2.2 Preparation of styrene/methyl methacrylate copolymer

We dissolved 1 mg of Azobisisobutyronitrile (AIBN) in mixture of 90 μl of styrene, 110 μl of divinylbenzene and 100 μl of methyl methacrylate. This was then followed by prepolymerization at 70°C for 3 hrs to reach the gel point. Afterwards, we spin-coated the prepolymer mixture onto the QCM electrode using 5 μl drop of the mixture and 2000 rpm spinning to obtain the thin layer in the range of 250-350 nm thickness. The electrode was left its to polymerize overnight under UV light at 254 nm and was verified by network analyzer.

2.3 Cells culture

A431 human epidermoid carcinoma cells were maintained in Dulbecco's modified Eagle's medium (DMEM) containing 10% fetal calf serum in a humidified 5% CO₂- air atmosphere at 37 °C. For all experiments, cells were cultured so as to be 60-90% confluent at the time of use. In order to transfer the cells to the sterilized QCM electrodes, the cultured cells were detached from the cultured flask by rinsing one times with phosphate buffered saline (PBS) and subsequently treating with 2.5 % trypsin/EDTA for 5 min at 37 °C. Cell detachment was stopped by adding culture medium excessively. A431 cells were grown on a pair of styrene/methyl methacrylate copolymer coated QCM electrode as a working electrode and gold coated QCM sheet as a reference electrode. After 2 days of cells culturing, the electrode was rinsed with 1X phosphate buffered saline solution (PBS) for 3 times before used.

Before the experiment the quartz was equilibrated with phosphate buffered saline. Bradykinin acetate salt was dissolved with phosphate buffered saline in different concentrations, 0.1 mg/ml, 0.5 mg/ml and 1.0 mg/ml. Firstly the 0.1 mg/ml bradykinin solution was injected onto the QCM for 60 min. Afterwards, 0.5 mg/ml and 1.0 mg/ml of bradykinin were changed for measuring the frequency response at the second and third hour respectively. Since the solutions had similar viscosities, frequency shifts were assigned to the response of bradykinin attached on the A431 cells coated electrodes.

3. Results and Discussion

The result showed the change in QCM signal with BK added onto the QCM (Figure 1). The frequency shift was observed during the binding of A431 cells up to 300 min after injection. Each concentrations of bradykinin were measured for 60 min. The frequency decreased immediately when each concentrations of bradykinin were injected. This is indicated that bradykinin can bind onto the B2 receptor of A431 membrane.

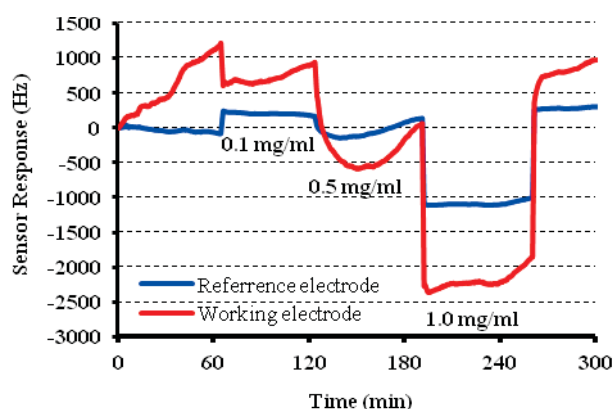


Figure 1 Binding of bradykinin to A431 cells attached on styrene/methyl methacrylate copolymer (working electrode) and gold surface (reference electrode)

The frequency response was increased with bradykinin concentrations as shown in figure 2. This demonstrated that A431 cells can spread on copolymer surface and still has a function as B2 receptor to bind BK..

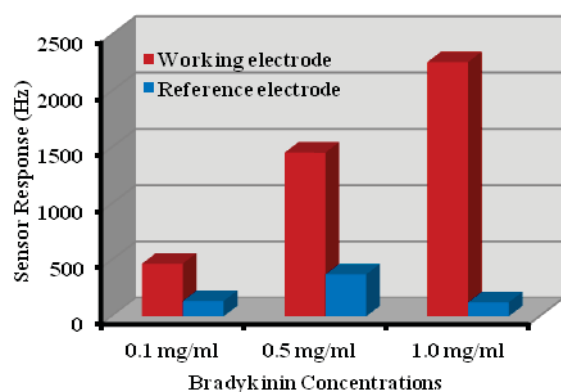


Figure 2 Sensor response of A431 human epidermoid carcinoma cells on electrodes in different concentrations of bradykinin.

Conclusions

The QCM technique can be used to study the binding of bradykinin and B2 receptors on A431 human epidermoid carcinoma cells line as indicated by the reduction in frequency baseline. Furthermore A431 can attach on styrene/methyl methacrylate copolymer which is a suitable surface for cell culture. The labeling-free QCM technique is also believed to be another method to monitor the cell adhesion on the modified surface for other cell lines.

Acknowledgements

This work was supported by the Royal Golden Jubilee Ph.D. Program (RGJ) under the Thailand Research Fund (TRF) and the institute of Analytical Chemistry, University of Vienna. The A431 cell line was kindly donated by Professor Dr. Doris Marko of institute of Food Chemistry and Toxicology, University of Vienna, Austria.

References

- [1] L. Kupcsik, in: M. J. Stoddart (Ed.), *Mammalian Cell Viability*, Vol. 740, Humana Press, Switzerland (2011), pp. 13-19.
- [2] D. Bogojevic, M. D. Chamberlain, I. Barbulovic-Nad and A. R. Wheeler, *LAB CHIP* 12 (2012) 627-634.
- [3] W. Huber, F. Hahne, in: R. Gentleman, V. Carey, W. Huber, R. Irizarry, S. Dudoit (Eds), *Bioinformatics and Computational Biology Solutions Using R and Bioconductor*, Springer New York (2005), pp. 71-90.
- [4] D. J. Campbell, *Clin. Exp. Pharmacol. Physiol.* 28 (2001) 1060-1065.
- [5] C. Golias, A. Charalabopoulos, D. Stagikas, K. Charalabopoulos and A. Batistatou, *Hippokratia* 11 (2007) 124-128.
- [6] D. Regoli, J. Barabé, in S. Giovanni Di (Ed), *Methods in Enzymology*, Vol. 163, Academic Press, New York (1988), pp. 210-230.
- [7] C. Liebmann, A. Graness, B. Ludwig, A. Adomeit, A. Boehmer, F. D. Boehmer, B. Nürnberg and R. Wetzker, *Biochem. J.* 313 (1996) 109-118.

INFLUENCE OF CULTURE CONDITIONS ON THE PRODUCTION OF ANTIBACTERIAL SUBSTANCES BY *BACILLUS LICHENIFORMIS*

Supranee Khuna¹, Nopakarn Chandet², Angkana Saovapakhiran^{3*}

¹Division of Biochemistry and Biochemical Technology, Department of Biotechnology, Graduate School, Chiang Mai University, Chiang Mai, 50200, Thailand

²Department of Chemistry, Faculty of Science, Chiang Mai University, Chiang Mai, 50200, Thailand

³Bio-organic synthesis and Molecular Biochemistry, Department of Chemistry, Faculty of Science, Chiang Mai University, Chiang Mai, 50200, Thailand

*E-mail: angkana.s@cmu.ac.th or s.angkana@gmail.com

Abstract: Antibacterial substances producing strains J503C, J504C, R101 and R301 were isolated from soil and identified as *Bacillus licheniformis*. Four distinct strains, J503C, J504C, R101 and R301, showed antibacterial activity against *Staphylococcus aureus* TISTR 1466. The production of antibacterial substances is mainly influenced by the culture conditions. Thus, this study focuses on the effect of media, initial pH and temperature on antibacterial productions by four strains of *B. licheniformis* in order to obtain the important factors affecting antibacterial substances production. The maximum productions of antibacterial substances of *B. licheniformis* J503C, J504C and R101 were observed in nutrient broth with initial pH 6, 7 and 8, respectively, whereas maximum antibacterial production by *B. licheniformis* R301 was obtained in both nutrient broth and tryptic soy broth with initial pH 8. The supernatant of *B. licheniformis* J503C, J504C, R101 and R301 exhibited strong inhibitory activity against *S. aureus* TISTR 1466 when these bacteria were grown at 37°C. The antibacterial activities of these inhibitory substances produced by *B. licheniformis* were also evaluated for their stabilities at different temperatures, organic solvents and enzymes. It was revealed that the inhibitory substances of *B. licheniformis* J503C, J504C, R101 and R301 were stable at 100°C for 15 min with clear zone of 0.76±0.01, 0.70±0.01, 0.83±0.05 and 0.82±0.01 cm, respectively. These substances showed remarkable stability in 50% (v/v) aqueous butanol. They also were resistant to amylase and lipase but completely inactivated by trypsin. The other chemical and biological characteristics of these active substances are under investigation to gain more information for further improving their antibacterial activities and practical applications.

1. Introduction

Antibacterial resistance has become a serious healthcare worldwide problem. The search for new antibacterial substances is also required [1]. The screening of antibacterial producer from natural sources may provide new antibacterial substance with a broad-spectrum activity.

The large number of antibacterial substance produced by *Bacillus* species with difference basic chemical structures, for example, gramicidin from *Bacillus brevis*, subtilin from *Bacillus subtilis*, polymyxin from *Bacillus polymyxa* and bacitracin from *Bacillus licheniformis* [2, 3]. *Bacillus* species are increasingly being used for production of antibiotics due to their stability and ability to grow at high

temperature. Additionally, various antibacterial substances derived from *Bacillus* species exhibited a broad range inhibition of bacteria strains and it also showed thermostability, pH stability and stability against surfactants [4].

2. Materials and Methods

2.1 Microorganisms

Bacteria were isolated from 13 soil samples in Thailand using dilution technique. Antibacterial substance producing strains were screened by using agar spot and agar-well diffusion assay. *Staphylococcus aureus* TISTR1466 and *Escherichia coli* TISTR 780 were used as indicator bacteria.

2.2 Antibacterial activity assay

Agar spot: Each isolated bacterium was spotted onto the surface of agar plate and allowed colony to develop at 37°C. The agar plate was overlaid with 5 mL soft-agar medium containing 6 mL of the indicator strain. Inhibition zone was determined after 24 h of incubation at 37°C [5].

Agar-well diffusion: Agar medium was mixed with indicator strain and poured into Petri dishes to solidify. Well of 6 mm diameter were cut and filled with 100 µL of cell free supernatant of isolated bacteria. The agar plate was incubated at 37°C for 24 h. The inhibition zone was detected [6].

2.3 Bacterial identification

The potential antibacterial substance producing strains were analysed by sequencing of 16S ribosomal RNA (rRNA). The 16S rRNA gene sequence of isolated bacterium was amplified using Universal primers 20F, 1500R, 520F, 920F and 920R. BLAST analysis of DNA sequence was performed using the NCBI database [7].

2.4 Effect of culture conditions on antibacterial production

Medium: The appropriated medium for antibacterial production was determined using different medium that are nutrient broth (NB), tryptic soy broth (TSB), brain heart infusion (BHI) and synthetic medium. The isolated bacteria were grown in each media at 37°C for 96 h in a rotary shaker at 160 rpm. Cell free supernatant was obtained by centrifuge

at 6000×g for 15 min and tested for antibacterial activity.

Initial pH: The appropriated production medium was adjusted to pH 4, 5, 6, 7, 8 and 10 before inoculating isolated bacteria producers. Cultures were centrifuged at 6000×g for 15 min after incubating at for 96 h 37°C in a rotary shaker at 160 rpm. Antibacterial activity was tested.

Temperature: The isolated bacteria were grown in production medium at 37, 45 and 50°C for 96 h in a rotary shaker at 160 rpm. Cultures were centrifuged at 6000×g for 15 min after 96 h and examined for antibacterial activity.

Aeration: The experiment was carried out by using 250 ml Erlenmeyer flask and Baffle flask containing production medium. Cultures were incubated at 37°C for 96 h in a rotary shaker at 160 rpm. Cell free supernatant was obtained by centrifuge at 6000×g for 15 min and examined for antibacterial activity.

2.5 Effect of temperature, pH, enzyme and organic solvent on antibacterial activity

The effect of temperature, pH, enzyme and organic solvent on antibacterial activity was performed as previously described [8]. To determine effect of temperature on antibacterial activity, cell free supernatant was incubated in temperature range 60-100°C for 30 min and 121°C for 15 min. Cell free supernatant was treated with 1 mg/ml of either amylase, trypsin or lipase for 1 h at 37°C. Samples were heated for 2 min to inactivate enzyme after complete reaction. The organic solvents (butanol, acetone, chloroform and trichloroacetic acid) were used at working concentration of 50% (v/v). Each organic solvent was added with cell free supernatant and incubated for 1 h at 37°C. After treatment, the treated samples were tested for residual antibacterial activity against *S. aureus* TISTR1466. The percentage of residual activity was expressed as the relative percentage antibacterial activity after treatment to that of the initial antibacterial activity.

3. Results and Discussion

3.1 Screening for antibacterial substance producing bacteria

Several bacteria were isolated from soil samples in Thailand. Four isolated bacteria which are J503C, J504C, R101, and R103 showed high antibacterial activity against *S. aureus* TISTR1466 and *S. epidermis* TISTR518. The 16s rRNA partial sequence showed 99% homology with *Bacillus licheniformis*. Therefore, these four strains of *B. licheniformis* were selected for further study.

3.2 Effect of medium, initial pH, temperature and aeration on antibacterial production

For determination of the preferable conditions for antibacterial substances production, four strains of *B. licheniformis* were grown in NB, TSB, BHI and synthetic medium. The supernatant from NB of *B.*

licheniformis J503C, J504 and R101 exhibited high antibacterial activity with clear zone 0.77 ± 0.021 , 0.71 ± 0.032 , 0.76 ± 0.010 and 0.73 ± 0.052 cm, respectively (Table 1). In the addition, *B. licheniformis* R103 could produce antibacterial substance in both NB and TSB with clear zone 0.73 ± 0.021 and 0.70 ± 0.000 cm, respectively. It was found that NB was the suitable medium for antibacterial substances production when compared to TSB, BHI and synthetic medium. The results indicated that the antibacterial substance productions were influenced by components in medium especially glucose which was supplemented in TSB, BHI and synthetic medium. The results are agreement with Tabbene *et al.* (2009) who reported that monosaccharides in culture medium apparently supported bacterial growth but did not affect stimulation of antibacterial substances production. Glucose could interferes biosynthesis of bacitracin of *B. licheniformis* [9]. Moreover, the addition of glucose to medium may lead to the delay of bacitracin production [10].

Table 1: Effect of medium on antibacterial production

| Medium | Clear zone (cm) | | | |
|------------------|------------------|------------------|------------------|------------------|
| | J503C | J504C | R101 | R103 |
| NB | 0.77 ± 0.021 | 0.71 ± 0.032 | 0.76 ± 0.010 | 0.73 ± 0.052 |
| TSB | - | - | - | 0.70 ± 0.000 |
| BHI | - | - | - | - |
| Synthetic medium | - | - | - | - |
| Penicillin G | 3.24 ± 0.051 | | | |

Data are represented as the mean width of the clear zone \pm standard deviation of three replicates.

-; no clear zone

Table 2: Effect of initial pH on antibacterial production

| Initial pH | Clear zone (cm) | | | |
|------------|------------------|------------------|------------------|------------------|
| | J503C | J504C | R101 | R103 |
| 5 | - | 0.64 ± 0.010 | 0.90 ± 0.021 | - |
| 6 | 0.94 ± 0.095 | 0.71 ± 0.006 | 1.01 ± 0.006 | 0.83 ± 0.010 |
| 7 | 0.83 ± 0.026 | 0.82 ± 0.032 | 0.91 ± 0.012 | 0.83 ± 0.000 |
| 8 | 0.77 ± 0.025 | 0.75 ± 0.006 | 1.01 ± 0.006 | 0.85 ± 0.017 |
| 10 | 0.76 ± 0.062 | 0.77 ± 0.000 | - | - |

Penicillin G 3.24 ± 0.051

Data are represented as the mean width of the clear zone \pm standard deviation of three replicates.

-; no clear zone

Four candidate strains of *B. licheniformis* were grown in nutrient broth with initial pH 5, 6, 7, 8 and

10. The maximum antibacterial production produced by *B. licheniformis* J503C was observed in nutrient broth with initial pH 6 with clear zone 0.94 ± 0.095 cm. *B. licheniformis* J504C produced the highest antibacterial substance at pH 7 with clear zone 0.82 ± 0.032 cm. Additionally, *B. licheniformis* R101 produced high antibacterial production in nutrient broth with initial pH 8 (1.01 ± 0.006 cm), The supernatant with initial pH 8 of *B. licheniformis* R301 also showed maximum activity with clear zone 0.85 ± 0.017 cm as shown in Table 2. Similar finding has been report by Cladera-Olivera *et al.* (2004). *B. licheniformis* 26L-10/3RA showed the highest Lichenin production with initial pH 6.8 [11]. Inappropriate pH values cause reduction of their growth and low level of antibacterial substance production.

The effects of temperature and aeration on antibacterial production were also evaluated. The highest antibacterial activity produced by *B. licheniformis* J503C, J504C, R101, and R103 were detected at 37°C with clear zone 0.94 ± 0.006 , 0.88 ± 0.045 , 0.83 ± 0.000 and 0.78 ± 0.006 cm. These four bacteria strains of *B. licheniformis* were able to grow at 45 and 50°C but could not produce antibacterial substances. In Table 3, it was found that the antibacterial production was not significantly affected by the aeration.

Table 3: Effects of temperature and aeration on antibacterial production

| Temperature, type of flask | Clear zone (cm) | | | |
|-------------------------------|------------------|------------------|------------------|------------------|
| | J503C | J504C | R101 | R103 |
| 37°C, Erlenmeyer flask | 0.94 ± 0.006 | 0.88 ± 0.045 | 0.83 ± 0.000 | 0.78 ± 0.006 |
| 45°C, Erlenmeyer flask | - | - | - | - |
| 50°C, Erlenmeyer flask | - | - | - | - |
| 37°C, Baffle flask | 0.84 ± 0.021 | 0.82 ± 0.015 | 0.76 ± 0.012 | 0.76 ± 0.012 |
| Penicillin G | 3.24 ± 0.051 | | | |

Data are represented as the mean width of the clear zone \pm standard deviation of three replicates.
-; no clear zone

3.3 Effects of temperature, pH, enzyme and organic solvent on antibacterial activity

The effects of temperature, pH, enzyme and organic solvent on antibacterial activity of four strains of *B. licheniformis* were also presented in this study. The antibacterial activities from all tested strains of *B. licheniformis* were stable at temperature 60, 80 and 100°C for 30 min. In the addition, these substances showed antibacterial activities after treated at 121°C, 103.5 kPa for 15 min. All antibacterial substances were completely lost activity after treatment with trypsin, whereas remained stable in α -amylase and lipase. These results suggest that all antibacterial substances from *B. licheniformis* J503C, J504C, R101 and R103 have protein moieties of their structures. The antibacterial activities of all tested cell-free supernatants were lost after treatment with acetone, chloroform and trichloroacetic acid but resistance to butanol. Effect of pH on antibacterial activity was evaluated by measuring the retained activity after incubated at difference pH values. The supernatant of four strains of *B. licheniformis* remained active after exposure to the pH range of 5-10 for 2 hours (Table 4). These characteristics may useful in various industrial processes which use high temperature or wide range of pH values.

Table 4 Effect of pH on antibacterial activity

| pH | Residual activity (%) | | | |
|----|-----------------------|----------------|----------------|----------------|
| | J503C | J504C | R101 | R103 |
| 5 | 79.2 ± 0.7 | 83.3 ± 0.7 | 94.4 ± 3.2 | 89.8 ± 2.0 |
| 6 | 78.0 ± 0.7 | 85.0 ± 0.7 | 92.2 ± 3.5 | 88.3 ± 2.6 |
| 7 | 93.2 ± 6.9 | 91.5 ± 1.2 | 93.1 ± 4.5 | 89.8 ± 4.1 |
| 8 | 93.2 ± 6.9 | 91.5 ± 1.2 | 93.8 ± 3.0 | 89.0 ± 2.4 |
| 9 | 97.0 ± 2.9 | 88.6 ± 0.7 | 92.2 ± 3.5 | 88.3 ± 0.7 |
| 10 | 80.3 ± 3.5 | 83.7 ± 0.7 | 88.2 ± 0.0 | 92.4 ± 2.6 |

Data are represented as the mean percentage of the residual activity \pm standard deviation of three replicates.

Table 5 Effects of temperature, enzymes and organic solvents on antibacterial activity

| Treatment conditions | Residual activity (%) | | | |
|--------------------------|-----------------------|----------|----------|----------|
| | J503C | J504C | R101 | R103 |
| Temperature | | | | |
| 60°C/ 30 min | 100±1.3 | 100±3.3 | 100±6.7 | 100±1.1 |
| 80°C/ 30 min | 99.0±3.0 | 99±3.0 | 90±6.7 | 96±3.0 |
| 100°C/30 min | 98.1±2.6 | 98±0.0 | 90±7.1 | 97±1.0 |
| 121°C/ 103.5 kPa/ 15 min | 86.0±2.0 | 89.7±0.0 | 87.3±2.8 | 85.2±1.1 |
| Enzymes | | | | |
| α-amylase | 94.0±3.7 | 99.2±4.1 | 98.4±2.8 | 99.1±0.7 |
| Trypsin | 0 | 0 | 0 | 0 |
| Lipase | 90.4±3.4 | 96.6±4.7 | 98.8±2.1 | 98.3±1.3 |
| Organic solvents | | | | |
| Butanol | 100±12.9 | 100±4.6 | 100±4.9 | 100±2.2 |
| Acetone | 0 | 0 | 0 | 0 |
| Chloroform | 0 | 0 | 0 | 0 |
| Trichloroacetic acid | 0 | 0 | 0 | 0 |

Data are represented as the mean percentage of the residual activity ± standard deviation of three replicates.

4. Conclusions

The antibacterial substances produced by *B. licheniformis* J503C, J504C, R101 and R103 exhibited antibacterial activity against gram positive bacteria, *S. aureus* TISTR1466 and *S. epidermis* TISTR518. All substances showed excellent thermal stability, board pH stability and organic solvent stability. These substances should be further investigate in order to gain more their biological and chemical information for improving their antibacterial activities and practical applications.

Acknowledgements

Authors gratefully acknowledge the Graduate School, Chiang Mai University, Thailand.

References

- [1] G. Didier, *Curr. Opinion in Microbiol.*, 2 (1999) 494-498.
- [2] K. Edwards, L.D. Arnold, *Bacteriol. Rev.*, 41 (1977) 449-474.
- [3] A. Muhammad, A.S. Aamer, H. Abdul, H. Fariha, *Pak. J. Biol. Sci.*, 39 (2007) 1303-1312.
- [4] M.L. Teixeira, F. Cladera-Olivera, J. dos Santos, A. Brandelli, *Food. Res. Int.*, 42 (2009) 63-68.

- [5] U. Schillinger, F.K. Lucke, *Appl. Environ. Microbiol.*, 55 (1989) 1901-1906.
- [6] N. Kayalvizhi, P. Gunasekaran, *Biotechnol. Bioproc. E*, 15 (2010) 365-370.
- [7] J. Brosius, T.J. Dull, D.D. Sleeter, H.F. Noller, *J. Mol. Biol.*, 148 (1981) 107-127.
- [8] F. Cladera-Olivera, G.R. Caron, A. Brandelli, *Lett. Appl. Microbiol.*, 38 (2004) 251-256.
- [9] O. Tabbene, I.B. Slimene, K. Djebali, M.-L. Mangoni, M.-C. Urdaci, F. Limam, *Biotechnol. Prog.*, 25 (2009) 1267-1274.
- [10] H.O. Haddar, G.M. Aziz, M.H. Al-Gelawi, *Pak. J. Biol. Sci.*, 10 (2007) 972-976.
- [11] P. Pattnaik, S. Grover, V. Kumar Batish, *Microbiol. Res.*, 160(2005)213-21

LACTIC ACID PRODUCTION FROM BY-PRODUCTS IN CANNED SWEET CORN INDUSTRY

Nannaphat Sujit¹, Nopakarn Chandet^{2*}

¹ Division of Biochemistry and Biochemical Technology, Department of Biotechnology, Graduate School, Chiang Mai University, Chiang Mai, 50200, Thailand.

² Department of Chemistry, Faculty of Science, Chiang Mai University, Chiang Mai, 50200, Thailand.

*E-mail: nopakarn@gmail.com, Tel. +6653-943336 #103

Abstract: Production of lactic acid from inexpensive raw materials becomes more attention recently due to the cost reduction and utilization of agricultural wastes. In this study, canned sweet corn industrial wastes including corn hull, corncob, discarded seed and residual water, were evaluated as feedstock for lactic acid production. The amounts of reducing sugar and lactic acid in the fermentation broth were measured by DNS method and Barker-Summerson method, respectively. The amounts of initial sugar in corn hull, corncob, discarded seed and residual water were investigated. Three strains of homofermentative lactic acid bacteria (LAB); *Pediococcus pentosaceus* TISTR 954, *Pediococcus acidilactici* TISTR 425 and *Streptococcus lactis* TISTR 457, were cultivated in the medium containing discarded seed as a carbon source. The amounts of lactic acid produced in 5 days cultivation of *P. pentosaceus* TISTR 954, *P. acidilactici* TISTR 425 and *S. lactis* TISTR 457 were 0.087, 0.024, and 0.140% (w/v), respectively. Corn hull and corncob were chosen for substrate pretreatment to enhance the amount of usable sugar. Among hydrolyzing agents, the diluted sulfuric acid was the most suitable hydrolyzing agent for substrate pretreatment giving 2.6% (w/v) of initial sugar in corn hull and corncob. The hydrolysate of corn hull and corncob were used as a substrate for lactic acid fermentation. For further study, partial purification of lactic acid will be done using Amberlite IRA-67 column chromatography.

1. Introduction

Lactic acid is an important organic acid that has been widely used in the food, leather, cosmetic, pharmaceutical and chemical industries. Recently, a polymer of lactic acid (PLA) becomes worldwide attention due to its biodegradable character and potential applications [1]. Traditional production of lactic acid normally uses starch as the fermentation substrate [2]. Alternatively, indeed, agro-industrial and forestry sources represent a potentially inexpensive and renewable carbohydrate feedstock for fermentation of lactic acid due to their abundance, low cost and high polysaccharide contents [3]. Such lignocellulose waste products are accumulated in large quantities every year and are mainly composed of three groups of polymers: cellulose, hemicellulose and lignin. Cellulose and hemicellulose are sugar rich fractions of interest for use in many fermentation processes, since microorganisms can use the sugars for growth and production of value added compounds such as ethanol, food additives, organic acids, enzymes, and other products [4].

Due to the requirement of large amount-low cost of lactic acid, biotechnological production from agricultural biomass is attended from biopolymer producers. The raw materials which are used to produce lactic acid should have the following characteristics: cheap to produce, low levels of contaminants, rapid production rate, high yield, no or less by-product formation, the ability to be fermented with no or less pre-treatment and year-round availability [5].

Lactic acid bacteria (LAB) can be classified into two groups: homofermentative and heterofermentative lactic acid bacteria. While the homofermentative LAB convert glucose almost exclusively into lactic acid, the heterofermentative LAB catabolize glucose into ethanol and CO₂ as well as lactic acid [6]. The homofermentative LAB usually metabolize glucose via the Embden-Meyerhof pathway (i.e. glycolysis). Since glycolysis results only in lactic acid as a major end-product of glucose metabolism, two lactic acid molecules are produced from each molecule of glucose with a yield of more than 0.90 g/g [7]. Only the homofermentative LAB are currently used for the commercial production of lactic acid [6].

In this study, lactic acid will be produced by submerged fermentation of corn hull hydrolysate (CHH) and corncob hydrolysate (CCH) using *Pediococcus pentosaceus* TISTR 954. The fermentation broth will then be separated and purified using ion exchange chromatography.

2. Materials and Methods

2.1 Materials

Corn hull and corncob were kindly obtained from Lanna Product Company in Lamphun Province. Those biomass were dried in the sunlight, milled to give a particle size of approximately 5 mm and 1 mm thickness for corn hull and corncob, respectively. Raw material was air dried at 65 °C for 24 hours and stored in plastic bag and kept at 4 °C until used.

2.2 Microorganisms and inoculum preparation

Pediococcus pentosaceus TISTR 954, *Pediococcus acidilactici* TISTR 425 and *Streptococcus lactis* TISTR 457 were purchased from Thailand Institute of Scientific and Technology Research (TISTR). The culture of *P. pentosaceus* TISTR 954 and *P. acidilactici* TISTR 425 were

maintained in Glucose extract-yeast extract-peptone (GYP) sodium acetate mineral salts agar and *S. lactis* TISTR 457 was maintained in Nutrient agar (NA). For using as starter cultures, the inoculums of those LABS were in MRS broth. A loopful of starter cultures from agar slant (GYP or NA) were inoculated into 10 ml of MRS medium. The culture was incubated at room temperature for overnight. The 24 hours-grown LAB was used as the inoculum.

2.3 Selected strains of Lactic Acid Bacteria

Erlenmeyer flasks (250 ml) containing 10 g of discarded seed and 180 ml of water used fermentation experiment. The fermentation medium was sterilized at 121 °C for 20 min. one milliliter of each strain inoculum was added into fermentation medium and incubated at 28 °C for 5 days. Samples were removed for analysis.

2.4 Pretreatment

Various kinds of chemicals were used for substrate pretreatment.

Dilute sulfuric acid pretreatment: 5.0 g of corn hull and corncob residue were mixed with 50 ml of 1.5% H₂SO₄ and kept at 100 °C for 6 hours. The mixtures were filtered to separate the solid residue and the filtrate fraction. The pH of filtrate fractions was adjusted to pH 7.0 with 6 M NaOH.

Lime pretreatment: 5.0 g of corn hull and corncob residue were mixed with 2 g of calcium hydroxide. Water (50 ml) was added on dried samples. The pretreated sample was autoclaved at 121 °C for 20 minutes. The mixtures were treated as described above in the section of diluted sulfuric acid pretreatment.

Aqueous ammonia pretreatment: 5.0 g of corn hull and corncob residue were mixed with 50 ml of 10% NH₄OH and incubated at room temperature for 24 hours. Then the residue was separated from the mixture by filtration. The filtrate was treated with 6 M HCl for pH neutralization

Sodium hydroxide pretreatment: 5.0 g of corn hull and corncob were soaked in 40 ml of 2% NaOH solution. The mixture was autoclaved at 121 °C for 20 minutes. The pH of filtrate fractions was adjusted to pH 7.0 with 6 M HCl.

2.5 Hydrolysate fermentation

One milliliter of inoculum of *P. pentosaceus* was added into test tube containing 9 ml of sterilized hydrolysate. The sample was incubated at 28 °C for 5 days. To scale up, the culture was added into 90 ml of hydrolysate in Erlenmeyer flask. The culture was incubated at 28 °C for 10 days and sampling at 0, 2, 4, 6, 8 and 10 days of cultivation to measure the amount of reducing sugar and concentration of lactic acid.

2.6 Analytical methods

The reducing sugar was determined by colorimetric method using 3, 5-dinitrosalicylic acid

(DNS) and lactic acid concentration was measured by the Barker- Summerson method [8].

3. Results and Discussion

3.1 The amount of reducing sugar of materials

Initially, experiment was carried out to determine the amount of reducing sugar in each material. Agricultural biomasses from canned sweet corn industry were corn hull, corncob, discarded seed and residual water. Corn hull and corncob were resized and pretreatment for further experiment. Table 1 shows the amounts of initial sugar in canned sweet corn industry. The amounts of initial sugar in dried corn hull and milled corncob were 0.05 and 0.09 %w/v, respectively. Due to the lowest amount of reducing sugar and biomass in industry (corn hull and corncob) were accumulated in large quantities. Corn hull and corncob were mainly composed of three groups of polymers: cellulose, hemicellulose and lignin. Therefore, the further experiment will focus on the pretreatment of corn hull and corncob to use as substrate for lactic acid production which is an essential step for substrate preparation.

Table 1 The amounts of initial sugar in Canned Sweet Corn Industry wastes

| Material | Reducing sugar |
|-----------------|----------------|
| corn hull | 0.44* |
| dried corn hull | 0.05** |
| milled corncob | 0.09** |
| discarded seed | 0.27* |
| residual water | 0.24** |

*%w/w, ** %w/v

3.2 Selection of Lactic acid bacteria (LAB) strains for lactic acid fermentation from discarded seed

Lactic acid production from discarded seed during Solid-state fermentation (SSF) by three strains of LAB was shown in Fig 1 and Fig 2. When the strain of *P. pentosaceus*, *P. acidilactici* and *S. lactis* were inoculated in the SSF process, the initial reducing sugar concentration decreased during the fermentation process, indicating that the reducing sugar was utilized by *P. pentosaceus*, *P. acidilactici* and *S. lactis*. The lactic acid concentration reached to 0.087, 0.024, and 0.140 % (w/v) for *P. pentosaceus*, *P. acidilactici* and *S. lactis*, respectively. Although *S. lactis* seems to be a good lactic acid producer in fermentation using discarded seeds as substrate, *P. pentosaceus* is better lactic acid producer in the fermentation using cellulosic biomass (corn hull, corncob) as substrate (data not shown). As explained above, *P. pentosaceus* was selected for further experiment of lactic acid production.

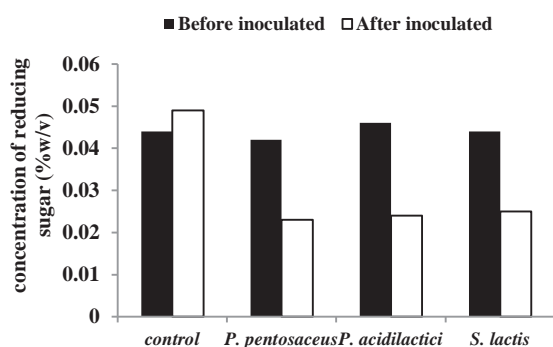


Figure 1 Concentration of reducing sugar during lactic acid fermentation for 5 days in each LAB strain

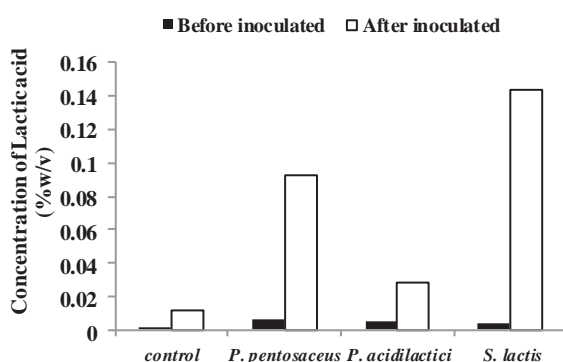


Figure 2 Concentration of lactic acid during lactic acid fermentation for 5 days in each LAB strain

3.3 Four different chemical pretreatments of corn hull and corncob

Corn hull and corncob were subjected to four chemical pretreatments with diluted sulfuric acid, lime, aqueous ammonia and sodium hydroxide, respectively. The pretreatment results, were expressed as the amount of reducing sugar of pretreated sample. Table 2 shows the amount of reducing sugar in each pretreatment. Pretreatment with sulfuric acid effectively released sugar 2.6% (2,600 mg/100 ml) of corn hull and corncob hydrolysate and detected as 44 times higher than the amount of sugar in untreated residues. Compared with the lime, aqueous ammonia and sodium hydroxide released more reducing sugar fraction from raw material because the hemicellulose of corn hull and corncob could be hydrolyzed to their sugar constituents using dilute acid that is necessary for effective production of lactic acid. Therefore, in this study, acid hydrolysis by dilute sulfuric acid was selected to use as the method of substrate pretreatment (corn hull and corncob).

Table 2 Effect of reducing sugar in each pretreatment

| Pretreatment | Reducing sugar (%w/v) | |
|---------------------------------------|-----------------------|---------|
| | corn hull | corncob |
| Dilute H ₂ SO ₄ | 2.6 | 2.6 |
| Lime | 0.039 | 0.029 |
| 10% NH ₄ OH | 0.023 | 0.024 |
| 2% NaOH | 0.034 | 0.039 |

3.4 Lactic acid production from corn hull and corncob hydrolyzed by *Pediococcus pentosaceus* TISTR 954

Lactic acid production from corn hull and corncob hydrolyzed by *Pediococcus pentosaceus* TISTR 954 was studied to produce lactic acid from substrate pretreatment (corn hull and corncob). Figure 3 and Figure 4 shows the reducing sugar consumption and lactic acid during fermentation of corn hull and corncob hydrolysate. The rate of lactic acid production gave the highest amount of lactic acid in 10 days of cultivation, 0.054 and 0.079 % (w/v) in corn hull and corncob hydrolysate. Theoretically, the amount of reducing sugar should be decreased due to the conversion to lactic acid. However, the amount of reducing sugar seemed to be constant while lactic acid amount was increased. This phenomenon was found because of other chemicals, such as furfural and 5-hydroxymethylfurfural, results as by-products from pretreatment utilizing either high temperatures and pressures or acid [9]. They may interfere with DNS by supplying reactive reducing groups as well as a characteristic interfering color.

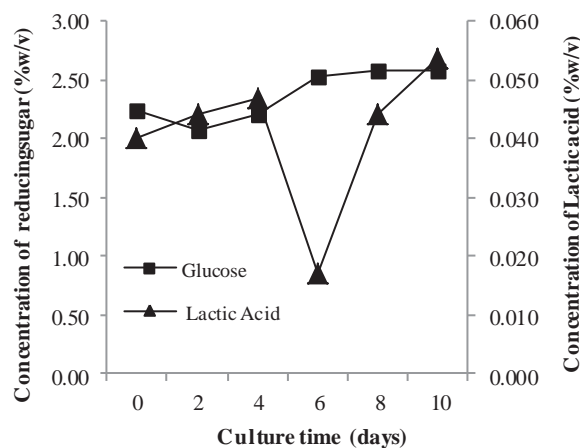


Figure 3 Reducing sugar consumption and lactic acid during fermentation of corn hull hydrolysate

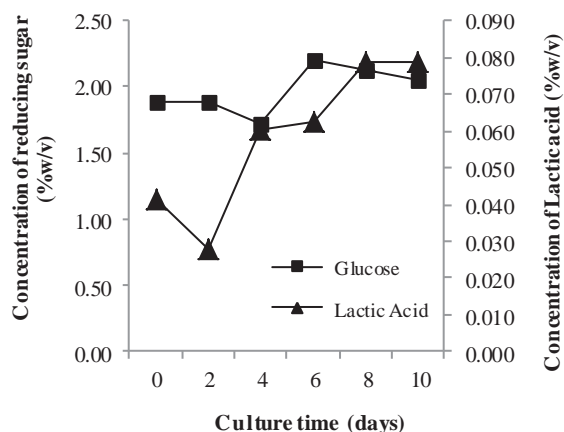


Figure 4 Reducing sugar consumption and lactic acid during fermentation of corncob hydrolysate

4. Conclusions

Lactic acid production by *P. pentosaceus* was done by using corn hull and corncob as substrates. It was found that, substrate pretreatment is necessary for increasing of reducing sugar. Corn hull and corncob were hydrolyzed by diluted sulfuric acid. Reducing sugar was increased up to 44 times in pretreated substrate compared to untreated. The amount of lactic acid produced in the fermentation using corn hull and corncob as substrate were detected as 0.054 and 0.079 % w/v respectively. For further study, partial purification of lactic acid will be done using Amberlite IRA-67 column chromatography.

Acknowledgements

The authors would like to thank Lanna Product Company in Lamphun Province for raw materials donation and this research work was supported by Center of Excellence for Innovation in Chemistry (PERCH-CIC).

Reference

- [1] J. Tuominen, J. Kylmä, A. Kapanen, O. Venelampi, M. Itävaara and J. Sappala, *Biomacromolecules*, 3 (2002), pp. 445-455.
- [2] L. Olsson and B. Hahn-Hägerdal, *Enzyme Microb. Technol.*, 18 (1996), pp. 312-331.
- [3] J.C. Parajo, J.L. Alonso and V. Santos, *Process Biochem.*, 31 (1996), pp. 271-280.
- [4] S.I. Mussatto and J.A. Telxeira, *Appl. Microbiol. And Microb. Biotechnol.*, (2010), pp. 897- 907.
- [5] T.B. VickRoy, Lactic Acid. In: *Comprehensive Biotechnology*, Vol. 3, Moo-Young M. (Eds.), Pergamon Press, New York, USA (1958).
- [6] K. Hofvendahl and B. Hahn-Hägerdal, *Enzyme Microb. Technol.*, 26 (2000), pp. 87-107.
- [7] T.D. Thomas, D.C. Ellwood and M.C. Longyear, *J. Bacteriol.*, 138 (1979), pp. 109-117.
- [8] S.B. Barker and W.H. Summerson, *J. Biol. Chem.*, 138 (1941), pp. 535-554

- [9] G.H. Horton, D.B. Rivers and G.H. Emert, *Ind. Eng. Chem. Prod. Res. Dev.*, 19 (1980), pp. 422

ANTIBACTERIAL ACTIVITY AND CYTOTOXICITY OF ANTIBIOTICS IMPREGNATED NANOSILVER-DOPED CALCIUM PHOSPHATE BONE GRAFT

Watchara Chokevivat, Faungchat Thammarakcharoen, Waraporn Suvannapruk,
Phetrung Phanphiriya, Jintamai Suwanprateeb*

National Metal and Materials Technology Center, National Science and Technology Development Agency,
114 Paholyothin Road, Klong 1, Klongluang, Pathumthani, 12120 Thailand

* Author for correspondence; E-Mail: jintamai@mtec.or.th, Tel. +66 2 5646500, Fax. +66 2 5646446

Abstract: It was shown that antibiotics impregnated calcium phosphate could provide an effective means for bone infection treatment by providing local, sustained and high concentrations of antimicrobial agents to the area of infected bone without systemically exposing the patient to high antibiotic levels that would cause toxic side effects while also function as a bone graft for new bone formation in the injured area eliminating the need for secondary reconstruction by additional grafting materials. Apart from antibiotics, silver has been known to possess inhibitory and antibacterial properties against a broad spectrum of bacterial strains while being relatively low toxic to human cells. Unlike antibiotics, silver is less prone to cause the resistance of bacteria. Recently, nanosilver has increasingly gained much interest due to its unique properties resulting from the nanoscale features and the ability to rapidly release of several silver species. It is envisioned that by combining both antibiotics and nanosilver could provide the synergic effect on bacterial eradication performance. In this study, nanosilver loaded calcium phosphates which were prepared by a novel low temperature phosphorization of 3D printed calcium sulfate dihydrate at the nanosilver concentration of 0.001 M and 0.005 M were impregnated by two antibiotics namely gentamicin (CN) and vancomycin (VC) under vacuum condition. Antibacterial activity of the samples against two bacterial strains (Gram negative *Pseudomonas aeruginosa* and Gram positive *Staphylococcus aureus*) was carried out by agar diffusion of the extraction at different periods. It was found that the combination of antibiotics and nanosilver could enhance the antibacterial activity of the samples by increasing the duration which the materials exhibited antibacterial property and the size of the inhibition zone for both bacterial strains compared to those of using antibiotics alone. Cytotoxicity against osteoblast of the samples as determined by MTT assay showed that no cytotoxic potential (cell viability > 70 %) at all extraction periods was observed for VC sample. However, 0.001 M nanosilver doped VC sample showed cytotoxic potential at day 1 extraction while 0.005 M doped VC sample showed cytotoxic potential even at day 3 extraction (cell viability \approx 30 %). CN sample and 0.005 M nanosilver CN sample displayed cytotoxic potential at day 1 extraction whereas cytotoxic potential was observed until day 2 extraction for 0.001 M nanosilver CN sample. Greater amount of nanosilver and antibiotics loading tended to enhance the antibacterial performance, but also increased the cytotoxic potential of the samples.

1. Introduction

Infection is a common incidence that could occur after surgical intervention. Treatment is usually carried out by systemic intravenous injection of antibiotics. However, in the case of bone tissue, the limited blood circulation normally results in poor antibiotic distribution at the infection regions. High dose and prolong injection are; thus, needed for effective eradication of the bacteria which can induce toxicity to the patients. Polymethylmethacrylate (PMMA) is used successfully with antibiotics impregnation for treating bone infection. However, several problems have been associated with PMMA use, including the requirement for material removal by a second surgical procedure and poor antibiotic elution properties. It was proposed that antibiotics impregnated calcium phosphate could also provide an effective means for bone infection treatment by providing local, sustained and high concentration of antimicrobial agents while also function as a bone graft for new bone formation in the injured area [1-5]. Apart from antibiotics, several metallic ions especially silver ions were known to possess inhibitory and antibacterial properties against a broad spectrum of bacterial strains while being relatively low toxic to human cells [6-8]. Silver is also less prone to cause the resistance of bacteria which is an advantage compared to antibiotics. Recently, silver nanoparticles have increasingly been used and gained much interest for infection treatment due to its unique properties resulting from the nanoscale features and the ability to rapidly release of several silver species which were seen to improve the treatment efficiency [7, 9]. It is thought that the combination of both antibiotics and nanosilver could provide the synergic effect on antibacterial performance. In this study, nanosilver-doped calcium phosphates were; thus, impregnated with two types of antibiotics including gentamicin and vancomycin. Their antibacterial activity and cytotoxicity of the samples were determined and compared with un-doped samples.

2. Materials and Methods

2.1 Materials

Raw materials used in this study were calcium sulfate hemihydrate (Lafarge Prestia Co.,Ltd, Thailand) and pre-gelatinized starch (Thaiwah Co.,Ltd, Thailand). These materials were supplied in the form of powders and used without further sieving. Antibiotics used were gentamicin sulfate (T.P Drug Laboratories (1969) Co., Ltd) and vancomycin hydrochloride (CJ CheilJedang Corporation, Korea), abbreviated as CN and VC respectively. Chemical structures of these antibiotics and their properties are shown in table 1 and figure 1.

Table 1: Properties of antibiotics used in this study [10].

| Antibiotics | Spectrum of activity | Molecular mass [g.mol ⁻¹] |
|-------------|------------------------------|---------------------------------------|
| Gentamicin | Gram positive /Gram negative | ≈ 723 |
| Vancomycin | Gram positive | ≈ 1486 |

2.2 Sample preparation

Calcium sulfate hemihydrate powders was mixed with pre-gelatinized starch powders using a mechanical blender and loaded into a three dimensional printing machine (Z400, Z Corporation) to print 7 mm in diameter spherical specimens. Water-based binder was used as a jetting media. The as-fabricated samples were then transformed to nanosilver-doped calcium phosphate by phosphorization reaction. Solutions containing 1M of disodium hydrogen phosphate (Fluka) and two concentration of silver nitrate (BDH) and glucose (Merck) (0.001 and 0.005 M) were prepared, designated CaP_001 and CaP_005 respectively. Ammonium (BDH) was then added dropwise to the solution until clear solutions were obtained. The fabricated 3DP beads were then immersed in the solution and kept at 80 °C for 24 hours in the air circulated oven. Samples were then taken out, rinsed by distilled water and oven dried. The calcium phosphate beads were then loaded with two types of antibiotics; using vacuum-assisted method similarly to previous studies [3-5].

2.3 Characterization

Microstructures of nanosilver loaded calcium phosphate samples were examined using a transmission electron microscope (JEOL JEM-2010). All samples were grinded into powders and then dispersed onto continuous carbon film grids prior to observation. The total antibiotics concentration in the sample beads were determined by elution in 2.4 M HCl and analysed by using UV-VIS spectrophotometer (Jasco V-530). In the case of antibacterial and cytotoxicity test, all the samples were sterilized by ethylene oxide gas prior to the tests. Antimicrobial

susceptibility test were carried out by modified agar diffusion assay. Two bacterial strains (Gram negative *Pseudomonas aeruginosa* ATCC 27853 and Gram positive *Staphylococcus aureus* ATCC 25923) were inoculated on each agar plates. The sample beads were submerged in simulated body fluid (SBF) at 37 °C for 10 days and the beads were withdrawn and placed in a new SBF at every 24 hours. Each eluates were placed in the bored holes in the agar plates and incubated at 37 °C. Antibiotic assay was performed by measuring inhibition zone by a venier caliper. In the case of cell cytotoxicity, each sample bead was incubated in 1 ml of DMEM (Biowhittaker) completed medium at 37 °C for 3 days. The eluates were drawn at 24, 48 and 72 hours with replenishment of a new medium after each eluate aspiration. The elutes were then added to each tissue culture dish which contained 1x10⁵ human osteoblast cells per one milliliter of DMEM medium and incubated for 24 hours. After incubation, 100 µl of 0.5 mg ml⁻¹ MTT (Sigma-Aldrich) was added in each well and incubated for another 2 hours. Dimethyl sulfoxide was then added and transferred to a 96-well plate. Optical density was measured at the wavelength of 570 nm using a microplate reader (Easys Model UVM 340) to quantify the cell viability.

3. Results and Discussion

Figure 1 shows the typical microstructures of fabricated nanosilver-doped calcium phosphate samples, CaP_001 and CaP_005, which similarly comprised the nanosized crystals of calcium phosphate with the distribution of spherical-shaped silver nanoparticles within the cluster. Larger silver particles were observed in CaP_005 compared to CaP_001. Figure 2 shows the total antibiotics loading in the nanosilver-doped calcium phosphate at different silver content. It could be seen that drug loading in pure calcium phosphate samples was greater than nanosilver-doped samples for both type of antibiotics. In the case of vancomycin, the drug content in CaP_VC_001 was lower than that of CaP_VC_005. In contrast, the drug content in CaP_CN_001 was greater than that of CaP_CN_005. This difference in drug loading efficiency could be related to the microstructure of the fabricated samples. The increase in degree of silver incorporation tended to decrease the adsorption sites for the drugs in the samples due to the greater in number and size of formed silver particles which could obstruct the diffusion of antibiotics solution into the samples. In the case of VC samples, the re-increase in antibiotics content in CaP_VC_005 was noted. Further investigation is needed to clarify this observation, but it is possibly related the greater gelling tendency of vancomycin on the surface of the samples than gentamicin.

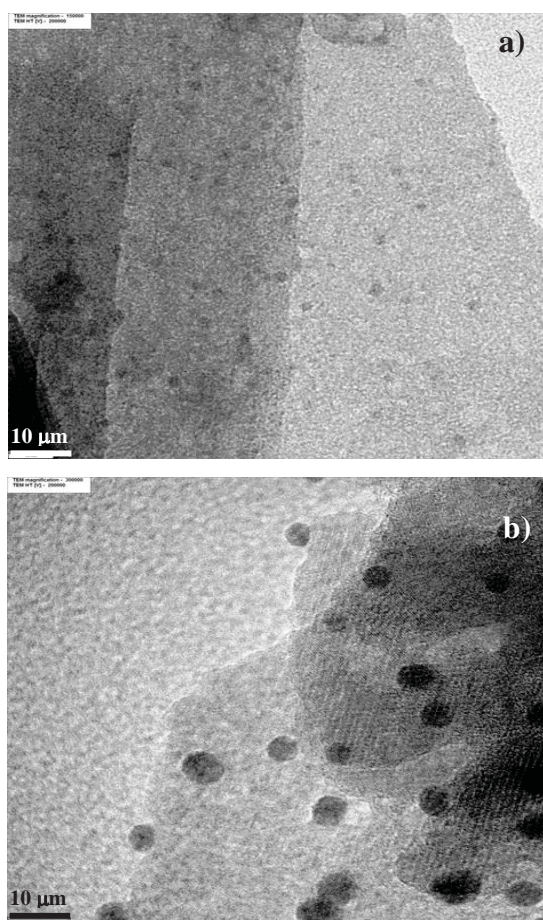


Figure 1. TEM images of fabricated nanosilver-doped calcium phosphates; a) CaP_001; b) CaP_005.

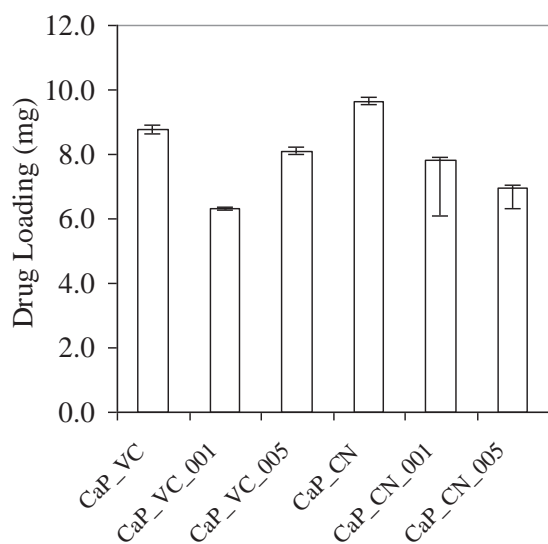


Figure 2. Total antibiotics content in the calcium phosphate and nanosilver-doped calcium phosphate samples.

Figures 3-4 show the antimicrobial profiles as indicated from the inhibition zone or clear zone on the agar plate against two bacterial strains, *Pseudomonas aeruginosa* and *Staphylococcus aureus* respectively. It was found that pure calcium phosphate (without

antibiotics) had no bactericidal properties at all extraction periods against both bacterial strains since no inhibition zone was observed (data not shown). In the case of *Pseudomonas aeruginosa*, inhibition zone was seen for CaP_CN, but not observed for CaP_VC sample since vancomycin was known to be inactive against gram negative strains [10]. After loading with nanosilver, the inhibition zone could be observed for all samples with the increase in antibacterial duration with increasing silver content especially for vancomycin loaded samples. In the case of *Staphylococcus aureus*, inhibition zones were seen for all samples. The antibacterial performance of CaP_VC and CaP_VC_001 did not differ much, but CaP_VC_005 showed longer antibacterial duration. In contrast, both CaP_CN_001 and CaP_CN_005 showed significantly longer antibacterial duration than CaP_CN sample. The combination of nanosilver and gentamicin seemed to give greater enhancement than vancomycin. This is possible due to the greater spectrum of activity, lower molar mass and lower minimum inhibitory concentration (MIC) of gentamicin [11].

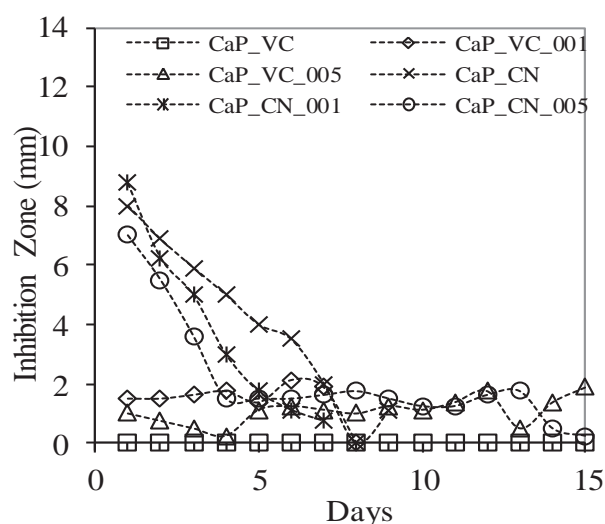


Figure 3. Antibacterial profile of antibiotics impregnated calcium phosphate and nanosilver-doped calcium phosphate (*Pseudomonas aeruginosa* ATCC 27853).

Cytotoxicity test indicated that no cytotoxic potential at all extraction periods was observed for CaP_VC sample since the cell viability levels was above 70 % (figure 5). However, CaP_VC_001 sample showed cytotoxic potential at day 1 extraction while CaP_VC_005 sample showed cytotoxic potential even at day 3 extraction. The increase in silver content and vancomycin loading in samples might be the cause of the increase in cytotoxic potential of CaP_VC_001 and CaP_VC_005 samples. In the case of gentamicin impregnated samples, CaP_CN and CaP_CN_005 samples displayed cytotoxic potential at day 1 extraction whereas cytotoxic potential was observed until day 2 extraction for CaP_CN_001 sample. This might be due to the synergistic effect of both toxicity potential of

gentamicin and nanosilver in CaP_CN_001 compared to the toxicity potential of gentamicin only in CaP_CN and lower gentamicin content and higher silver content in CaP_CN_005.

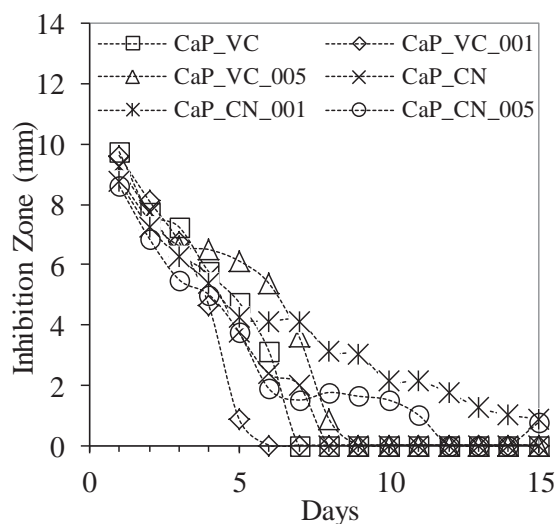


Figure 4. Antibacterial profile of antibiotics impregnated calcium phosphate and nanosilver-doped calcium phosphate (*Staphylococcus aureus* ATCC 25923).

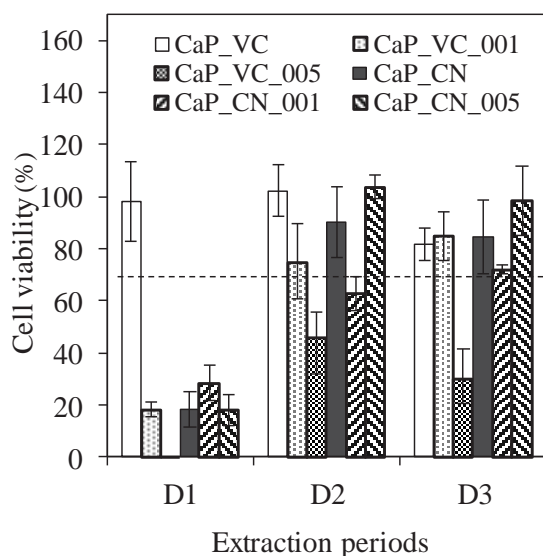


Figure 5. Cell viability of antibiotics impregnated nanosilver-doped calcium phosphate samples using serial extraction technique.

4. Conclusions

It could be concluded that the combination of nanosilver and antibiotics could enhance the antibacterial performance of the calcium phosphate samples. The enhancement depended on the type and loading of antibiotics and nanosilver concentration. Greater content of nanosilver and antibiotics loading tended to increase the antibacterial performance, but also increased the cytotoxic potential of the samples.

Acknowledgements

Lafarge Prestia Co.,Ltd, Thailand is thanked for the supply of calcium sulfate and Thaiwah Co.,Ltd, Thailand for the supply of pre-gelatinized starch. Cluster and Program Management Office, National Science and Technology Development Agency is acknowledged for financial support.

References

- [1] M. Diefenbeck, T. Mückley and G.O. Hofmann, *Injury*. **37** (2006) S95-S104.
- [2] G.H.I.M. Walenkamp, L.L.A. Kleijn and M. de Leeuw, *Acta. Ortho.* **69** (1998) 518-522.
- [3] P. Phanphiriya, W. Suwannapruk, B. Chernchujit, Y. Siripakarn, T. Suntharapa and J. Suwanprateeb, *Antimicrobial Property of Gentamicin Loaded 3DP Calcium Phosphate Sphere*, 7th Thailand Materials Science and Technology Conf. Proc., Bangkok, Thailand (2010), pp. 406-408.
- [4] F. Thammarakcharoen and J. Suwanprateeb, *The effect of bead size on drug loading and releasing characteristic of antibiotic loaded 3DP calcium phosphate bead*, Pure and Applied Chemistry International Conf. Proc., Bangkok, Thailand (2011), pp. 473-476.
- [5] P. Phanphiriya, F. Thammarakcharoen, W. Chokevivat and J. Suwanprateeb., *Adv. Mater. Res.* **506** (2012) 513-516.
- [6] C. Marambio-Jones and E.M.V. Hoek., *J. Nanopart. Res.* **12** (2010) 1531-1551.
- [7] S. Sarkar, A. D. Jana, S. K. Samanta and G. Mostafa., *Polyhedron*. **26** (2007) 4419-4426.
- [8] R. Janardhanana, M. Karuppaiah, N. Hebalkara and T. N. Rao., *Polyhedron*. **28** (2009) 2522-2530.
- [9] H. Q. Yin, R. Langford and R. E. Burrell., *J. Burn Care Rehabil.* **20** (1999) 195-200.
- [10] O.S. Kluin, H.C. van der Mei, H.J. Busscher and D. Neut., *Biomaterials*. **30** (2009) 4738-4742.
- [11] S. Alvarez, M. Jones and S. L. Berk., *Antimicrob. Agents Chemother.* **Nov.** (1985) 689-?.

CHARACTERISTICS AND CELL RESPONSES ON SILK FIBROIN FILM PREPARED FROM THREE THE SILKWORMS, *Bombyx Mori*

Kanyaluk Kaewprasit¹, Amornrat Promboon² and Siriporn Damrongsakkul^{1*}

¹ Department of Chemical Engineering, Faculty of Engineering, Chulalongkorn University, Bangkok, 10330 Thailand

² Department of Biochemistry, Faculty of Science, Kasetsart University, Bangkok, 10900 Thailand

* Author for correspondence; E-Mail: siriporn.d@chula.ac.th, Tel: +66-2-2186862, Fax: +66-2-2186877

Silk is a natural material composed of two proteins. The core structural protein is fibroin and the glue-like protein that holds fibroin fiber together so called sericin. Silk fibroin has been increasingly studied because of its biocompatibility, good mechanical properties, comparing to other natural materials, and slow biodegradation rate. Silk cocoons derived from the silkworm, *Bombyx mori* are of the most widely studied silk species in tissue engineering. In the present study, we aimed to compare the characteristics of three silkworm races, including Thai race (Nangnoi-Srisaket 1; NN), Japanese race (K1) and Chinese race (K8). The thermal property in term of degradation temperature of silk fibroin films was investigated by thermogravimetric analyzer (TGA). The difference in degradation temperature among silk fibroin films could not be observed. For the chemical conformation, beta-sheet structures of silk fibroin films were examined by fourier transform infrared spectrophotometer (FTIR). The determination of amino acid composition of three silk fibroins showed that the main amino acid residues of silk fibroin were glycine (Gly), alanine (Ala), serine (Ser) and tyrosine (Tyr). The amino acid composition of three silk fibroins showed slightly different. The *in vitro* attachment and proliferation of rat bone marrow-derived stem cells (MSC) cultured on three different fibroin films were evaluated. It was found that the numbers of cell attached and proliferated on tissue culture plate were significantly higher than those cultured on all silk fibroin films. Japanese fibroin film (K1) was found to promote cell attachment and proliferation of MSC slightly greater than fibroin films prepared from other silkworm races, although the significant difference among fibroins derived from three silkworm races was not observed.

1. Introduction

Many natural proteins have been studied for their mechanical, chemical, electrical and electromagnetic properties. Elastins, collagens, silks, keratins, and resilins are ones of the most common proteins widely studied as protein-based biomaterials [1]. Silk fibroin has been used in a wide variety of biomedical applications, for example, surgical suture or scaffolds to promote cell growth and tissue regeneration [2]. Silk fibroin derived from the *Bombyx mori* silkworm is of the most widely studied silk species in tissue engineering. For the general domesticated *Bombyx mori* silkworm, silk fibroin fibers consist of two proteins: a light chain (26 kDa) and a heavy chain (390 kDa) which are presented in a 1:1 ratio and linked by a single disulfide bond. These proteins are coated with a family of hydrophilic proteins called sericins (20 – 310

kDa) [3]. The amino acid components of silk fibroin including glycine, alanine, serine and tyrosine form antiparallel β -sheets in the spun fibers, leading to the stability and mechanical features of the fibers [4].

In Thailand, the domesticated *Bombyx mori* silkworm, especially Nangnoi-Srisaket 1, has recently studied by many researchers. Chamchongkaset et al. [5] developed three-dimensional silk fibroin-based scaffolds from Nangnoi-Srisaket 1 silkworms using salt-leaching method. The scaffolds were conjugated with type A gelatin and *in vitro* test was studied using mouse preosteoblast cell line (MC3T3-E1). The results showed that gelatin conjugation could promote the cell proliferation in silk fibroin-based scaffolds. Vachiraroj et al. [6] have fabricated the hybrid scaffolds from silk fibroin (Nangnoi-Srisaket 1), gelatin, lowdeacetylation degree chitosan and hydroxyapatite (HA). *In vitro* biocompatibility and osteoconductivity of these materials were investigated using MC3T3-E1 and rat bone marrow-derived stem cells (MSC). Also, they concluded that protein-based material showed high potential to promote cell attachment and proliferation while HA hybrid materials supported osteogenic differentiation.

From other countries, the *Bombyx mori* silkworm was also studied. Kim et al. [7] used silk fibroin supplied by Institute of Sericulture in Japan to prepare silk fibroin scaffolds with the addition of polyaspartic acid during processing. These mineralized protein-composite scaffolds were subsequently seeded with human bone marrow stem cells (hMSC) and cultured *in vitro* for 6 weeks under osteogenic conditions with or without BMP-2. The results suggest increased osteoconductive outcomes with an increase in initial content of apatite and BMP-2 in the silk fibroin porous scaffolds. She Z. et al. [8] used the silk cocoons purchased from Yi Xian Raw Silk Factory in China to fabricate the three-dimensional porous silk fibroin/chitosan (SFCS) scaffolds by freeze-drying technique. SFCS scaffolds degraded quickly during the first 2 weeks, and the weight loss reached 19.28 wt% after 8 weeks of degradation.

Because there are several *Bombyx mori* silkworm races obtained from different sources, in this work, the comparison on the characteristics and cell responses of silk fibroin from three *Bombyx mori* silkworm races, including Thai race (Nangnoi-Srisaket 1; NN), Japanese race (K1) and Chinese race (K8) were studied. Thermal property, chemical conformation, and

amino acid composition of silk fibroin were evaluated. Rat bone marrow-derived stem cells (rMSC) were cultured on three different silk fibroin films in order to investigate the attachment and proliferation, comparing to those culture on tissue culture plate (TCP).

2. Materials and Methods

2.1 Materials

Bombyx mori cocoons, including Thai race (Nangnoi-Srisaket 1; NN), Japanese race (K1) and Chinese race (K8) were kindly given by Queen Sirikit Sericulture Center, Nakornratchasima province, Thailand. Other chemicals used in this study were analytical grade.

2.2 Preparation of silk fibroin solution

Silk fibroin solution was prepared as described by Kim et.al. [7]. Briefly, cocoons were boiled in an aqueous solution of 0.02 M Na₂CO₃ and then rinsed thoroughly with deionized water to remove sericin protein. After drying, the degummed silk fibroin was dissolved in 9.3 M LiBr solution at 60 °C for 3-4 h. The solution was dialyzed against deionized water using cellulose dialysis bag (MWCO 12000 - 16000, Viskase Companies Inc., Japan) for 2 days until the conductivity of dialyzed water was the same as that of deionized water. The solution was centrifuged at 10,000 rpm to remove the small amount of silk residue that formed during the process. The final concentration of silk fibroin aqueous solution was about 6.5-7.0 wt%.

2.3 Preparation of silk fibroin film

To prepare films for the physicochemical characterizations, the silk fibroin solution was cast onto a teflon mold. For the *in vitro* cell culture test, silk fibroin solution was diluted to 0.5wt% and cast onto 24-well tissue culture plate (TCP). The silk fibroin films were obtained after air drying overnight. Then, the silk fibroin films were immersed in 70 vol% methanol for 30 min to induce the conformation change of silk fibroin from random coil to β -sheet.

2.4 Physicochemical characterizations

The degradation temperature (T_d) of different silk fibroins was analyzed by thermogravimetric analyzer (TGA Q50, TA Instrument, USA). The test was performed under a nitrogen atmosphere with a gas flow of 90 ml/min and heated up to 700 °C at the heating rate of 10 °C/min.

FTIR spectra of the silk fibroin films were analyzed by fourier transform infrared spectrometer (Spectrum GX, Perkin Elmer, UK) in the spectral region of 2500 – 750 cm⁻¹ with an attenuated total reflection mode (ATR) to determine the conformations of silk fibroin films.

Amino acid compositions of different silk fibroins were analyzed using high performance liquid chromatography (LC-10A, Shimadzu Corporation, Japan). Each sample was analyzed twice. The

quantitative amino acid composition, determined by external standard calibration, was expressed as mol% for each amino acid.

2.5 Isolation and culture of rat bone marrow-derived mesenchymal stem cells

Rat bone marrow-derived mesenchymal stem cells (MSC) were isolated from the bone shaft of femurs of 3-week-old Wistar rats according to the technique reported previously [9]. Briefly, after cutting off both ends of rat femurs, the bone marrow was flushed out with 1 ml of Alpha-modified Eagle minimal essential medium (α -MEM). After that, the cell suspension was cultured in tissue culture plate containing α -MEM supplemented with 15 vol% fetal bovine serum (FBS) and 100 U/ml penicillin/streptomycin at 37 °C in a 5% CO₂ condition. The medium was refreshed on the 4th day after isolation to remove non-adherent cells and continuously refreshed every 3 days. The cells of passages 2–3 at the sub confluent condition were used for the following experiments.

2.6 *In vitro* attachment and proliferation tests

MSC were seeded onto the silk fibroin films at 2×10^4 cells/film for adhesion and proliferation tests and incubated at 37 °C in a 5% CO₂. Cells cultured on TCP at the same conditions were served as control. After culture for 6, 24, 72, 120 h, the number of cells was evaluated using MTT assay [10]. Briefly, MTT was first prepared as a stock solution of 0.5 mg/ml in phosphate buffer (PBS, pH 7.4). To prepare for MTT measurement, the culture media was removed from the well plate. The plates were washed with PBS. Then 350 μ l of MTT solution was added. The well plates were incubated at 37°C, 5% CO₂ for 30 min. After removing MTT solution, DMSO was added to elude the purple ice crystals of MTT. The absorbance of the solution was measured at 570 nm using a micro plate reader (Perkin Elmer, 1420 multilabel counter, USA). All data were expressed as mean \pm SD (n = 4). The percentage of cell attachment was calculated according to the following equation where N_1 and N_0 are the numbers of cells attached at 6 h and initial seeded, respectively [11].

3. Results and Discussion

3.1 Physicochemical characteristics of different silk fibroins

The degradation temperature of silk fibroin films from three silkworm races were shown in Table 1. The degradation temperature (T_d) of NN film was at 264.8 °C while those K1 and K8 films were at 264.2 °C and 265.0 °C, respectively. The difference in degradation temperature of different silk fibroin films could not be obviously noticed.

Table 1: The degradation temperature (T_d) of *Bombyx mori* silk fibroin films from three silkworm races.

| Silkworm races | T_d (°C) |
|-------------------------|------------|
| Nangnoi-Srisaket 1 (NN) | 264.8 |
| Japanese race (K1) | 264.2 |
| Chinese race (K8) | 265.0 |

The conformation of silk fibroin films investigated by ATR-FTIR was shown in Figure 1. It could be seen that three peak positions including amide I (C=O stretching), amide II (N-H deformation and C-N stretching) and amide III (C-N stretching and N-H deformation) were found at 1610–1630 cm^{-1} , 1510–1520 cm^{-1} , and 1230 - 1270 cm^{-1} , respectively. These amide bands were attributed to the secondary structure (β -sheet) of protein as previously reported [12–14]. ATR-FTIR results revealed that the structure of silk fibroin films from three silkworm races were similar.

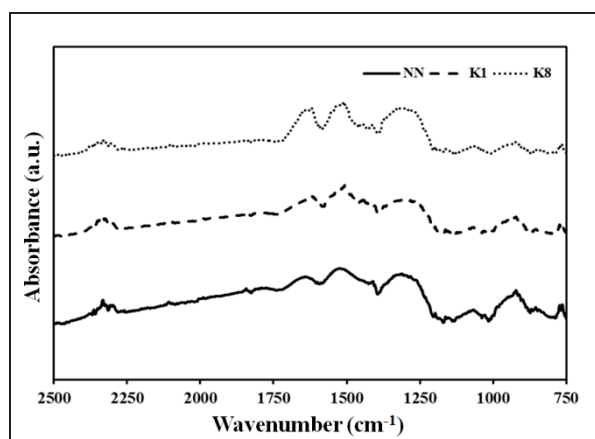


Figure 1. FTIR spectra of silk fibroin films from three silkworm races, (—) Nangnoi-Srisaket 1 : NN, (---) Japanese race : K1 and (.....) Chinese race: K8.

The amino acid compositions of *Bombyx mori* silk fibroin from three silkworm races were demonstrated in Table 2. The common amino acids of all silk fibroin were alanine, glycine, serine and tyrosine. The amino acid components were classified into 2 groups; hydrophilic and hydrophobic groups. The percentage of hydrophilic amino acid groups in K1 (22.93%) was similar to K8 (22.83%) while that of NN (18.33%) was lowest. On the other hand, NN (81.67%) contained higher percentage of hydrophobic amino acid groups than other two silkworm races, indicating the most hydrophobicity of NN.

Table 2: Amino acid composition (% by mole) of *Bombyx mori* silk fibroin from three silkworm races (Nangnoi-Srisaket 1: NN, Japanese race: K1 and Chinese race: K8).

| | NN | K1 | K8 |
|--------------------|-------|-------|-------|
| Hydrophilic | | | |
| Acidic | | | |
| Aspartic acid | 1.63 | 2.08 | 2.18 |
| Glutamic acid | 1.15 | 1.52 | 1.51 |
| Basic | | | |
| Arginine | 0.30 | 0.31 | 0.44 |
| Lysine | 0.20 | 0.26 | 0.30 |
| Histidine | 0.83 | 0.81 | 1.02 |
| Polar | | | |
| Serine | 13.42 | 16.87 | 16.30 |
| Threonine | 0.80 | 1.08 | 1.08 |
| Cysteine | - | - | - |
| Total | 18.33 | 22.93 | 22.83 |
| Hydrophobic | | | |
| Non- polar | | | |
| Glycine | 38.32 | 33.00 | 35.76 |
| Alanine | 34.29 | 31.26 | 29.39 |
| Proline | 0.42 | 0.64 | 0.64 |
| Valine | 1.15 | 1.67 | 1.53 |
| Leucine | 0.27 | 0.38 | 0.43 |
| Isoleucine | 0.20 | 0.31 | 0.32 |
| Methionine | 0.08 | 0.13 | 0.10 |
| Aromatic | | | |
| Tyrosine | 5.75 | 7.66 | 7.16 |
| Phenylalanine | 0.98 | 1.69 | 1.39 |
| Tryptophan | 0.21 | 0.33 | 0.45 |
| Total | 81.67 | 77.07 | 77.17 |

3.3 *In vitro* attachment and proliferation of MSC on silk fibroin films

The number of MSC attached and proliferated on silk fibroin films were presented in Figure 2. There was no significant difference in the number of cells attached on different silk fibroin films after 6 h of culture. At 24, 72 and 120 h of culture, the number of cells proliferated on K1 films was slightly greater than other silk fibroin films, however, the significant difference was not found. On the other hand, cells attached and proliferated on TCP showed the greatest number along culture period.

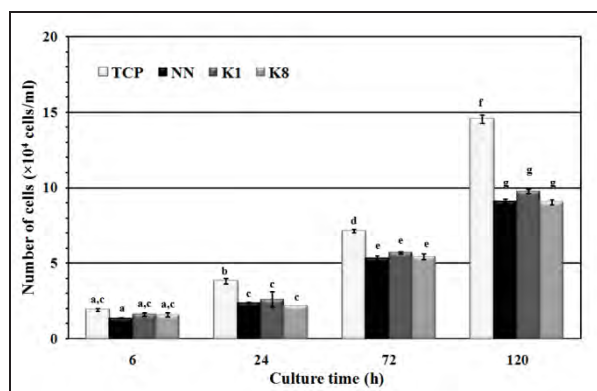


Figure 2. The number of MSC attached and proliferated on silk fibroin films prepared from three silkworm races (Nangnoi-Srisaket 1: NN, Japanese race: K1 and Chinese race: K8) and tissue culture plate (TCP). a - g represented significant difference among samples at $p < 0.05$.

Table 3 presented the percentage of cell attachment. The percentage of cell attachment on TCP was highest (95.6 ± 5.1), while those of NN, K1 and K8 films were at 68.9 ± 1.9 , 81.1 ± 5.1 and 78.9 ± 6.9 , respectively. The percentage of cell attachment on K1 film was slightly higher than other two silk fibroin films. On the other hand, NN film showed the lowest percentage of cell attachment. This might be related to hydrophilic/hydrophobic properties of silk fibroins. Yang et al. [15] reported that a material's hydrophilicity enhanced the absorption of fibronectin, which is essential for the adhesion of osteoblast in vitro. There were two phases in the process of cell attachment. The first is non-specific adsorption of cells on the materials mainly mediated by the physico-chemical interaction between cells and materials. Hydrophilicity contributes to this physicochemical interaction. When material surfaces are exposed to a dilute serum, hydrophilic surfaces are better than hydrophobic surfaces for cell attachment, spread, and cytoskeletal organization. The second phase is the specific adsorption of cells on the materials. After non-specific adhesion, cells will secrete some extracellular matrix (ECM) which can be adsorbed on the material surface, then bind the integrins on the surface of cells, and mediate the specific interaction between cells and materials. Therefore, in this study, the hydrophilic surface of K1 and K8 films might promote the attachment of MSC rather than the more hydrophobic surface of NN film.

Table 3: The percentage of cell attachment on *Bombyx mori* silk fibroin films prepared from three silkworm races.

| Substrate | Cell attachment (%) |
|----------------------------|---------------------|
| Tissue culture plate (TCP) | 95.6 ± 5.1 |
| Nangnoi-Srisaket 1(NN) | 68.9 ± 1.9 |
| Japanese race (K1) | 81.1 ± 5.1 |
| Chinese race (K8) | 78.9 ± 6.9 |

4. Conclusions

In this work, the preliminary results of the physicochemical characteristics of three silkworm races including, Thai race (Nangnoi-Srisaket 1; NN), Japanese race (K1) and Chinese race (K8) showed that all silk fibroins had the similar conformation structure and degradation temperature. From amino acid composition analysis, Japanese race (K1) and Chinese race (K8) silk fibroins had the higher percentage of hydrophilic amino acid groups than Nangnoi-Srisaket 1 (NN) silk fibroin. After culture of cell attached and proliferated on Japanese race (K1) silk fibroin film was slightly greater than those of silk fibroin films prepared from other silkworm races (Nangnoi-Srisaket 1 and Chinese races), possibly due to the most hydrophilicity of Japanese race (K1) silk fibroin that could enhance biological functions. Although the significant difference among fibroins derived from three silkworm races was not observed.

Acknowledgements

Financial supports from The National Research University Project of CHE and the Ratchadaphiseksomphot Endowment Fund (AS615A-55) and Chulalongkorn University Centenary Academic Development Project are gratefully acknowledged. We thank Tanom Bunaprasert, M.D. for the use of cell culture facilities at i-Tissue Laboratory, Faculty of Medicine, Chulalongkorn University.

References

- [1] X. Hua, P. Cebe, A. S. Weiss, F. Omenetto and D.L. Kaplan, *Materialstoday*. **15** (2012) 208-215.
- [2] H. Mori and M. Tsukada, *Rev. Mol. Biotechnol.* **74** (2000) 95-103.
- [3] C. Vepari and D.L. Kaplan, *Prog. Polym. Sci.* **32** (2007) 991-1007.
- [4] U.J. Kim, J. Parka, H.J. Kima, M. Wada, D.L. Kaplan, *Biomaterials* **26** (2005) 2775-2785.
- [5] J. Chamchongkaset, S. Kanokpanont, D.L. Kaplan, S. Damrongsakkul, *Advanced Materials Research* **55-57** (2008) 685-688.
- [6] N. Vachiraroj, J. Ratanavaraporn, S. Damrongsakkul, R. Pichyangkura, T. Banaprasert, S. Kanokpanont, *Int. J. Biol. Macromol.* **45** (2009) 470-477.
- [7] H.J. Kim, U.J. Kim, H.S. Kim, C. Li, M. Wada, G.G. Leisk and D.L. Kaplan, *Bone* **42** (2008) 1226-1234.
- [8] Z. She, B. Zhang, C. Jin, Q. Feng and Y. Xu, *Polym. Degrad. Stabil.* **93** (2008) 1316-1322.
- [9] Y. Takahashi, M. Yamamoto and Y. Tabata, *Biomaterials*. **26** (2005) 3587-3596.
- [10] T. Mosmann, *J. Immunol. Methods*. **65** (1983) 55-63.
- [11] I. Prasertsung, S. Kanokpanont, R. Mongkolnavin, C. S. Wong, J. Panpranot and S. Damrongsakkul, *Journal of Biomaterials Science*. **23** (2012) 1485-1504.
- [12] I. Taketani, S. Nakayama, S. Nagare, M. Senna, *Appl. Surf. Sci.* **244** (2005) 623-626.
- [13] A.R. Murphy, P. St. John, D.L. Kaplan, *Biomaterials*. **29** (2008) 2829 - 2838.

- [14] E. S. Gil, D. J. Frankowski, S. M. Hudson, R. J. Spontak, *Materials Science and Engineering C*. **27** (2007) 426–431.
- [15] M. Yang, S. Zhu, Y. Chen, Z. Chang, G. Chen, Y. Gong and N. Zhao, *Biomaterials*. **25** (2004), 1365–1373.

DEVELOPMENT OF SILK FIBROIN/GELATIN HYDROGELS FOR CONTROLLED RELEASE OF CURCUMIN

Kantarat Lerdchai¹, Jutarat Kitsongsermthorn², Juthamas Ratanavaraporn¹, Sorada Kanokpanont¹, Siriporn Damrongsakkul^{1*}

¹ Department of Chemical Engineering, Faculty of Engineering, Chulalongkorn University, Bangkok, 10330 Thailand

² Department of Pharmaceutics and Industrial Pharmacy, Faculty of Pharmaceutical Sciences, Chulalongkorn University, Bangkok, 10330 Thailand

* Author for correspondence; E-Mail: siriporn.d@chula.ac.th, Tel: +66-2-2186862, Fax: +66-2-2186877

Abstract: Gelatin (G), obtained by acid or alkaline hydrolysis of collagen, is extensively used for pharmaceutical and medical purposes because of its inexpensiveness biocompatibility, biodegradability, and water solubility. Silk fibroin (SF), a natural protein derived from *Bombyx mori* silkworm, is one of the most interesting biomaterials because of its non-toxicity, biocompatibility, remarkable mechanical properties, and slow biodegradation rate. In this study, silk fibroin extracted from Thai cocoons (Nangnoi Srisaket 1) and type A gelatin obtained by an acidic treatment of porcine skin collagen were used to fabricate hydrogels for a controlled release application. Curcumin, a medicinal herbal compound with an anti-cancer activity, was selected as a model drug. Silk fibroin and gelatin solutions were blended at different SF/G weight blending ratios of 0/100, 20/80, 50/50, 80/20 and 100/0, crosslinked with 0.2% v/v glutaraldehyde, and freeze-dried to obtain the SF/G hydrogels. Morphology of SF/G hydrogels was observed on a scanning electron microscope (SEM). The crosslinking degree of SF/G hydrogels was determined by 2, 4, 6-trinitrobenzenesulfonic acid (TNBS) method. The *in vitro* biodegradation of hydrogels in collagenase solution was assessed. The SF/G hydrogels were loaded with curcumin and the *in vitro* release of curcumin from hydrogels was evaluated. From the results, all SF/G hydrogels showed homogeneous porous structure. It was found that the crosslinking degrees of SF/G blended hydrogels at 20/80, 50/50 and 80/20 were significantly higher than those of pure silk fibroin and pure gelatin hydrogels. The pure gelatin hydrogels showed the fastest biodegradation. The release test demonstrated that the SF/G blended hydrogels at 20/80, 50/50 and 80/20 could control the release of curcumin, comparing to the pure silk fibroin and pure gelatin hydrogels. The highly crosslinked SF/G hydrogels showed slowly release of curcumin, possibly due to the slow biodegradability of hydrogels. Therefore, the SF/G blended hydrogels were introduced as alternative carriers for controlled release of curcumin.

1. Introduction

Controlled release system has been used to deliver drugs in order to achieve a therapeutic effect at a target site. The advantages of controlled release system are to reduce dose of drug required and avoid the side effect of drug to other organs. Various controlled release systems such as specially-designed tablets that can be taken orally, injectable microspheres or implants have been developed. [1, 2]. Both synthetic and natural

polymers are used as materials to prepared controlled release carriers. Natural polymers are widely studied due to their biocompatibility and biodegradability. Recently, the binary blends of natural polymers such as silk fibroin/gelatin [3] and hyaluronic acid/chitosan [4] were selected to fabricate the controlled release carriers.

Gelatin is a protein obtained by partial hydrolysis of collagen which is an insoluble fibrous protein mainly found in skin, bones and connective tissue [5, 6]. Gelatin is of interest due to its inexpensiveness and excellent biological properties such as biocompatibility and biodegradability [7]. However, the fast biodegradation rate of gelatin limits its applications [8]. Then, gelatin is modified through several methods such as crosslinking or blending with slow degrading materials like silk fibroin to extend its biodegradation rate [3].

Silk fibroin, a natural protein polymer, is derived from silkworm (e.g. *Bombyx mori*.) Recently, silk fibroin is one of the most attractive biopolymers used in biomedical applications because of its biocompatibility, slow biodegradation and remarkable mechanical properties [9, 10]. In addition, Silk fibroin is blended with other polymers such as hyaluronic acid, gelatin and collagen to enhance its biological functions [10, 11].

Curcumin, a yellow polyphenol extracted from the rhizome of turmeric (*Curcuma longa*), is known as a herbal compound with potent anti-inflammatory, anti-oxidant, and anti-cancer activities [12-14]. It was reported that curcumin induced apoptosis of various cancer cells such as colorectal, lung, breast, pancreatic and prostate carcinoma [15]. Curcumin was then selected as a model drug for the development of controlled release system in this study.

In this work, Thai silk fibroin/gelatin (SF/G) hydrogels at different SF/G weight blending ratios were fabricated by freeze-drying and glutaraldehyde crosslinking techniques. The morphology and *in vitro* biodegradation of the SF/G hydrogels were investigated. The *in vitro* release test of curcumin from the developed hydrogels was performed to demonstrate its controlled release behavior.

2. Materials and Methods

2.1 Materials

Thai silk cocoons, Nangnoi-Srisaket 1, were obtained from Queen Sirikit Sericulture Center, Nakornratchaima province, Thailand. Type A gelatin by an acidic treatment of porcine skin collagen was kindly supplied from Nitta Gelatin Inc., Japan. Curcumin was purchased from Sigma-Aldrich (USA). Other chemicals used in this study were analytical grade.

2.2 Preparation of silk fibroin aqueous solution

Silk fibroin solution was prepared using the method of Kim et al. [16]. In brief, Thai silk cocoons were boiled for 20 min in an aqueous solution of 0.02 M Na₂CO₃ and rinsed thoroughly with deionized water to remove sericin protein and wax. The fibroin fiber was dissolved in 9.3 M LiBr solution at 60°C for 4 h. This solution was dialyzed in deionized water for 2 days. The dialyzed water was changed regularly until its conductivity was the same as that of deionized water. The silk fibroin solution obtained was then centrifuged at 9,000 rpm, 4°C for 20 min to remove insoluble debris. The final concentration of silk fibroin solution was about 6.5-7% w/v.

2.3 Fabrication of silk fibroin/gelatin hydrogels

The concentration of silk fibroin solution was diluted to 4% w/v. Type A gelatin was dissolved in deionized water under agitation to obtain gelatin solution at a concentration of 4% w/v. The final concentration of SF/G blend solutions was fixed at 4% w/v and different weight blending ratios of SF/G (0/100, 20/80, 50/50, 80/20 and 100/0) were studied. After the blended solution was mixed under stirring for 20 min, glutaraldehyde solution was added in the solution at a final concentration of 0.2% v/v. The crosslinked SF/G solution was then frozen overnight prior to lyophilization for 72 h. The freeze-dried SF/G hydrogels were immersed with 0.1 M glycine solution for 3 h to block the residual aldehyde groups of glutaraldehyde and washed 3 times with deionized water for 15 min each. After refreeze-drying, the SF/G hydrogels were obtained.

2.4 Morphological observation

The cross-sectioned morphology of SF/G hydrogels was observed on a scanning electron microscope (SEM, JSM 5400, JEOL, Japan). The SF/G hydrogels were cross-sectioned, fixed on stubs and coated with gold prior to SEM observation.

2.5 Determination of crosslinking degree

The determination of crosslinking degree was performed using the modified method of Bubins et al. [17]. Briefly, One ml of 0.5% 2,4,6-trinitrobenzene sulphonic acid (TNBS) solution and one ml of 4% NaHCO₃ were added in the known-weight SF/G hydrogels. The mixture was heated at 40°C for 2 h. After that, 4 ml of 37% HCl solution was added and

heated at 60°C overnight. The absorbance of the solution was measured at 415 nm. The crosslinking degree was calculated as follows:

$$\text{Crosslinking degree (\%)} = (1 - A_c/A_n) \times 100$$

where A_c and A_n represented the absorbance of crosslinked and non-crosslinked hydrogel, respectively.

2.6 *In vitro* biodegradation test

The SF/G hydrogels (10 mg) were incubated in 1 U/ml collagenase solution (pH 7.4) containing 0.01% w/v sodium azide as an antibiotic at 37°C [11]. The enzyme solution was changed every 2 days to ensure continuous enzyme activity. At each pre-determined time, the remained hydrogels were taken out of the solution, rinsed repeatedly with deionized water, and freeze dried. The dried hydrogels were weighed and the percentage of remaining weight was calculated as follows:

$$\text{Remaining weight (\%)} = \frac{W_f}{W_i} \times 100$$

where W_f and W_i represented the final and initial weights of hydrogels, respectively.

2.7 *In vitro* release test of curcumin from hydrogels

Curcumin was dissolved in ethyl alcohol (99.9% v/v) to obtain a concentration of 0.3% w/v. The curcumin solution (100 µl) was loaded onto a SF/G hydrogel (5×5×3 mm³) by physical absorption. The hydrogels were left at 4°C for 12 h to allow complete adsorption. After air-drying at room temperature, the curcumin-loaded hydrogels were immersed in 1 ml of phosphate buffer saline (PBS, pH 7.4) containing 0.01% v/v of Tween 80 [18] and incubated at 37°C. At each pre-determined time, the PBS solution was collected and replaced with the equal volume of fresh PBS. The absorbance of curcumin released into the PBS solution was determined using a spectrophotometer at the wavelength of 430 nm [14]. The amounts of curcumin were obtained by comparing with the standard curve of curcumin prepared at different concentrations.

3. Results and Discussion

3.1 Morphology of Thai silk fibroin/gelatin hydrogels

The cross-sectioned morphology of SF/G hydrogels was showed in Figure 1. The homogeneous porous structure and interconnected pores were observed throughout the obtained hydrogels, which indicated that the SF/G hydrogels would be able to absorb and entrap curcumin in porous structure.

3.2 Crosslinking degree of SF/G hydrogels

The concept of determination of crosslinking degree by 2,4,6-trinitrobenzene sulphonic acid (TNBS) is to react with free amino groups in protein [17]. The crosslinking degree was calculated from the

concentration of free amino groups of hydrogels. Figure 2 and 3 illustrated free amine groups of non-crosslinked and crosslinked hydrogels and the crosslinking degree of hydrogels, respectively. It was found that the pure gelatin hydrogels showed the highest content of free amino groups for both non-crosslinked and crosslinked ones. The contents of free amino groups decreased along the increasing content of silk fibroin. It was noted that the contents of free amino groups of the SF/G blended hydrogels (20/80, 50/50, 80/20) dramatically decreased after the crosslinking, indicating their high crosslinking degrees.

From Figure 3, the crosslinking degrees of pure gelatin and pure silk fibroin hydrogels were 33% and 48%, respectively. Interestingly, the SF/G blended hydrogels had significantly higher crosslinking degrees than those of pure gelatin and pure silk fibroin hydrogels. This corresponded to the results of free amino groups. This indicated that glutaraldehyde could be used to crosslink both gelatin and silk fibroin by the reaction of free amino groups of lysine residues and the N-terminal amino groups of proteins with aldehyde groups of glutaraldehyde [8, 19]. Both gelatin and silk fibroin contained free amino acids, therefore, the SF/G blended hydrogels were crosslinked at the higher extent.

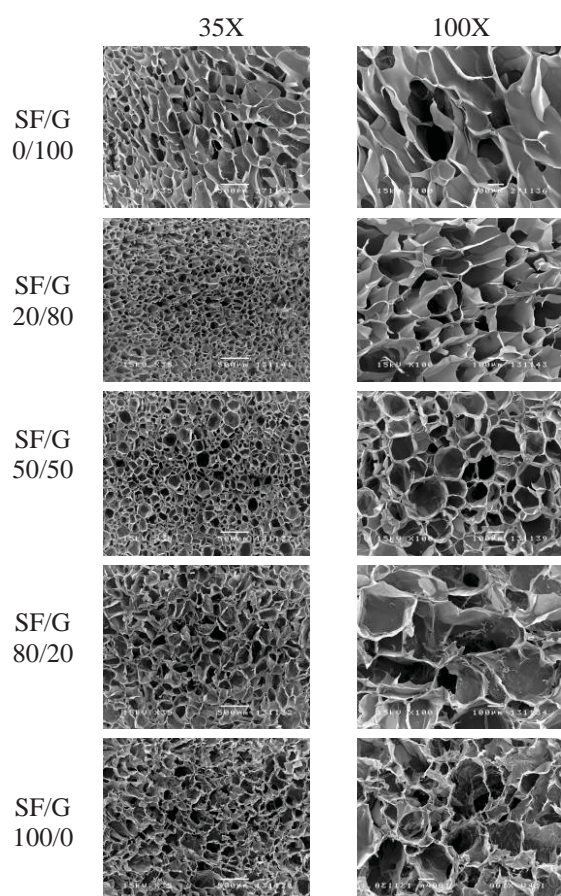


Figure 1. SEM micrographs of SF/G hydrogels with different weight blending ratios.

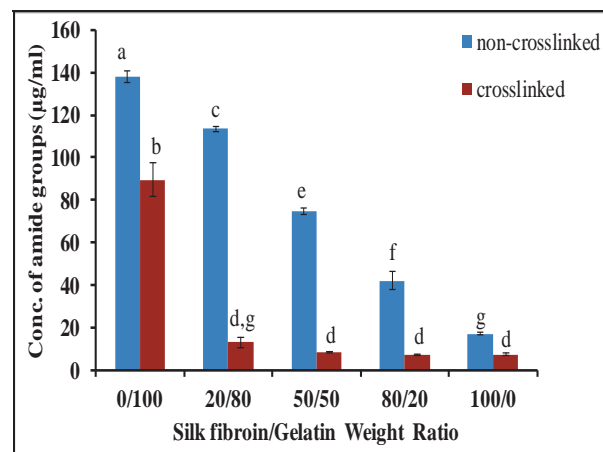


Figure 2. Concentration of amide groups of non-crosslinked and crosslinked SF/G hydrogels (a-g represent the significant difference ($p < 0.05$). Results with the same alphabet indicates that they are not significantly different.)

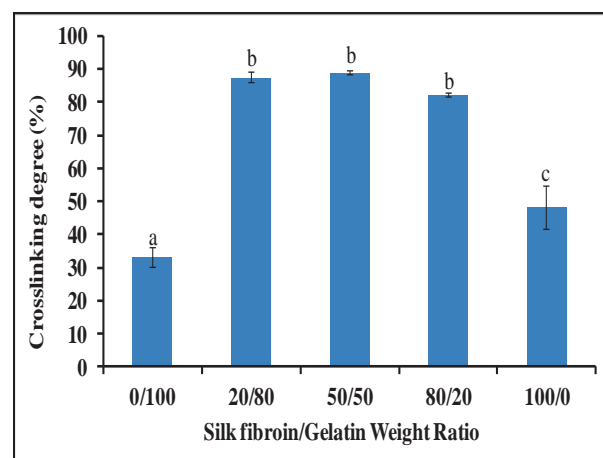


Figure 3. Crosslinking degree (%) of SF/G hydrogels after crosslinking with 0.2% v/v glutaraldehyde. (a-c represent the significant difference ($p < 0.05$). Results with the same alphabet indicates that they are not significantly different.)

3.3 *In vitro* biodegradation of hydrogels

The biodegradation of SF/G hydrogels plays an important role to control the release of curcumin. The results of *in vitro* biodegradation of hydrogels and were presented in Figure 2. Along 28 days of degradation period, the percentages of remaining weight of pure gelatin hydrogels (G100) were lower than those of other hydrogels, indicating its fastest biodegradation. On the other hand, the blended and pure silk fibroin hydrogels were slowly degraded. Since collagenase is an enzyme that specifically digests collagen [3, 11] it could specifically degrade gelatin, a denatured collagen, rather than silk fibroin. In addition, the blended and pure silk hydrogels had higher crosslinking degrees as compared to the pure gelatin hydrogels, resulting in the slow degradation.

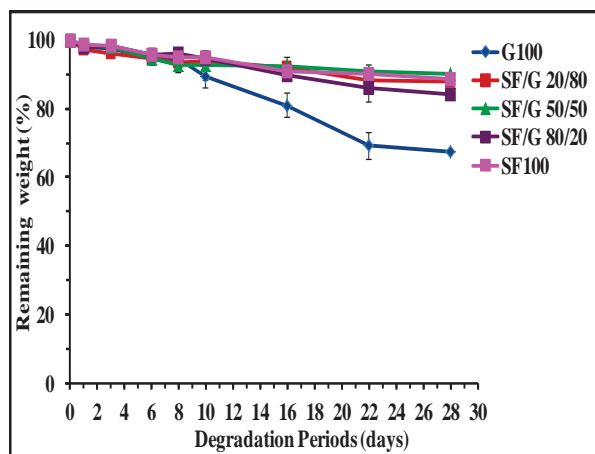


Figure 4. Percentage of remaining weight of Thai silk fibroin/gelatin hydrogels with different weight blending ratios after incubated in 1 U/ml collagenase solution (pH 7.4) containing 0.01% w/v sodium azide at 37°C.

3.4 *In vitro* release of curcumin from hydrogels

The release behavior of curcumin from SF/G hydrogels was demonstrated in Figure 3. All hydrogels showed initial burst release of curcumin at initial 3 days. This may be due to diffusional release of curcumin from the surface of hydrogels. At the later time, pure gelatin hydrogels (G100) showed the highest amounts of curcumin released, followed by the pure silk fibroin hydrogels (SF100). On the other hand, the SF/G blended hydrogels showed controlled release of curcumin, due to the higher crosslinking degrees. Highly crosslinked hydrogels would slowly release curcumin. The results indicated that the release behavior of curcumin from SF/G hydrogels was governed by the weight blending ratios of hydrogels, the crosslinking degrees and the biodegradability of hydrogels.

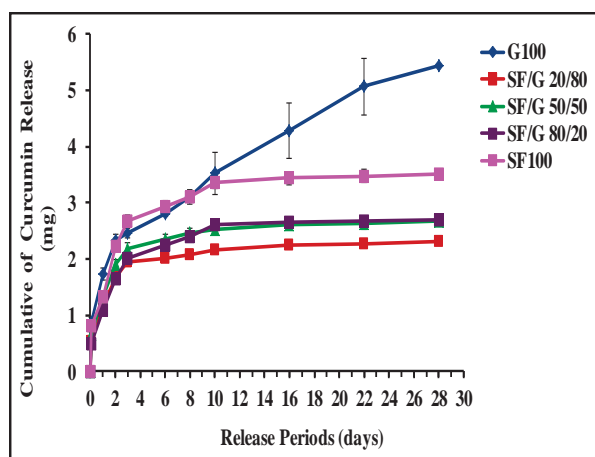


Figure 5. *In vitro* release of curcumin from Thai silk fibroin/gelatin hydrogels with different weight blending ratios after incubated in PBS solution (pH 7.4) containing 0.01% v/v of Tween 80 at 37°C.

4. Conclusions

Silk fibroin/gelatin hydrogels were successfully fabricated at different weight blending ratios for the controlled release of curcumin. The SF/G blended hydrogels at 20/80, 50/50 and 80/20 showed higher crosslinking degrees, slow biodegradation and slow controlled release of curcumin, comparing to the pure gelatin and pure silk fibroin hydrogels. The results suggested that the SF/G blended hydrogels could be alternative carriers for the controlled release of curcumin.

Acknowledgements

Financial supports from The National Research University Project of CHE and the Ratchadaphiseksomphot Endowment Fund (AS615A-55) and Chulalongkorn University Centenary Academic Development Project are gratefully acknowledged.

References

- [1] R. Langer, *Acc. Chem. Res.* **26** (1993) 537-542.
- [2] K.W. Leong, and R. Langer, *Adv. Drug Delivery Rev.* **1** (1988) 199-233.
- [3] B.B. Mandal, J.K. Mann, and S.C. Kundu, *Eur. J. Pharm. Sci.* **37** (2009) 160-171.
- [4] S.T. Lim, et al., *J. Controlled Release.* **66** (2000) 281-292.
- [5] S. Young, et al., *J. Controlled Release.* **109** (2005) 256-274.
- [6] Y. Tabata and Y. Ikada, *Adv. Drug Delivery Rev.* **31** (1998) 287-301.
- [7] B.B. Mandal, A.S. Priya, and S.C. Kundu, *Acta Biomater.* **5** (2009) 3007-3020.
- [8] A. Bigi, et al., *Biomaterials.* **22** (2001) 763-768.
- [9] Q. Lu, et al., *Macromol. Biosci.* **10** (2010) 289-298.
- [10] N. Bhardwaj and S.C. Kundu, *Carbohydr. Polym.* **85** (2011) 325-333.
- [11] P. Jetbumpenkul, et al., *Int. J. Biol. Macromol.* **50** (2012) 7-13.
- [12] H. Hatcher, et al., *Cell. Mol. Life Sci.* **65** (2008) 1631-1652.
- [13] J. Ravindran, S. Prasad, and B. Aggarwal, *AAPS J.* **11** (2009) 495-510.
- [14] S.S. Bansal, et al., *Eur. J. Pharm. Biopharm.* **80** (2012) 571-577.
- [15] S. Manju and K. Sreenivasan, *Colloids Surf., B.* **82** (2011) 588-593.
- [16] U.J. Kim, et al., *Biomaterials.* **26** (2005) 2775-2785.
- [17] W.A. Bubnis and C.M. Ofner Iii, *Anal. Biochem.* **207** (1992) 129-133.
- [18] J. Rujisomnana, *Modification Of Gelatin Structure with Cholesterol for Curcumin Delivery*, Master's Thesis, Chulalongkorn University, (2005).
- [19] E. Leo, et al., *Int. J. Pharm.* **155** (1997) 75-82.

ENZYMATIC SILK DEGUMMING USING A PROTEASE FROM BACTERIAL STRAIN CRC_6NB

Sawaros Pookajorn^{1,2}, Utai Uyen^{1,2}, Pramvadee Y. Wongsangchantra^{1,2*}

¹ Department of Biotechnology and ²Center for Excellence in Protein Structure and Function, Faculty of Science, Mahidol University, Ratchathewi, Bangkok, 10400, Thailand

* Author for correspondence; E-Mail: pramvadee.yuv@mahidol.ac.th, Tel. +66 22015859, Fax. +66 22015843

Abstract: Silk fiber produced from silkworm, *Bombyx mori*, consists of two main proteins. Silk sericin, which is a group of gelatinous proteins, surrounds on the fibroin fiber as layers to glue the fiber together for the formation of a cocoon, a shelter for a silkworm. However, with the textile industries' points of view, sericin proteins and other impurities are the cause of hardness and coarseness of silk texture and must be removed by a process called silk degumming. Traditional silk degumming methods can remove sericin as well as damage fibroin. They pollute environment and require a large amount of water and energy. On the other hand an enzymatic silk degumming process provides an alternative milder condition to the fibroin. In addition the process is more eco-friendly, and the sericin hydrolysate can be recovered with less effort. A bacterial strain, CRC_6NB, isolated from an area of silk industrial waste in Thailand, possesses a potential enzyme for silk degumming. The crude enzyme produced extracellularly under a specific condition was relatively exhibited degrading activity on sericin but not fibroin based on a semi-quantitative assay called radial diffusion on thin-layer enzyme assay (RD-TEA). The enzyme was not only tested on an immobilized form of the substrate in the RD-TEA but also tested on silk yarn, the real substrate, in order to compare silk degumming efficiency of enzyme doses at 1, 2, and 3 ISU (immobilized sericin unit based on the RD-TEA) under pH 8, at 37°C. With boiling in a synthetic detergent (SILKOBLANC BN[®]), a positive control, and according to scanning electron micrographs and staining tests, the enzyme produced from the bacterial strain, CRC_6NB showed similar result in sericin removal from silk yarn without pre-treatment. The degumming results were also better than a commercial enzyme (Alcalase[®]) in terms of the remaining sericin residues and fibroin fibrillation under the same enzyme doses and conditions.

1. Introduction

Silk degumming is an important process for removal of sericin and other impurities, which surround as layers on fibroin. This process makes sericin more soluble by breaking down the peptide bonds of sericin; thus provide the supple, smooth, lustrous, and whitened of silk fiber. The traditional methods involve boiling in different degumming agents such as water under high pressure, soap, synthetic detergents, alkaline, and acid [1]. These methods possibly remove sericin at the expense of damage to fibroin.

They require large amount of water and energy as well as polluting environment. On the other hand, in theory, enzymatic silk degumming involves proteolytic degradation of sericin at milder conditions. Thus, it should minimize damaging to the surface of fibroin fiber. Additionally, it can save more energy, and do harmless to environment. Therefore, enzymatic silk degumming process should be the alternative method to replace the conventional degumming methods to obtain the better quality of silk fiber.

In order to apply an enzyme for silk degumming, at least two factors are concerned. Firstly, the enzyme should be able to access and hydrolyze silk sericin on natural silk yarn, which is sericin in complex with fibroin [2]. Secondly, the enzyme should degrade only sericin effectively but not fibroin. In this study, we have investigated substrate specificity of the crude enzyme from bacterial strain CRC_6NB toward sericin rather than fibroin in comparison with Alcalase[®], a known commercial enzyme for silk degumming [1-3]. The study was based on both Radial diffusion on Thin-layer Enzyme Assay (RD-TEA) and silk degumming test. In RD-TEA, substrates are regenerated silk proteins in an immobilized form on polystyrene surface [3] whereas, in silk degumming, the solid form of substrates or silk yarn is used for evaluation.

2. Materials and Methods

2.1 Bacterial strain and enzymes

The bacterial strain CRC_6NB was isolated from an area of silk industrial waste in Khonkaen province, Thailand (unpublished results) and maintained as lyophilized gelatin

disc. One disc was used as a starting inoculum for pre-culture in Nutrient Broth (NB). The pre-culture was used as inoculum at 1% to NB supplemented with silk yarn at 37°C with shaking incubator at 160 rpm for 72 h. The cell-free supernatant (CFS) was collected by centrifugation and used as the crude extracellular enzyme. Alcalase® as a reference enzyme was purchased from Merck, Germany.

2.2 Radial diffusion in agar gel and the Thin-layer Enzyme Assay (RD-TEA)

The RD-TEA was performed according to Rodbumrer *et al.* [3]. Briefly, skimmed milk, sericin, or fibroin solution was immobilized on a hydrophobic surface of polystyrene petri dish, and agar was layered on top of the protein-coated surface. An enzyme was dropped into a punched well and then incubated. Proteolytic activity was detected by water-vapor condensation on the protein-coated surface. A diameter of each enzyme-affected surface was measured horizontally and vertically across a well using a digital calliper. One immobilized sericin unit (ISU) of protease is defined as the amount of enzyme at 50 µl that hydrolyzes immobilized sericin, giving a 1-cm diameter of the enzyme-affected zone under standard conditions of 100 mM phosphate buffer, pH 7 at 37°C for 16 h.

2.3 Determination of silk degumming efficiency

Degumming: According to Rodbumrer *et al.* [3], the crude enzyme or Alcalase® (as a commercial enzyme reference) with activity of 1, 2, and 3 ISU was incubated with raw silk yarn (solid form of silk) at 37°C for 24 and 48 h under pH 8. The degummed silk yarn was washed in boiling water for 3 min, rinsed at room temperature, and dried at 60°C. A *negative control* was the buffer without enzyme under the same condition. A *positive control* was boiling of raw silk yarn for 45 min in 0.4% (w/v) of SILKOBLANC BN®, a synthetic detergent supplied by CHT R. Beitlich GmbH (Germany) for silk degumming.

Selective staining of sericin: A degummed silk sample was boiled in 0.05% Sirius Red F3B (DyStar) for 2 min, rinsed with distilled water to remove the excess dye, and then dried at 60°C for 1 day.

Scanning electronic microscopy (SEM): Silk samples were mounted and coated with gold using Sputter coater, Balzers model SCD 040. The mounted samples were scanned by SEM (JOEL, JSM-5410LV).

3. Results and Discussion

Substrate specificity

The crude enzyme from bacterial strain CRC_6NB and Alcalase® were compared for their substrate specificity among skimmed milk, sericin, and fibroin using RD-TEA under standard conditions of 100 mM phosphate buffer, pH 7 at 37°C for 16 h. The results in Table 1 showed that with the same level of protease activity on skimmed milk, the crude enzyme CRC_6NB has slightly less activity on sericin than Alcalase®. However, while Alcalase® could hydrolyze fibroin in some extent, no activity could be detected on fibroin using the crude enzyme. Thus, it is clear that different enzymes exhibit different substrate preferences.

Table 1 Comparison of substrate specificity of the crude enzyme from bacterial strain CRC_6NB and Alcalase® using RD-TEA.

| Enzymes | Total protein* (µg/ml) | Average diameters of enzyme affected surface zone (mm) | | |
|---------------|------------------------|--|---------|--------------|
| | | Skimmed milk | Sericin | Fibroin |
| Alcalase® | 36 | 26.17 | 27.78 | 22.60 |
| Crude CRC-6NB | 630 | 26.50 | 26.60 | Not detected |

*Total proteins were determined using the Micro BCA Protein Assay kit from Pierce (USA) with BSA as a standard protein.

Silk degumming efficiency

Silk degrading ability was also tested on real solid substrate form of silk (silk degumming). Here in order to compare 2 different proteolytic enzymes, crude enzyme CRC_6NB and Alcalase®, we have standardized the amount of the enzymes used based on their proteolytic activity on sericin

using RD-TEA. This strategy should provide more relevant assay to the real conditions in silk degumming than using a general substrate such as casein or skimmed milk. The treatments were carried on at different enzyme doses (1-3 ISU) and times (24 and 48 h) at pH 8 and 37°C. Negative and positive controls were a buffer at pH 8 and SILKOBLANC BN detergent, respectively.

The results shown in Figure 1 suggested that selective staining of the remaining sericin with Sirius Red F3B (Figure 1) provided a gross view of degummed samples. Sericin was stained in red whereas fibroin was not as shown in the negative and positive controls, respectively. A general observation was that the more the enzyme used, the less the remaining sericin, and the more the exposure time (48 h), the better the removal of sericin. From the external appearance with the staining, it could roughly estimate that both enzymes with 3 ISU could completely remove sericin within 24 h. However, when compare the crude enzyme CRC_6NB with Alcalase®, the crude enzyme CRC_6NB could remove sericin better than Alcalase® at all enzyme doses treated.

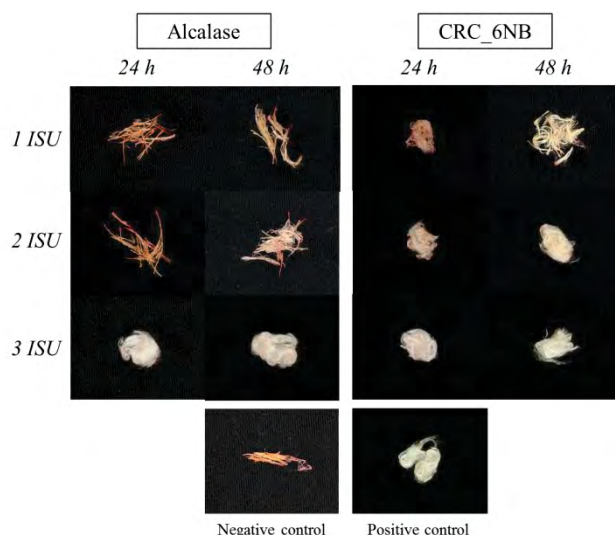


Figure 1. Silk degumming efficiency determined by selective staining of the remaining sericin with Sirius Red F3B.

The scanning electron micrographs (Figure 2) have confirmed that the crude enzyme CRC_6NB could effectively remove sericin from the fibroin fiber. This is shown by gradual increase of area of smooth surface in the treatments with the crude enzyme CRC_6NB from low to high doses and from 24 h to 48 h without a sign of fibroin damage even at the highest dose. In contrast, Alcalase® could not remove sericin evenly from the fiber; it also damaged fibroin. Therefore, the enzymatic degumming by the crude enzyme from bacterial strain CRC_6NB showed the higher degumming efficiency than Alcalase®.

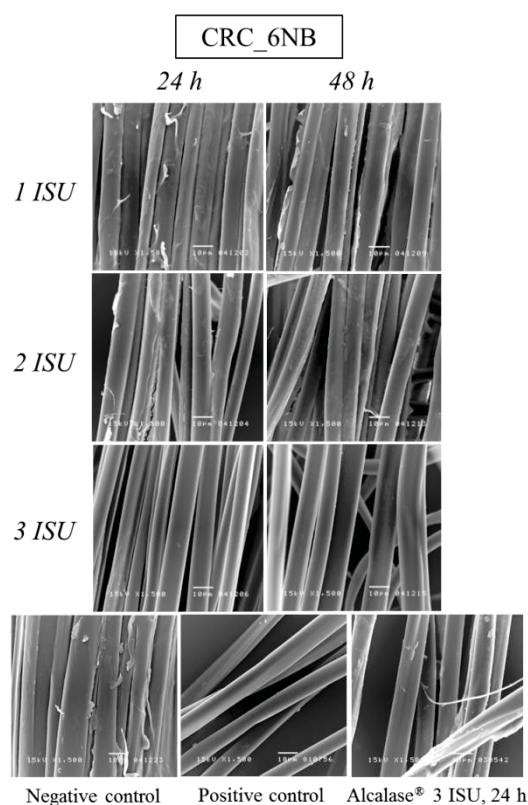


Figure 2. Scanning electron micrographs demonstrated silk degumming efficiency of the crude enzyme from bacterial strain CRC_6NB and Alcalase®.

4. Conclusions

This study showed that crude enzyme from the bacterial strain CRC_6NB is obviously more specific to sericin than fibroin in comparison with the commercial enzyme Alcalase[®]. The greater specificity of the enzyme to sericin on silk yarn will make enzymatic silk degumming process more controllable. Therefore, crude enzyme CRC_6NB is considered more suitable for improvement of silk degumming process in Thailand, in which water and energy consumption can also be reduced. Sericin can be recovered from the waste effluent as a high value by-product, thus reducing environmental problems.

Acknowledgements

This work was supported by the grants from the Mahidol University Research Program Budget to Pramvadee Y. Wongsangchantra, and through a scholarship by Biotechnology Alumni to Sawaros Pookajorn. The authors are grateful to previous works of Chantima Kaeyanon.

References

- [1] S. Chopra, M.L. Gulrajani. *Indian J Fibre Text Res.* **19** (1994) 76-83.
- [2] P. Rodbumrer, D. Arthan, U. Uyen, J. Yuvaniyama, J. Svasti, P.Y. Wongsangchantra. *Acta Biochim Biophys Sin.* **44** (2012) 974-983.
- [3] M. Arami, S. Rahimi, L. Mivehie, F. Mazaheri, N.M. Mahmoodi. *J. Appl. Polym. Sci.* **106** (2007) 267-75.

STRUCTURAL INSIGHTS INTO THE INTERACTION OF CATHEPSIN S, H, L AND B WITH CYSTATIN D BY PROTEIN-PROTEIN DOCKING METHOD

Surapong Pinitglang^{1*}, Ratchanee Saiprajong¹, Krongsakda Phakthanakanok²,
Khanok Ratanakhanokchai³

¹ Department of Food Science and Technology, School of Science and Technology, University of the Thai Chamber of Commerce, Bangkok 1040Thailand.

² Department of Food Science and Technology, School of Science and Technology, Muban Chombueng Rajabhat University, Ratchaburi 7015Thailand.

³ Department of Biochemical Technology, School of Bioresources and Technology, King Mongkuts University of Technology, Thonburi, Bangkok 1015Thailand.

*Author for correspondence; E-mail: surapong_pin@utcc.ac.th, Tel. +66 26976525, Fax. +66 2 2777007

Abstract: Cathepsin S, H, L, and B are cysteine proteinases found in many types of cells. In mammals, cystatins inhibit cathepsins B, H, L, and S both intra- and extracellular following a reversible, tight-binding mechanism. X-ray crystal structures of cathepsin S (2H7J), H (1NB3), L (2YJC) and B (3K9M) and the three-dimensional structure of cystatin D (1ROA) have been reported, but, there has been limited success when using crystallography to study the interaction of these cathepsins with cystatin D. The aim of this research was to investigate the interaction-between cystatin D presents inhibition profiles with a preferential inhibition cathepsin S > Cathepsin H > cathepsin L, and no inhibition of cathepsin B. To elucidate the structural reasons for this specificity, we have used X-ray crystallographic data to derive models of the cathepsin S, H, L, and B -cystatin D complex by using the HADDOCK protein-protein docking program. The results were shown that cathepsin S-cystatin D complex of positioning the L1 loop of cystatin D and form hydrogen bonds with amino acid residues in S1-subsite of cathepsin S. Valine 5in L1 loop of cystatin D interacts with methionine 71, phenylalanine 7and 211 of cathepsin S. While cathepsin H has leucine7and proline 71 in the S1-subsite, which proline71 has a shorter side chain than methionine 71 of cathepsin S. These reason would then make cathepsin H being less hydrophobic effective than cathepsin S. Leucine 69, methionine 7and 161 are in the S₁'-subsite of Cathepsin L to make the hydrophobic pocket notably longer in cathepsin L when compare with cathepsin S. Cystatin D could not inhibit cathepsin B was that the L1 loop cannot make contact with the S₁' subsite due to the Val 59 in the cystatin D is being close to Trp221 in the S₁' subsite and deep hydrophobic pocket of cathepsin B.

1. Introduction

Cathepsins are cysteine proteinase papain C1 family that hydrolysis peptide bond of the proteins, found in many types of cell including in animal. There are approximately a dozen members of this family, which are distinguished by their structure and catalytic

mechanism. Most of the members become activated at the low pH found in lysosomes [1]. Cystatins are natural inhibitors of cysteine proteinases. In mammals cystatins inhibit peptidases such as cathepsin S, H, L, and B both intra-and extracellular following a reversible, tight binding mechanism [2]. Recently, a new protein-protein interaction domain termed PB₁ (Phox and Berm1) was identified by docking of the two PB₁ domains with HADDOCK program [3]. Studies on cathepsins interactions between cystatin D presents inhibition profiles with a preferential inhibition cathepsin S > Cathepsin H > cathepsin L, and no inhibition of cathepsin B [4]. These conclusions were investigated to elucidate the structural reasons for this specificity of cathepsin S, H, L, and B-cystatin D adsorptive complex by using the HADDOCK protein-protein docking program [5-6].

2. Materials and Methods

Studies on cathepsin S, H, L and B interactons with cystatin D were determined by HADDOCK 2.1 protein-protein docking program. The cryltallographic structure of cathepsin S (2H7J) [7], cathepsin H (1NB3) [1], cthepsin L (2YJC) [8], cathepsin B (3K9M) [9] and cystatin D (1ROA) [4] were retrieved from Protein Data Bank (PDB) [10]. Molecular visualization of cathepsin S, H, L and B complex with cystatin D were visualized by Discovery Studio 2.5 [11-13]. Molecular dynamics simulations of free form of cathepsin S and B were studied by GROMACS program [14]. HADDOCK 2.1 was run on all targets using default parameter, including random removal 50% of the data for each separate docking trial, automatic definition of flexibility, and sampling of 180° rotated solutions in it, but excluding solvated docking. The structures were clustered using a cut-off 7.5 Å 1-RMDS, only counting the interface backbone atoms of the ligand. The clusters

were ranked according to the CARPI evaluation criteria.

3. Results and Discussion

The results of cathepsin S, H, L, and B interactions with cystatin D by HADDOCK protein-protein docking program were shown in Figure 1-8. The results of studies on molecular dynamics simulations of cathepsin S and B were shown in Figure 9-11. The L1 loop of the binding site Val59 is close contact with the amino acid residues in the S_1' pocket of the cathepsin S. The hydrophobic pocket of S_1' subsite cathepsin S, the major inhibitor recognition site is formed by the amino acid residues of Gly68, Gly69, Phe70, Met71, Val162, Gly165, and Phe211. Previous studies have shown that a L1 loop of binding site of cystatin D close contact with the amino acid residues forming in the S_1' pocket in the enzyme [4]. The hydrophobic pocket of S_1' subsite of cathepsin H associated with Leu70 there is a significant difference in the residue 70 is Phe in Cathepsin S Leu in cathepsin L and Met in cathepsin L. It may be that the hydrophobic effect seen with Cathepsin S, H, and L interaction with the L1 loop of cystatin D depends on hydrophobic of the nature of binding interactions. The major change is that Met71 at the end of S_1' -subsite in cathepsin S, become Pro71 making the pocket notably shorter in cathepsin H.

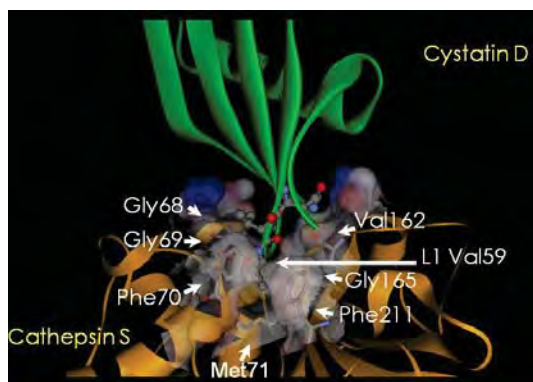


Figure 1. Molecular docking model of cathepsin S adsorptive complex with L1 loop of cystatin D. The cystatin D showed in green ribbon and the enzyme represented in yellow ribbon and electrostatic surface. Amino acid residues of Phe70, Phe211, Met71 and Val162 are essential for binding interactions between cathepsin S and cystatin D.

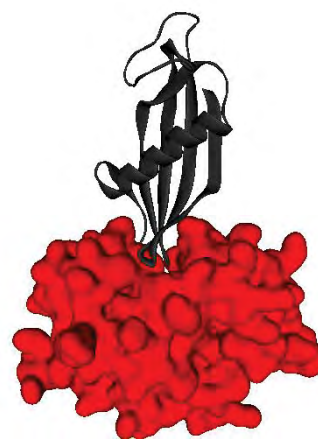


Figure 2. The Poisson-Boltzmann electrostatic potential displayed on the protein surfaces of cathepsin S in complex with ribbon diagram of L1 loop of cystatin D.

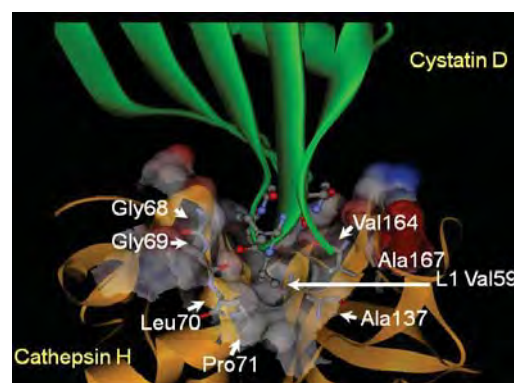


Figure 3. Molecular docking model of cathepsin H adsorptive complex with L1 loop of cystatin D. Amino acid residues of Leu70, Pro71 and Val164 are binding sites for interactions between cathepsin H and L1 loop of cystatin D.

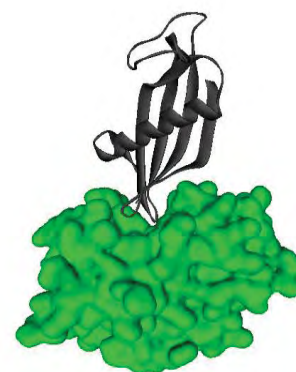


Figure 4. The Poisson-Boltzmann electrostatic potential displayed on the protein surfaces of cathepsin H in complex with ribbon diagram L1 loop of cystatin D .

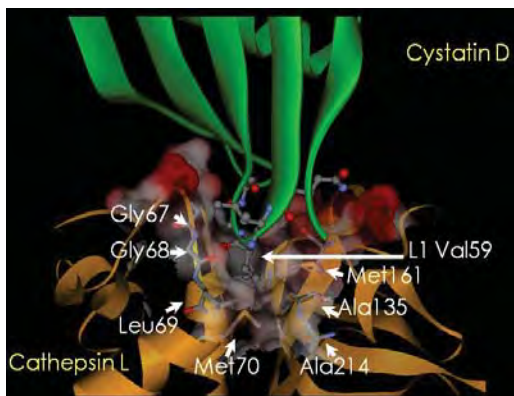


Figure 5. Molecular docking of cathepsin L adsorptive complex with L1 loop of cystatin D. Amino acids residues of Leu6 and Met7 and Met161 are essential binding site interactions of cathepsin L-cystatin D complex.

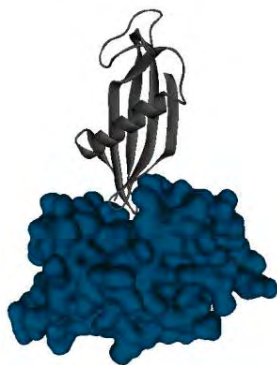


Figure 6. The Poisson-Boltzmann electrostatic potential displayed on the protein surfaces of cathepsin L complex with ribbon diagram L1 loop of cystatin D.

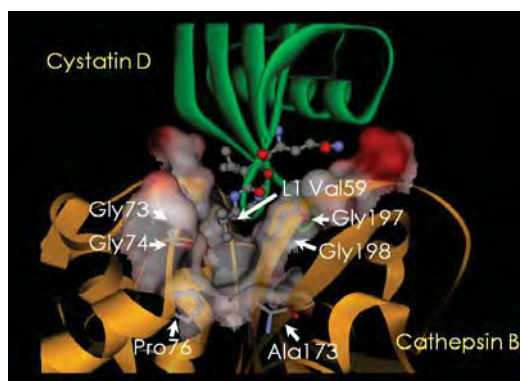


Figure 7. Molecular docking model of cathepsin B adsorptive complex with L1 loop of cystatin D. Amino acid residues of Gly73-74, Pro76, Val15 and Gly197-198 are binding site region deep hydrophobic pocket.



Figure 8. The Poisson-Boltzmann electrostatic potential displayed on the protein surfaces of cathepsin B in complex with ribbon diagram L1 loop of cystatin D.

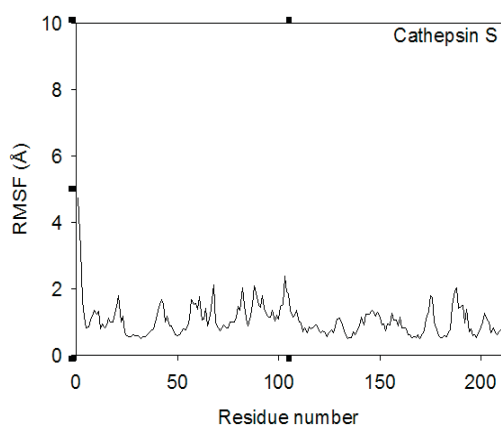


Figure 9. Molecular dynamics simulations profiles representation of Root-mean-square fluctuation (RMSF) of cathepsin S.

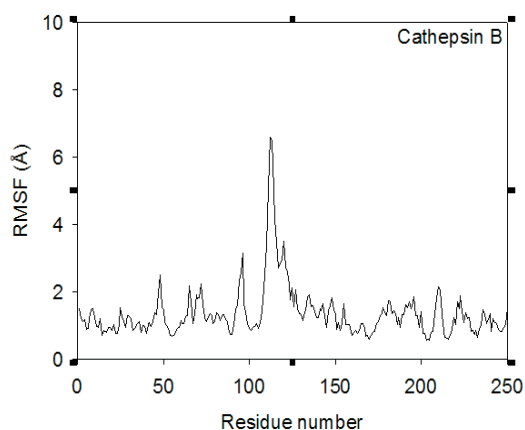


Figure 10. Molecular dynamics simulations profiles representation of Root-mean-square fluctuation (RMSF) of cathepsin B. The amino acid residues number 109-122 were shown a high fluctuation.

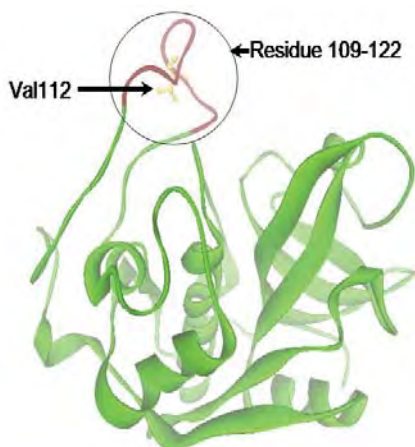


Figure 11. Conformation of cathepsin B collected from molecular dynamics simulations studies at equilibrium. Amino acid residues number 109-122 were shown a high fluctuation.

4. Conclusions

Cystatin D was presented inhibition cathepsin S> cathepsin H> cathepsin L and no inhibition of cathepsin B. Structural hydrophobic differences in the S_1' binding site for cathepsin S, H, L and B are clearly present in cystatin D and are most likely the reason why cystatin D is not an inhibitor of cathepsin B. The L1 loop of the binding site of cystatin D was shown close contact with amino acid residues forming the S_1' pocket of the enzyme. Studies on protein-protein interactions to elucidate the structural reasons for specificity models of the cathepsin S, H, L, and B - cystatin D adsorptive complex were investigated by using GROMACS program. Comparison on molecular dynamics simulations studies on the conformation of cathepsin S and cathepsin B were determined. The profiles of Root-mean-square fluctuation (RMSF) of amino acid residues number 109-122 of cathepsin B were shown high fluctuation all the times and propose that these part of amino acid residues possible to prevent binding interactions with cystatin D.

Acknowledgements

This research was supported by the Thailand Research Fund under a grant of the Royal Golden Jubilee Ph.D. program to K.P. Dr. Chandra Verma, Head of Computer modeling Unit, Bioinformatics Institute, A* STAR, Singapore is gratefully acknowledged for supporting this research. National Electronics and Computer Technology Center (NECTEC) is also acknowledged for computing facilities Itanium Cluster for molecular docking and molecular dynamics simulations studies.

References

- [1] S. Jenko, I. Dolenc, G. Guncar, A. Dobersek, M. Podobnik and D. Turk, *J. Mol. Biol.* **326**(2003) 875-885.
- [2] M. Abrahamson, M. Alvarez-Fernandez and C.M. Nathanson. *Biochem Soc Symp.* **70**(2003) 179-199.
- [3] A.van Drogen-Petit, C. Zwahlen, M. Peter and A.M.J.J. Bonvin, *J. Mol. Biol.* **336**(2004) 1195-1210.
- [4] M. Alvarez-Fernandez, Y-H. Liang, M. Abrahamson and X-D. Su, *J. Biol. Chem.* **280**(2005) 18221-18228.
- [5] C. Dominquez, R. Boelens and A.M.J.J. Bonvin, *J. Am. Chem. Soc.* **125**(2003) 1731-1737.
- [6] S.J. de Vries, A.D.J. van Dijk, M. Krzeminski, M. van Dijk, A. Thureau, V. Hsu, T. Wassenaar and A.M.J.J. Bonvin, *Protein: Struc. Funct. & Bioinformatic.* **69** (2007) 726-733.
- [7] A.W. Patterson, W.J. Wood, M. Hornsby, S. Lesley, G. Spraggon and J.A. Ellman. *J. Med. Chem.* **49**(2006) 6298-6307.
- [8] L.A. Hardegger, B. Kuhn, B. Spinnler, L. Anselm, R. Ecabert, M. Stihle, B. Gsell, R. Thoma, J. Diez, J. Benz, J.-M. Plancher, G. Hartmann, Y. Isshiki, K. Morikami, N. Shimma, W. Haap, D.W. Banner, and F. Diederich, *Chem Med Chem.* **6**(2011) 2048-2054.
- [9] M. Renko, U. Pozgan, D. Majera and D. Turk, *Febs. J.* **277**(2010) 4338-4345.
- [10] H.M. Berman, J. Westbrook, Z. Feng, G. Gilliland, T.N. Bhat, H. Weissing, I. Shindyalov and P.E. Bourne, *Nucleic. Acids. Res.* **28**(2000) 235-242.
- [11] B. Honig, K. Sharp and A.S. Yang, *J. Phys. Chem.* **97**(1993) 1101-1109.
- [12] A. Nicholls and B. Honig, *J. Comp. Chem.* **12**(1991) 435-445.
- [13] K.A. Sharp, A. Nichols, R. Friedman and B. Honig, *Biochemistry.* **30**(1991) 9686-9697.
- [14] D.S.D. Van, E. Lindahl, B. Hess, G. Groenhof, A.E. Mark and H.J. Berendsen, *J. Comput. Chem.* **26** (2005) 1701-1718.

EQUILIBRIUM AND KINETIC STUDIES OF METHYL ORANGE AND METHYL VIOLET ADSORPTION ON ACTIVATED CARBON PREPARED FROM FRUIT OF *WODYETIA BIFURCATE* A.K. IRVINE

Nopparat Poolsawat¹, Warinna Borirak¹, Apichat Klayanon², Uthia Tippomuang², Akapong Suwattanamala^{3*}

¹Department of Chemistry Teaching, Faculty of Education, Burapha University, Bangsaen, Chonburi, 20131 Thailand

²Department of Chemistry, Faculty of Science, Burapha University, Bangsaen, Chonburi, 20131 Thailand

* Author for correspondence; E-Mail: akapong@buu.ac.th, Tel. +66 38103053, Fax. +66 38 393494

Abstract: In this study, activated carbon derived from fruit of *Wodyetia bifurcate* A.K. Irvine was prepared by using zinc chloride as an activated reagent. The optimum conditions for the preparation were the weight ratio of carbon to zinc chloride at 1: 2 and the temperature for carbonization at 80 °C, which provided highest adsorption efficiency iodine. Activated carbon prepared from fruit of *Wodyetia bifurcate* A.K. Irvine was utilized as a potential adsorbent for the removal of methyl orange and methyl violet dyes from aqueous solutions. The adsorption by a batch method was evaluated by changing various parameters such as initial concentration of dyes, contact time and solution temperature. The equilibrium adsorption isotherm was well represented by Langmuir isotherm models. Both methyl orange and methyl violet adsorptions followed the pseudo-second-order kinetic models. The thermodynamic parameters, such as the enthalpy, entropy, and Gibbs free energy changes were calculated and these values showed that the adsorption of both dyes by activated carbon was spontaneous endothermic process, which favored high temperature.

1. Introduction

Dyes are the major pollutants of waste water from textile, cosmetic, paper, printing, pharmaceutical and coloring industries, so the removal of dyes from waste water has attracted considerable aspect in environmental science. Several treatment methods have been applied to remove pollutants from waste water such as photochemical degradation, biological degradation, coagulation, chemical oxidation, and adsorption [1]. Among these mentioned methods, adsorption on activated carbons is commonly used due to its high efficiency and ability to separate a wide range of chemical compounds [2], simplicity of design [3] and economic feasibility. In recent years, the low cost materials and readily available material, mainly industrial and agricultural byproducts have been considered to be a very interesting precursor to prepare activated carbon [4, 5].

In this study, fruit of *Wodyetia bifurcate* A.K. Irvine was used as a novel alternative to derive activated carbon for the removal of methyl orange (MO) and methyl violet (MV) from aqueous solutions. MO and MV had harmful effects on living organisms in a short period of exposure considered as

choice of acid and basic dyes, respectively. The main goal of the present work is to investigate the potentiality of this novel activated carbon for the adsorption of MO and MV from aqueous solutions. Equilibrium and kinetic data analysis were performed to understand the adsorption mechanism and different models were evaluated by fitting to the experimental data.

2. Materials and Methods

2.1 Preparation adsorbent and adsorbate solution

Activated carbon prepared from fruit of *Wodyetia bifurcate* A.K. Irvine by using zinc chloride as an activated reagent. The optimum conditions for the preparation were the weight ratio of carbon to zinc chloride at 1: 2 and the temperature for carbonization at 80 °C, which provided highest adsorption efficiency iodine.

Methyl orange (MO) and methyl violet (MV) were analytical grade and were used without any further purification to prepare stock solution by dissolving accurately weighted amounts in doubly distilled water. Solutions of desired concentration of MO and MV were prepared from the stock solution.

2.2 Batch experiments

The adsorption of MO and MV from aqueous solution onto derived activated carbon was performed using batch equilibrium technique. A suspension containing 0.05 g of adsorbent was mixed with a definite volume (30 mL) of fixed initial concentrations of dyes solution in a flask, which was immersed in a thermostated water bath keeping constant working temperature. The sample solutions at the pre-determined time intervals, were filtered using filter paper to obtain the residual concentrations. The residual dye concentration in the filtrate was subsequently determined using spectronic 20 at wavelength (505 nm for MO and 590 nm for MV) corresponding to the maximum absorbance. The adsorption tests were continued until the equilibrium concentration was reached. The effect of contact time on the amount of dye absorbed was studied as a function of initial concentration of dye and

temperature. The obtained data from the adsorption tests were then used to calculate the adsorption capacity, q_e (mg/g), of the adsorbent by the following relation :

$$q_e = \frac{(C_0 - C_e)V}{m} \quad (1)$$

where C_0 and C_e (mg/L) are the liquid-phase concentrations of dye at initial and equilibrium time, respectively. V (L) is the volume of solution, and m (g) is the mass of adsorbent used.

3. Results and Discussion

3.1 Effect of contact time and initial concentration

Equilibrium time is one of the most important parameters in the design of economical wastewater treatment systems. Rapid uptake and quick establishment of equilibrium time imply the efficiency of particular adsorbent in terms of utility in wastewater treatment. The adsorption of dyes onto derived activated carbon at various initial dye concentration (164, 327, 655 mg/L for MO; 150, 200, 250 mg/L for MV) was investigated as function of contact time in order to determine the necessary adsorption equilibrium time as shown in Figure 1. The adsorption process at different dye concentrations was rapid at the beginning and then gradually decreased with the progress of adsorption until the equilibrium was reached. As shown in Figure 1, the contact time needed for MO and MV solutions to reach equilibrium was 90 min. The rate of removal is higher at the initial contact time due to larger surface are available of the adsorbent. After adsorption, the rate of dye uptake is controlled by the rate of dye transported from the exterior to interior sites of the adsorbent particles.

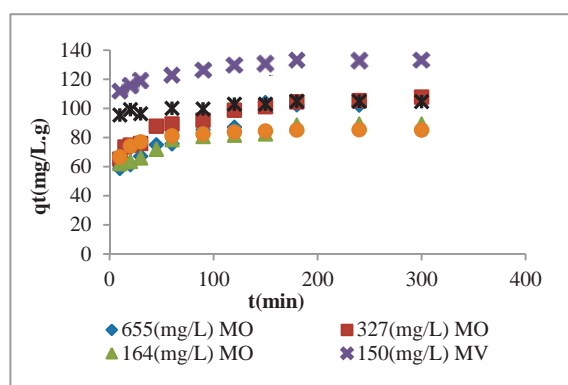


Figure 1. Effect of contact time and initial dye concentration on the adsorption of MO and MV onto derived activated carbon at temperature 30 °C.

3.2 Effect of temperature on adsorption capacity of activated carbon

Temperature is an important parameter for the adsorption process and batch adsorption studies were carried out at three different temperatures (15, 30, 45

°C for MO and 20, 25, 30 °C for MV). Results showed that the adsorption capacity increased with increasing temperature, which suggests that the adsorption is favored at high temperature. To compare the kinetic of adsorption of both MO and MV onto activated carbon, the optimal temperature was 30 °C to select on the study due to the same temperature performed for both dyes.

3.3 Kinetic of adsorption

Two important kinetic models (pseudo-first-order and pseudo-second-order) are applied to investigate the behavior dynamics of adsorption process of MO and MV dyes on to derived activated carbon.

The pseudo-first-order kinetic model can be represented by the following Lagergren equation [6] :

$$\log(q_e - q_t) = \log q_e - \frac{k_1}{2.303} t \quad (2)$$

where q_e and q_t are the amounts of adsorbate adsorbed (mg/g) at equilibrium and at contact time t (min), respectively and k_1 is the pseudo-first-order rate constant (min^{-1}). The values of q_e and k_1 were determined from the intercepts and the slopes of the graphs of $\log(q_e - q_t)$ versus t , respectively. The k_1 , correlation coefficient (R^2) and q_e values (experimental and calculated) are given in Table 1.

Table 1: Kinetic parameters of pseudo-first-order model for the adsorption of MO and MV onto derived activated carbon at different initial concentrations.

| Dye | C_0 (mg/L) | $q_{e, \text{exp}}$ (mg/g) | Pseudo-first-order | | |
|-----|-----------------|-------------------------------|--------------------------------|-------------------------------|--------|
| | | | k_1 (min^{-1}) | $q_{e, \text{cal}}$ (mg/g) | R^2 |
| MO | 164 | 89.16 | 2.51×10^{-2} | 55.42 | 0.5997 |
| | 327 | 107.65 | 1.27×10^{-2} | 42.81 | 0.9815 |
| | 655 | 106.30 | 1.31×10^{-2} | 55.95 | 0.8212 |
| MV | 150 | 84.20 | 9.9×10^{-3} | 11.60 | 0.8383 |
| | 200 | 104.63 | 1.08×10^{-2} | 9.90 | 0.8509 |
| | 250 | 130.22 | 9.3×10^{-3} | 20.28 | 0.8960 |

The results show that the experimental values, $q_{e, \text{exp}}$ did not agree with the calculated value, $q_{e, \text{cal}}$ obtained from the linear plots. It suggests that the adsorption kinetics for MO and MV were not in a good corresponding to the pseudo-first-order kinetic model.

The pseudo-second-order kinetic model can be expressed as [7] :

$$\frac{t}{q_t} = \frac{1}{k_2 q_e^2} + \frac{1}{q_e} t \quad (3)$$

where k_2 is the pseudo-second-order rate constant (g/mg min). The plot of t/q_t versus t is a straight line, as shown in Figure 2. The values of k_2 and q_e determined from the slopes and intercepts of the graph are summarized in Table 2.

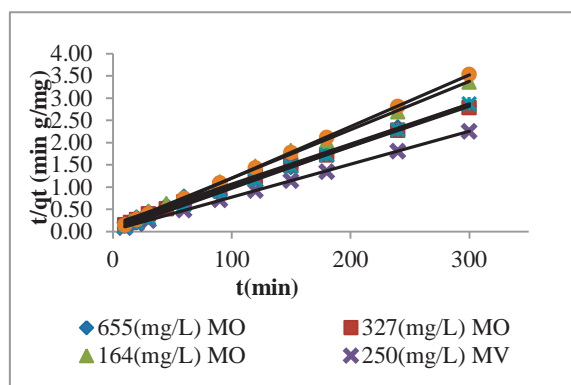


Figure 2. Pseudo-second-order kinetic plots for the adsorption of MO and MV onto derived activated carbon.

Table 2: Kinetic parameters of pseudo-second-order model for the adsorption of MO and MV onto derived activated carbon at different initial concentrations.

| Dye | C_0 (mg/L) | $q_{e,exp}$ (mg/g) | Pseudo-second-order | | |
|-----|-----------------|-----------------------|-----------------------|-----------------------|--------|
| | | | k_2 (g/mg.min) | $q_{e,cal}$ (mg/g) | R^2 |
| MO | 164 | 89.16 | 1.07×10^{-3} | 91.74 | 0.9985 |
| | 327 | 107.65 | 7.58×10^{-4} | 111.11 | 0.9987 |
| | 655 | 106.30 | 4.74×10^{-4} | 111.11 | 0.9935 |
| MV | 150 | 84.20 | 3.42×10^{-3} | 86.20 | 1 |
| | 200 | 104.63 | 3.61×10^{-3} | 105.26 | 0.9997 |
| | 250 | 130.22 | 1.80×10^{-3} | 135.14 | 0.9998 |

The linear plot provides a good agreement between the experimental and the calculated q_e values. The corresponding correlation coefficient (R^2) values for the pseudo-second-order kinetic model were greater than 0.99 for all MO and MV initial concentrations. Thus the adsorption of MO and MV onto the prepared activated carbon was described by the pseudo-second-order kinetic model. These results showed a good agreement with the previous study on MO and MV adsorption onto activated carbon derived from *Phragmites australis*[8].

3.4 Adsorption isotherm and equilibrium

The equilibrium adsorption isotherm plays an important role in the design adsorption system. The equilibrium adsorption is usually described by an isotherm equation characterized by the surface properties of adsorbent and its affinity to the adsorbate. Two important adsorption isotherms, the Freundlich and Langmuir isotherms are applied in this study.

The Langmuir isotherm is based on the assumption that the adsorption process takes place at specific homogeneous sites within the adsorbent surface and that once a dye molecule occupies a site, which suggested that the adsorption process is monolayer in nature [9,10]. A well known linear form for the Langmuir equation is given as:

$$\frac{C_e}{q_e} = \frac{1}{q_m} C_e + \frac{1}{q_m K_L} \quad (4)$$

where C_e is the equilibrium concentration (mg/L), q_e is the amount of adsorbate adsorbed per unit mass of adsorbent at equilibrium (mg/g). q_m is the theoretical maximum adsorption capacity corresponding to complete monolayer coverage on the surface (mg/g). K_L is the Langmuir isotherm constant related to the energy of adsorption (L/mg). The values of q_m and K_L can be evaluated from the slope and intercept of the linear plot of C_e/q_e versus C_e .

The Freundlich isotherm is an empirical equation assumed that the adsorption process takes place on a heterogeneous surface through a multilayer adsorption and adsorption capacity is related to the concentration of dye at equilibrium[11]. A linear expression of the Freundlich equation is generally represented as:

$$\ln q_e = \ln K_F + \frac{1}{n} \ln C_e \quad (5)$$

where q_e is the amount of adsorbate adsorbed per unit mass of adsorbent at equilibrium (mg/g), C_e is the equilibrium concentration of the adsorbate (mg/L), K_F is the Freundlich adsorption constant related to adsorption capacity of the adsorbent ((mg/g) (L/mg)^{1/n}) and $1/n$ is the heterogeneity factor. The values of K_F and $1/n$ were calculated from the intercept and slope of the plot of $\ln q_e$ versus $\ln C_e$.

All correlation coefficient, R^2 values and the constants obtained from two isotherm models are presented in Table 3.

Table 3: Isotherm parameters obtained from the two isotherm models for the adsorption of MV and MO onto derived activated carbon.

| Isotherm models | MV | | | MO | | |
|---------------------------------------|--------|--------|--------|--------|--------|--------|
| | 20°C | 25°C | 30°C | 15°C | 30°C | 45°C |
| Langmuir | | | | | | |
| q_m (mg/g) | 104.16 | 116.28 | 128.61 | 166.67 | 158.73 | 153.85 |
| K_L (L/mg) | 0.197 | 0.098 | 0.121 | 0.32 | 0.63 | 0.78 |
| R^2 | 0.9992 | 0.9991 | 0.9998 | 0.9915 | 0.9942 | 0.9969 |
| Freundlich | | | | | | |
| K_F (mg/g) (L/mg) ^{1/n} | 61.46 | 49.36 | 57.82 | 78.89 | 93.80 | 115.56 |
| n | 9.97 | 6.17 | 6.50 | 5.35 | 7.12 | 5.95 |
| R^2 | 0.9090 | 0.8722 | 0.9265 | 0.8963 | 0.9243 | 0.9397 |

The Langmuir isotherm model yielded a much better fit than the Freundlich isotherm model. In addition, the Langmuir isotherm model yielded the highest R^2 values which were greater than 0.99 at all the temperatures studied. It shows that the adsorption of both dyes on derived activated carbon was best described by this model. A linear plot of Langmuir isotherm model in this study was presented in Figure 3.

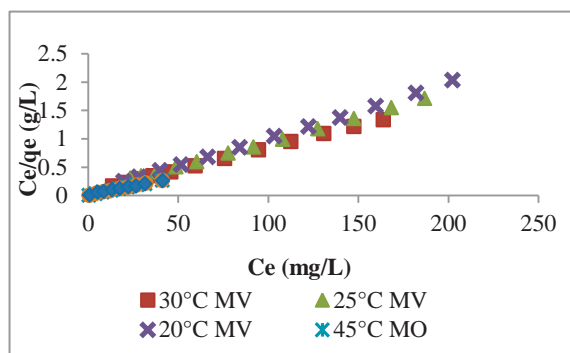


Figure 3. Langmuir plots for the adsorption of MV and MO onto derived activated carbon

The maximum monolayer sorption capacity, q_m , obtained with the Langmuir isotherm at 30°C, was 158.73 and 128.61 mg/g for MO and MV, respectively.

3.5 Thermodynamic studies

The thermodynamic parameters such as change in standard free energy (ΔG^0), enthalpy (ΔH^0) and entropy (ΔS^0) were calculated by the following expressions:

$$\Delta G^0 = -RT \ln K_c \quad (6)$$

$$K_c = \frac{q_e}{C_e} \quad (7)$$

$$\ln K_c = \frac{\Delta S^0}{R} - \frac{\Delta H^0}{RT} \quad (8)$$

where R (8.314 J/molK) is the gas constant, T (K) is the absolute temperature and K_c (L/g) is the standard thermodynamic equilibrium constant expressed by q_e/C_e . By plotting a graph of $\ln K_c$ versus $1/T$ (K⁻¹), the values of ΔH^0 and ΔS^0 can be calculated from the slopes and intercepts. The results are summarized in Table 4.

Table 4: Thermodynamic parameters of the adsorption process at different temperature.

| Dye | T (°C) | ΔG^0 (kJ/mol) | ΔH^0 (kJ/mol) | ΔS^0 (kJ/mol/K) | R^2 |
|-----|--------|-----------------------|-----------------------|-------------------------|--------|
| MO | 15 | -6.852 | | | |
| | 30 | -7.952 | 14.280 | 73.337 | 0.9204 |
| | 45 | -9.052 | | | |
| MV | 20 | -0.397 | | | |
| | 25 | -0.708 | 35.59 | 122.49 | 0.9733 |
| | 30 | -1.628 | | | |

The obtained negative values of ΔG^0 and positive values ΔH^0 showed that the adsorption of both MO and MV dyes are spontaneous endothermic process, which favored high temperature. The positive value of ΔS^0 suggests the increasing randomness at the solid/solution interface during the adsorption process.

4. Conclusions

In this study, the utility of activated carbon prepared from the fruit of *Wodyetia bifurcata* A.K. Irvine as an adsorbent was investigated for the removal of MO and MV from aqueous solutions. Both dyes were found to adsorb on the surface derived activated carbon. The batch study parameters such as dyes initial concentration, contact time and solution temperature, were found to be effective on the adsorption efficiency of MO and MV. The experimental data obtained from adsorption kinetic and isotherm studies can be successfully fitted to pseudo-second-order kinetic model and Langmuir isotherm model. The maximum sorption capacity was obtained with the Langmuir isotherm at 30 °C and found to be 158.73, 128.61 mg/g for MO and MV, respectively. The adsorption of MO and MV dyes by derived activated carbon is spontaneous endothermic process, which favored high temperature.

Acknowledgements

This work was partially supported from financial support via the Center of Excellence for Innovation in Chemistry (PERCH-CIC), Office the Higher Education Commission, the Ministry of Education and the grant from Research and Graduate School Division, Faculty of Science, Burapha University are also gratefully acknowledged.

References

- [1] N. Dizge, C. Ayiner, E. Demirbas, M. Kobya, S. Kara, *J. Hazard. Mater.* **150** (2008) 737–746.
- [2] H. Cherifia, S. Haninia, F. Bentahar, *Desalination*. **244** (2009) 177–187.
- [3] I.A.W. Tan, A.L. Ahmad, B.H. Hameed, *J. Hazard. Mater.* **153** (2008) 709–717.
- [4] I.D. Mall, V.C. Srivastava, N.K. Agarwal, *Dyes Pigments*. **69** (2006) 210–223.
- [5] B.H. Hameed, *J. Hazard. Mater.* **154** (2008) 204–212.
- [6] S. Lagergren, B.K. Svenska, *Veterskapsakad Handlingar* **24** (1898) 1–6.
- [7] Y.S. Ho, G. McKay, *Chem. Eng. J.* **70** (1998) 115–124.
- [8] S. Chen, J. Zhang, C. Zhang, Q. Yue, Y. Li, and C. Li, *Desalination*. **252** (2010) 149–156.
- [9] I. Langmuir, *J. Am. Chem. Soc.* **40** (1918) 1361–1403.
- [10] A. Afkhami, T. Madrakian, A. Amini, *Desalination*. **243** (2009) 258–264.
- [11] H.M.F. Freundlich, *J. Phys. Chem.* **57** (1906) 385–470.

SMALL-SCALE CHEMISTRY FOR GEOLOGY STUDENTS; ACID RAIN EXPERIMENT

Warunee Manosong¹, Pimchana Hoktha^{2*}

Department of Chemistry, Faculty of Science, Thaksin University, Patthalung, 93110 Thailand

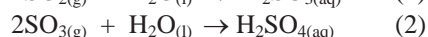
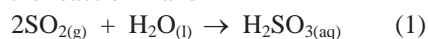
*E-mail: Hoktha@gmail.com

Abstract : In this study describe the study of acid rain by small-scale laboratory for the geology students. In this experiment, the principle of acid rain was designed for students who usually nervous and unfamiliar in chemical laboratory. As a result, students were motivated by integrating chemical knowledge with geology. This experiment was to promote knowledge of chemistry to geology students successfully.

Keywords Small-Scale Chemistry, Acid Rain Experiment

1. Introduction

Acid rain is the rain with pH about < 5.6. Acid rain occurs when emissions of sulfur dioxide (SO₂) or sulfur trioxide (SO₃) react in the atmosphere with water as the reaction 1 and 2



SO₂ and SO₃ can dissolve readily in rain to form acid solutions or acid rain.

The geology students with the non-science major faculty of Humanities and Social Sciences, Thaksin University are required to study general chemistry laboratory course as a basic required course.

The geology students are required to apply the chemical knowledge to the geology context such as factors that affect corrosion of shelters, concrete or marble sculptures, defoliation, bark damaging, wither and dead of plants, acid soil formation that affects plants and underground animals and acidity water in stream or natural sources that affects water animals' population.

The simplicity of the acid rain small-scale laboratory is aimed to engage geology students to learn chemistry with a pleasure. The acid rain by small-scale laboratory was a short experiment which provided accurate results in a short time, used a smaller quantity of chemicals, lower cost, used easier preparation and experimentation, reduced amount of chemicals in the reaction, avoided the dangers from using a larger scale of chemicals and reduced waste disposal.

Hypothesis

Geology students pass the preset criteria at the good level after learning through experimenting about acid rain by using the acid rain small-scale laboratory.



Figure 1 a. Effects of acid rain on stone monument and carvings

(<http://gardenofeaden.blogspot.com/2012/07/effects-of-acid-rain.html>)

b. Effect of acid rain on plants

(http://www.rspg.or.th/plants_data/plantdat/commelin/tspath_1.htm)

2. Materials and Methods

2.1 A set of the acid rain small-scale laboratory with handout was distributed to students.

2.2 Collecting data:

2.2.1 The pre – test of acid rain including 4 items, 10 marks for measuring students' ability to answer the main idea, details, meaning, causes and effects of acid rain prior to form the experiment.

2.2.2 A laboratory report and answered questions of students were collected.

2.2.3 A criteria of quality levels were assigned in table1.

Table 1. The preset criteria.

Efficiency level range of the student's score

| Score | Efficiency Level |
|---------|------------------|
| 8 – 10 | Excellent |
| 7 – 7.9 | Good |
| 6 – 6.9 | Fair |
| 5 – 5.9 | Poor |
| 0 – 4.9 | Very Poor |

2.3 The management procedures for the acid rain small-scale laboratories are below;

The laboratory report of acid rain including 6 items, 10 marks for measuring students' ability to answer the main idea, details, meaning, causes and effects of acid rain prior to form the experiment.

Research Methodology

Within 3 hours, the 56 students have to do A – E activities as following:

- A. (10 min) Students quiz the pre-test exam.
- B. (30 min) Students learn substances, the acid rain theory, cautions of the experiment and check their understanding.
- C. (60 min) Students do the experiment :
 - Part 1: the sources of Sulfur dioxide and acid rain
 - Part 2: the oxidized of SO_2 with H_2O_2 to form SO_3 and H_2SO_4
 - Part 3: Observation and setting situations of dangers (effects) of acid rain
- D. (40 min) Students write the laboratory report and answer the questions.
- E. Collect, analyze and interpret the data before and after doing experiment in mean, SD and percentage.



Figure 2: students are doing pre-test.



Figure 3: Students are doing the experiment.

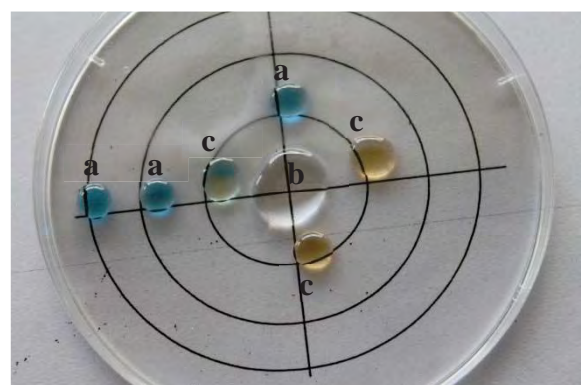


Figure 4: Part 1: the sources of Sulfur dioxide and acid rain

- a. Distilled water + Bromocresol green (blue colored solution)
- b. $\text{Na}_2\text{SO}_3(\text{aq}) + \text{H}_2\text{SO}_4(\text{aq}) \rightarrow \text{Na}_2\text{SO}_4 + \text{H}_2\text{O}(\text{l}) + \text{SO}_2(\text{g})$
- c. $2\text{SO}_2(\text{g}) + \text{H}_2\text{O}(\text{l}) \rightarrow \text{H}_2\text{SO}_3(\text{aq})$
(blue \rightarrow yellow ; indicated the acidity of solution)

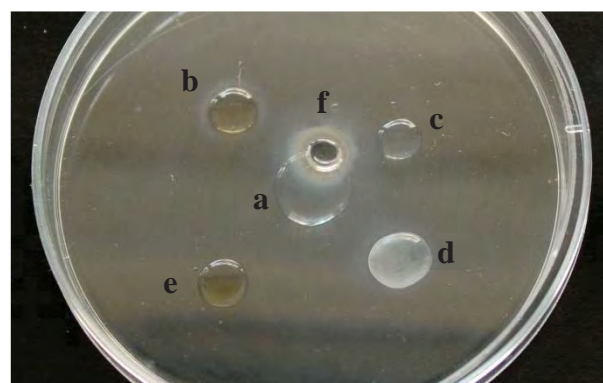


Figure 5: Part 2: the oxidized of SO_2 with H_2O_2 to form SO_3 and H_2SO_4

- a. $\text{Na}_2\text{SO}_3 + \text{H}_2\text{SO}_4 \rightarrow \text{Na}_2\text{SO}_4 + \text{H}_2\text{O} + \text{SO}_2(\text{g})$
- b. $\text{H}_2\text{O} + \text{H}_2\text{O}_2 + \text{SO}_2(\text{g}) \rightarrow \text{H}_2\text{SO}_4(\text{aq}) + \text{H}_2\text{SO}_4(\text{aerosol})$
- c. $\text{BaCl}_2 + \text{H}_2\text{O} + \text{SO}_2(\text{g}) \nrightarrow$
- d. $\text{BaCl}_2 + \text{H}_2\text{O} + \text{H}_2\text{O}_2 + \text{SO}_2 \rightarrow \text{BaSO}_4(\text{s})$
- e. $2\text{SO}_2(\text{g}) + \text{H}_2\text{O}(\text{l}) \rightarrow \text{H}_2\text{SO}_3(\text{aq})$
- f. $\text{H}_2\text{O}_2 + \text{SO}_2(\text{g}) \rightarrow \text{H}_2\text{SO}_4(\text{aerosol})$



Herbaceous plants are 20-60 cm tall. There are largely plump stems that leaves are stacked around as lanceolate and sharp. Also there are cutting base, trunk encircling and smooth edges as well as thick, dark green leaves. There are both single channel and multi-channel. Each channel consists of 2 outer spathe bract is greenish purple. Cone outer two adjacent overlapped, stacked and wrapped jacket white small aggregate clusters. There are calyx three white petals oval, greenish, oblong, some clear petals 3, white oval plate as thick petals and having six stamens. The ovary wall has three holes in a small flat oval seeds.

Anthocyanins are purple or red-purple pigments inside leaf cells. When the leaf is torn, SO_2 in the air touches those pigments and will change the color rapidly. Unlike unbroken leaf, the covered wax will protect the anthocyanins inside from SO_2 . That makes anthocyanins are not changed color.

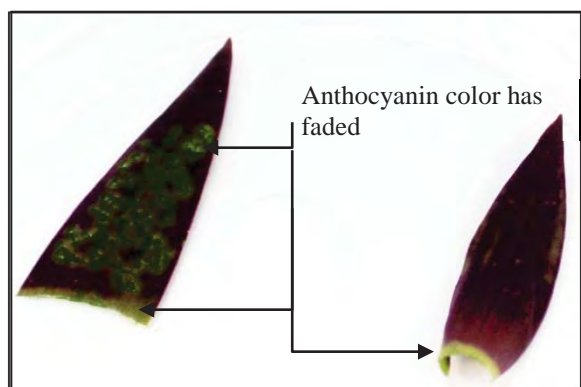
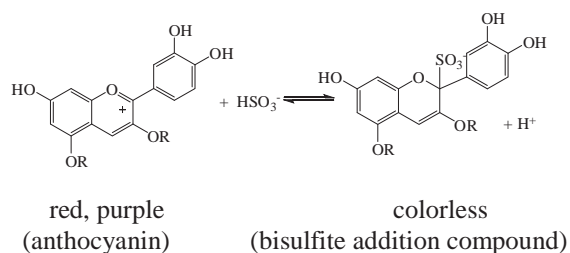


Figure 6 : Part 3: Observation and setting situations of dangers (effects) of acid rain.



3. Results and Discussion

1. 75.81% of students got increased score after teaching by using the proposed method.

2. The scores of pre-test and report were shown in table 2. The results illustrated that the students tested in pre-test obtained score in the very poor level (less than 4.9) However, after teaching, they got the score in good level. Then, it means that these students gained the knowledge of acid rain after teaching them by using the proposed method.

Table 2 Scores and efficiency level of the students in this class room

| Test | Score | | | Efficiency level |
|--------------|-------|------|-------|------------------|
| | Mean | SD | % | |
| Pre-test | 4.31 | 2.04 | 78.57 | Very poor |
| Report score | 7.07 | 0.45 | 91.07 | Good |

4. Conclusion

The observe behaviors of students were recorded. The student reports ($n = 56$) were inspected. The students' acid rain knowledge scores were higher from the poor level up to the good level after learning through doing the experiment by using the acid rain small-scale laboratory.

As a result, students were motivated by integrating chemical knowledge with geology. The experiments were obtained including the origin, diffusion and solubility of sulfur dioxide and then sulfur dioxide was oxidized by hydrogen peroxide to produce sulfuric acid. Clearly, this result can be related to the student's learning theory. Therefore, this experiment is to promote knowledge of chemistry to geology students appropriately.

Acknowledgement

I would like to thank Department of Chemistry., Faculty of Science, Thaksin University.

References

- [1] David R. Schryer *Heterogeneous Atmospheric Chemistry..* American Geophysical Union. 1985.
- [2] Diana H. Carlson, Charles C. Plummer, The Late David Mcgeary. *Physical Geology Eearth Revealed.* McGraw-Hill, 2008.
- [3] Edward L. Waterman, Steven Thompson. *Small-Scale Chemistry Laboratory Manual.* Addison – Wesley Publishing Company, 1995.
- [4] Elizabeth Kay Berner, Robert A. Berner. *Global environment. Water, Air and Geochemical Cycles.* Prentic Hall, Inc. 1996.
- [5] Stephen Thompson, *Chemtrek:Small-Scale Experiments for General Chemistry.* Prentice Hall, 1990.
- [6] http://www.epa.gov/acidrain/effects/surface_water.html
- [7] http://en.wikipedia.org/wiki/Acid_rain
- [8] <http://www.smallscalechemistry.colostate.edu>

EFFECT OF POLYETHYLENE GLYCOL 400 ON ENTRAPMENT EFFICIENCY OF ELLAGIC ACID-LOADED NIOSOMES

Samonthorn Poomsiripaiboon¹, Varaporn Buraphacheep Junyaprasert^{1*}

¹ Department of Pharmacy, Faculty of Pharmacy, Mahidol University, Rajthevi, Bangkok, 10400 Thailand

* Author for correspondence; E-Mail: varaporn_jun@mahidol.ac.th, Tel. +66 26448677-91, Fax. +66 26448694

Abstract: Ellagic acid (EA) is a potent antioxidant phytochemical substance which has shown a whitening property. Due to the low solubility of EA, it is difficult to formulate into a cosmetic product. This study aimed to develop niosomes of EA and to investigate the influence of polyethylene glycol (PEG) 400, used as a solubilizer, on the entrapment efficiency of EA-loaded niosomes. EA-loaded niosomes were prepared by reverse phase evaporation (REV) method using Span 60, Tween 60 and cholesterol as vesicle forming agents. To solubilize EA, 10-25% (v/v) PEG 400 was added into an aqueous phase containing EA. In order to reduce the particle size of niosomes with homogeneous size, probe sonication was applied to REV vesicles. Particle size and polydispersity index (PI) of niosomes were measured by photo correlation spectroscopy (PCS). The results showed that after being subjected to the probe sonication process, the mean particle sizes of EA-loaded niosomes was in the range of 150-200 nm with PI values less than 0.4. An increase in PEG 400 amount did not alter the vesicle size and PI value of niosomes. Moreover, the entrapment efficiency of EA in niosomes was determined by ultrafiltration technique and the concentrations of EA were analyzed using HPLC spectrophotometry. The addition of PEG 400 increased solubility and entrapment efficiency of EA. Increasing concentration of PEG 400 in aqueous phase from 10-25%, entrapment efficiency of EA was found to be 8.65-60.06%. In conclusion, this study indicated that the Span 60/Tween 60 niosomes of EA were successfully developed with the use of PEG 400 as a solubilizer. An increase in concentration of PEG 400 could increase the entrapment efficiency of EA-loaded niosomes.

1. Introduction

Melanin is a key factor determining the color of skin. The tyrosinase enzyme plays the most important role in melanin synthesis. Several tyrosinase inhibitors have been proposed, based on the view that melanogenesis can be controlled and skin-whitening products can be developed if tyrosinase activity can be suppressed [1]. One such compound is ellagic acid (EA), a major polyphenolic antioxidant, found in wide varieties of berries and nuts. EA has been already proven its antioxidant potential both *in vitro* and *in vivo*. Like other polyphenols, EA possesses a wide range of biological activities such as antioxidant, antimutagenic, antitumor, antihyperglycemic and anti-infective effects [2]. In addition, *in vitro* studies found that EA could inhibit mushroom-derived tyrosinase competitively and in a dose-dependent manner. The inhibition constant (k_i) is 81.6 μ M [3]. According to the results of the animal studies using the brownish

guinea pig, EA is a more efficient skin whitener and suppressor of pigmentation than arbutin or kojic acid, other active skin whiteners, at the same dose level (1%) and its efficacy is almost the same as that of hydroquinone without injuring cells. However, there is no cosmetic product available that can deliver therapeutically adequate dose due to the poor aqueous solubility (~9.7 μ g/ml) [4] and low skin penetration of EA. Thus, there is a strong need to deliver this molecule by unconventional means which can circumvent biopharmaceutical and pharmacokinetic issues related with EA without compromising its therapeutic potential.

Encapsulation of a drug in vesicular structures can be predicted to prolong the existence of the drug in the systemic circulation, enhance the solubility and thus enhance penetration into target tissues. Non-ionic surfactant based vesicles (niosomes) are formed from the self-assembly of non-ionic amphiphiles in aqueous media resulting in closed bilayer structures which can entrap both hydrophilic and lipophilic drugs either in an aqueous layer or in vesicular membrane. These structures are analogous to phospholipids vesicles (liposomes) and serve as drug carriers. The low cost, greater stability and resultant ease of storage of non-ionic surfactants has lead to the exploitation of these compounds as alternatives to phospholipids [5].

Niosomes are versatile carrier systems that can be administered through various routes including dermal and transdermal. In terms of transdermal or topical drug delivery, niosomes appear to be gaining in popularity. They are thought to improve the horny layer properties, both by reducing transepidermal water loss and by increasing smoothness via replenishing lost skin lipids. Non-ionic surfactants normally show favorable dermatological properties, being very mild to the skin and eye [6]. Therefore, niosomes are interesting for a development into carriers for dermal and transdermal delivery of active substances.

In the present work, the niosomes obtained from the mixtures of Tween 60 and Span 60 using reverse phase evaporation (REV) method were developed to encapsulate EA for dermal delivery. Due to the low solubility of EA, polyethylene glycol (PEG) 400 was used as solubilizer at various concentrations. The influences of PEG 400 on the entrapment efficiency of EA-loaded niosomes and their particle size were investigated.

2. Materials and Methods

2.1 Materials

Sorbitan monostearate (Span 60) and polyethylene glycol sorbitan monostearate (Tween 60) were obtained from Uniqema (Chicago, USA). EA and PEG 400 were purchased from Fluka (West St. Paul, USA). Cholesteryl poly-24-oxyethylene ether (Solulan C24) was received as a gift sample from Amerchol (NJ, USA). All other solvents were of HPLC grade and triple distilled water was used.

2.2 Preparation of EA-loaded niosomes

The Span 60/Tween 60 niosomes of EA were prepared by reverse phase evaporation (REV) method [7]. Briefly, the mixture of surfactants (2:1 Span 60 and Tween 60) and cholesterol in 1:1 mole ratio and Solulan C24 were dissolved in diethyl ether (organic phase). To solubilize EA, 10, 15, 20 and 25% (v/v) PEG 400 was added into aqueous phase containing EA. At 1.5:1 the organic phase: the aqueous phase, the aqueous phase was added to the lipid mixture and mixed until a homogeneous w/o emulsion was obtained. The w/o emulsion was sonicated at 7°C for 10 min. Then, diethyl ether was slowly removed under reduced pressure using rotary evaporator (60 rpm) until niosomal suspension was completely formed. The dispersion was evaporated about 15 min and then nitrogen gas was purged into dispersion for substitution of diethyl ether. In order to reduce the particle size of niosomes with homogeneous size, probe sonication was applied to REV vesicles. The niosome formulations were placed in an ice bath to prevent overheating and sonication was applied by a probe sonicator at 60% amplitude with a pulse of 30 sec for a period of 15 min. The composition of each formulation is listed in Table 1.

Table 1: The composition of niosome formulations (in 50 ml water)

| Formulation | E-10P | E-15P | E-20P | E-25P |
|---------------------------------|-------|-------|-------|-------|
| Span 60 (μmole) | 500 | 500 | 500 | 500 |
| Tween 60 (μmole) | 250 | 250 | 250 | 250 |
| Cholesterol (μmole) | 750 | 750 | 750 | 750 |
| Solulan C24 (mol%) ^a | 5 | 5 | 5 | 5 |
| EA (mol%) ^a | 1 | 1 | 1 | 1 |
| PEG 400 (%v/v) ^b | 10 | 15 | 20 | 25 |

^a The amount of Solulan C24 and EA were calculated in mol% of total lipid (1500 μmole)

^b The amount of PEG 400 was calculated in %v/v of aqueous phase

2.3 Measurement of vesicle size and size distribution of niosomes

Vesicle size and size distribution of niosomes were determined by photo correlation spectroscopy (PCS) with a Malvern Zetasizer ZS (Malvern Instruments, UK). The mean vesicle size (z-ave) and polydispersity index (PI) were obtained by averaging of 10 measurements at an angle of 90° in 10 mm diameter cells at 25°C. The real refractive index and the imaginary refractive index were set at 1.456 and 0.001, respectively.

2.4 Determination of entrapment efficiency

The prepared niosomes of EA were separated from unentrapped EA by ultrafiltration using centrifugal filter tubes with a molecular weight cut-off of 30 kDa which were centrifuged (Optima™ Model LE-80K, Beckman, USA) at 12,500 rpm for 30 min. The isolated pellets were dissolved in methanol (MeOH) and then diluted 10 folds with MeOH and 0.1% (v/v) phosphoric acid in water (1:1, v/v). The concentration of EA in niosomes and ultrafiltrate (free drug) were analyzed using HPLC method. The percentage of EA entrapment efficiency (% E.E.) was defined as follows:

$$\% \text{ E.E.} = \frac{\text{Amount of EA loaded in niosomes}}{\text{Total amount of EA added}} \times 100$$

2.5 HPLC analysis

The concentrations of EA were measured by HPLC (Model LC-10AD, Shimadzu, Japan). The stationary phase was Hypersil® ODS C18 reverse-phase column (250×4.6 mm, 5 μm) used in isocratic mode at ambient temperature. The mobile phase was a mixture of 0.1% phosphoric acid, MeOH and acetonitrile (42:48:10, v/v). The UV detection was performed at a wavelength of 254 nm, the flow rate was 0.8 ml/min and the injection volume was 20 μl. Prior to the analysis, validation of the HPLC method was performed to ensure linearity of the calibration curve between 0.05 and 10 μg/ml with a correlation coefficient value of 0.9999. The high precision for repeatability and reproducibility with coefficients of variation of less than 2% was found. The accuracy was determined by three replicate injections of three different concentrations of EA, and the percent recovery was found to be 100.11±0.06%. Therefore, the HPLC method used in this study demonstrated good linearity, precision and accuracy for determination of EA concentration.

2.6 Statistical analysis

Statistical analysis of the differences in the physicochemical properties among predetermined intervals in the same formulation and between formulations was performed by using paired-t test and one-way analysis of variance (one-way ANOVA), respectively. The level of significance was taken at *p* value of 0.05.

3. Results and Discussion

The Span 60/Tween 60 niosomes of EA were prepared using different concentrations of PEG 400, used as a solubilizer, by REV method. The results showed that all formulations were able to form vesicles. Theoretically, a non-ionic surfactant with single alkyl tail such as Span 60 can form vesicular structure since it has relatively large hydrophobic moiety (HLB = 4.7) with low water solubility. In contrast, some surfactants with higher HLB (hydrophilicity) such as Tween 60 cannot form vesicle. These surfactants can form vesicle only in the presence of suitable amounts of cholesterol [8]. Hence, the mixtures of Span 60, Tween 60 and cholesterol in this study provided the ability to form vesicles.

3.1 Vesicle size and size distribution

Figure 1 shows the mean vesicle size (z-ave) and polydispersity index (PI) of EA-loaded niosomes evaluated by PCS after production. The vesicle size and PI values of EA-loaded niosomes before probe sonication were 449-803 nm and 0.517-0.764, respectively. After probe sonication, the vesicle size and PI reduced to 151-157 nm and less than 0.4, respectively. In general, the PI values higher than 0.4 indicating large size distributions which lead to aggregates [7]. Therefore, probe sonication was found to be effective on size reduction of the niosomes. In addition, an increase in the amount of PEG 400 did not significantly affect the niosome size and PI value ($p>0.05$).

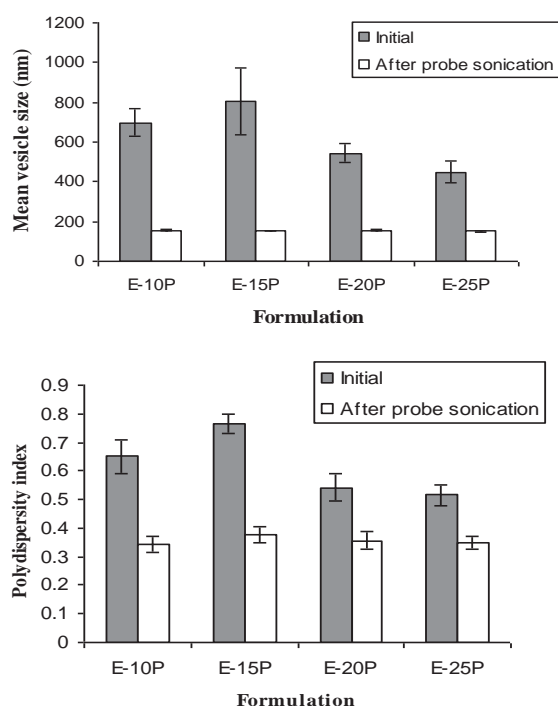


Figure 1. Mean vesicle size (z-ave, upper panel) and polydispersity index (PI, lower panel) of EA-loaded niosome formulations before and after probe sonication.

3.2 Entrapment efficiency

The entrapment efficiency of EA-loaded niosomes after probe sonication was determined by analysis of entrapped drugs presented in the niosomal pellets and free drugs presented in the ultrafiltrate after separation by ultrafiltration. The drug content in the vesicles and the ultrafiltrate were analyzed by HPLC spectrophotometry using the conditions as previously described. The entrapment efficiency (% E.E.) of EA in the niosomes varied between 8.65% and 60.06% depending on the amount of PEG 400 used. The highest entrapment efficiency was found in niosomes prepared with the highest amount, 25% (v/v), of PEG 400, as shown in Table 2. The results indicated that the entrapment of EA in niosomes was significantly elevated with increasing the concentration of PEG 400 in the system ($p<0.05$). This may be resulted from the localization of PEG 400 molecules between double layers of vesicle and the high solubility of EA in PEG 400 which can form suitable hydrogen bonds by the interactions between phenolic groups and lactone moiety of EA and polyoxyethylene groups of PEG 400. Moreover, mixtures of Span 60 and Tween 60 created suitable hydrophobic and hydrophilic properties provide these systems excellent entrapment of solubilized forms of EA [7].

Table 2: Entrapment efficiency of EA-loaded niosomes

| Formulation | PEG 400 (%v/v) | % E.E. ^a |
|-------------|----------------|---------------------|
| E-10P | 10 | 8.65 ± 0.72 |
| E-15P | 15 | 22.06 ± 1.03 |
| E-20P | 20 | 39.63 ± 0.69 |
| E-25P | 25 | 60.06 ± 1.30 |

^a The values are expressed as the mean ± SD, n = 3

4. Conclusions

The Span 60 and Tween 60 niosomes of EA were successfully developed with the use of PEG 400 as a solubilizer. The Span 60/Tween 60 niosome formulations were able to effectively encapsulate EA and had small nanosized vesicles with a monodisperse distribution. This study indicated that an increase in concentration of PEG 400 could increase the entrapment efficiency of EA-loaded niosomes. This system may be used for the development of EA-loaded niosomes, which may be good candidates for EA delivery.

Acknowledgements

The authors would like to thank the Graduate College of Mahidol University for the support of this work.

References

- [1] Y. Tanaka In: M. Paye, A.O. Barel and H.I. Maibach, Editors, *Handbook of Cosmetic Science and Technology*, Taylor & Francis, Florida (2006), pp.313-318.
- [2] J.M. Landete, *Food. Res. Int.* **44** (2011) 1150-1160.
- [3] H. Shimogaki, Y. Tanaka, H.Tamai and M. Masuda, *Int. J. Cosmetic. Sci.* **22** (2002) 291-303.
- [4] I. Bala, V. Bhardwaj, S. Hariharan and M.N.V. Ravi Kumar, *J. Pharm. Biomed. Anal.* **40** (2006) 206-210.
- [5] I.F. Uchegbu and A.T. Florence, *Adv. Colloid. Interface. Sci.* **58** (1995) 1-55.
- [6] A.S. Guinedi, N.D. Mortada, S. Mansour and R.M. Hathout, *Int. J. Pharm.* **306** (2005) 71-82.
- [7] V.B. Junyaprasert, P. Singhsa, J. Suksiriworapong and D. Chantasart, *Int. J. Pharm.* **423** (2012) 303-311.
- [8] A. Pardakhty, J. Varshosaz and A. Rouholamini, *Int. J. Pharm.* **328** (2007) 130-141.

INFLUENCE OF LIQUID LIPID ON SIZE, ZETA POTENTIAL AND ENTRAPMENT EFFICIENCY OF LUTEIN-LOAD NANOSTRUCTURED LIPID CARRIERS

Putita Boribalnukul¹, Varaporn Buraphacheep Junyaprasert^{1*}

Department of Pharmacy, Faculty of Pharmacy, Mahidol University, Bangkok, 10400 Thailand

* Author for correspondence; E-Mail: varaporn.jun@mahidol.ac.th, Tel. +66 26448677-91, Fax. +66 26448694

Abstract: Lutein is the subclass of non-provitamin A carotenoids known as xanthophylls which is able to increase the elasticity and hydration of the skin. The aim of this study was to formulate a delivery system of lutein for dermal and cosmetic applications by incorporation into nanostructured lipid carriers (NLC) using glyceryl monostearate as a solid lipid and various amounts of coconut oil, rice bran oil or palm oil as a liquid lipid in the formulations. The lipid nanoparticles were produced by high pressure homogenization method. By photon correlation spectroscopy, the mean particle size of all formulations was in the range 100-130 nm and the negative charge of zeta potential values were lower than 30 mV. An increase in oil loading did not affect the mean particle size and zeta potential of NLC formulations. In addition, the solubility of lutein in oil and the entrapment efficiency was evaluated by high-performance liquid chromatography and found that the solubility of lutein in coconut oil, rice bran oil and palm oil was not difference while the entrapment efficiency of lutein in NLC increased when increasing liquid oil concentration.

1. Introduction

Solid lipid nanoparticles (SLN) are the nano-carriers which are in solid state at room temperature and change to liquid while melting at increasing temperature. Generally, SLN are composed of 0.1% (w/w) to 30% (w/w) solid lipid dispersed in an aqueous medium and if necessary stabilized with preferably 0.5% (w/w) to 5% (w/w) surfactant [1]. Solid lipid nanoparticles have been introduced as a potent carrier system for various pharmaceutical and cosmetic active compounds. They are capable of protecting unstable active compounds against degradation, releasing the active ingredients in a controlled way and prolonging residence time of some actives such as sunscreens in the stratum corneum, as well as targeting drug to the upper layer of skin [2]. However, some problems also occurred including low drug loading and drug expulsion from the carrier during storage time owing to the crystal lattice upon polymorphic transitions into perfect crystals with a limited number of imperfections. These problems arise from the composition of solid lipids, which generally are pure lipids and/or a blend of solid lipids [3,4]. To overcome the limitations of SLN, nanostructured lipid carriers (NLC) have been developed and reported as the second generation of lipid nanoparticles. In

contrast to SLN being produced from solid lipids, the NLC are produced using blends of solid lipids and liquid lipids (oils) [5]. The solubility of active ingredients in oils is generally much higher than in solid lipids. For this reason, the higher loading capacity can be achieved by the development of NLC. With this approach, drug expulsion during storage time is also minimized. Admixture of liquid with solid lipids leads to the creation of a less ordered inner structure. Thus, the drug molecules can be accommodated in between lipid layers and/or fatty acid chains [6].

Lutein is a member of the carotenoid family of lipid soluble pigments. It has gained recognition as being potentially beneficial to human health, particularly to prevent the development of certain chronic eye diseases. Recent studies showed a beneficial association between consumption of lutein and a lower incidence of age-related macular degeneration (AMD) and cataracts, the leading causes of acquired blindness in the elderly population around the world [7,8]. The benefit of lutein in humans does not stop with eye health but also more generally as an antioxidant. It is able to quench singlet oxygen, a highly reactive free radical that can damage deoxyribonucleic acid (DNA) [9]. In addition, consumption of carotenoids, including lutein, is believed to play a role in maintaining skin health by reducing UV-induced erythema [10, 11]. In 2006, a clinical trial was designed to study the efficacy of lutein and zeaxanthin on the skin. This study demonstrated that the topical treatment with lutein (50 ppm, 2 times per day) showed an immediate increase in superficial skin lipids, significant reduction in skin lipid peroxidation, increasing in the photoprotective activity, skin elasticity and skin hydration. Even the combined oral and topical treatment of lutein exhibited the greatest efficacy in most previous cases [12], lutein is liposoluble and an unstable molecule. To avoid these problems, it should be encapsulated into lipid nanoparticle.

Palm oil, rice bran oil and coconut oil are among the most widely used vegetable oils in Thailand. They have been used in many cosmetic products as skin hydrating agents and emollients for a long time. In present study, palm oil, rice bran oil and coconut oil were used as liquid lipid in lutein-loaded NLC formulation which was aimed to investigate an effect

of the amount of each oil on particle size, zeta potential and entrapment efficiency of lutein-loaded NLC.

2. Materials and Methods

2.1 Materials

The materials used in this study were Cithrol® GMS 40 (Glyceryl monostearate, Croda, Germany), lutein powder 80% (Xian Huarui Bio-engineering, China), poloxamer 188 (BASF, Germany), rice bran oil (King, Thailand), coconut oil (Pure magic, Thailand), palm oil (Lam Soon Public, Thailand), acetonitrile and methanol HPLC grade (Burdick & Jackson, Korea).

2.2 Preparation of NLC

Lutein-loaded NLC were prepared by hot high pressure homogenization technique in 100 ml batches. Briefly, the lipid phase containing solid lipid, liquid lipid was melted at 80°C, followed by an addition of lutein. The hot aqueous surfactant solution was added to the melted lipid phase under stirring by high speed homogenizer (Ultra-Turrax T25, IKA, Germany) for 1 min at 8000 rpm. The pre-emulsion was further processed by high pressure homogenizer (APV-2000, SPX Flow Technology, Germany) applying three homogenization cycles at 500 bar. The lipid dispersion was cooled down under ambient conditions to room temperature and formed into NLC dispersions. The composition of all formulation is show in Table 1.

2.3 Particle size

Particle size (z-ave) and polydispersity index (PI), a measure of the width of the size distribution, were determined by photon correlation spectroscopy (PCS) using Zetasizer Nano ZS (Malvern Instruments, UK). The z-ave and PI values were obtained being the average of 10 measurements at an angle of 90° in 10 mm diameter cells at 25 °C. All samples were diluted with deionized water to a suitable scattering intensity. To observe the presence of microparticles, the laser diffractometry (LD) using Mastersizer 2000 (Malvern Instruments, UK) was applied. The obtained data were

evaluated using the volume distribution ($d_{10\%}$, $d_{50\%}$, $d_{90\%}$) and span values. The diameter values indicate the percentage of particles possessing an equal to or lower than the given value. The Span value is a statistical parameter useful to evaluate the particle size distribution and calculated applying the following equation:

$$\text{Span} = \frac{d_{90\%} - d_{10\%}}{d_{50\%}}$$

2.4 Zeta potential

The zeta potential (ZP) is assessed by determining particle electrophoretic mobility using Zetasizer NanoZS (Malvern Instruments, UK). Zeta potential values were calculated using the Helmholtz-Smoluchowsky equation.

2.5 Determination of entrapment efficiency

The entrapment efficiency of lutein-loaded NLC is determined directly by ultrafiltration method using centrifugal filter tubes (Amicon Ultra-4, Millipore, Ireland) with a 30 kDa molecular weight cut-off. The lipid nanoparticles were dissolved with acetone and then diluted with methanol. The percentage of incorporated lutein was determined by high performance liquid chromatography (HPLC) at wavelength of 450 nm running in the isocratic mode. The system consisted of Hypersil® ODS C18 RP column (Thermo scientific, USA). The mobile phase was a mixture of methanol and acetonitrile (90:10, v/v). The flow rate was 1 mL/min at room temperature. Encapsulation efficiency was calculated based on the following equation:

$$\text{E.E. (\%)} = \frac{\text{Lutein in nanoparticle}}{\text{Total amount of lutein}} \times 100$$

2.6 Solubility study

The solubility of lutein in various oils such as coconut oil, palm oil and rice bran oil was determined by placing an excess amount of lutein in a test tube containing 1 mL of each oil. The mixtures were vortexed and equilibrated at room temperature for 48 h in shaker bath. Undissolved lutein was removed by centrifuged at 3,000 g for 15 min. Supernatant was taken and dissolved with acetone, then diluted with methanol. The solubility of lutein was determined by

Table 1: Formulation of Lutein-loaded NLC system (% w/w)

| Formulations | GMS | Palm oil | Coconut oil | Rice bran oil | Poloxamer 188 | Lutein | Water q.s. |
|----------------|------|----------|-------------|---------------|---------------|--------|------------|
| Lutein-NLC-P5 | 9.31 | 0.49 | | | 2.5 | 0.2 | 100 |
| Lutein-NLC-P10 | 8.82 | 0.98 | | | 2.5 | 0.2 | 100 |
| Lutein-NLC-P20 | 7.84 | 1.96 | | | 2.5 | 0.2 | 100 |
| Lutein-NLC-C5 | 9.31 | | 0.49 | | 2.5 | 0.2 | 100 |
| Lutein-NLC-C10 | 8.82 | | 0.98 | | 2.5 | 0.2 | 100 |
| Lutein-NLC-C20 | 7.84 | | 1.96 | | 2.5 | 0.2 | 100 |
| Lutein-NLC-R5 | 9.31 | | | 0.49 | 2.5 | 0.2 | 100 |
| Lutein-NLC-R10 | 8.82 | | | 0.98 | 2.5 | 0.2 | 100 |
| Lutein-NLC-R20 | 7.84 | | | 1.96 | 2.5 | 0.2 | 100 |

HPLC as previously described.

2.7 Statistics

The data are presented as mean values \pm standard deviation (SD). Significance of difference was evaluated using Student's *t*-test and one way ANOVA at probability level of 0.05.

3. Results and Discussion

3.1 Particle size and zeta potential analysis

Aqueous lutein-loaded NLC dispersions composed of 10% lipid phase (solid lipid, liquid lipid and lutein) were prepared using different ratios between solid lipid and liquid lipid, i.e. 95:5, 90:10, 80:20 and different type of liquid lipid. Table 2 shows the mean particle size (z-ave) of NLC evaluated by PCS. After production, it was found that the amount of oil loading did not affect the particle size of NLC. In general, the mean particle size of lipid nanoparticles depends on several factors, e.g. type and concentration of lipids and surfactants, and the viscosity of the lipid phase. However, the z-ave values of NLC with various carrier oils were slightly different, indicating that the liquid oils did not affect the particle size of the NLC. This may be due to the fact that during the production process of NLC, the lipid and aqueous phases were heated up to 80 °C, thus the viscosity of the lipid phase composed of different oil should be nearly similar [13]. In addition, LD was performed due to the limitation of PCS to detect the presence of microparticles. Table 3 shows that the obtained volume distribution diameter of 90% particles was lower than 420 nm. Furthermore, PI value of all formulations was lower than 0.3 indicating the narrow size distribution.

Table 2: Mean particle size (z-ave), polydispersity index (PI) and zeta potential values of lutein-loaded NLC formulations by PCS (25°C) on the day of production

| Formulations | Z-ave | PI | ZP (mV) |
|----------------|-----------------|-------------------|-----------------|
| Lutein-NLC-P5 | 109.6 \pm 2.7 | 0.235 \pm 0.017 | -25.3 \pm 4.8 |
| Lutein-NLC-P10 | 115.3 \pm 2.6 | 0.254 \pm 0.013 | -27.6 \pm 2.7 |
| Lutein-NLC-P20 | 116.3 \pm 2.6 | 0.261 \pm 0.021 | -29.1 \pm 1.9 |
| Lutein-NLC-C5 | 106.0 \pm 2.8 | 0.232 \pm 0.025 | -17.4 \pm 1.1 |
| Lutein-NLC-C10 | 105.2 \pm 3.1 | 0.278 \pm 0.021 | -18.8 \pm 1.8 |
| Lutein-NLC-C20 | 103.9 \pm 2.2 | 0.240 \pm 0.022 | -20.5 \pm 1.0 |
| Lutein-NLC-R5 | 123.9 \pm 1.8 | 0.217 \pm 0.025 | -28.5 \pm 1.9 |
| Lutein-NLC-R10 | 117.2 \pm 3.7 | 0.243 \pm 0.022 | -25.6 \pm 4.8 |
| Lutein-NLC-R20 | 122.7 \pm 4.4 | 0.262 \pm 0.038 | -25.9 \pm 5.7 |

The analysis of the ZP, which is the electric potential at plan of shear, is a useful tool to predict the physical storage stability of colloidal systems. Normally, negative/positive charge of ZP values lower than 30 mV is considered a slight stable formulation. The stable formulation should present the

negative/positive charge of ZP higher than 30 mV. In the present study, the zeta potential values were in the range of -17.4 to -29.1 mV (Table 2). This might be attributed to poloxamer 188, a nonionic surfactant which decreases the electrostatic repulsion between the particles and sterically stabilizes the nanoparticles by forming a coat around their surface [14].

Table 3: Volume distribution diameters in micrometer (μ m) (d10%, d50%, d90%) and Span values obtained by LD on the day of production

| Formulations | d10% | d50% | d90% | Span |
|----------------|-------|-------|-------|-------|
| Lutein-NLC-P5 | 0.140 | 0.190 | 0.302 | 0.851 |
| Lutein-NLC-P10 | 0.143 | 0.196 | 0.320 | 0.901 |
| Lutein-NLC-P20 | 0.143 | 0.197 | 0.328 | 0.942 |
| Lutein-NLC-C5 | 0.140 | 0.199 | 0.390 | 1.024 |
| Lutein-NLC-C10 | 0.140 | 0.197 | 0.340 | 1.014 |
| Lutein-NLC-C20 | 0.143 | 0.197 | 0.345 | 1.025 |
| Lutein-NLC-R5 | 0.141 | 0.194 | 0.336 | 1.140 |
| Lutein-NLC-R10 | 0.143 | 0.198 | 0.369 | 1.143 |
| Lutein-NLC-R20 | 0.140 | 0.199 | 0.412 | 1.365 |

3.2 Entrapment efficiency and solubility study

The effect of oil content on drug entrapment efficiency of NLC was also investigated. Figure 1 shows that the drug entrapment efficiencies were increased with increasing the amount of oil ($P < 0.05$). This is due to an increase in the number of imperfections in the particle matrix, providing space for the accommodation of drug molecules. Table 4 show the solubility of lutein in palm oil, coconut oil and rice bran oil. The results shown that the solubilities of lutein in various oils were comparable which may be related to the results that %E.E of the NLC formulations of all oils was not different when using at the same concentration ($p > 0.05$).

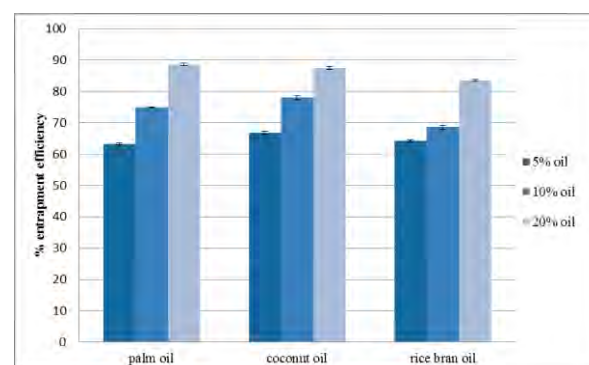


Figure 1. Drug entrapment efficiency of lutein-loaded NLC.

Table 4: Solubility of lutein in various oils

| Oils | Lutein (mg/oil 1 g) |
|---------------|---------------------|
| Palm oil | 0.67 |
| Coconut oil | 0.46 |
| Rice bran oil | 0.55 |

4. Conclusions

In this work, lutein-loaded NLC were formulated using glyceryl monostearate as a solid lipid and various amounts of coconut oil, rice bran oil or palm oil as a liquid lipid in the formulations. The mean particle size of all formulations was in the range 100-130 nm with a narrow size distribution. The negative charge of zeta potential values were lower than 30 mV. The results from this study indicated that type of oil and the amount of oil did not affect the mean particle size and zeta potential of NLC formulations. In addition, the solubility of lutein in coconut oil, rice bran oil and palm oil was comparable leading to similar entrapment efficiency of NLC at the same concentration of oils used. However, the entrapment efficiency of lutein in NLC increased when increasing liquid oil concentration.

Acknowledgements

The authors express thanks to the Graduate Collage of Mahidol University for support this work.

References

- [1] K. Jaspreet, S. Gurpreet, S. Seema and R AC, *JDDT* **2** (2012) 146–150.
- [2] E.S. Farboud, S.A. Nasrollahi and Z. Tabbakhi, *Int J Nanomedicine* **6** (2011) 611-617.
- [3] V. Teeranachaideekul, E.B. Souto, V.B. Junyaprasert and R.H. Muller, *Eur J Pharmaceut Biopharmaceut* **67** (2007) 141-148.
- [4] A. Saupe, S.A. Wissing, A. Lenk, C. Schmidt and R.H. Muller, *Biomed Mater Eng* **15** (2005) 393-402.
- [5] R.A. Sanad, N.S. AbdelMalak, T.S. elBayoomy and A.A. Badawi, *AAPS PharmSciTech* **11** (2010) 1684-1694.
- [6] R.H. Muller, M. Radtke and S.A. Wissing, *Adv Drug Deliv Rev* **54** (2002) S131–S155.
- [7] B. Olmedilla, F. Granado, I. Blanco and M. Vaquero, *Nutrition* **19** (2003) 21–24.
- [8] S. Richer, W. Stiles, L. Statkute, J. Pulido, J. Frankowski, D. Rudy, K. Pei, M. Tsipursky and J. Nyland, *Optometry* **75** (2004) 216–230.
- [9] B. Lockwood, *Pharmaceutical Press* **2** (2007) 1-3.
- [10] W. Stahl and H. Sies, *Appl Skin Physiol* **15** (2002) 291-296.
- [11] A.A. Rodrigues and A Shao, *Toxicology Letters* **150** (2004) 57-83.
- [12] P. Palombo, G Fabrizi, V. Ruocco, E. Ruocco, J. Fluhr, R. Roberts and P. Morganti, *Skin Pharmacol Physiol* **20** (2007) 199-210.
- [13] V. Teeranachaideekul, P. Boonme, E.B. Souto, R.H. Muller and V.B. Junyaprasert, *J Control Release* **128** (2008) 134-141.
- [14] H. Jifu, F. Xinsheng, Z. Yanfang, W. Jianzhu, G. Fengguang, L. Fei and P. Xinsheng, *Int J Nanomedicine* **6** (2011) 683-692.

METHYL SALICYLATE ENCAPSULATED IN BIODEGRADABLE POLYMER MICROCAPSULES

Sarinya Shawaphun^{1,2*}, Thara Manangan^{1,2}

¹Department of Industrial Chemistry, Faculty of Applied Science, King Mongkut's University of Technology North Bangkok, Bangsue, Bangkok, Thailand

²Research Center of Nano Industries and Bio-plastics, King Mongkut's University of Technology North Bangkok, Bangsue, Bangkok, Thailand

*Sarinya Shawaphun; E-Mail: Sarinya73@yahoo.com, Tel. +66 25552000 ext 4823

Abstract: Methyl salicylate (MS) is an organic ester drug that is naturally produced by many species of plants. MS is used in high concentrations as a rubefacient in deep heating liniments to treat joint and muscular pain. Biodegradable polymer microcapsules, made of Poly(lactic acid) (PLA) and Poly(butyleneadipate-co-terephthalate) (PBAT), have been used to encapsulate MS for preventing fast evaporation when using as coating material on elastic bandage to treat joint and muscular pain. These microcapsules were prepared by emulsification evaporation technique by using Poly(vinyl acetate-co-vinyl alcohol) (PVAc-co-VA) as an emulsifier. Some parameters such as polymer matrix, amount of MS and % of vinyl alcohol in P(VAc-co-VA) emulsifier have been studied to find the optimal condition. Then, MS encapsulated in both types of biodegradable polymers microcapsules were separated by extracting with methanol and quantified the amount by spectrophotometric method to determine the efficiency of container pellets. From our results, we found that MS was encapsulated up to 93.54% in PLA microcapsule and 86.60% in PBAT microcapsule.

1. Introduction

The encapsulation of drugs in biocompatible and biodegradable polymer microcapsules is a promising advancement to protect the functional properties of the encapsulated bioactive agents that have to be delivered active, pure and untransformed [1]. In addition to maintain the drug in the desired therapeutic range with a single administration, controlled release systems may offer other favourable prospects such as to localize the delivery of drug to particular sites, to stabilize rapidly vaporized drugs and to increase patient comfort. Surfactant and/or polymer based emulsions have been widely used as drug carriers in pharmacy as well as templates in the production of micro/nanocapsules and particles for controlled/targeted release and/or drug protection against environmental conditions [2]. The common structure of these potential drug-delivery scaffold consist of a hydrophobic interior (hydro-phobic core of a surfactant micelle or polymer matrix in a core of micelle) and a hydrophilic shell, which is mostly intended to entrap and deliver small molecule drugs *via* hydrophobic interactions to obtain increased solubility and stability [3]. The most important key factors of tailor-made drug carrier micro/nanocapsules and particles that determine their efficacy are particle

morphology (including size and shape), drug loading, and most important, drug release profiles. It is expected that the release pattern of the drugs from polymer microcapsule is affected by the rate of drug diffusion out of the polymer matrix, which in turn depends on the chemical structure of the polymer (polarity, glass transition temperature, flexibility of the polymer backbone) and the drug-polymer matrix interaction that can be achieved through the choice of the matrix material and size control of the microspheres [4].

Various methods for the preparation of solid dispersions or micro/nanoparticles using enteric polymers have been developed including solvent evaporation, co-precipitation, emulsification/solvent evaporation, emulsification/diffusion and salting-out method [5]. For these methods, the emulsification/solvent evaporation method is popularly used for microspheres preparation because of its simplicity, reproducibility and fast processing with minimum controllable process variables that can be easily implemented [6-7]. In this method, a volatile organic phase containing dissolved polymer is emulsified in an aqueous phase under constant stirring. The drugs are usually incorporated into the organic phase, in dissolved or dispersed stages and then evaporating the solvent. Among other uses, biodegradable polymers are on high demand for production of microparticles for micro/nanoencapsulation and controlled, slow and targeted release of bioactive agents in industrial application including pharmaceutical, food and medical industries.

The aim of this research was to conduct a systematic investigation on polymer matrix influence on the morphology, size, polydispersity index, and bioactive compound loading efficiency of polymer microcarriers and define the preferred condition for the preparation of optimum biodegradable polymer based carriers. For that purpose, methyl salicylate (MS) as a hydrophobic drug was encapsulated into biodegradable polymer microcapsules. In this communication, MS which is widely used in muscular and joint pain treatment was selected as model drug to be used in the form of controlled release formulation because of its small molecular size, poor water solubility, measurable activity in release studies, and high thermodynamic

stability. Based on a preliminary study, we supposed that the size and encapsulation efficiency could be influenced by the compositions and the amount of the polymer matrix phase. In addition, the latter can have a crucial importance in many certain pharmaceutical applications. Therefore, the main objective of the present work is to investigate the effect of polymer matrix of the MS loaded microcapsules on the encapsulation efficiency of MS in the polymer microcapsules. Hence, Poly(lactic acid) (PLA) and Poly(butylene adipate-co-terephthalate) (PBAT) were selected as the polymeric carrier because of their well-established biodegradability and biocompatibility manifested by their wide spread applications as therapeutic carrier materials. Accordingly, in this work attempt had been made to prepare microspheres of different polymer matrix (PLA and PBAT) using emulsification/solvent evaporation method in emulsion composed of P(VAc-co-VA). The parameters influencing the formation of enteric microparticles such as polymer type, concentration and type of emulsifier were investigated. The MS-loaded microparticles with different polymer matrix were characterized by optical microscopy, turbidity study, and encapsulated MS analysis. In a study on MS-loaded microparticles, UV spectrophotometry was found to be an easy and sensitive method for direct estimation of drug amount. In addition to encapsulation efficiency and drug loading, the MS loaded microcapsules are evaluated in terms of their size, morphology and production yield.

2. Materials and Methods

2.1 Materials

Analytical grade Polyvinylacetate (PVAc) (Mw 100,000 g/mol), methyl salicylate (MS), ferric chloride hexahydrate ($\text{FeCl}_3 \cdot 6\text{H}_2\text{O}$), dichloromethane, methanol and potassium hydroxide were purchased from Sigma Aldrich. Polylactic acid (PLA) and poly(butylene adipate-co-terephthalate) (PBAT) purchased from NatureWorks LLC (MN, USA) were used. Controllable high speed mechanical stirrer (Yellowline OST 20 Digital, IKA) was used in emulsion preparation. Degree of hydrolysis of PVAc was determined from carbonyl index (CI) using a Perkin Elmer Spectrum 2000 Fourier-Transform Infrared Spectrophotometer (Perkin-Elmer), emulsion particle size and distribution were measured using 400X optical zoom Stereo Microscope (Meiji) and % light transmittance of colloid were determined using a ThermoSpectronic 20 (Perkin-Elmer).

2.2 Synthesis of Poly(vinyl acetate-co-vinyl alcohol) emulsifiers

To an oven dried 250-mL round bottomed flask containing a vigorously stirred solution of PVAc (1.00 g) in 30 mL of methanol equipped with a reflux condenser and a drying tube, at room temperature was gradually added a solution of 0.029 M methanolic KOH solution. The mixture then was set to reflux at 60°C for 20, 30, 40, 50, 60, 70 and 80

minutes, respectively. After removal of the heat source, the flask then was cooled down to room temperature by means of water bath and then ice bath in order to stop further reaction. Methanol was removed *in vacuo* using rotary evaporator at room temperature to obtain about 1 mL of the residue. Then it was poured into a Petri dish and put in a vacuum desiccators for 24 hours. The obtained copolymer was then subjected to a carbonyl index determination using FTIR spectroscopy.

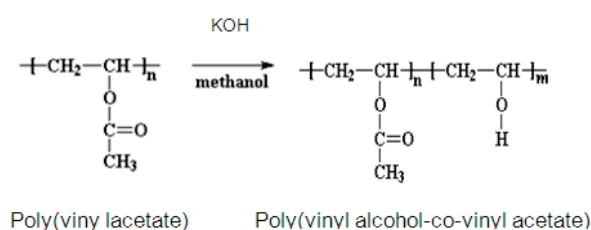


Figure 1. Partial hydrolysis of P(VA-co-VAc) [8]

2.3 Degree of hydrolysis (%HD) determination of Poly(vinyl acetate-co-vinyl alcohol)

FT-IR spectrum of each P(VAc-co-VA) film was obtained from Perkin Elmer Spectrum 2000 Fourier-Transform Infrared Spectrophotometer. Carbonyl index (CI) then was first measured by the ratio of absorption peak area at 1640-1840 cm^{-1} (corresponding to C=O stretching mode of vibration) to peak area at 1350-1470 cm^{-1} (corresponding to C-H bending modes of vibration) as described below [9]:

$$\text{Carbonyl index (CI)} = \frac{A_{1640-1840}}{A_{1350-1470}}$$

Degree of hydrolysis (%HD) then was calculated as follows:

$$\%HD = \left(1 - \frac{CI_{P(VA-co-VAc)}}{CI_{PVAc}} \right) \times 100$$

2.4 Formulation of MS-loaded PLA/PBAT microparticles

Briefly, the organic phase was formed by dissolving 2.0 g of PLA or PBAT and 0.10 g of MS into 200 mL methylene chloride. This solution was added dropwisely into 120 mL of 0.05% aqueous P(VAc-co-VA) (at 35, 67 and 82%HD, respectively) solution. The resulting o/w emulsion was then mechanically stirred at 1,000 rpm for 8 hours at ambient temperature to allow methylene chloride evaporation to obtain solidified microspheres. The resulting microparticles suspension is left overnight at room temperature to evaporate off the methylene chloride present in the aqueous phase.

2.5 Size determination of microparticles

Dilute aqueous suspensions of microparticles were placed on microscope slides and covered by a cover slide. Those specimens were further analyzed by transmission light microscopy (TLM) and

representative micrographs were obtained by using a digital camera. Polarized light may be also used if necessary. The obtained TLM micrographs were processed with the image analysis software, for determination of the average size of polyester microparticles.

2.6 Droplet stability of MS-loaded PLA/PBAT microparticles suspension

The coalescence stability of MS-loaded PLA/PBAT emulsion droplets has been investigated by measuring % light transmittance at 600 nm. Droplet coalescence kinetics was determined during storage.

2.7 Determination of the actual MS loading and Encapsulation efficiency (EE)

Actual MS loading of microparticles was determined by extracting the MS from the polymer. Firstly, the MS-loaded PLA or PBAT microparticles were isolated from the suspensions by twice centrifugations at 9,000 rpm for 5 min and two washing cycles. The supernatant containing the non-encapsulated MS was discarded and the pellet was vacuum dried for 24 hours. The microparticles production yield was calculated by dividing total weight of microspheres formed by weight of all nonvolatile components used for preparation of microspheres. The MS content of the microparticles (1.5-2.0 g, accurately weighed) was extracted with 200 ml methanol by using Soxhlet extractor for 6 hours. MS concentration in the resulting clear solutions obtained was determined by spectrophotometric method assay of MS-iron complex. Briefly, the 0.01M ferric chloride solution was prepared freshly in 25 mL of water. Either MS sample or standard MS solution (1 mL) were mixed with the 0.2 mL of ferric chloride reagent solution and incubated for 5 minutes at room temperature. Subsequently, the color intensity developed was measured at 595 nm by using UV-Vis spectrophotometer (Lambda2S 6998, Perkin Elmer, Germany). The percent (0.1%) extinction coefficient of MS standard concentrations (between 1×10^{-4} and 8×10^{-4} M) was detected as $0.866 \text{ M}^{-1}\text{cm}^{-1}$. The MS loading is determined from the mass ratio of the encapsulated MS to the total microparticles produced. The encapsulation efficiency of MS in the microspheres was calculated from the actual loading with respect to the theoretical loading of MS (% w/w) in the microspheres.

3. Results and Discussion

Concentration of KOH used in the methanolysis reaction of PVAc showed major impact on degree of hydrolysis. As shown in Table 1, very low catalyst concentration was required to obtain up to 80 % HD after refluxed 60 °C for 80 minutes. However, catalyst concentration below 0.02 M did not react with PVAc while catalyst concentration above 0.20 M gave complete hydrolysis (data not shown). In order to avoid catalysts removal process, minimum catalyst

concentration at 0.029 M was used. So, investigation of time depending hydrolysis was done at a constant 60 °C. The results in Table 1 demonstrated that degree of hydrolysis (%HD) in P(VAc-co-VA) increased with reaction time at 0.029M catalyst concentration used.

Table 1: Degree of hydrolysis at various reactiontime

| Reaction time (min) | Carbonyl index (CI) | Degree of hydrolysis (% HD) |
|---------------------|---------------------|-----------------------------|
| 0 | 1.653 | 0 |
| 20 | 1.059 | 35.95 |
| 30 | 0.850 | 48.56 |
| 40 | 0.654 | 60.45 |
| 50 | 0.530 | 67.58 |
| 60 | 0.463 | 71.09 |
| 70 | 0.406 | 77.50 |
| 80 | 0.285 | 82.82 |

To study the influence % HD of P(VAc-co-VA) emulsifier in the external aqueous phase on the particle size of PLA and PBAT suspensions, we prepared biodegradable polymer suspensions by using P(VAc-co-VA) copolymer consisting of different degree of hydrolysis. This result was monitored during optical microscope observation at 400x–1000x magnification (Figure 1). The morphology looked nearly spherical with slightly rough external surface due to solvent evaporation and internal solid formation. It could be noticed that PLA encapsulated particles appeared to be rougher surface and larger sized than PBAT encapsulated particles in general.



Figure 1. MS-loaded particles in PLA matrix (left) and PBAT matrix (right) using 67.58% HD P(VAc-co-VA) emulsifier

Table 2: Particle size of MS-loaded PLA and PBAT encapsulated microspheres using various %HD of P(VAc-co-VA) emulsifier

| Degree of hydrolysis (%HD) | Particle Size (μm) | |
|----------------------------|--------------------|------------|
| | PLA | PBAT |
| 35.95 | 11.54±7.04 | 14.96±6.51 |
| 67.58 | 11.20±9.43 | 9.13±5.53 |
| 82.82 | 10.10±4.89 | 7.94±6.03 |

The variation of %HD of P(VAc-co-VA) emulsifiers produces different sizes of biodegradable polymer suspensions shown in Table 2. The sizes of the resulting suspensions range from 8 to 15 μm. When using PBAT as a matrix, the smaller particles sizes

were obtained from the greater %HD of P(VAc-co-PVA) emulsifier. However, there is no significant difference in size with %HD when using PLA as a matrix. At high %HD, the increase of VA content in P(VAc-co-VA) causes considerable decrease in the particles size of PBAT microparticles and *vice versa*, probably due to the decrease of hydrophobic capture volume in P(VAc-co-VA) emulsifier caused quick evaporation of methylene chloride making small crystal or denser structure in PBAT, hence, causing a contraction in size in PBAT particles. In PLA matrix, however, methylene chloride could be swelled and trapped with PLA to form amorphous gel, therefore, no crystal structure in PLA causing contraction in particle size.

Table 3: % Light transmittance of PLA and PBAT suspensions at various %HD of P(VAc-co-VA) emulsifier after 1 day and after 5 days.

| Degree of hydrolysis (% HD) | % Light Transmittance at 600 nm | | | |
|-----------------------------|---------------------------------|--------------|-------------|--------------|
| | PLA | | PBAT | |
| | After 1 day | After 5 days | After 1 day | After 5 days |
| 35.95 | 24.2 | 1.6 | 1.9 | 0.7 |
| 48.56 | 19.6 | 4.6 | 9.7 | 1.4 |
| 60.45 | 13.4 | 6.2 | 1.6 | 1.8 |
| 67.58 | 27.4 | 8.6 | 0.8 | 0.5 |
| 82.82 | 11.7 | 7.7 | 3.6 | 5.5 |

However, the prepared PLA suspension tended to be less stable with time than PBAT suspension, because % light transmittance of PLA suspension decreased with storage time (Table 3). A reasonable explanation could be that a residual solvent left in PLA which took more time to disperse out than PBAT as mentioned earlier.

Table 4: Encapsulation Efficiency of MS in PLA and PBAT microparticles using 67.58% HD of P(VAc-co-VA) emulsifier

| Matrix | Micro-particle Yield | MS loading (theoretical) | MS loading (actual) | EE |
|--------|----------------------|--------------------------|---------------------|-------|
| PLA | 94.19 | 4.80 | 4.49 | 93.54 |
| PBAT | 87.15 | 4.79 | 4.15 | 86.60 |

Under this condition, MS could be encapsulated up to 93.54% in PLA matrix microparticles and 86.60% in PBAT matrix microparticles as shown in Table 4. Thus, PLA matrix particles tend to encapsulate more hydrophobic drug than PBAT matrix microparticles. The influence of polymer matrix on encapsulation efficiency of the PBAT matrix was lower than PLA matrix due to the faster crystallization kinetic and denser structure of PBAT.

4. Conclusions

The aqueous suspensions of PLA matrix and PBAT matrix were prepared using P(VAc-co-VA) with various degree of hydrolysis from 35.95 to 82.82%

synthesized from alkali methanolysis of PVAc. PLA matrix encapsulated particles generally provide a constant particle size at 10-11 μm , while PBAT matrix encapsulated particles significantly reduced in size as %HD of emulsifier increased. It is also important to note that particle size of PBAT suspension was generally smaller than that of PLA suspension. Finally, PLA matrix microparticles could encapsulate hydrophobic MS drug more than PBAT microparticles.

Acknowledgements

We would like to thank Faculty of Applied Science, KMUTNB for the financial support of this research.

References

- [1] X. Cheng, R. Liu, and Y. He, European Journal of Pharmaceutics and Biopharmaceutics, 76(2010) pp 336-341
- [2] W. S. Cheow and K. Hadinoto, Colloids and Surfaces A: Physicochem. Eng. Aspects, 370(2010) pp 79-86.
- [3] L. Deladino, P. S. Anbinder, A. S. Navarro, and M. N. Martino, Carbohydrate Polymers, 71(2008) pp 126-137
- [4] I. J. Castellanos, G. Cruz, R. Crespo, and K. Griebenow, Journal of Controlled Release, 81(2002) pp. 307-319
- [5] K. Elkharraz, A. R. Ahmed, A. Dashevsky, and R. Bodmeier, International Journal of Pharmaceutics, 409 (2011) pp. 89-95
- [6] X. Zeng, J. Li, J. Zheng, Y. Pan, J. Wang, L. Zhang, X. He, and D. Liu, Colloids and Surfaces B: Biointerfaces, 94(2012) pp. 324-332
- [7] C. T. Brunner, E. T. Baran, E. D. Pinho, R. L. Reis, N. M. Neves, Colloids and Surfaces B: Biointerfaces 84 (2011) pp. 498-507
- [8] Y. Yuan-Hsiang, L. Ching-Yi, Y. Jui-Ming and L. Wei-Hsiang, Polymer, 44 (2003) pp. 3553-3560.
- [9] H. S. Mansur, C.M. Sadahira, A.N. Souza and A. A.P. Mansur, Material Science and Engineering, 28 (2008) pp. 539-548.
- [10] N. Anton, J-P. Benoit and P. Saulnier, J. of Controlled Release, 128 (2008) pp 185-199.
- [11] P.B. O'Donnell and J.W. McGinity, Advanced Drug Delivery Reviews, 28 (1997) pp 25-42.
- [12] K.S. Soppimath, T. M. Aminabhavi, A.R. Kulkarni and W.E. Rudzinski, J. of Controlled Release, 70 (2001) pp 1-20.
- [13] S. Freitas, H.P. Merkle and B. Gander, J. of Controlled Release, 102 (2005) pp 313-332.

ENCAPSULATION OF MENTHOL IN RICE STARCH BY SPRAY DRYING

Pitchvipa Prommas¹, Uracha Ruktanonchai², Hidefumi Yoshii³, Apinan Soottitantawat¹

¹Center of Excellence in Particle Technology, Department of Chemical Engineering, Faculty of Engineering, Chulalongkorn University, Bangkok 10330, Thailand

²National Nanotechnology Center (NANOTEC), National Science and Technology Development Agency 111 Thailand Science Park, Pathumtani, Thailand

³Department of Applied Biological Science Kagawa University 2393, Ikenobe, Miki-cho, Kita-gun, Kagawa 761-0795, Japan

* Author for correspondence; E-Mail: apinan.s@chula.ac.th, Tel. +66 22186999, Fax. +66 22186877

Abstract: Menthol, a cyclic terpene alcohol, is found in peppermint. It is widely used in many products such as shampoo, cigarette and candy. However, there are some kind of products that uses latent heat from the menthol including cooling body powder. The main ingredients in cooling powder are menthol and talcum but menthol easily sublimates so it has a problem of short efficiency time and the talcum may cause health problems. For solving this problem, in this study the encapsulation technique by spray drying was used to produce encapsulated menthol body powder for a long lasting efficiency time cooling powder. The rice starch, organic substance, was used as a wall material instead of talcum. The effects of air inlet temperature, atomizer speed and feed flow rate on the menthol retention after spray drying process were investigated. Furthermore, effect of maltodextrin content in the wall materials was also studied. The results were found that the lower air inlet temperature and lower feed flow rate resulted in the higher menthol retention. The higher atomizer speed increased the retention. The retention was also increased by the additional of maltodextrin at 10 wt% to the feed mixture.

1. Introduction

Menthol, a cyclic terpene alcohol, is found in peppermint. The melting point of menthol is 41-43 °C¹. Although menthol is a solid at room temperatures, it is very volatile. Menthol also uses in food and cosmetic industries. One example of using is in the cooling body powder.

Encapsulation is defined as a process by which one material or mixture of materials is coated or entrapped within another material². The primary reasons for encapsulation of flavours are to protect them from chemical reaction (e.g. light-induced or oxidation), to retain them during storage and to prevent interactions with food components and other flavours³. Encapsulation technology is now well developed and accepted within the pharmaceutical, chemical, cosmetic, foods and printing industries⁴. In food products, fats and oils, aroma compounds, vitamins, minerals, colorants and enzymes have been encapsulated⁵. The process for encapsulation of sensitive compounds consists of two steps: first step is often emulsification of a core material, such as aroma, with a wall material such as a polysaccharide or protein. Second step is drying or cooling of the emulsions obtained. The retention of flavour is governed by factors related to the chemical nature of

the core material, including its molecular weight, chemical functionality, polarity and relative volatility⁶. Types of wall material⁶, ratio of the core material to wall material⁷, encapsulation method⁸ and storage conditions⁹ are also affected the retention of flavors. According to the encapsulation process used, the encapsulated powder presents various shapes (films, spheres, particles irregular), various porous structures (porous or compact) and various solid states (amorphous or crystalline dehydrated solid, rubbery or glassy matrix) that influences diffusion of flavours or external substances (oxygen, solvent) as well as the food product stability during storage.

Spray drying is a commercial processes which is widely used in large-scale production of encapsulated flavours and volatiles¹⁰. The merits of the process are low processing cost, wide choice of carrier solids, good retention of volatiles, good stability of the finished product, and large-scale production in continuous mode¹¹. The process of spray drying involves the dispersion of the substance to be encapsulated in a carrier material, followed by atomization and spraying of the mixture into a hot chamber^{12,13}. The resulting encapsulated powder are then transported to a cyclone separator for recovery. The development of spray-drying technology has been intimately associated with dairy, food, biotechnology and pharmaceutical industries where heat-sensitive materials have to be dried while maintaining the prerequisite microbiological stability in the dried particles. However, the main problem of the cooling powder is the short efficiency cooling time. For solving this problem, spray drying technique was used to produce a long efficiency time cooling body powder. The aim of this research was to investigate the effect of air inlet temperature, feed flow rate, atomizer speed and maltodextrin content on menthol retention, particle size, water content and morphology of encapsulated powders prepared by spray drying technique.

2. Materials and Methods

2.1 Preparation of emulsified solution

The rice starch in the form of flour starch at 65% (Bangkok Inter Food Co. Ltd, Thailand), maltodextrin at 20% and casein at 5% of solid content (Mitsubishi Kagaku Foods Cor.) were mixed with distilled water for preparation of wall material at 40% of total solid content. The melted menthol (Soda Aromatic Co., Ltd.) was added to the solution at 10% of solid content. Then, the mixture was homogenized by a high speed homogenizer at 8000 rpm for 3 min.

2.2 Preparation of encapsulated powder

The emulsified solution was fed to as pray dryer (Ohkawara L8) at feed flow rate 25 and 35 ml/min., speed of atomizer 10000 and 30000 rpm, air flow rate 110 kg/h and air inlet temperature 120-180 °C.

2.3 Analysis of menthol content

0.1 g of encapsulated powder was dispersed in 1 ml of distilled water and 4 ml of hexane with cyclohexanone (1µl/ml) and then the solution was mixed by vortex machine 1 min after that heats the solution by water bath at 90°C for 30 min (every 10 min, vortex 1 min). The 2 µl of cooled solution was injected to GC (GC-2014, Shimadzu) at column temperature 150°C, injection temperature 180°C, detector temperature 200°C and N₂ flow rate 60 ml/min. The menthol retention was calculated using the following equation.

$$\text{Retention (\%)} = (R2 \times 100) / R1$$

R1= initial menthol content in feed solution

R2= menthol content retained in the powder product

2.4 Measurement of emulsion size

The emulsified dispersion was diluted with distilled water and analyzed by SALD-7100 (Shimadzu Corporation, Kyoto, Japan)

2.5 Measurement of particle size

The sieve analysis was used for measuring the particle size (aperture size 150, 106, 75, 53, 32 and 20 µm). The encapsulated powder was mixed with 3% w/w of silica and sieved for 3 hr.

2.6 Measurement of water content

The encapsulated powder was weighted and dried by vacuum dryer (ADP-21, Yamato Scientific America) at 90°C for 20 hr. Water content was calculated using the following equation:

$$\text{Water content} = W1 - W2 - [M1 - M2]$$

W1= weight of encapsulated powder before drying

W2= weight of encapsulated powder after drying for 20 hr

M1= weight of menthol in encapsulated powder before drying

M2= weight of menthol in encapsulated powder after drying for 20 hr

2.7 Analysis of morphology

A scanning electron microscope (JSM-6060, JEOL Co., Ltd, Tokyo, Japan) was used to observe the structure of encapsulated powder at 10 kV.

3. Results and Discussion

3.1 Effect of air inlet temperature

The results showed that increasing the air inlet temperature results in lower retention (Table 1). This may be explained by the fact that menthol easily evaporates when contacts with the high temperature. Additionally, increasing temperature also enhances the water evaporation and thus water content of powder obtained was shown to be decreased. Similar findings have been reported by Kadamet al¹⁴. (2011) in microencapsulation of ginger oil and Mortazaet al¹⁵. (2012) in microencapsulation of fish oil that resulted in increasing retention with decreasing temperature. In the case of menthol encapsulated powder, there is no significance difference between emulsion and particle size between each inlet air temperature conditions. The morphology of encapsulated powder shows in Figure 1. It was indicated that increasing the air inlet temperature resulted in powders with rough surface.

Table 1: Effect of air inlet temperature on the properties of encapsulated powders.

| Inlet temperature (°C) | Retention (%) | Emulsion size (µm) | Partical size (µm) | Water content (%) |
|------------------------|---------------|--------------------|--------------------|-------------------|
| 120 | 63.1 | 4.3 | 52 | 7.9 |
| 140 | 54.4 | 4.1 | 56 | 6.4 |
| 160 | 48.2 | 4.3 | 58 | 5.3 |
| 180 | 48.8 | 4.0 | 54 | 2.9 |

3.2 Effect of feed flow rate

An increasing in feed flow rate resulted in the lower retention. The size of sprayed droplet is increased. The longer time to form the dry solid crust around the droplets which act as the solid membrane is expected. Therefore, more losses of menthol are observed according to Petiraksakul et al¹⁶ (2011) and Tantratian et al¹⁷(2005). Morphology of the powders also show in Figure 2. There wasno different between these structures.

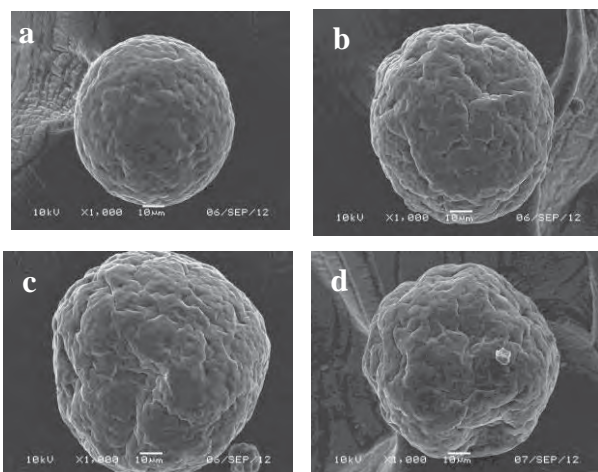


Figure 1 SEM images of encapsulated powders obtained when using different air inlet temperature (a) 120°C (b) 140°C (c) 160°C (d) 180°C at1000x magnification

Table 2: Effect of feed flow rate on the properties of encapsulated powders

| Feed flow rate (ml/min) | Retention (%) | Emulsion size (µm) | Particle size (µm) | Water content (%) |
|-------------------------|---------------|--------------------|--------------------|-------------------|
| 25 | 73.7 | 4.8 | 54 | 6.2 |
| 35 | 40.8 | 4.0 | 42 | 8.5 |

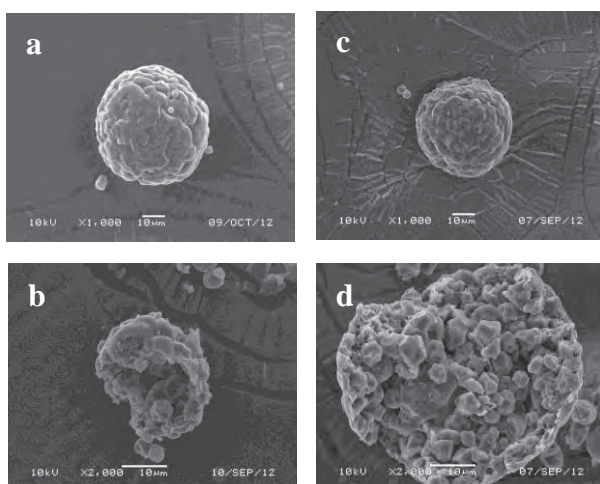


Figure 2 SEM images of encapsulated powders (a) surface structure, feed rate 25 ml/min (b) internal structure, feed rate 25 ml/min (c) surface structure, feed rate 35 ml/min (d) internal structure, feed rate 35 ml/min at1000x magnification

3.3 Effect of atomizer speed

An increasing in atomizer speed yielded smaller droplet size of feed emulsion (Table 3). It uses a short time to form solid wall that is why higher atomizer

speed makes high retention. Morphology of powder show in Figure 3

Table 3: Effect of atomizer speed on the properties of encapsulated powders.

| Atomizer speed(rpm) | Retention (%) | Emulsion size (µm) | Particle size (µm) | Water content (%) |
|---------------------|---------------|--------------------|--------------------|-------------------|
| 10000 | 63.1 | 4.3 | 52 | 7.9 |
| 30000 | 73.7 | 4.8 | 54 | 6.2 |

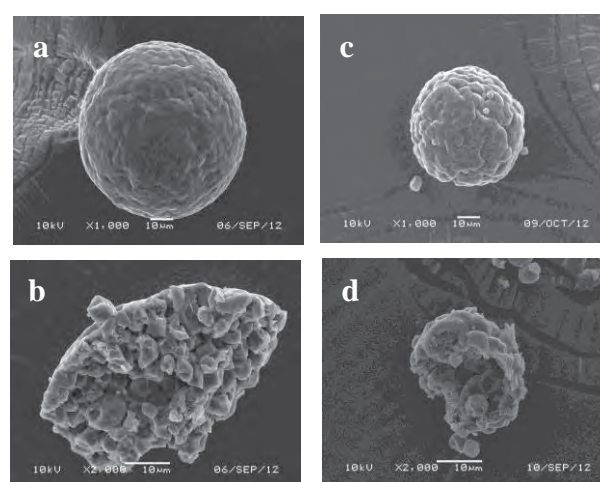


Figure 3 SEM images of encapsulated powders(a) surface structure, atomizer speed 10000 rpm at 1000x magnification(b) internal structure, atomizer speed10000 rpm at 2000x magnification (c) surface structure, atomizer speed 30000 rpm at 1000x magnification(d) internal structure, atomizer speed30000 rpm at 2000x magnification

3.4 Effect of maltodextrin content (MD)

Maltodextrins are formed by partially hydrolyzing cornstarch with acids or enzymes. They manifest the ability to form matrices that are important in forming wall systems^{18,19}. In selecting the wall materials for encapsulation, maltodextrin is a good compromise between cost and effectiveness. This is the reason why adding maltodextrin in feed emulsion. Table 4 shows the effect of maltodextrin addition. The results showed that increasing maltodextrin content up to 10% could increase menthol retention. This may be due to the maltodextrin acts as a film forming that covers the granule of rice starch (Figure 4). However, when content of maltodextrin increased to 20%, menthol retention decreased. These results may be from the increasing of feed viscosity with maltodextrin content. The larger sprayed droplet size is expected at the higher viscosity of feed.

Table 4: Effect of maltodextrin content on the properties of encapsulated powders

| Maltodeatrin Content (%) | Retention (%) | Emulsion size (μm) | Partical size (μm) | Water content (%) |
|--------------------------|---------------|--------------------|--------------------|-------------------|
| 0 | 13.5 | 4.0 | 42 | 8.6 |
| 5 | 36.7 | 4.2 | 44 | 5.5 |
| 10 | 73.7 | 4.8 | 54 | 6.2 |
| 20 | 57.1 | 2.3 | 48 | 4.1 |

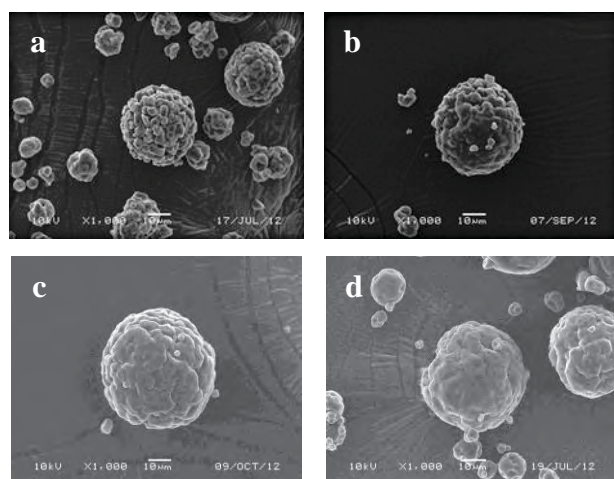


Figure 4 SEM images of encapsulated powders obtained when adding maltodextrin at (a) 0% (b) 5% (c) 10% and (d) 20% at 1000x magnification

4. Conclusions

The air inlet temperature and feed flow rate have an influence on the retention and morphology of the powders. Using lower air inlet temperature and feed flow rate yielded powders with higher retention. Furthermore, adding maltodextrin to a certain amount could increase menthol retention. To produce the best properties of cooling body powder, the spray drying should be operated at air inlet temperature 120°C, feed flow rate 25 ml/min, atomizer speed 30000 rpm and adding maltodextrin at 10% of solid content.

References

[1] CRC Handbook of Chemistry and Physics, 88th edition (2007)
 [2] Risch SJ. *In Encapsulation and Controlled Release of Food Ingredients*, American Chemical Society: Washington, DC, (1995), pp. 2–7.
 [3] Reineccius GA. *Source Book of Flavors*. Aspen: Gaithersburg, MD, (1999)

[4] Augustin, M.A., Sanguansri, L., Margetts, C. and Young, B. *Microencapsulation of food ingredients*. Food Australia, **53**(2001), pp. 220–223.
 [5] Dziezak, J.D. *Microencapsulation and encapsulation ingredients*. Food Technology, **42**(1988), pp.136–151.
 [6] Imagi, J., Muraya, K., Yamashita, D., Adachi, S. and Matsuno, R. *Retarded oxidation of liquid lipids entrapped in matrixes of saccharides or protein*. Bioscience, Biotechnology, and Biochemistry **56**(1992), pp. 1236–1240.
 [7] Minemoto, Y., Adachi, S. and Matsuno, R. *Autoxidation of linoleic acid encapsulated with polysaccharides of differing weight ratio*. Bioscience, Biotechnology, and Biochemistry, **63**(1999), pp. 866–869
 [8] Minemoto, Y., Adachi, S. and Matsuno, R. *Comparison of oxidation of menthyl linoleate encapsulated with gum arabic by hot-air-drying and freeze-drying*. Journal of Agricultural and Food Chemistry, **45**(1997), pp.4530–4534.
 [9] Yoshii, H., Furuta, T. and Kawasaki, K. *Oxidative stability of powder tridocosahexanoic acid included in cyclodextrin and its application to fish meal paste*. Bioscience, Biotechnology, and Biochemistry, **61**(1997), pp.1376–1378.
 [10] Deis, R.C. *Spray-drying-innovative use of an old process*. Food Product Design, **7** (1997), pp. 97–113
 [11] Reineccius, G.A. *Flavor encapsulation*. Food Reviews International, **5**(1989), pp. 147–176
 [12] Dziezak, J.D. *Microencapsulation and encapsulation ingredients*. Food Technology, **42**(1988), pp. 136–151.
 [13] Watanabe, Y., Fang, X., Minemoto, Y., Adachi, S. and Matsuno, R. *Suppressive effect of saturated Lascorbate on the oxidation of linoleic acid encapsulated with maltodextrin or gum arabic by spray-drying*. Journal of Agricultural and Food Chemistry, **50**(2002), pp.3984–3987.
 [14] Kadam M.L., Syed I. and Kale R.V. *Study on Extraction of Ginger Oil and its Microencapsulation*. EJEAFChE (2011), pp. 1579–4377
 [15] Mortaza A., Hossien M., Ashkan M. and Shahin R. *Influence of Wall Material and Inlet Drying Air Temperature on the Microencapsulation of Fish Oil by Spray Drying*. Food Bioprocess Technol (2012)
 [16] Pinsupha P., Kanitha J. and Anurak P.. *Influence of spray drying conditions on the physical properties of rice-milk powders*. 37th Congress on Science and Technology of Thailand (2011)
 [17] Sumate T., Pranee J., Rangsimat. and Sajeepon T.. *Production of Chicken Flavor Powder from Chicken Cooking Drip by Spray Drying*. Section T, **3**(2005): pp. 203–210
 [18] Kenyon, M.M. and Anderson, R.J. *Maltodextrins and low-dextrose-equivalence corn syrup solids: production and technology for the flavor industry*. In: Flavor Encapsulation (edited by S.J. Risch & G.A. Reineccius). (1988), pp. 7–12
 [19] Shahidi, F. and Han, X.Q. *Encapsulation of food ingredients*. Critical Reviews in Food Science and Nutrition, **33**(1993), pp.501–547

SUN PROTECTION PROPERTIES OF SUNFLOWER OIL EXTRACTED ASTAXANTHIN FROM ALGAE *HAEMATOCOCCUS PLUVIALIS*

Itthayakorn Promputtha^{1*}, Narumon Saytakep¹, Trai Pekthong²

¹ School of Cosmetic Science, Mae Fah Luang University, 333 Moo 1, Tasud, Muang, Chiang Rai, 57100, Thailand

² School of Science, Mae Fah Luang University, 333 Moo 1, Tasud, Muang, Chiang Rai, 57100, Thailand

* Author for correspondence; E-Mail: itthayakorn.pro@mfu.ac.th, Tel. +66 53 916837, Fax. +66 53 916831

Abstract: Astaxanthin is an attractive compound in food, cosmetic, and pharmaceutical applications as it has essential biological functions of strong antioxidant, immune response enhancer, coloring agent, and UV ray protecting agent. The red cyst of microalgae *Haematococcus pluvialis* is a major source of astaxanthin and the extraction using various bio-solvent vegetable oils has performed a better value of astaxanthin than using other organic solvents. The highest yield has currently been expressed in sunflower oil extract and its colorant property has been established, while its sun protection properties have not yet explored. This study intended to examine the sun protection properties of the sunflower oil extracted astaxanthin from *H. pluvialis* for application in sunscreen product. The culture broth containing red cyst of *H. pluvialis* was extracted with equal volume of sunflower oil under vigorous stirring on magnetic stirrer for 48 h, the oil extracted supernatant was collected and quantified for astaxanthin. The extract was analyzed for the Sun Protection Factor (SPF) and Boots Star Rating values both before and after added in sunscreen formula. The sunflower oil extracted astaxanthin obtained the SPF value of 2.28 and Boots Star Rating value of 3. Nevertheless, astaxanthin content and SPF value were not stable after accelerated conditions, except the Boots Star Rating value. The extract was compatible for sunscreen formulation at concentration of 2.5-5.0% (w/w) and able to enhanced the SPF while was not for Boots Star Rating value. More concentration of the extract provided higher SPF of sunscreen formula, unfortunately the SPF of sunscreen formula was not stable under accelerated conditions. This study indicated that sunflower oil extracted astaxanthin from *H. pluvialis* was efficiency to enhanced the SPF value of sunscreen formula. However, the improvement of its stability is needed for further investigation.

1. Introduction

Astaxanthin is an attractive compound in food, cosmetic, and pharmaceutical applications [1] as it has essential biological functions of strong antioxidant, immune response enhancer, coloring agent, and UV ray protecting agent [2]. The red cyst of microalgae *Haematococcus pluvialis* is a major source of astaxanthin [1,3]. Nevertheless, the thicken wall of red cyst of *H. pluvialis* is a major difficulty to extract astaxanthin. This problem resulted to extraction method using organic solvent comprise high energy consumption, multiple separation steps, and remain undesirable chemicals which not suitable for cosmetic formulation [4]. Therefore, the extraction using various

bio-solvent vegetable oils have been used instead and has performed a better value of astaxanthin than using other organic solvents [4-5]. The highest yield has currently been expressed in sunflower oil extract and its colorant property has been established [5], while its sun protection properties have not yet explored. This study intended to examine the sun protection properties of the sunflower oil extracted astaxanthin from *H. pluvialis* for application in sunscreen product.

2. Materials and Methods

2.1 Cultivation of *H. pluvialis* for astaxanthin accumulation

Haematococcus pluvialis was obtained from Thailand Institute of Scientific and Technological Research (TISTR), Thailand, and cultured in Modified COMBO Medium (MCM) which composed of the following (mg/l): KNO₃ 200, KH₂PO₄ 20, NaHCO₃ 450, MgSO₄·7H₂O 100, V_{B12} 4×10⁻³, Na₂EDTA·2H₂O 3.36, FeCl₃·6H₂O 2.44, ZnCl₂ 4.1×10⁻³, H₃BO₃ 6.1×10⁻³, CoCl₂·6H₂O 5.1×10⁻³, MnCl₂·4H₂O 4.1×10⁻³, (NH₄)₆Mo₇O₂₄·7H₂O 38×10⁻³ [6]. The culture flasks were incubated on 60 rpm orbital shaker. To induce high astaxanthin synthesis (red phase), the exponentially grown culture was continuously illuminated with 4000 Lux at 28±1 °C [5]. The induced cells were collected by centrifugation at 8000 rpm for 10 min, counted, re-suspended in fresh culture medium, and kept for astaxanthin extraction step.

2.2 Extraction of astaxanthin from *H. pluvialis* with sunflower oil

The extraction method was performed following the protocol of Kang and Sim and Promputtha et al. [4-5] with some modification. A 20 ml of 7.6×10⁶ cells/ml of induced cyst culture was mixed with 20 ml of sunflower oil. The mixture was vigorously stirred on magnetic stirrer at room temperature for 48 hrs., leaved to settle under gravity, and the oil extracted supernatant (top layer) was collected (Figure 1). The absorbance of the extract was scanned (350-650 nm) and astaxanthin was quantified at 480 nm compared with standard astaxanthin (0.5 µg/ml). The sunflower oil extracted astaxanthin extract were named as SEA for compacted communication.

2.3 Preparation of sunscreen base formula and sunscreen containing SEA

The ingredients of the sunscreen formula were listed in Table 1. Oxybenzone, ethylhexyl methoxycinnamate, butyl-methoxydibenzoylmethane, finsolve TN, dimethicone and PEG-12 dimethicone were weighted and pooled into 250 ml beaker, heated in water bath until all ingredients dissolved (mixture A). The 74.3 g of water was weighted and poured into a 400 ml beaker. Carbopol, propylene glycol, disodium EDTA, triethanolamine and ethanol were added into the water. The mixture was stirred and heated at 80-85 °C, the mixture was then slowly poured into the mixture A and stirred constantly. To prepare the sunscreen containing SEA, the concentration of 2.5% and 5.0% (w/w) of SEA were formulated as the recipes shown in Table 1. Emulsion was stirred vigorously until the extract was homogenously mixed.

Table 1: Ingredients of sunscreen base formula and sunscreen containing SEA.

| Part | Ingredients | % (w/w) | | |
|------|-----------------------------------|---------|------|------|
| | | Base | SEA | |
| | | | 2.5 | 5.0 |
| A | Water | 69.5 | 69.5 | 69.5 |
| | Carbopol 940 | 0.4 | 0.4 | 0.4 |
| | Propylene glycol | 2.0 | 2.0 | 2.0 |
| | Disodium EDTA | 0.1 | 0.1 | 0.1 |
| | Triethanolamine | 1.0 | 1.0 | 1.0 |
| | Ethanol | 3.0 | 3.0 | 3.0 |
| B | Oxybenzone | 3.0 | 3.0 | 3.0 |
| | Ethyl hexyl methoxycinnamate | 3.0 | 3.0 | 3.0 |
| | Butyl-methoxydibenzoyl methane | 3.0 | 3.0 | 3.0 |
| | C ₁₂₋₁₅ Alkyl Benzoate | 8.0 | 5.5 | 3.0 |
| | Dimethicone | 1.0 | 1.0 | 1.0 |
| | Cyclomethicone | 2.0 | 2.0 | 2.0 |
| | PEG-12 dimethicone | 3.0 | 3.0 | 3.0 |
| C | Uniphen-P23 | 1.0 | 1.0 | 1.0 |
| E | SEA extract | - | 2.5 | 5.0 |

2.4 Measurement of sun protection properties of SEA and sunscreen containing SEA

The measurements were performed by standard protocol by using the SPF 290S Analyzer with latest version of WinSPF software. The sample was accurately weighed of 0.22 mg and injected with 1 ml syringe and evenly spread across the entries surface of 25 cm² of the substrate using Transpore® 3M attached on the square disk using a gloved finger. The sun protection factor (SPF) and Boots Star Rating values of SEA were determined under transmission between 290-400 nm in autoscan program. All of the measurements were performed in triplicate and statistical analyzed.

2.5 Stability test of SEA and sunscreen containing SEA

The SEA was analyzed for the stability of the color, astaxanthin content, SPF and Boots Star Rating values at initial stage and under accelerated conditions of dark/light, freeze/thaw, and heating/cooling cycles. The color of SEA was measured by Chromameter KONICA MINOLTA CR-400 at room temperature. The data value L* (clarity), a* (green-red spectrum), and b* (blue-yellow spectrum) were recorded in triplicate. The astaxanthin content was quantified as the absorbance at 480 nm.

The centrifugation, freeze/thaw cycle, and heating/cooling cycle methods were performed for stability test of the sunscreen formulas. For the centrifugation method, the sunscreen sample was weigh for 1.5 g into a 1.5 ml centrifuge tube and centrifuged at acceleration of 6000 rpm for 30 min. For the freeze/thaw cycle method, the sunscreen sample was vertically stored in -20 °C freezer for 12 h, and stored at room temperature for 12 h, repeated this cycle for six times. For heating/cooling cycle method, the sunscreen sample was vertically stored in 55 °C hot air oven for 12 h followed by stored in 4 °C refrigerator for 12 h, the cycle was repeated six times. After completed each accelerated conditions, the separation layer of emulsion or any changes of the physicochemical features of the sample were observed.

3. Results and Discussion

3.1 SEA preparation

The red cyst of a 9-day cultivation of *H. pluvialis* were harvested and extracted for astaxanthin with sunflower oil for 48 h. The sunflower oil phase containing astaxanthin (top layer) was collected (Figure 1). The astaxanthin content was quantified at 480 nm compared with standard astaxanthin (Figure 2). Almost astaxanthin content was released from the red cyst to sunflower oil phase after 48 h of extraction. This result correlated to the report of Kang and Sim [4] that *Haematococcus* astaxanthin extraction with soybean, corn, grape seed, and olive oils, provides the highest recovery yields after extraction for 48 h. Longer than 48 h of extraction, the astaxanthin content was gradually declined. This may caused from unstable property of astaxanthin [7].

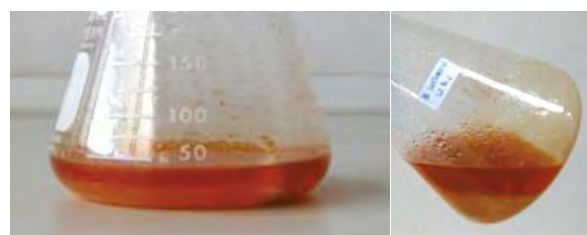


Figure 1. The separation layer of the sunflower oil phase containing astaxanthin substance (top layer) and water phase packed with algal cell debris (below).

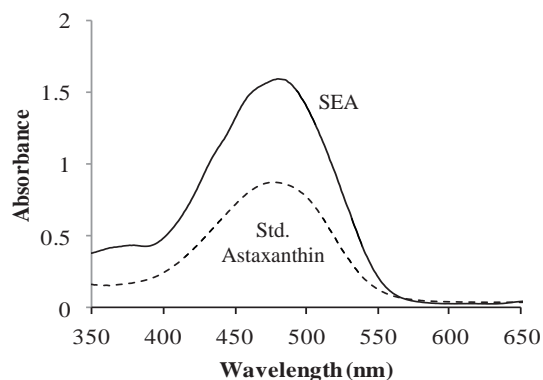


Figure 2. Absorbance spectra of SEA compared with 0.5 µg/ml standard astaxanthin. Astaxanthin content is quantified at 480 nm. SEA extract was diluted 10 fold before measuring the absorbance.

3.2 Stability of SEA extract

From Table 2, the a^* value of 6.83 at initial stage indicates the redness of the extract, however redness of extract is drastically decreased after accelerated conditions. The L^* value which indicates the lightness of the sample was also decreased after accelerated conditions. Astaxanthin content quantified at 480 nm was reduced after accelerated conditions (Figure 3). This result indicated that the astaxanthin content was parallel reduced with decreasing of the redness of the extract. Astaxanthin is a highly unsaturated molecule, it can easily decomposed by light and oxygen, which can cause the loss of antioxidant properties [7], and current study demonstrated that the accelerated condition of dark/light was reduced the stabilization of astaxanthin.

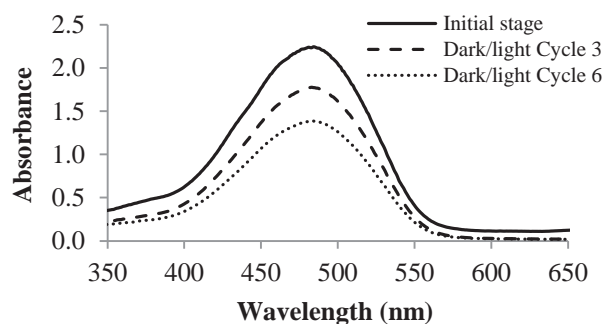


Figure 3. Absorbance spectra of SEA after cycle 3 and 6 of dark/light accelerated condition compared with the initial stage.

3.3 Sun protection properties of SEA and sunscreen formula containing SEA

The SEA extract and the sunscreen formula containing SEA extract were analyzed for the SPF and Boots Star Rating values both before and after accelerated conditions. The SEA was initially obtained the SPF value of 2.28 and Boots Star Rating value of 3, and the critical wavelength was 373.4 nm. After cycle 3 and 6 of the accelerated conditions of dark/light, freeze/thaw, and heating/cooling, the SPF

value of the SEA was reduced while the Boots Star Rating value was stable (Table 2).

SEA extract was compatible for sunscreen formulation at concentration of 2.5-5.0% (w/w) and able to enhanced the SPF, while was not for Boots Star Rating value. The sunscreen base formula was expressed the SPF value of 6.09 at the beginning and SPF value was increased to 9.73 and 13.16 after additional of 2.5% and 5.0% (w/w) of SEA, respectively, while the SEA was not enhanced the Boots Star Rating value. The result indicated that more concentration of astaxanthin extract enhanced higher SPF value of the sunscreen formula (Table 3).

The SPF value of sunscreen base formula and formula containing 2.5% and 5.0% (w/w) of SEA were declined after accelerated conditions of freeze/thaw and heating/cooling cycle. The SPF of formula containing 2.5% SEA were reduced from 9.73 to 6.5 after 6 cycles of freeze/thaw and reduced to 7.28 after heating/cooling acceleration. The SPF of formula containing 5.0% extract were reduced from 13.16 to 9.62 and 9.22 after 6 cycles of freeze/thaw and heating/cooling accelerated conditions, respectively (Table 3). The Boots Star Rating value of sunscreen base formula and formula containing extract were increased after 6 cycles of freeze/thaw and heating/cooling accelerated conditions from level 3 (good) to 4 (superior). It may be possible that the substance in sunscreen formula was interacted with synergistic activity under accelerated conditions.

Haematococcus astaxanthin has been verified that able to superior protection of the skin from UV and provided 100 times better protection against UVA light-induced oxidative stress in rat kidney fibroblasts compared to lutein [8].

3.4 Physicochemical properties of sunscreen containing SEA










The physicochemical properties of sunscreen containing SEA including of the appearance, color, texture, pH, viscosity, and layer separation were observed before and after accelerated conditions. Before acceleration, the appearance of the sunscreen base formula was pure white in color, smooth texture, and absence of layer separation after centrifugation. The sunscreen containing 2.5% and 5.0% (w/w) of SEA were appeared in color of light orange-white and light orange, respectively. The appearance of light orange color was affected from the red color of astaxanthin content. The pH value of sunscreen containing SEA were slightly increased from 6.62 to 7.08 in formula containing 2.5% SEA, and to 7.13 in formula containing 5.0% SEA. This result indicated that more concentration of SEA enhanced higher pH value. Therefore, pH about 7 of sunscreen product is acceptable for cosmetic safety. The viscosity of sunscreen containing SEA was slightly decreased without causing of layer separation and the texture stayed smooth. All physicochemical properties described above are summarized in Table 3.

Table 2: Satbility test of color, SPF, and Boots Star Rating values of SEA at initial stage and after accelerated conditions.

| Parameter | Initial stage | Accelerated conditions | | | | | | Δ Cycle6-Initial stage | | |
|--------------------------|---------------|------------------------|-------|-------------|-------|-----------|-------|-------------------------------|-------------|-----------|
| | | Dark/Light | | Freeze/Thaw | | Heat/Cool | | Dark/Light | Freeze/Thaw | Heat/Cool |
| | | C3 | C6 | C3 | C6 | C3 | C6 | | | |
| Color | | | | | | | | | | |
| L* | 26.41 | 25.11 | 22.36 | 25.04 | 24.60 | 21.51 | 20.40 | -4.05 | -1.81 | -6.01 |
| a* | 6.83 | 2.48 | 0.67 | 2.05 | 0.70 | 3.53 | 0.95 | -6.16 | -6.13 | -5.88 |
| b* | 4.36 | 1.43 | 0.44 | 1.98 | 0.07 | 1.54 | 0.13 | -3.92 | -4.29 | -4.23 |
| SPF | 2.28 | 1.76 | 1.14 | 1.8 | 1.34 | 1.81 | 1.19 | -1.14 | -0.94 | -1.09 |
| Boots Star Rating* | 3 | 3 | 3 | 3 | 3 | 3 | 3 | 0 | 0 | 0 |
| Critical Wavelength (nm) | 373.4 | 373.7 | 373.3 | 373.7 | 373.8 | 374.0 | 373.8 | -0.4 | 0.4 | 0.4 |

*Boots Star rating; 3=Good, 4=Superior, 5=Ultra

Table 3: Comparison of physicochemical properties, SPF, and Boots Star Rating values of sunscreen base formula, sunscreen formula containing 2.5% and 5.0% (w/w) SEA at initial stage and after accelerated conditions.

| Parameter | Sunscreen base formula | | | Sunscreen containing 2.5% SEA | | | Sunscreen containing 5.0% SEA | | |
|----------------------|--|--|--|--|--|---|--|--|--|
| | Initial stage | Freeze/Thaw | Heat/Cool | Initial stage | Freeze/Thaw | Heat/Cool | Initial stage | Freeze/Thaw | Heat/Cool |
| Appearance and color |  |  |  |  |  |  |  |  |  |
| | Pure white | Pure white | Pure white | Light orange-white | Cream | Cream | Light orange | Light orange-white | Light orange-white |
| Texture | Smooth | Smooth | Smooth | Smooth | Smooth | Smooth | Smooth | Smooth | Smooth |
| pH | 6.62 | 6.70 | 6.79 | 7.08 | 7.12 | 7.18 | 7.13 | 7.19 | 7.24 |
| Viscosity (cP) | 3343 | 3317 | 3303 | 3270 | 3183 | 3210 | 3290 | 3220 | 3243 |
| Layer separation | No | No | No | No | No | No | No | No | No |
| SPF | 6.09 | 5.25 | 4.03 | 9.73 | 6.5 | 7.28 | 13.16 | 9.62 | 9.22 |
| Boots Star Rating | 3 | 4 | 4 | 3 | 4 | 4 | 3 | 4 | 4 |

4. Conclusions

The SEA obtained the SPF and Boots Star Rating value. Nevertheless, astaxanthin content, recolor, and SPF value were not stable after accelerated conditions, except the Boots Star rating value. The SEA was compatible for sunscreen formulation at concentration of 2.5-5.0% (w/w) and able to enhanced the SPF while was not for Boots Star Rating value. More concentration of the extract provided higher SPF of sunscreen formula. Unfortunately, the SPF of sunscreen formula containing SEA was not stable under accelerated conditions. This study indicated that sunflower oil extracted astaxanthin from *H. pluvialis* was efficiency to enhanced the SPF value of sunscreen formula. However, the improvement of its stability is needed for further investigation

Acknowledgement

This worked was supported by the research grant of Mae Fah Luang University, Chiang Rai , Thailand.

References

- [1] D.K. Kim, S.J. Hong, J.H. Bae, N. Yim, E.S. Jin and C.G. Lee, *Biotechnol. Bioprocess. Eng.* **16** (2011) 698–705.
- [2] M. Guerin, M.E. Huntley and M. Olaizola, *Trends Biotechnol.* **21** (2003) 210–216.
- [3] J.K. Park, P.N. Tran, J.D. Kim, S.L. Hong and C.G. Lee, *J. Microbiol. Biotechnol.* **19** (2009) 918–921.
- [4] C.D. Kang and S.J. Sim, *Biotechnology Letters* **30** (2008) 441–444.
- [5] I. Promputtha and T. Pekthong, *Extraction of natural red color from microalgae Haematococcus pluvialis using bio-solvent vegetable oils for application in cosmetics*, The 4th International Conference on Natural Products for Health and Beauty Conf. Proc., Chiang Mai, Thailand, (2012), In press.
- [6] J.G. Liu, M.Y. Yin and J.R. Zhang, *Chin. J. Oceanol. Limnol.* **4** (2002) 358–394.
- [7] A.R. Rao, R. Sarada and G.A. Ravishankar, *J. Sci. Food Agr.* **87** (2007) 957–965.
- [8] N.M. Lyons and N.M. O'Brien, *J. Dermatol. Sci.* **30** (2002) 73–84.

PREPARATION OF COPPER NANOPARTICLES USING GALLIC ACID AS REDUCING AGENT

Panchanin Wongsuwat, Ampa Jimtaisong*, Sirirat Mookriang

School of Cosmetic Science, Mae Fah Luang University, Muang, Chiang Rai, 57100 Thailand

*Author for correspondence; E-mail: ampa@mfu.ac.th, Tel. +66 53 916843, Fax. +66 53 916831

Abstract: The preparation of copper nanoparticles using safe antioxidant gallic acid as reducing agent in the presence of various polymers (PVP, polyquaternium-7 and carboxymethyl chitosan) was studied. The factors that affected the preparation of copper nanoparticles, including reactant ratio, reaction temperature, and stabilizing agent were investigated. The copper nanoparticles were characterized by UV-Vis absorption spectroscopy and TEM techniques. The preparation of copper nanoparticles using gallic acid in various aqueous polymer solutions showed no peak of copper nanoparticles. However, the particle size of copper nanoparticles determined by TEM revealed that the size was about 14 nm in average diameter.

1. Introduction

The research of nanoparticle and nanotechnology field is fast-growing. Research has already led to significant breakthroughs, and several products are available commercially. Nanoparticles can be classified on the basis of the type of material into metallic, semiconductor and polymeric nanoparticles. They exhibit unique physical properties (such as particle aggregation, photoemission, electrical and heat conductivities), chemical properties (such as catalytic activity), and hence have received much attention from scientists and researchers in different areas of biological science [1]. Copper nanoparticles have attracted considerable attention because of their catalytic, optical, and electrical conducting properties. Several methods were developed for the preparation of copper nanoparticles, including thermal reduction, metal vapor synthesis, radiation methods, microemulsion techniques, laser ablation, mechanical attrition, and chemical reduction [2]. The nanoparticles are widely synthesized from gold and silver, in spite of their high cost while copper nanoparticles have more attraction because of their high conductivity and lower cost but these are difficult to apply because they are easily oxidized in ambient air. To protect copper nanoparticles against oxidation and agglomeration, the synthesis can be done with the polymer acts as capping agent to stabilize and improve characteristic of copper nanoparticles [3]. In this study, the preparation of copper nanoparticles using safe antioxidant substance (gallic acid) as reducing agent was studied. The factors that affect the preparation of copper nanoparticles, including reactant ratio, reaction temperature, and stabilizing agent were investigated. The copper nanoparticle was characterized by UV-Vis absorption spectroscopy and TEM techniques.

2. Materials and Methods

2.1 Reagents for copper nanoparticles synthesis

Solvent for copper nanoparticles synthesis was deionized water. Copper sulfate pentahydrated and gallic acid were of A.R. grade.

2.2 Preparation of copper nanoparticles

2.2.1 Preparation of copper nanoparticles in aqueous poly(vinylpyrrolidone) (PVP)

PVP K-90 (1% w/v solution) were varied at 2 and 4 ml. Gallic acid (2.5 mM) concentration in aqueous PVP K-90 were studied by varying at 2, 5, 10, and 20 ml at room temperature for 30 min. The effect of reaction time was compared between 30, 60, and 180 min at room temperature (RT) and 80 °C for 30min.

2.2.2 Preparation of copper nanoparticles in aqueous Polyquaternium-7

The synthesis of copper nanoparticles at different pH values was studied by mixing 0.01M of $\text{CuSO}_4 \cdot 5\text{H}_2\text{O}$, 0.10M Gallic acid, and 10 ml of Polyquaternium-7 (1% w/v) at 85 °C for 30 min. The effects of gallic acid concentration in aqueous Polyquaternium-7 solution were studied in two different ways. First, the concentration of gallic acid was varied at 0.025, 0.05, 0.1, and 0.25 % w/v. The reaction mixture was prepared by 0.01M $\text{CuSO}_4 \cdot 5\text{H}_2\text{O}$ pH 6.5, 10 ml of Polyquaternium-7 (1% w/v) at 85 °C for 30 min. Second, the concentration of gallic acid was varied at 2.5, 2.0, and 1.25 mM. The reaction mixture was prepared by 0.3 mM $\text{CuSO}_4 \cdot 5\text{H}_2\text{O}$ at pH 6.5, 4 ml Polyquaternium-7 at room temperature for 60 min.

2.2.3 Preparation of copper nanoparticles in aqueous carboxymethyl-chitosan (CM-chitosan)

The effect of gallic acid concentration at 0.01M and 0.10M was used to react with 0.01M $\text{CuSO}_4 \cdot 5\text{H}_2\text{O}$ at pH 6.5, CM-chitosan (0.1% w/v) 5 ml at 85 °C for 30 min. The reaction mixture prepared by 0.01M $\text{CuSO}_4 \cdot 5\text{H}_2\text{O}$ and 0.10M gallic acid synthesized at 85 °C for 30 min. Effect of concentration of CM-chitosan was studied at 0 ml and 5ml.

2.3 Particle size of copper nanoparticles

The size of copper nanoparticles was investigated by transmission electron microscopy (TEM, JEOL model JEM-2010). A drop of copper nanoparticles solution was placed on copper grid. The size distribution was calculated from the measurement of

particle size for more than 300 particles in the TEM picture.

3. Results and Discussion

3.1 Preparation of copper nanoparticles in aqueous poly (vinylpyrrolidone) (PVP)

3.1.1 Effect of PVP and gallic acid concentration

PVP K-90 (1% w/v solution) was varied at 2 and 4 ml. Gallic acid (2.5 mM) concentration in aqueous PVP K-90 were studied by varying at 2, 5, 10, and 20 ml at room temperature for 30 min (Table 1). The color of the solution is different when amount of PVP and gallic acid was decreased it resulted in color change from brown to yellow color (Figure 1). The progress of the reaction was monitored from color changes by UV-Vis absorption spectra of nanoparticles, but there is no surface plasmon peak of copper nanoparticles showed at 580 nm (Figure 2).

Table 1. Synthesis of copper nanoparticles using 0.3 mM $\text{CuSO}_4 \cdot 5\text{H}_2\text{O}$ (30 min, room temperature)

| Sample | 1%w/v of PVP (ml) | 2.5 mM gallic acid (ml) |
|--------|-------------------|-------------------------|
| S1 | 4 | 20 |
| S2 | 4 | 10 |
| S3 | 2 | 20 |
| S4 | 2 | 10 |
| S5 | 2 | 5 |
| S6 | 2 | 2 |

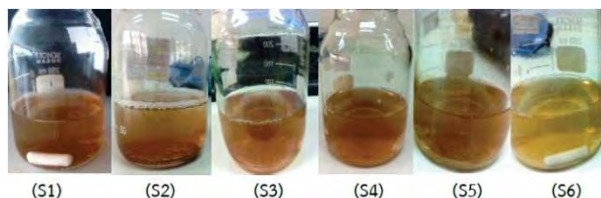


Figure 1. Copper nanoparticles prepared at different quantities of PVP and gallic acid

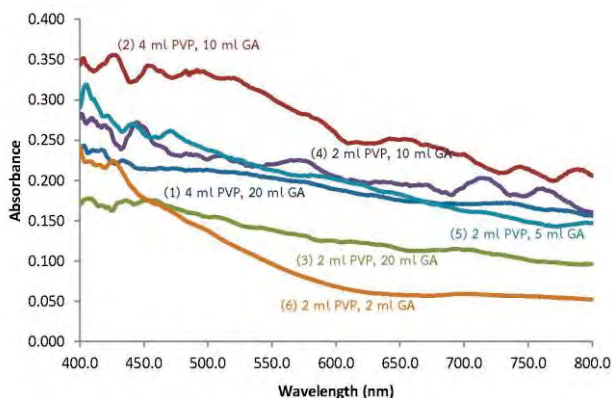


Figure 2. UV-Vis absorption spectra of copper nanoparticle at different quantities of PVP and gallic acid concentration

3.1.2 Effect of reaction time and temperature

The reaction time was compared between 30, 60, and 180 min (Table 2). In addition, the effect of temperature was also studied at room temperature (RT) and 80 °C for 30 min (Figure 3). The blue color of copper sulphate in the reaction mixture changed to light brown but there is no surface plasmon peak of copper nanoparticles observed at 580 nm.

Table 2. Copper nanoparticles synthesized in aqueous poly(vinylpyrrolidone) at different reaction time and temperature.

| Sample | 2.5 mM gallic acid (ml) | Temperature * (°C) | Time (minute) |
|--------|-------------------------|--------------------|---------------|
| S7 | 2 | RT | 30 |
| S8 | 2 | RT | 60 |
| S9 | 2 | RT | 180 |
| S10 | 2 | 80 | 30 |
| S11 | 5 | RT | 60 |
| S12 | 5 | 80 | 30 |

RT= room temperature (28-35 °C)

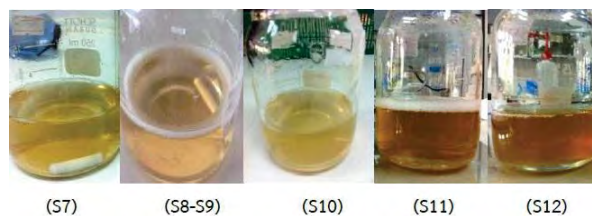


Figure 3. Effect of reaction time and temperature on copper nanoparticles prepared by gallic acid in aqueous PVP

3.2 Preparation of copper nanoparticles in aqueous Polyquaternium-7

3.2.1 Effect of pH

The synthesis of copper nanoparticles at different pH values was studied (Figure 4). The reaction mixtures were prepared by 0.01M of $\text{CuSO}_4 \cdot 5\text{H}_2\text{O}$, 0.10M Gallic acid, and 10 ml of Polyquaternium-7 at 85 °C for 30 min. The characteristic absorption showed no peak of copper nanoparticles at 580 nm (Figure 5).

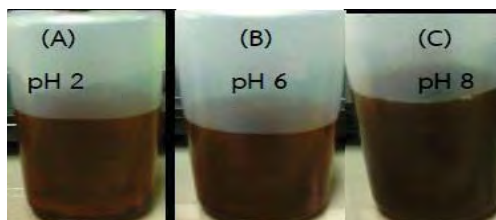


Figure 4. Preparation of copper nanoparticles at different pH values (85°C, 30 min)

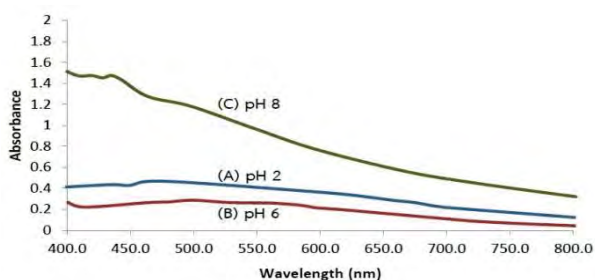


Figure 5. UV-Vis absorption spectra of reaction at different pH (Polyquaterrum-7, 85 °C, 30 min)

3.2.2 Effect of gallic acid and $\text{CuSO}_4 \cdot 5\text{H}_2\text{O}$ concentration

The effect of gallic acid concentration in aqueous Polyquaterrum-7 solution was studied in two different ways. First, the concentration of gallic acid was varied at 0.025, 0.05, 0.1, and 0.25 %w/v (Figure 6, A-D). The reaction mixture was prepared by 0.01M $\text{CuSO}_4 \cdot 5\text{H}_2\text{O}$ pH 6.5, 10 ml of Polyquaterrum-7 at 85 °C for 30 min. Second, the concentration of gallic acid was varied at 2.5, 2.0, and 1.25mM (Figure 6, E-G). The reaction mixture was prepared by 0.3mM $\text{CuSO}_4 \cdot 5\text{H}_2\text{O}$ at pH 6.5, 4ml of Polyquaterrum-7 at room temperature for 60 min. UV-Vis absorption spectra showed no peak of copper nanoparticles at 580 nm.

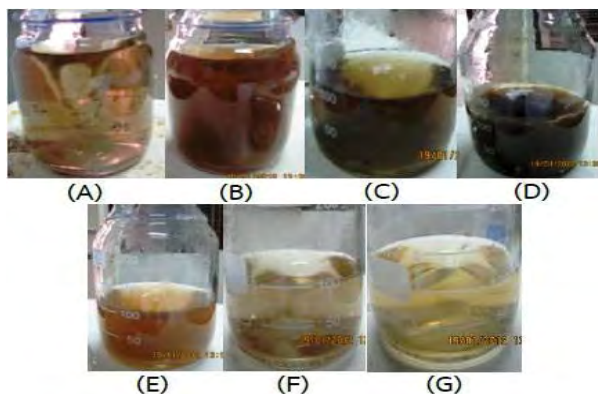


Figure 6. Effect of reaction at different concentration of gallic acid (GA); (A) 0.025, (B) 0.05, (C) 0.1, (D) 0.25 % w/v GA at 85°C for 30 min., (E) 2.5mM, (F) 2.0mM, and (G) 1.25mM GA at room temperature for 60 min.

3.3 Preparation of copper nanoparticles in aqueous carboxymethyl-chitosan (CM-chitosan)

3.3.1 Effect of gallic acid concentration

Gallic acid at 0.01M and 0.10M concentration were used to react with 0.01M $\text{CuSO}_4 \cdot 5\text{H}_2\text{O}$ at pH 6.5, CM-chitosan (0.1%) 5 ml at 85 °C for 30 min. Gallic acid interacted with copper sulfate, the color changed and precipitate was formed, and when concentration of gallic acid increased color of solution showed darker brown color (Figure 7). UV-Vis absorption spectra showed no peak of copper nanoparticles at 580 nm (Figure 8).

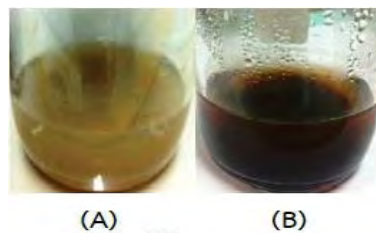


Figure 7. The effect of reaction at different concentration of gallic acid (CM-chitosan, 85 °C, 30 min); (A) 0.01M and (B) 0.10M

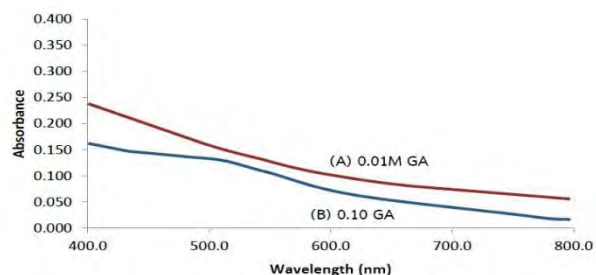


Figure 8. UV-Vis absorption spectra of reaction at different gallic acid concentration (CM-chitosan, 85 °C, 30 min)

3.3.2 Effect of CM-chitosan concentration

The reaction mixture prepared by 0.01M $\text{CuSO}_4 \cdot 5\text{H}_2\text{O}$ and 0.10M gallic acid synthesized at 85 °C for 30 min. Carboxymethyl-chitosan (0.01 % CM-chitosan) at 0 ml, and 5 ml was studied and it was found that both have brown precipitation (Figure 9), but the UV-Vis absorption spectra showed no peak of copper nanoparticles at 580 nm (Figure 10).

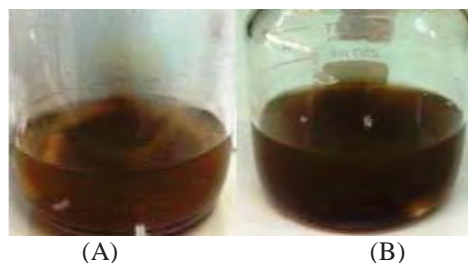


Figure 9. The effect of reaction at different quantity of 0.01% CM-chitosan (A) 0 ml, and (B) 5 ml (85 °C, 30 min)

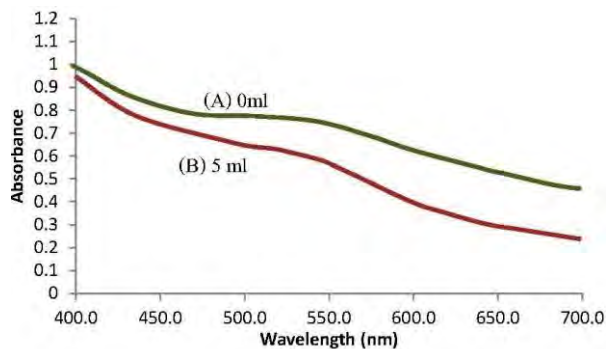


Figure 10. UV-Vis absorption spectra of reaction at different CM-chitosan quantity (85 °C, 30 min)

3.4 Particle size of copper nanoparticles

Transmission electron microscopy studies revealed that the particle size of copper nanoparticles prepared by 0.01M $\text{CuSO}_4 \cdot 5\text{H}_2\text{O}$ and 0.01M gallic acid with 5 ml of 0.1% CM-chitosan as stabilizing agent (85 °C for 30 min) is about 14.05 nm in average diameter and showed the normally round of particles (Figure 11). According to Samin et al., (2007) [4], copper nanoparticles size <5 nm diameter synthesized at low copper ion concentration, the corresponding UV-Vis absorption spectrum demonstrated a featureless Mie scattering profile without the appearance of an apparent surface plasmon band (Figure 12). This might, at least in part, be attributed to the small particles size, while large size copper nanoparticles at ~55 nm showed a characteristic peak at around 570 nm [4].

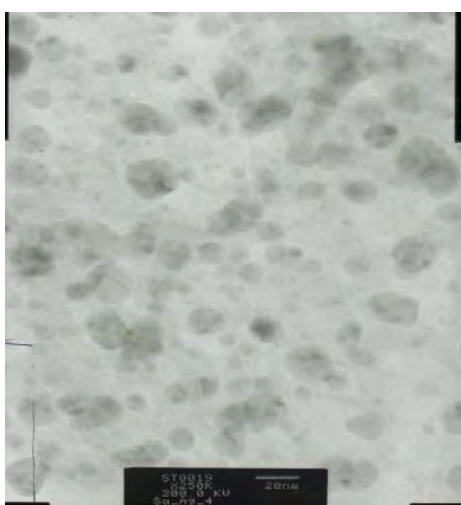


Figure 11. TEM image of copper nanoparticles

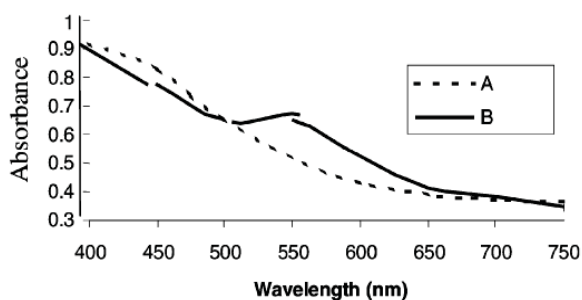


Figure 12. UV-Vis absorption spectra of copper nanoparticles; (A) smaller size Cu nanoparticles (<12 nm diameter) showing no SPR absorption band and (B) particles of size, 55 nm diameter, showing characteristic peak of copper nanoparticles at 570 nm [4].

4. Conclusions

This work reported the preparation of copper nanoparticle using gallic acid in aqueous solution of various polymers (CM-chitosan, PVP-K90, and polyquaternium-7). The studies indicate that preparation conditions, i.e. concentration of reaction,

polymer stabilizers, pH and reaction time and temperature massively affected the produced copper nanoparticles. UV –Vis absorption spectroscopy technique was used for preliminary monitor the reaction but established a featureless Mie scattering profile without the appearance of an apparent surface plasmon band (550-650 nm) which may due to the smaller size of copper nanoparticles as the TEM analysis revealed that the particle size of the synthesized copper nanoparticles is around 14 nm.

Acknowledgements

The author would like to thank Mae Fah Luang University for providing space and facilities.

References

- [1] S. Robert, "Health Effects of Nanoparticles", Robert-Sauvé en santé et en sécurité du travail (IRSST), August 2006.
- [2] LQ. Pham et al, *J. Colloid Interface Sci* **365** (2012) 103-109.
- [3] M. Bicer and I. Sisman, *Power Technology Inc* **198** (2010) 279-284.
- [4] M. Samin et al, *Bull. Mater. Sci* **30** (2007) 535-540.

Environmental Chemistry

CRUDE GLYCEROL PURIFICATION BY ADSORPTION VIA ACTIVATED CARBON DERIVED FROM SEWAGE SLUDGE

Chaowat Autthanit^{1*}, Mali Hunsom^{1,2}

¹ Department of Chemical Technology, Faculty of Science, Chulalongkorn University, Bangkok, 10330 Thailand

² Center of Excellence on Petrochemical and Materials Technology, Chulalongkorn University, Bangkok 10330, Thailand

* Author for correspondence; E-Mail: ch.resolves@gmail.com, Tel. +66 02 218 7516, Fax. +66 02 255 5831

Abstract: This work was carried out to investigate the effect of parameters on the preparation of activated carbon from sewage sludge for crude glycerol purification. Types of activating agent (KOH, H₃PO₄ and K₂CO₃), ratio of activating agent to char (1.0-6.0 w/w), impregnation time (5-25 hrs) and carbonization temperature (500-900°C) were explored. The preliminary results indicated that among the utilized activating agents, the activated carbon activated by KOH provided the best efficiency for crude glycerol purification. The purity of crude glycerol increased from 35 to 89 wt.% in the presence of activated carbon activated by KOH at ratio of 5:1, impregnation time of 25 hr and carbonization temperature of 800 °C. Moreover, the oxygen-containing surface groups on the surface of activated carbon played a key role on the purity of crude glycerol.

1. Introduction

Interest in biodiesel based on fatty acid methyl esters has grown considerably worldwide. This is also the case in Thailand where the recent increase in biodiesel production is predicted to be at least four-fold over just four years, from less than 2.1×10^6 l/day in 2008 to an expected 8.4×10^6 l/day in 2012 [1]. The production of 10 kg of biodiesel yields approximately 1 kg of crude glycerol [2]. Increasing the share of biodiesel in transportation fuels may decrease the net emission of CO₂ and alleviate the global warming problem. However, the increase in biodiesel production rates will significantly raise the quantity and surplus of crude glycerol and partially waste in the environment. This is because the crude glycerol discharged from biodiesel production plants consists not only of glycerol but also many other chemicals such as water, salts, soap, alcohol, traces of glycerides, and vegetable colors [3]. In addition, high-purity glycerol is still required as it is an important industrial feedstock for applications in the food, cosmetic and pharmaceutical industries, as well as other more minor uses [4]. Because the separation of glycerol via conventional distillation processes is not economically viable, removal of impurities via adsorption by a selective adsorbent is one of the possible ways to purify crude glycerol to acceptable standards [5].

Considering the potential commercial application of selective adsorption of glycerol, it is certainly necessary to find a cheaper and efficient adsorbent for treatment of crude glycerol [6]. The aqueous-phase adsorption of crude glycerol has been concerned mainly on activated carbon.

In this work, the purification of crude glycerol derived from a waste used-oil utilizing biodiesel (methyl ester) production plant was carried out using activated carbon derived from industrial sewage sludge by chemical activation method. Effects of ratio of activating agent to char, impregnation time and carbonization temperature on the properties of activated carbon as well as the crude glycerol purification efficiency were investigated

2. Materials and Methods

2.1 Pre-treatment of crude glycerol

Initially, the free fatty acid and salt contents were reduced by acidification. In each trial, 300 g of crude glycerol was acidified by the addition of phosphoric acid (85% H₃PO₄) to the desired pH 2.5, and then left for 12 h until the solution had phase separated into three distinct layers, that is a top layer of free fatty acids, the middle glycerol-rich layer and, if present, the bottom inorganic salt-rich layer. The top layer was removed by slow decantation and the middle glycerol-rich layer was separated from the bottom inorganic salt-rich layer, if present, by filtration. Prior to removal of the residue salts from glycerol-rich layer, it was neutralized by the addition of 12.5 M NaOH to pH 7.0, left for a while and then filtered to eliminate the precipitated salt [1].

2.2 Preparation of activated carbons

Activated carbons from sewage sludge were prepared in a two-step process: pyrolysis and chemical activation processes. In the pyrolysis process, sewage sludge was first washed with water to remove the water-soluble impurities, dried at 105 °C for 24 hrs. Then the precursor was heated to 400 °C at the rate of 10 °C/min for 2 hrs under N₂ atmosphere at flow of 50 ml/min, and then cooled to room temperature at the same rate. The resulting material was called chars.

The chars were then subjected to chemical activation. In the chemical activation process, 10.0 g of the pyrolyzed carbon were mixed with 100 mL of distilled water and amount of activation agent, depending on the ratios of activation reagent/pyrolyzed carbons desired (1:1, 2:1, 3:1, 4:1, 5:1 and 6:1 by weight) for each activation agent (KOH, H₃PO₄ and K₂CO₃). The mixture was shaken at 200 rpm depending on the set time (5-25 hrs). Finally, the carbonization was conducted at one of five different temperatures (500-900 °C) under nitrogen flow at heating rate of 10°C/min, and held at 30 min. After

activation, the derived activated carbons were removed from the reactor. Then, it was rinsed with 3.0 M HCl and deionized water for several times to remove other inorganic matter until the pH become neutral, filtered and finally dried at 105 °C for 24 hrs.

2.3 Adsorption with produced activated carbon

Adsorption of pretreated crude glycerol was conducted at room temperature in conical flasks with continuous shaking. Prior to use, the produced activated carbon was dried at 105 °C for 30 min to eliminate free moisture. In the adsorption stage, activated carbon was mixed with pretreated crude glycerol at ratio of 67 g/l pretreated crude glycerol, mixed at 250 rpm for 90 min and then subjected to vacuum filtration to remove the activated carbon.

2.4 Analysis

The glycerol content in purified crude glycerol was measured according to the standard method (ASTM D7637-10) [1] by a titration with sodium metaperiodate. This test method is based on the cold oxidation of the glycerol by sodium metaperiodate in a strong acidic medium. The glycerol content can be calculated by using Eq. (1)

$$\text{Glycerol content (\%)} = \frac{1.15125 \times (V_1 - V_2)}{m} \quad (1)$$

Where:

V_1 = volume of sodium hydroxide used in glycerol titration (mL)

V_2 = volume of sodium hydroxide used in blank titration (mL)

m = weight of glycerol sample used (g)

Ash content was analyzed according to the Standard method (ISO 2098-1972) by burning 1 g glycerol in a muffle furnace at 750 °C for 3 h. The MONG (Matter Organic Non-glycerol) levels and water was measured in terms of contaminants, which were calculated by the difference from a hundred of the previous three compositions [100-(% glycerol content+% ash content)]. The contents of oxygen-containing surface functional groups with varying acidity were determined by the Boehm's method of

titration with basic solutions of different base strengths (NaHCO_3 , Na_2CO_3 and NaOH) [7]. The superiority of sewage sludge for activated carbon production was first checked using proximate analysis.

3. Results and Discussion

3.1 Properties of crude glycerol

The original crude glycerol was a dark brown liquid with a pH of 8-9. It contained a low content of glycerol but a relatively high ash and contaminant contents (Table 1). The ash content was largely composed of inorganic matter such as sodium salts that originated from the utilized catalyst (NaOH) in the transesterification process. By far the largest contaminant was MONG, which indeed exceeded the glycerol levels, and was generated by the contamination of soap, methanol and methyl esters in the glycerol residue from the biodiesel production process. During the pre-treatment stage, some of the fatty acids were released as soluble soap and some of methyl esters dissolved or suspended in the glycerol solution. These free fatty acids and methyl esters then reacted with the excess NaOH in the subsequent neutralization step to re-form soap which remained in the glycerol residue [8].

3.2 Effect of parameters on crude glycerol purification by adsorption with activated carbon derived from sludge

3.2.1 Effect of weight ratio of activating agent to char

Effects of weight ratio of activating agent to char on crude glycerol purification were carried out at the weight ratio of 1 by using three types of activating agent including KOH , K_2CO_3 and H_3PO_4 at constant activating time of 20 hr and carbonized in N_2 atmosphere at 500 °C for 30 min. The surface oxygen containing functional groups including carbonyl, carboxyl, hydroxyl and lactone were first measured. As shown in Figure 1, large quantity of carbonyl was generated on the surface of activated carbon compared with other types of activating agent. This group increased as the increase of weight ratio of KOH to char while the other measured groups remained

Table 1. Characteristics of crude glycerol, pretreated crude glycerol and purified crude glycerol by adsorption process

| Parameters | BS 2621:1979 [9] | Crude glycerol | Pretreated crude glycerol | Purified crude glycerol by adsorption process | |
|-------------------------|------------------|----------------|---------------------------|---|-----------------------------|
| | | | | Activated carbon derived from sludge ^a | Commercial activated carbon |
| pH | | 8.0-9.0 | 7.0 | 7.0 | 7.0 |
| Glycerol content (wt.%) | ≥ 80 | 27.23 ± 0.84 | 35.76 ± 0.27 | 89.35 ± 1.72 | 84.1 ± 0.85 |
| Ash content (wt.%) | ≤ 10 | 36.18 ± 0.20 | 29.07 ± 0.51 | 9.94 ± 1.21 | 13.10 ± 0.13 |
| Contaminant (wt.%) | ≤ 10 | 36.59 | 35.17 | 0.71 ± 0.50 | 2.9 ± 0.72 |
| Color (Pt-Co unit) | | 172,857 | 154,038 | 2,426 ± 39 | 46,627 ± 2678 |

^a At the activated carbon dose of 67 g/l glycerol at 250 rpm for 90 min (KOH 5:1, 25 hr and 800 °C)

constant or decrease slightly. The similar trend of quantity change was observed in the case of K_2CO_3 . However, in the presence of H_3PO_4 , more quantities of hydroxyl and carboxyl were generated compared with carbonyl and lactone. The hydroxyl and carboxyl groups were 4.9 and 4.1 mEq/g at weight ratio of 6, while only 2.1 and 1.5 mEq/g of carbonyl and lactone were generated. This might be attributed to the fact that KOH and K_2CO_3 are the basic chemicals, which can enhance high generation of basic oxygen functional groups (carbonyl group), while H_3PO_4 is the acid chemical which can enhance a more generation of acid oxygen functional groups (carboxyl, hydroxyl and lactone).

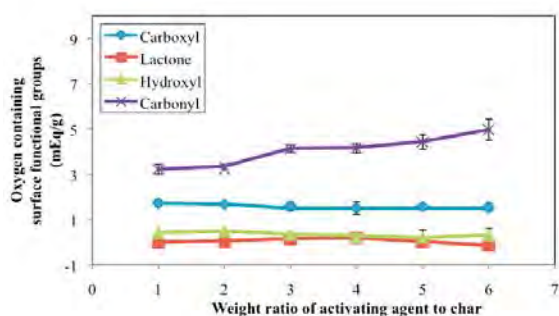


Figure 1. Contents of oxygen containing surface functional groups of the activated carbon with KOH at difference activating ratios.

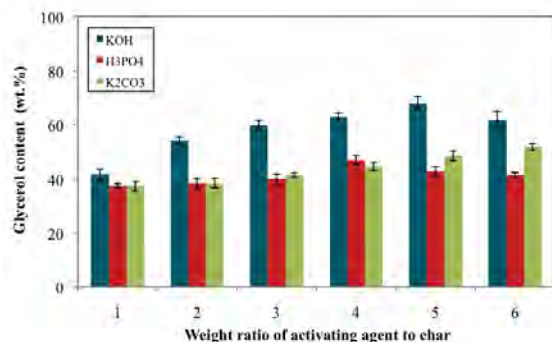


Figure 2. Effect of weight ratio of activating agent to char on the purity of crude glycerol.

Figure 2 shows variation of glycerol content in crude glycerol purified by adsorption with activated carbon activated by KOH, K_2CO_3 and H_3PO_4 . It was found that the activated carbon activated by KOH at the weight ratio of KOH to char of 5:1 provided the best purity of crude glycerol compared with other types of activating agent. It can enhance the purity of crude glycerol from 35.76 to 68.08 wt.%, while K_2CO_3 and H_3PO_4 can increase the purity of crude glycerol to 51.7 and 40.8 wt.% at the weight ratio of 6 and 4, respectively. This is because the KOH can enhance a high formation of carbonyl group on the surface of activated carbon. As proposed by Pereira et al. [10], the carbonyl group is the basic functional group containing high quantity of electron acceptor [11] [12], which can bond as well to the anionic charge of FAME or FFAs (R-COO⁻), resulting to the decrease of contaminant in

purified crude glycerol. Thus, it favors to bond with the negative charged acid groups. In this case, the crude glycerol contained large quantity of free fatty acid, which has negatively charged acid groups [13]. Thus, the presence of high quantity carbonyl group can reduce high quantity of fatty acid containing in crude glycerol. However, if the ratio of KOH was increased to 6:1, the purity of crude glycerol also decreased from 68.08 to 61.82 wt.%. This was possibly due to the decomposition of excessive KOH molecules to water which can gasify with carbon to form CO and H_2 [14]. Over-gasification might reduce the specific surface area and adsorption of crude glycerol.

3.2.2 Effect of impregnation time

Effect of impregnation time on crude glycerol purification by the adsorption with activated carbon activated by KOH at the weight ratio of 5:1 and carbonize under N_2 atmosphere at 500 °C for 30 min was investigated in the range of 5-25 hrs. The glycerol content in purified crude glycerol increased as the increase of impregnation time (Figure 3). This is might be attributed to the fact that long impregnation time would promote the diffusion of KOH in the char, resulted to the formation of large quantity of carbonyl group from 1.98 mEq/g at 5 hr to 4.66 mEq/g at 25 hr. Hence, the impregnation time of 25 hr was required and was used in subsequent experiments.

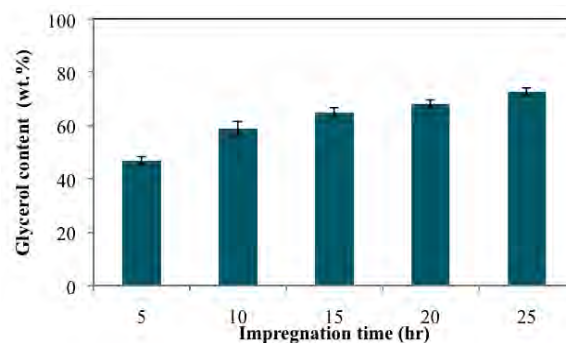


Figure 3. Effect of impregnation time on the purity of crude glycerol purified by adsorption with KOH at weight ratio to char of 5.

3.2.3 Effect of carbonization temperature

Effect of carbonization temperature on crude glycerol purification by the adsorption with activated carbon activated by KOH at the weight ratio of 5:1 and carbonize under N_2 atmosphere at different temperature in the range of 500-900 °C for 30 min was investigated at constant impregnation time of 25 hr. As shown in Figure 4, the glycerol content in purified crude glycerol increased from 72.68 to 89.35 wt.% as the increase of carbonization temperature of 500 to 800 °C. This corresponds to the increase of carbonyl group on the surface of activated carbon from 4.67 mEq/g to 7.08 mEq/g. However, further increase the carbonized temperature from 800 to 900 °C results to the decrease of glycerol content to 67.01 wt.%, consistent with the decrease of the quantity of carbonyl group to 4.15

mEq/g. This is because the carbonyl groups can decompose around 850 °C [11], resulting to the decrease of the adsorption capacity of contaminants from crude glycerol. In addition, KOH can convert to potassium carbonates at higher temperature [15], resulting to the decrease of surface area as well as the low the capacity to adsorb contaminants in crude glycerol.

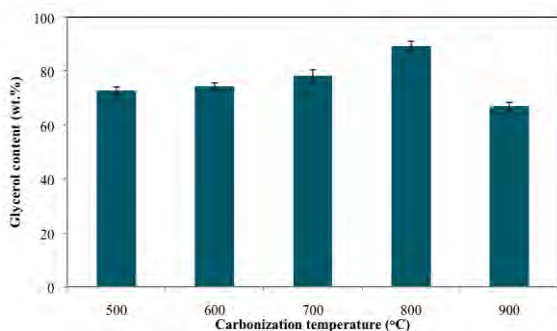


Figure 4. Effect of carbonization temperature on the purity of crude glycerol purified by adsorption with KOH at weight ratio to char of 5.

The properties of purified crude glycerol purified by the adsorption with activated carbon derived from sludge and commercial one were demonstrated in Table 1. It was clearly seen that the crude glycerol purified by the activated carbon derived from sludge had high glycerol content than that purified by commercial activated carbon. In addition, the color of the former case was lower than the latter case as demonstrated in Figure 5.

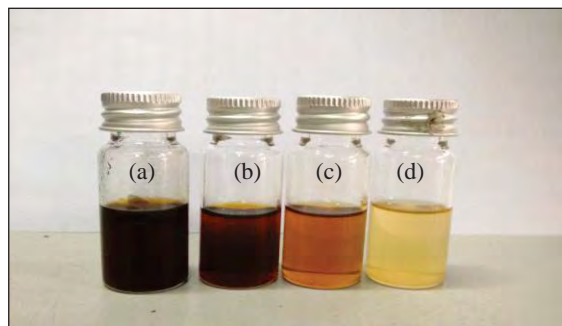


Figure 5. Color of (a) crude glycerol, (b) pretreatment crude glycerol and purified crude glycerol by adsorption with (c) commercial activated carbon and (d) activated carbon derived from sludge.

4. Conclusions

In this study, sewage sludge has been shown to be a feasible source for crude glycerol purification. Among utilized chemical agent, KOH showed the performance compared with K_2CO_3 and H_3PO_4 because it can enhance the large generation of carbonyl group on the surface of activated carbon. Thus, it was chosen as the most effective activation reagent for activation of sewage sludge for producing the best result in percentage of glycerol. The optimum condition for

preparation of activated carbon from sewage sludge was obtained at activated carbon activated by KOH at ratio of 5:1, impregnation time of 25 hr and carbonization temperature of 800 °C. This condition provided the best activated carbon which gave the most efficiency for crude glycerol purification.

Acknowledgements

The authors acknowledge the Department of Chemical Technology, Faculty of Science, Chulalongkorn University for financial support, the Nanyang Textile Co., Ltd for raw material support.

References

- [1] R. Manosak, S. Limpattayanate and M. Hunsom, *Fuel Processing Technology*, **92** (1), 2011: 92-99.
- [2] Z. Chi, D. Pyle, Z. Wen, C. Frear and S. Chen, *Process Biochem.* **42** (2007) 1537-1545.
- [3] M. Hajek and F. Skopal, *Bioresource Technol* **101** (2010) 3242-3245.
- [4] D.T. Johnson and K.A. Taconi, *Eng. Progress* **26** (2007) 338-346.
- [5] F. Karaosmanoglu, K.B. Cigizoglu, M. Tuter, and S. Ertekin, *Energy Fuels* **10** (1996), 890-895.
- [6] L. Peereboom, B. Koenigsnecht, M. Hunter, J.E. Jackson, and D.J. Miller, *Carbon* **45** (2007) 579-586.
- [7] X. Chen, S. Jeyaseelan and N. Graham, *Waste Manage* **22** (2002) 755-760.
- [8] D.T. Johnson and K.A. Taconi, *Eng. Progress* **26** (2007) 338-346.
- [9] T.L. Ooi, K.L. Yong, K. Dzulkafly, W.M.Z. Wan Yunus and A.H. Hazimah, *J. Palm Oil Res.* **13** (2001) 16-22.
- [10] M. F. R. Pereira, S. F. Soares, J. J. M. Orfao, and J. L. Figueiredo, *Carbon* **41** (2003) 811-821.
- [11] N.D. Epitotis, *Journal of the American Chemical Society* **94** (1972) 1946.
- [12] G.X. Yu, S.X. Lu, H. Chen and Z.N. Zhu, *Carbon* **43** (2005) 2285.
- [13] G. Vivekanand, *Surface modification of activated carbon for the removal of water impurities*, The Center for Microfibrous Material Manufacturing, Department of Chemical Engineering, Auburn University, USA (2008).
- [14] J. GUO and A. C. LUA, *Chemical Engineering Research and Design* **81** (2003) 585-590.
- [15] A. Nasser and A. El. Hendawy, *Applied Surface Science* **255** (2009) 3723-3730

NONYLPHENOL POLYETHOXYLATE DEGRADATION BY MEANS OF FENTON AND PHOTO-FENTON PROCESSES

Nisakorn Thongkon^{1*}, Patraphon Kaewthumrong¹, Watchara Mungmai¹

¹ King Mongkut's University of Technology Thonburi/Department of Chemistry, Bangkok, Thailand

* Author for correspondence; E-Mail: Nisakorn.tho@kmutt.ac.th, Tel. +66 02 4708964, Fax. +66 02 4708843

Abstract: In the present experimental work, the degradation of nonylphenol polyethoxylate (NPnEO; $n = 3-13$, $n \sim 9$) was investigated using Fenton and Photo-Fenton processes. Characterization of the composition of NPnEO was exploited for the qualitative determination of their degradation products. The separation of individual nonylphenol by ethoxylated units was performed by normal-phase high performance liquid chromatographic (HPLC)-FL employing amino column. The optimum condition was achieved by using the mixture of 60% hexane and 40% isopropanol as mobile phase at a flow rate of 1.2 mL min^{-1} . Limits of detection were estimated to be 30, 5, 5, 5, 5, 10, 10 and 30 mg L^{-1} for NP3EO, NP4EO, NP5EO, NP6EO, NP7EO, NP8EO, NP9EO and NP10EO, respectively ($S/N = 3$). The relative standard deviation based on peak area of each ethoxylate homologue ranged from 0.09 to 4.7 %. The degradation products from Fenton process were $96.7 \pm 0.5\%$ of NP5EO, $2.2 \pm 0.3\%$ of NP4EO and $1.1 \pm 0.2\%$ of NP3EO by calculating from the relative peak area. The best performance was obtained using the following concentration: 50 mg L^{-1} of NPnEO ($n = 3-13$), 150 mg L^{-1} of Fe^{2+} and $50 \text{ mg L}^{-1} \text{ H}_2\text{O}_2$. In order to enhance NPnEO degradation, photolysis was also performed. The equipment and concentration of Fenton's reagent for Photo-Fenton treatment were the same used on Fenton process. The reaction solution was irradiated with a high-pressure mercury lamp emitting UV radiation at a wavelength of about 254 nm. Photo-Fenton process showed best results that provided less toxic chemical in solution after 6 h of reaction (100.0% NP5EO).

1. Introduction

Nonylphenol polyethoxylates (NPnEOs) are the most commonly used alkylphenol polyethoxylates (APnEOs) which are nonionic surfactants in industrial and household cleaning products [1]. Due to their widespread usage, NPnEOs and their degradation products are contaminants in environment [2, 3]. NPnEOs are broken down aerobically into nonylphenol ethoxy carboxylates and short-chain NPnEOs which can be further degraded to nonylphenol in anaerobic environment [4, 5]. Toxicity of NPnEOs are relatively low, however the concern on their degradation products become increasingly. Degradation products of NPnEOs have been reported to have greater toxicity than their parent compounds. They have caused estrogenic responses [6]. Many papers have been focused on the biodegradation of NPnEOs [7]. Biodegradation of NPnEOs is slow process and it produces highly and specially toxic and stable nonylphenol [8, 9]. There are, in fact, other

factors that cause degradation of NPnEOs. Oxidation processes are commonly used to eliminate organics from water and wastewater [10, 11, 12]. However, oxidation of NPnEOs has not previously been explored and determined in detail.

In this work, degradation of NPnEO ($n = 3$ to 13 , $n \sim 9$) by Fenton's reagent and Photo-Fenton reaction was proposed and followed up with High performance liquid chromatography – fluorescence spectroscopy instruments (HPLC-FL) for determination of NPnEO and their degradation products. Fenton's reagent is one of the most effective methods for the oxidation of organic pollutants. Reagent has been found effective in treating various industrial wastewater components [12]. It is very important that during treatment of industrial wastewater should not produce persistent and toxic chemicals. The aim of this work was to identify and compare the degradation products from fenton's reagent and photo-fenton processes.

2. Materials and Methods

2.1 Reagents and chemicals

All chemicals were reagent grade and used without further purification. Tergitol NP-9 (mixture of NPnEO from 3 to 13, $n \sim 9$) was purchased from Fluka (Germany). Hydrogen peroxide (30%) and ferrous sulfate heptahydrate were purchased from Ajax Chemicals, Australia. For high performance liquid chromatography (HPLC) measurements, HPLC-grade hexane and isopropanol (Fisher, Thailand) were used.

2.2 Methods

2.2.1 Degradation of NPnEO ($n = 3$ to 13 , $n \sim 9$)

Laboratory studies were investigated the possible degradation products of NPnEO ($n \sim 9$) under aerobic environment conditions. The concentration of NPnEO solution in all experiments was 50 mg L^{-1} . 25- mL of NPnEO solution was transferred to a vial left in laboratory for 2 days. A similar experiment was performed in the dark by covering the vial with aluminum foil for 2 days. For Fenton experiments, different concentrations of ferrous sulfate heptahydrate and hydrogen peroxide (30%) in the range of $50 - 150 \text{ mg L}^{-1}$ were used in order to examine the effect of ferrous ion and H_2O_2 concentration. A 25-mL of test solution, which contained 50 mg L^{-1} of NPnEO and ferrous ions or H_2O_2 with different concentration was stirred 300 rpm for 6 h in the dark. The Photo- Fenton process was carried out using Fenton's reagent under

UV irradiation. A high pressure mercury lamp (Applied photophilic Ltd. UK.) was used as UV source. The distance between UV source and a vial containing solution was 20 cm. The exposure time was 6 h.

2.2.2 HPLC-FL analysis

All measurements were performed using a Varian Model PROSTAR 230 instrument equipped with programmable fluorescence 363 detector. Analytes were monitored by fluorescence detection (λ_{ex} : 228 nm and λ_{em} : 305 nm). The solutions were introduced using micro syringe injection to a 20- μL loop and analytes were separated on a 250 x 4.6 mm I.D. column packed with 10 μm d_p NH_2 column from Phenomenex. The mobile phase was the mixture of hexane and isopropanol. The mobile phase solvent and flow rate were optimized for the identification and separation of each oligomer.

3. Results and Discussion

3.1 Optimization conditions for HPLC-FL analysis

Chromatographic separation of NPnEO ($n = 3 - 13$; $n \sim 9$) in a single run present several difficulties due to the mixtures of ethoxylate (EO) homologues. The appropriate analytical column and mode of separation were carefully chosen in order to obtain the best separation of NPnEO oligomers. Normal-phase liquid chromatography was tested for NPnEO analysis. Amino column (NH_2) was used for qualitative analysis of each EO homologue. Mobile phase, hexane and isopropanol in different ratios and their flow rate were optimized to obtain good resolution and separation of NPnEO. As can be seen in Fig. 1, the separation of NPnEO that has ethoxylate units' length from 3 to 13 was achieved when the mobile phase consisting of hexane-isopropanol (60-40) at a flow rate of 1.2 mL min^{-1} was used for isocratic analysis.

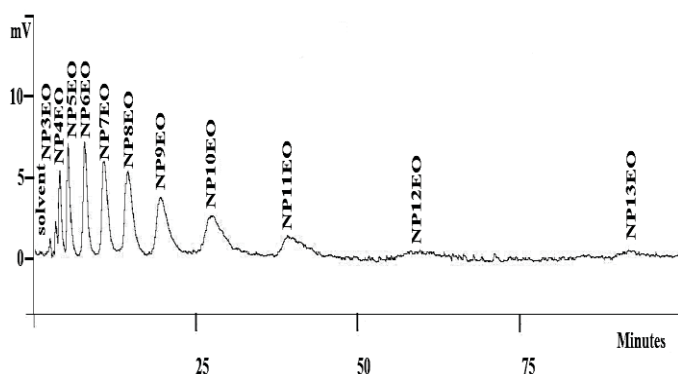


Figure 1 Chromatogram obtained from separation of NPnEO ($n = 3 - 13$; $n \sim 9$) at 50 mg L^{-1}

Fig. 1 shows the normal-phase chromatogram of mixture containing NPnEO with oligomer lengths of $n = 3 - 13$. Normal-phase HPLC provides better separation of NPnEO oligomers in comparison to reverse-phase. Separation was obtained with an NH_2 column under normal-phase condition using hexane

and isopropanol as the mobile phase. The NPnEO oligomers are separated according to the increasing number of EO units. Peaks of short-chain NPnEO, especially NP3EO and NP4EO are partly separated with a resolution value of 0.8 under these conditions. Chromatogram shows longer retention time and broader peaks of long-chain NPnEO. Analysis time was taken for 100 minutes to complete the whole peaks of NPnEO oligomers. Peaks of NP11EO, NP12EO and NP13EO were broad and difficult to observe in chromatogram due to very low sensitivity. In this work, the degradation products from oxidation process were qualitatively identified each homologue as NP3EO to NP10EO within 35 minutes. Limits of detection were estimated to be 30, 5, 5, 5, 5, 10, 10 and 30 mg L^{-1} for NP3EO, NP4EO, NP5EO, NP6EO, NP7EO, NP8EO, NP9EO and NP10EO, respectively when the injection volume was 20 μL . Over the established ranges (5-1000 mg L^{-1}) linear regression analysis of individual NPnEO concentration VS peak area obtained good fits ($r^2 > 0.9500$) for each homologue. The relative standard based on peak areas of each homologue ranged from 0.09 to 4.7 %.

3.2 Degradation of NPnEO ($n \sim 9$)

The HPLC patterns of NPnEO after leaving batch experiments with/without covering of aluminum foil for 2 days show no degradation process during analysis time. In previous work [13], degradation of 300 $\mu\text{g L}^{-1}$ of NPnEO solution was studied by using fluorescence spectrophotometer for measuring the total quantity of NPnEO in solution after degradation process. The results indicated that the maximum percentage degradation of NPnEO was 2.23 ± 0.11 and 1.36 ± 0.02 for solutions left in the laboratory and in the dark, respectively for 100 min. The results were corresponding with the present work that obtained no change in peak area of each NPnEO oligomer.

The effectiveness of Fenton's reagent pretreatment on the degradation of NPnEO was investigated. Experiments were conducted to examine the effect of the ferrous ions in the dark on peak area of each NPnEO oligomer. Fig. 2 shows that peak area of each homologue decreases significantly, especially the peaks of longer EO units of NPnEO ($n = 6 - 10$) when the concentration of Ferrous ions increases. No peaks of NPnEO ($n = 6 - 10$) are seen in chromatogram obtained from oxidation of NPnEO with a 150 mg L^{-1} of a solution containing ferrous ions (Fig. 2c). Two peaks of NP5EO could result from a degradation pathway described as a ω -oxidation. The terminal of alkyl or/and EO chain were oxidized to carbonylic groups. This degradation process occurred in combination with shortening of EO chain. Fig. 3 presents a concentration of ferrous ion series evaluation of the reaction products using peak area of each homologue that clearly indicate the formation of shorter chain length ethoxylates. The concentration of ferrous ions at 150 mg L^{-1} was chosen due to the best performance that resulted $97.5 \pm 0.2\%$ of NP5EO, $1.6 \pm 0.2\%$ of NP4EO and $0.9 \pm 0.1\%$ of NP3EO.

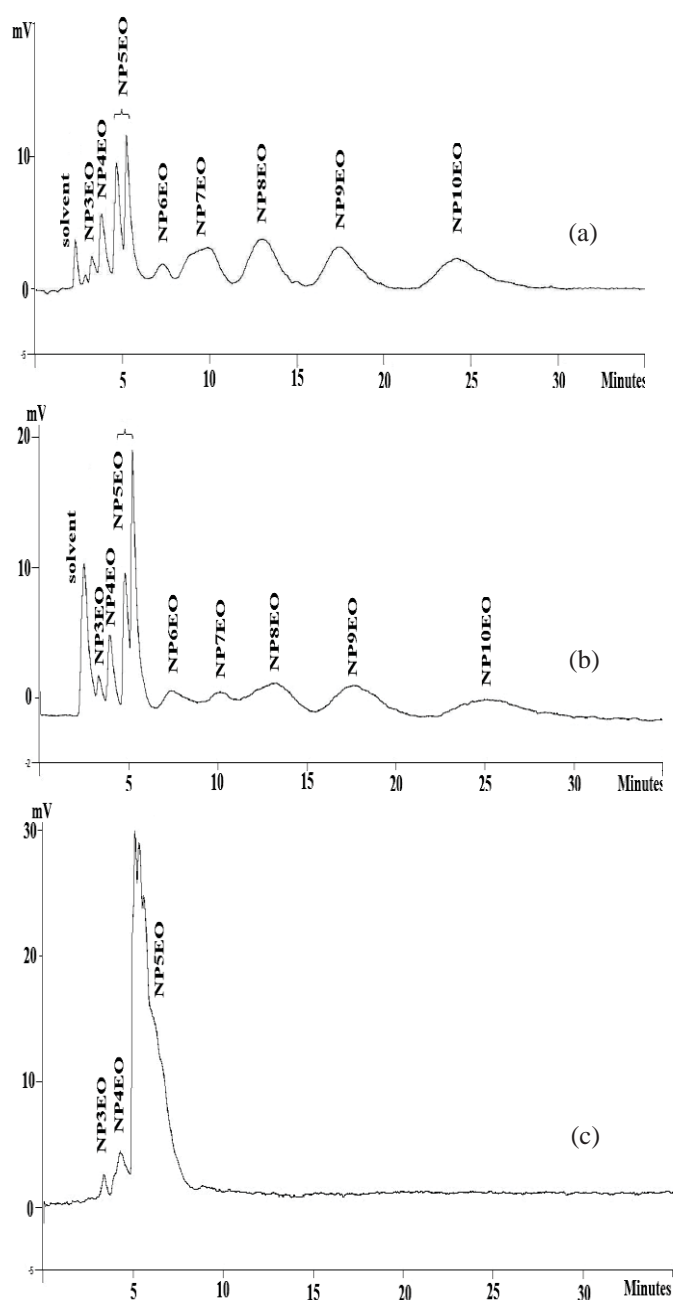


Figure 2 Degradation of NPnEO by ferrous ions at the concentration of (a) 50, (b) 100 and (c) 150 mg L⁻¹

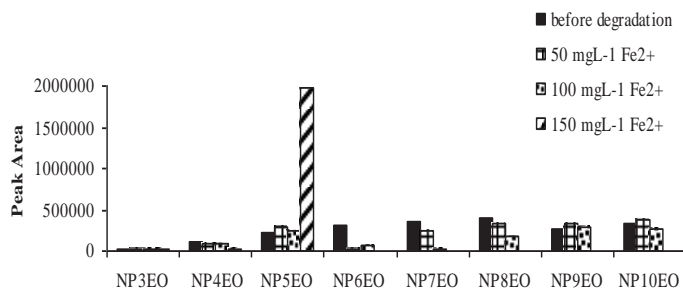


Figure 3 Peak area of individual NPnEO after the reaction of NPnEO (n= 3 to 10) with ferrous ions at different concentration

Next experiment was studied the effect of H₂O₂ in the dark for degradation of NPnEO. It could be seen in Fig. 4 and 5 that the potential of H₂O₂ is superior to of Fe²⁺. Longer EO units (n = 6-10) of NPnEO are not seen in HPLC chromatograms. The concentration of H₂O₂ at 50 mg L⁻¹ was chosen because increases in H₂O₂ concentration did not enhance the degradation process. The degradation products were 96.2±0.5% of NP5EO, 2.7±0.3% of NP4EO and 1.1±0.3% of NP3EO after using this reagent for 6 h.

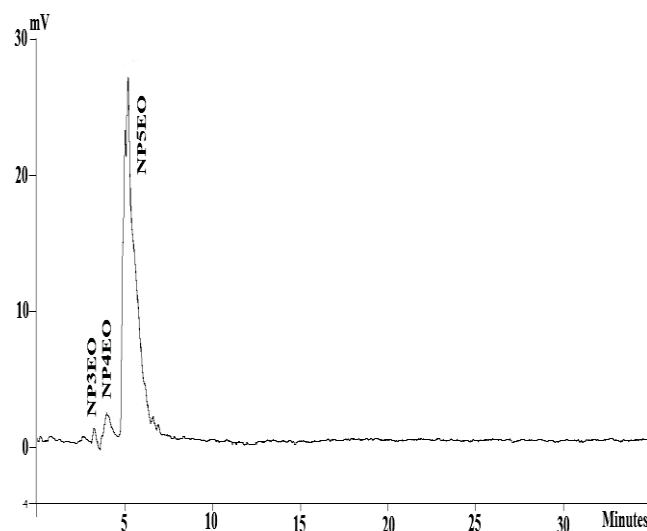


Figure 4 Degradation of NPnEO by H₂O₂ at the concentration of 50mg L⁻¹

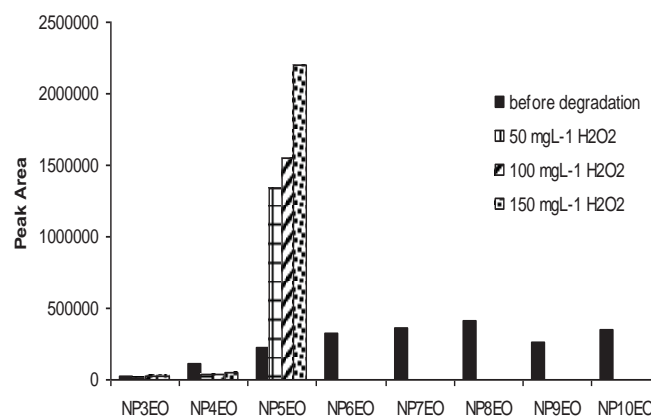
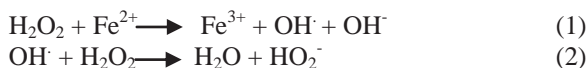


Figure 5 Peak area of individual NPnEO after the reaction of NPnEO (n= 3 to 10) with H₂O₂ at different concentration

Fenton's reagent is a mixture of H₂O₂ and ferrous ion which produces hydroxyl radicals. In this work, the mixture between 150 mg L⁻¹ of ferrous ions and 50 mg L⁻¹ of H₂O₂ was used for degradation enhancement of NPnEO in the dark. The HPLC chromatogram shows the same results as in Fig. 4. The degradation products from oxidation process of Fenton method were 96.7±0.5% of NP5EO, 2.2±0.3% of NP4EO and 1.1±0.2% of NP3EO. Degradation was not enhanced due to consumption of ferrous ions and hydroxyl radicals by H₂O₂ as can be seen in equation 1 and 2.



Study in the Photo-Fenton system was examined. Longer EO units of NPnEO is degraded to NP5EO the same as degradation by Fenton's reagent (Fig. 6). However, peak area of NP5EO is decreased significantly and no peaks of NP3EO and NP4EO are observed. The reason for disappearance of NP3EO and NP4EO in Photo-Fenton process may have been the destruction of the benzene ring. Hydroxyl radicals are generated as can be seen in equation 1. Ferric ions can react with water when ultraviolet is irradiated (equation 3). This reaction produces more hydroxyl radicals and gives Fe^{2+} back to a solution. NP3EO and NP4EO have short chain length ethoxylate that could be easily degraded to intermediate and to CO_2 and H_2O completely (equation 4 and 5). To enhance the degradation of NPnEO by Photo-Fenton method, increases in the UV light intensity should increase the number of hydroxyl radicals. Exposure time for Photo-Fenton process is also important for enhancement of degradation process producing less toxic chemicals.

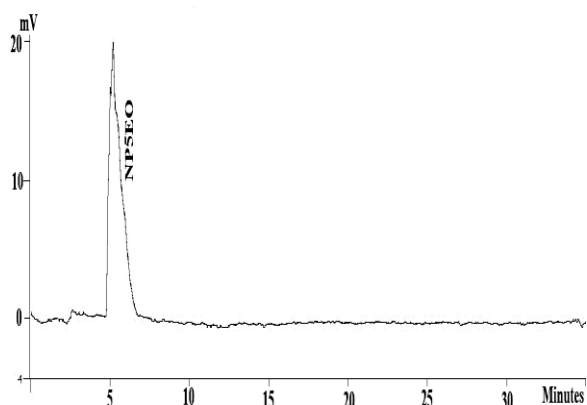
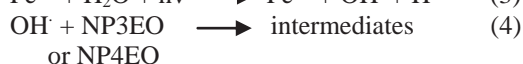


Figure 6 Degradation of NPnEO by photo- fenton process



4. Conclusions

In this work, normal-phase HPLC-FL showed the optimum performance for the selected NPnEO oligomers. HPLC patterns show how long-chain NPnEOs are degraded to short-chain NPnEOs or other products leading to the information about degradation processes. This method is rapid, simple and easy operation handle. Analysis can perform in a single run to obtain qualitative information.

Photo-fenton process tends to be the best treatment for NPnEO because of ability to destroy benzene ring. However, further study will concentrate on the UV light intensity, exposure time of irradiation and the effect of initial concentration of $\text{Fe}^{2+}/\text{H}_2\text{O}_2$. NPnEOs

are nontoxic chemicals but their degradation products from aerobic and anaerobic treatment causing pollutants widespread in the environment. Nontoxic chemicals from wastewater treatment are the most requirements for reducing accumulation of contaminants in environmental system. Therefore, information about the origin of pollutants and wastewater treatment are very important for removal all toxic chemicals from the environment.

Acknowledgements

The authors acknowledge financial support from department of chemistry, King Mongkut's University of Technology Thonburi, Thailand.

References

- [1] C. Planas, J.M. Guadayol, M. Droguet, A. Escals, J. Rivera and L. Caixach, *Water Res.* **36** (20002) 982-988.
- [2] D.W. Kolpin, E.T. Furlong, M.T. Meyer, E.M. Thurman, S.D. Zaugg, L.B. Barber and H.T. Buxton, *Environ. Sci. Technol.* **36** (2002) 1202-1211.
- [3] M.J. La Guardia, R.C. Hale, E. Harvey and T.M. Mainor, *Environ. Sci. Technol.* **35** (2001) 4798-4804.
- [4] H.A. Ball, M. Reinhard and P.L. McCarty, *Environ. Sci. Technol.* **23** (1989) 951-961.
- [5] W. Giger, P.H. Brunner and C. Schaffner, *Science*. **25** (1984) 623-625.
- [6] E. Galembeck, A. Alonso and N.C. Meirelles, *Chem. Biol. Interact.* **113** (1998) 91-103.
- [7] M.H.I. Comber, T.D. Williams and K.M. Stewart, *Water Res.* **27** (1993) 273-276.
- [8] H. Destailats, H.M. Hung and M.R. Hoffmann, *Environ. Sci. Technol.* **34** (2000) 311-317.
- [9] K. Hyunook, P. Guisu, Y. Myongjin, K. Eunjung, H. Youngkook and M.K. Colosimo, *Res. J. Chem. Environ.* **11** (2007) 72-84.
- [10] M. Fukushima and K. Tatsumi, *Environ. Sci. Technol.* **35** (2001) 1771-1778.
- [11] E.J. Rosenfeldt and K.G. Linden, *Environ. Sci. Technol.* **38** (2004) 5476-5483.
- [12] P.M. Nagarnaik and B. Boulanger, *Chemosphere*. **85** (2011) 854-860.
- [13] N. Thongkon, P. Samtong and N.Piyaphotchanakorn, *Burapha Science Journal*. **12** (2007) 14-27.

REUSING CULTURE MEDIUM FOR *CHAETOCEROS GRACILIS* CULTIVATION IN AIRLIFT PHOTOBIOREACTORS

Patthama Sung¹, Prasert Pavasant^{1*}

¹Chemical Engineering Research Unit for Value Adding of Bioresources, Department of Chemical Engineering, Faculty of Engineering, Chulalongkorn University, Phayathai Rd., Patumwan, Bangkok 10330, Thailand

*E-mail: prasert.p@chula.ac.th, Tel. +66 22186870, Fax. +66 22186877

Abstract: One of the major costs for the cultivation of *Chaetoceros gracilis* is the medium expenses. This work investigates the effectiveness in the reuse of culture medium and to examine preliminary economical analysis for such cultivation. In this work, the cultivation of *Chaetoceros gracilis* with an initial cell concentration of 5×10^5 cells mL⁻¹, light intensity of 10,000 lux and the total volume of 5 L airlift photobioreactor and with the modified F/2 medium with fresh sea water are examined. Major medium constituents are silicate (2.97 mg-Si/L), phosphate (1.02 mg-P/L) and nitrate (12.35 mg-N/L). The cost of initial major medium are 42.4% of silicate, 5.5% of phosphate and 33.1% of nitrate from total cost of initial medium. The work will start by collecting the medium after removing the harvested cell. The reused nutrients is then used silicate, phosphate and nitrogen for the cultivation and the performance of such system is compared with the original culture for economical comparison

1. Introduction

The production of biofuels from microalgae has stimulated numerous attention recently. Although the oil product from the microalgae still is quite costly when compared with oil derived from vegetation, the growth of algae is relatively faster leading to a better yield and there are room to improve on process efficiency. In addition, microalgae can be cultivated all year long and can be harvested on a daily basis which allows a better process management (rather than harvesting once a year and the raw material will have to be stored for months). Moreover the use of microalgae to produce biofuels does not lead to the problem of food security, unlike the other land-crops where the energy plants are blamed for the invasion and reduction of food-crop lands [1]. Marine microalgae have been applied in aquaculture industry, especially in hatchery of many aquatic lives, e.g. shrimp and fish [2]. For shrimp larvae, *Chaetoceros gracilis* is one of the most popular species in Thailand as it can be cultivated quite easily. Preliminary examination reveals that this alga contains a reasonable amount of triglyceride and might be a good source of biofuels.

Recently, there has been a study on the optimal growth and reactor design for the cultivation of *Chaetoceros calcitrans* (*Chaetoceros calcitrans* the same family but a different genus *Chaetoceros gracilis*) where the maximum cell density of approximately 8.88×10^6 cell mL⁻¹ with a maximum specific growth rate of 7.41×10^{-2} h⁻¹ were achieved [3]. Moreover, the culture could be grown in various

modes of operation both in semi-continuous and continuous, and both indoor and outdoor. One of the most important economical factors for the cultivation of *Chaetoceros* is the cost of nutrients, as the high cost silica which is one of the main nutritional components constitutes more than 80% of the overall cost and this makes the nutrient cost as high as more than 1 THB per litre.

This research investigates the effectiveness in the use of culture medium and to examine preliminary economical analysis for such *Chaetoceros gracilis* cultivation from the management of nutrient. The reuse of nutrients will also be examined in cases where excess nutrients have to be used for a better growth.

2. Materials and Methods

2.1 Cultivation of *Chaetoceros gracilis*

The cultivation of *Chaetoceros gracilis* was carried out in batch cultivation system with the initial cell concentration of 5×10^5 cells mL⁻¹. Employed in this work is 5 L acrylic airlift photobioreactor (ALPBR). Air was supplied through a porous sparger at a superficial velocity of 3 cm s⁻¹ [3]. The temperature was controlled at 24 – 30 °C. Light was supplied with fluorescent lamps where the intensity at the draft tube surface was maintained at 10,000 lux or 135 μ mol photon m⁻² s⁻¹. The light intensity was measured by Digicon LX-50 lux meter. The cultivation was grown in fresh seawater enriched with modified standard F/2 (Guillard's) stock solution [3].

The culture medium was measured for the consumed nutrients the reuse medium was examined for the remaining silicate, phosphate, and nitrate to determine the amount of extra nutrient needed to be added.

2.2 Determination of cell concentration

Cell concentration was determined using a microscope and the counting of cells was with Haemocytometer where the depth of the counting grid is 0.1 mm (Each counting grid is divided 25 channels) and the medium area is 0.04 mm². The cell number is calculated from:

$$N = n \times 10^4 \quad (1)$$

where N = Cell number (cells mL⁻¹) and n = Number of cells in the counting grid (cells).

2.3 Determination of specific growth rate

The cell concentrations at the two different time periods were employed for the calculation of the growth rate as expressed by

$$\mu = \frac{\ln(N_2) - \ln(N_1)}{t_2 - t_1} \quad (2)$$

where μ is the specific growth rate (h^{-1}), N_1 the cell concentration at t_1 (cells h^{-1}), N_2 the cell concentration at t_2 (cells h^{-1}), t_1 the first sampling time (h) and t_2 the second sampling time (h).

2.4 Determination of medium concentration

Silicate, phosphate, and nitrate were monitored by UV-Visible spectrophotometer at wavelength of 810 , 885, and 220 – 275 nm respectively.

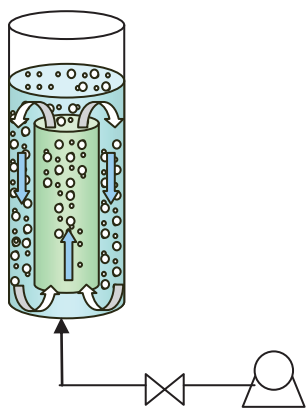


Figure 1 Schematic diagram for airlift photobioreactor

2.5 Determination of productivity

Productivity of *C. gracilis* can be calculated from Equation 3.

$$P = \frac{N_2 - N_1}{t_2 - t_1} \times V \times 1000 \times 24 \quad (3)$$

where P is the productivity (cells day^{-1}), N_1 the cell concentration at t_1 (cells h^{-1}), N_2 the cell concentration at t_2 (cells h^{-1}), t_1 the first sampling time (h), t_2 the second sampling time (h) and V the harvest volume (L).

2.6 Determination of specific productivity

Specific productivity of *C. gracilis* can be calculated from Equation 4.

$$SP = \frac{P}{V} \quad (4)$$

where SP is the specific productivity (cells $\text{L}^{-1} \text{day}^{-1}$), P the productivity (cells day^{-1}) and V the harvest volume (L).

3. Results and Discussion

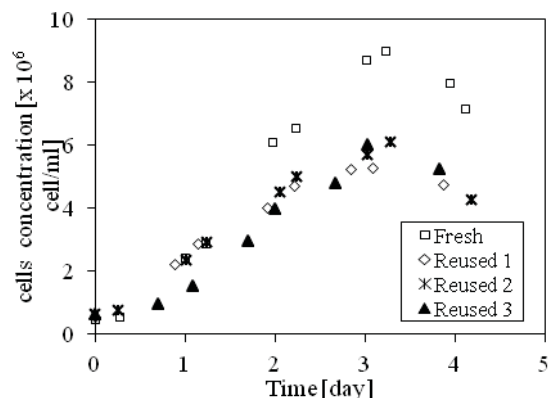


Figure 2 Growth behaviors of *C. gracilis* in fresh medium, 1st, 2nd and 3rd medium reuse

Figure 2 illustrates the result from the cultivation of the *C. gracilis* where Table 1 shows the cell concentration and specific growth rate from the cultivation with fresh medium, first, second and third reuses of medium. A maximum cell concentration obtained from the fresh medium was approximately $8.99 \times 10^6 \text{ cell mL}^{-1}$ with a maximum specific growth rate of 0.04 h^{-1} . The *C. gracilis* was then separated from the fresh culture medium by centrifugation at 4500 rpm, 15 min and 10°C . The resulting clear solution was then reused.

In the 1st, 2nd and 3rd medium reuses, the media were replenished with nutrients at the amounts that were consumed during their growth to maintain the medium composition as close to the original concentration (modified F/2 medium) as possible. The maximum cell concentration obtained from the 1st, 2nd and 3rd medium reuses were lower than that with fresh medium (5.28×10^6 , 6.09×10^6 , 6.02×10^6 and $8.99 \times 10^6 \text{ cell mL}^{-1}$, respectively). The maximum cell concentrations from the 2nd and 3rd medium reuses were higher than 1st, but the specific growth rate of 1st, 2nd and 3rd medium reuse equaled 0.03 h^{-1} .

The major medium constituents in the modified F/2 medium are silicate, phosphate and nitrate which take the following concentration: $2.965 \text{ mg-Si L}^{-1}$ of silicate, $1.0181 \text{ mg-P L}^{-1}$ of phosphate and $12.353 \text{ mg-N L}^{-1}$ of nitrate. This corresponds to the total cost of 0.17 THB per liter (of which 42.4% from silicate, 5.5% from phosphate and 33.1% from nitrate).

Table 1 Maximum cell concentration, specific growth rate in fresh medium, 1st, 2nd and 3rd medium reuses for the cultivation of *C. gracilis*

| System | Maximum cell concentration ($\times 10^6 \text{ cell mL}^{-1}$) | Specific growth rate (h^{-1}) |
|-----------------------|--|---|
| Fresh | 8.99 | 0.04 |
| 1 st reuse | 5.28 | 0.03 |
| 2 nd reuse | 6.09 | 0.03 |
| 3 rd reuse | 6.02 | 0.03 |

Table 2 Productivity and specific productivity in fresh medium, 1st, 2nd and 3rd medium reuses for the cultivation of *C. gracilis*

| System | Productivity ($\times 10^9$ cell day ⁻¹) | Specific Productivity ($\times 10^9$ cells L ⁻¹ day ⁻¹) |
|-----------------------|--|---|
| Fresh | 13.32 | 2.66 |
| 1 st reuse | 7.65 | 1.53 |
| 2 nd reuse | 8.29 | 1.66 |
| 3 rd reuse | 8.94 | 1.79 |

Table 3 Economic for the cultivation of *C. gracilis*

| System | Cost (THB L ⁻¹) | | | | Total (THB L ⁻¹) |
|-----------------------|-----------------------------|------|------|-------|---------------------------------|
| | Si | P | N | Other | |
| Fresh | 0.09 | 0.01 | 0.04 | 0.03 | 0.17 |
| 1 st reuse | 0.01 | 0.01 | 0.04 | 0.03 | 0.09 |
| 2 nd reuse | 0.01 | 0.01 | 0.04 | 0.03 | 0.08 |
| 3 rd reuse | 0.03 | 0.01 | 0.03 | 0.03 | 0.10 |

Figures 2, 3 and 4 demonstrate initial and final major medium concentrations where Table 3 illustrates the total cost of medium in fresh medium, reused mediums (from 1st, 2nd and 3rd reuse) for the cultivation of *C. gracilis*. Table 2 shows the productivity from the cultivation with fresh medium, first, second and third reuses of medium.

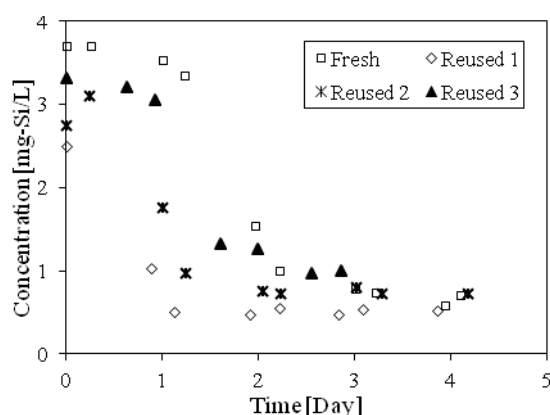


Figure 2 Silicate concentration for the cultivation of *C. gracilis* in fresh medium, 1st, 2nd and 3rd medium reuses

Although the reuse of medium resulted in a decreased in productivity, the total cost reduced as there was a less demand for additional nutrients (Table 3). The ratio of specific productivity and nutrient cost will indicate the amount of biomass generated from the same operating cost and this equals to: 15.6, 17, 20.7, and 17.9 for fresh, 1st, 2nd, and 3rd nutrients, respectively. This means that the reuse of medium offers a better enonomics for the cultivation of *C.*

gracilis.

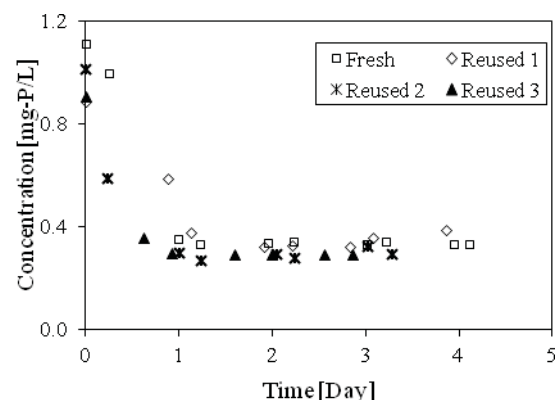


Figure 3 Phosphate concentration for the cultivation of *C. gracilis* in fresh medium, 1st, 2nd and 3rd medium reuses

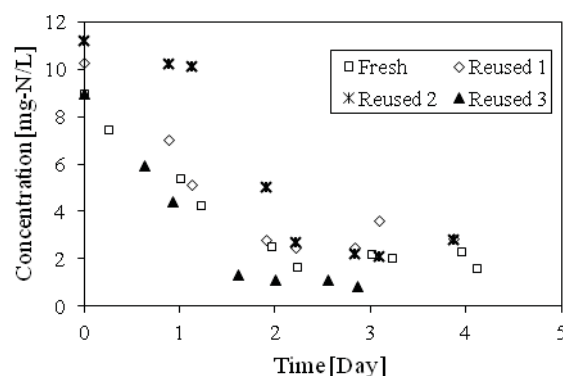


Figure 4 Nitrate concentration for the cultivation of *C. gracilis* in fresh medium, 1st, 2nd and 3rd reused medium.

When considering the cost of each medium component, nitrate and phosphate took the same cost contribution in both fresh and reused mediums (from 1st, 2nd and 3rd reuse) while productivity has decreased. As a result, the ratio between the cost of the media (nitrate and phosphate) increased productivity.

While in the case of silicate found that the cost of silicate most affects to the total cost of medium. When productivity reduced ratio between the cost of silicate and productivity will be have decreased. Silicate was a major medium can be reused in the repeated cultivation as much as approximately 10-20% of previously cultivation.

4. Conclusions

The work shows that, the cell concentration and specific growth rate of fresh medium, reused 1st, reused 2nd and reused 3rd medium. The fresh medium was found to the maximum specific growth rate of 0.04 h⁻¹ with maximum cell concentration 8.99 $\times 10^6$ cell mL⁻¹ in batch culture system. The reused 1st, reused 2nd and reused 3rd medium were lower than fresh medium (5.28 $\times 10^6$, 6.09 $\times 10^6$, 6.02 $\times 10^6$ and 8.99 $\times 10^6$ cell mL⁻¹, respectively). The total cost of reused 1st, 2nd and 3rd medium were lower than fresh medium.

The major medium was silicate the most effective of total cost.

Acknowledgements

The authors wish to acknowledge the Thailand Research Funds for their financial support.

References

- [1] L. Gouveia and A.C. Oliveira, *J. Ind. Microbiol. Biotechnol.* **36** (2009) 269-274.
- [2] B.H. Liang, P.S. Leung and Y.C. Shang, *Aquaculture Asia*, 2 (1997) 28-31.
- [3] S. Krichnavaruk, W. Loataweesup, S. Powtongsook and P. Pavasant, *Chemical Engineering Journal*, 105 (2005) 91-98.

PHOTOCATALYTIC DEGRADATION OF DIRECT YELLOW142 DYE BY CuO/ZnO

Thanaporn Buratipapong, Rattana Fungkiatkajorn and Aimorn Saksaengwijit*

Department of Chemistry, Faculty of Science, King Mongkut's University of Technology Thonburi, Bangkok, Thailand

*aimorn.sak@kmutt.ac.th

Crystalline zinc oxide particles covered with copper oxide on the surface (CuO/ZnO) were prepared by the sol-gel method. The CuO/ZnO sample was characterized by X-ray diffraction (XRD) and scanning electron microscope (SEM). The photodegradation of Direct Yellow 142 dye (DY142) under the daylight irradiation was used to determine the catalytic activity of CuO/ZnO. The influences such as pH, catalyst dosage, initial concentration of dye and temperature on the photodegradation efficiency were investigated. Under the daylight irradiation CuO/ZnO has the higher photocatalytic activity than ZnO with a factor of 1.64. Kinetic analysis on the photodegradation of DY142 indicated that the reaction can be described by the Langmuir-Hinshelwood model. By using CuO/ZnO as a catalyst, the activation energy E_a of the reaction under the daylight irradiation is 14.7 kJ/mol.

1. Introduction

Heterogeneous photodegradation of dyes and some organic compounds in wastewater has drawn increasing attention as one of efficiency ways for wastewater treatment. Metal oxides such as ZnO, TiO₂, SnO₂, WO₃ and CuO are widely presented as common photocatalysts for the oxidation processes in various reactions [1-5]. Due to the advantage of ZnO and TiO₂ such as the environmental stability, non-toxicity to human health, low cost and high photocatalytic efficiency, they are known catalysts to use widely in many fields. ZnO and TiO₂ are semiconductors with large energy gaps (about 3.2 eV, ~ 387 nm) between their valence and conducting bands. Therefore, only the light with high enough energy as UV irradiation can be absorbed and relevant in the exciting step in the photocatalytic process for ZnO and TiO₂. Since the light in UV range is just a small part (only 4-5 %) of the solar light, the use of ZnO and TiO₂ in solar light as a photocatalyst has low efficiency. In a decade, many attempts to overcome this disadvantage have been reported in several researches [3,6-7]. Some researchers had loaded some impurity metals such as Ag, Au, Cu and Zr [3-4, 8] into these metal oxides in order to improve their photocatalytic efficiencies. However, only some metals can give positive results, the others give the opposite results or less significance. Some researchers had modified the oxide catalysts by synthesizing the composites between ZnO (or TiO₂) and some other oxides. The copper semiconductor as CuO/ZnO, CuO-TiO₂, WO₃-TiO₂, ZnO-TiO₂ and ZnO/SnO₂ [2,6-9] were successfully synthesized and

used as photocatalysts in the degradation processes. Not only the oxide compound, some conjugated π -system also had been added to the oxide composite for improving the electron transfer efficiency in the photocatalytic process [7,10].

In the present work, we had synthesized the composite CuO/ZnO in order to improve the catalytic efficiency of ZnO by extending the absorbance range to the low-energy region of the solar spectrum. Since CuO semiconductor has a narrow band gap of 1.7 eV, it absorbs the visible light and generate an excited electron and hole for the oxidation process. Moreover, the photogenerated electrons from ZnO can transfer to CuO in order to reduce the recombination of electron and hole. ZnO coupled with CuO has already been reported in many applications [9,11]. In this work, we used the photodegradation of Direct Yellow 142 dye (DY142) under the daylight as a model to determine the enhancement of photocatalytic efficiency of CuO/ZnO comparing to ZnO. The kinetics of the reaction was also studied.

2. Materials and Methods

2.1 Chemicals

Direct Yellow 142 dye (DY142, CH) was purchased from Di-star Company. Zinc sulphate (ZnSO₄·7H₂O), Copper sulphate (CuSO₄·5H₂O) and sodium hydroxide (NaOH) are analytical grade from the AJAG Chemical Company (Australia). All reagents were used without further purification.

2.2 Preparation of ZnO and CuO/ZnO

For preparing the CuO/ZnO composite, the nano-zinc oxide (ZnO) powder was synthesized by the sol-gel method under the aging temperature-control. The 50 mL of 0.2 M ZnSO₄ and 50 mL of 0.45 M NaOH solution were cooled at 0 °C for 4 hours. Then, mixed the both solution and stirred the mixture in the aging bath at 28°C. The clear mixture solution became clouded and some white powder precipitated at the bottom. The white powder was dried at 120°C for 1 hour and then calcited at 550°C for 5 hours.

The composite CuO/ZnO was prepared by the impregnation method as reported in the literature [12]. The synthesized nano-zinc oxide powder was soaked and stirred in 0.5 M CuSO₄ solution for 24 hours. The copper ions Cu²⁺ adsorb and penetrate on the surface

of zinc-oxide crystal. The purple powder was filtered and dried at 120°C for 1 hour. The colour of the powder would change to black after calcination at 550°C for 5 hour.

2.3 Characterization

The crystal structures of the prepared photocatalysts were characterized by the X-ray powder diffraction with $\text{CuK}\alpha$ radiation scanning from $2\theta = 20$ -70 degrees. The particle morphology of CuO/ZnO composite was observed by the scanning electron microscope (SEM).

2.4 Photodegradation Studies

The photodegradation of DY142 dye was carried out in the thermostat bath at temperature 25, 35 and 45 °C. A 25 ml solution containing known concentration of the dye and amount of CuO/ZnO catalyst was prepared and stirred under the light source in the thermostat bath. A 8W daylight bulb was used as the light source. The reactor was set to have 8 cm distance between the solution surface and the light source. During irradiation, the solution was stirred continuously to keep the suspension homogeneous. The reaction was stopped at several setting times and the remain concentration of dye in the solution was determined by the spectrometric method. After centrifuging, the supernatant was collected and measured the absorption intensity at $\lambda_{\text{max}} = 405$ nm. By using the calibration curve, the remaining concentration of dye was determined. The degradation was carried out at natural pH of dye solution. Only the experiments on the pH effect, the pH of the solution was adjusted with hydrochloric acid and sodium hydroxide solution and monitored by a pH-meter.

The photodegradation efficiency of DY142 was defined as follows:

$$\text{Photodegradation efficiency (\%)} = \frac{C_0 - C_t}{C_0} \cdot 100 \quad (1)$$

where C_0 is the initial concentration of DY142 dye and C_t is the concentration of dye at certian reaction time t (minutes).

3. Results and discussion

3.1 Characterization

The powder X-ray diffraction pattern of ZnO/CuO is shown in figure 1(a). The triangle and square symbols locate the refraction peaks for ZnO and CuO, respectively. All characteristic peaks of ZnO are correlated to the XRD pattern for pure ZnO as shown in the figure. This pattern is for the hexagonal wurtzite structure. The refraction peaks for CuO have low intensities, therefore it is difficult to specify the crystal lattice for CuO. The SEM image of CuO/ZnO is shown in figure 1(b). The image indicates the aggregation of CuO/ZnO particles.

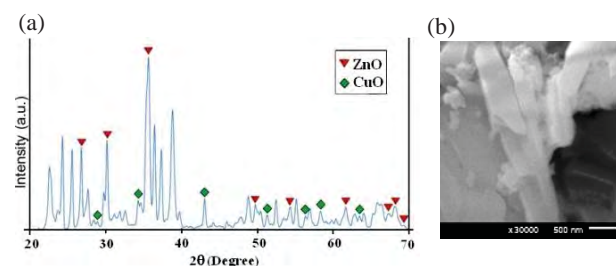


Figure 1. (a) XRD pattern and (b) SEM image of CuO/ZnO

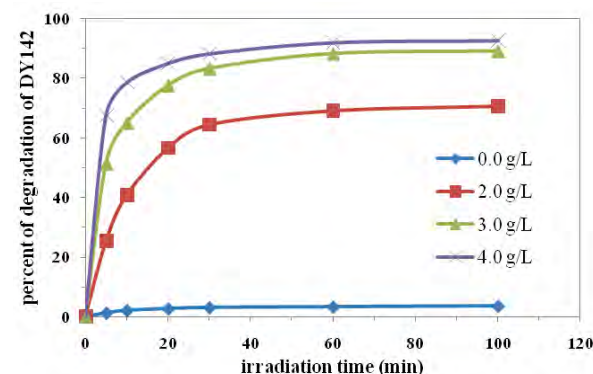


Figure 2. Percent of photodegradation of 40.32 mg/L DY142 as a function of catalyst dosage.

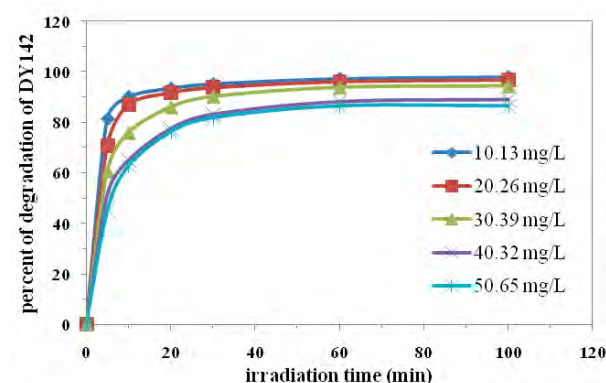


Figure 3. Percent of photodegradation of DY142 as a function of initial dye concentration. Catalyst dosage is 3g/L.

3.2 Effect of the photocatalyst dosage

In order to examine that to what extent DY142 could be degraded under the daylight without catalyst. A blank experiment was done by irradiating a 40.32 mg/L DY142 solution for 100 minutes. It turns out that the percent of photodegradation of DY142 without catalyst was only 3.6%. Therefore, it is interesting to determine that what the least amount of catalyst to give reasonable high degradation efficiency is. For this purpose, the experiment was done again with the various doses of catalyst (2.0, 3.0 and 4.0 g/L). The results are shown in the figure 2. By increasing the catalyst dose from 2.0 to 3.0 g/L, the percent of degradation increased from 70.5 to nearly 90 (89.7) after 100 minutes of irradiation. When the catalyst dose further increased to 4.0 g/L, the percent of degradation increased more slightly (only 2.3% more). Thus, the optimize amount of CuO/ZnO catalyst to give high degradation efficiency is 3.0 g/L.

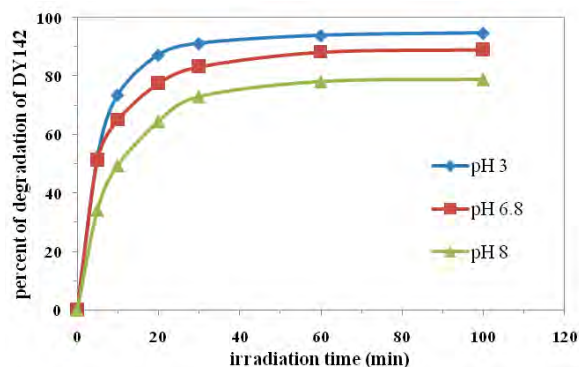


Figure 4. Percent of photodegradation of 40.32 mgL⁻¹ DY142 as a function of pH. Catalyst dosage is 3g/L.

3.3 Effect of the initial dye concentration

The initial concentration of DY142 was varied in the range of 10.13-50.65 mg/L while the catalyst dosage was kept to 3.0 g/L. As shown in figure 3, the photodegradation efficiency decreased as increasing the initial dye concentration. It is known that the generation of hydroxyl and superoxide radicals presents as an important step for the photodegradation reaction. More adsorbed dye molecules on the surface of catalyst obstruct the adsorption of hydroxyl ions and reduce the efficiency for absorbing photons. With high initial dye concentration, the degradation efficiency will therefore be low since the generation of oxidative radicals is decreased.

3.4 Effect of pH

The wastewater from textile industrials has a wide range of pH values. The natural pH of dye solution in this work is 6.88. In different pH conditions, the charge of dye molecule is different. The generation of hydroxyl radicals is also dependent on the pH of the solution. Thus, pH is an important parameter for ones to concern when studying the photodegradation. In order to study the effect of pH on the degradation efficiency, the behaviors of the photodegradation reaction in acid and base condition (pH=3 and pH=8) were investigated. The degradation efficiency at pH=3 is highest for this experiment. In figure 4, the efficiency decreased with increasing the pH value. This result implies that the photodegradation of DY142 with CuO/ZnO as a catalyst should be better to carry out in the acidic medium. This result is in agreement with the previous works on the similar type of dye degradation [13]. Generally, the reaction mechanisms for photodegradation can be contributed from three main processes;



The oxidation of dye via a positive hole (eq. 3) is regarded as the main degradation mechanism in the acidic medium, which should be also the main process for degradation of DY142 in this work.

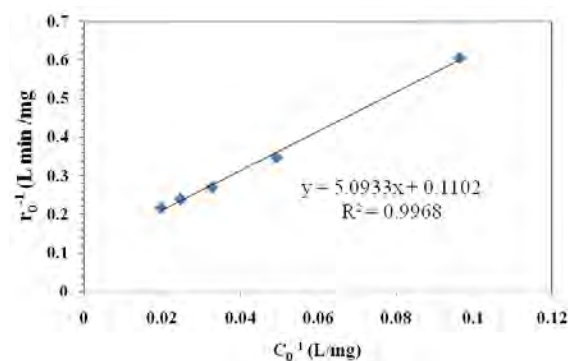


Figure 5. The relationship between the inverse of the initial rate r_0^{-1} and the inverse of initial concentration of dye, C_0^{-1} . Solid line is the linear fit to the Langmuir-Hinshelwood model.

The influence of pH generally depends on the type of dye and the properties of catalytic surface. In acidic medium, the surface of metal oxide is generally positive charged and changes to be negative charged in the alkaline medium. DY142 is a negative-charged dye with sulfonate groups ($-\text{SO}_3^-$) in its molecular structure. In alkaline medium, dye molecule still has negative charged, the electrostatic repulsion force between dye and the catalyst surface might be a reason to decrease the photodegradation efficiency at high pH condition.

3.5 Kinetic Analysis

Heterogeneous photocatalytic reaction is complicated, which is involving many processes (such as molecular diffusion, adsorption and chemical reaction) and having many parameters. In this work, we studied only on the kinetics under different initial concentrations of dye and the effect of the temperature. Photodegradation of DY142 was carried out in varying the initial concentration of dye in the range of 10 – 50 mg/L. Many researches on the heterogeneous catalytic reaction always used the Langmuir-Hinshelwood expression to explain the kinetics. Below are the equations to describe the kinetic behavior of the photodegradation of DY142 in the Langmuir-Hinshelwood model;

$$r = -\frac{d[\text{DY142}]}{dt} = k \frac{K_{\text{DY142}}[\text{DY142}]_0}{1 + K_{\text{DY142}}[\text{DY142}]_0} \quad (5)$$

$$r_0 = k \frac{K_{\text{DY142}}[\text{DY142}]_0}{1 + K_{\text{DY142}}[\text{DY142}]_0} \quad (6)$$

$$\frac{1}{r_0} = \frac{1}{k} + \frac{1}{kK_{\text{DY142}}[\text{DY142}]_0} \quad (7)$$

where r represents the rate of reaction that changes with time. The term r_0 represents the initial rate of reaction, $[\text{DY142}]_0$ is the initial concentration of DY142 dye (mgL⁻¹), K_{DY142} is the Langmuir-Hinshelwood adsorption equilibrium constant (Lmg⁻¹) and k is the rate constant of the reaction on the surface (mgL⁻¹min⁻¹).

According to the Langmuir-Hinshelwood form in the equation 5, the plot between r_0^{-1} and $[\text{DY142}]_0$ should give a linear relationship. The linearized